UNIVERSITY OF SOUTHAMPTON

FACULTY OF NATURAL AND ENVIRONMENTAL SCIENCES

School of Chemistry

Supramolecular porphyrin arrays on DNA and SWNT scaffolds

by

Ashley James Brewer

Thesis for the degree of Doctor of Philosophy

April 2011

ABSTRACT

UNIVERSITY OF SOUTHAMPTON

Abstract

FACULTY OF NATURAL AND ENVIRONMENTAL SCIENCES
SCHOOL OF CHEMISTRY

Doctor of Philosophy

SUPRAMOLECULAR PORPHYRIN ARRAYS ON DNA AND SWNT SCAFFOLDS

by Ashley James Brewer

A variety of supramolecular porphyrin arrays on DNA or single walled carbon nanotube scaffolds are presented herein. A novel porphyrin modified nucleoside with multiple degrees of freedom about the linking moiety has been synthesised. Oligonucleotide strands containing the novel 'flexible' porphyrin modified nucleoside or a previously published 'rigid' linked porphyrin modified nucleoside were synthesised. The resulting systems were analysed by photospectrometric techniques. Stable B form duplexes were observed in all cases, with the porphyrin modifications imparting a stabilising effect on the duplexes, the degree of stabilisation the novel porphryin monomer provides is of a similar level to that of the rigid linked monomer. Excitonic coupling of the porphyrins is observed; the different monomers incorporated into DNA show different effects in the circular dichroism spectra, which may be explained through the increased conformational freedom of the 'flexible' linker.

The synthesis of a novel anthraquinone modified nucleoside is presented. Modified DNA strands containing both porphyrin modifications and anthraquinone modifications were synthesised and analysed electrochemically. Cyclic voltammetry has shown that the inclusion of multiple porphyrin modifications increase the electron transfer rate to the anthraquinone redox marker.

The synthesese of a novel ferrocenyl modified nucleotide, a novel naphthalene diimide modified nucleotide and an alternative synthesis route for a ruthenium *tris*-bipyridyl nucleoside are presented.

Homo- and hetero-porphyrin single walled carbon nanotube adducts have been prepared with neutral, tetra-anionic and tetra-cationic porphyrins. Significantly elevated loading levels have been observed for the mixed charge species which forms a 1:1 salt on the nanotube surfaces.

Contents

List of figures

List of Schemes

List of tables

DECLARATION OF AUTHORSHIP

I, Ashley James Brewer

declare that the thesis entitled

Supramolecular porphyrin arrays on DNA and SWNT scaffolds

and the work presented in the thesis are both my own, and have been generated by me as the result of my own original research. I confirm that:

- this work was done wholly or mainly while in candidature for a research degree at this University;
- where any part of this thesis has previously been submitted for a degree or any other qualification at this University or any other institution, this has been clearly stated;
- where I have consulted the published work of others, this is always clearly attributed;
- where I have quoted from the work of others, the source is always given. With the exception of such quotations, this thesis is entirely my own work;
- I have acknowledged all main sources of help;
- where the thesis is based on work done by myself jointly with others, I have made clear exactly what was done by others and what I have contributed myself;
- parts of this work have been published as:
    - High loading of carbon nanotubes with hetero-porphyrin complexes. Brewer, A.; Lacey, M.; Owen, J. R.; Nandhakumar, I.; Stulz, E. *J. Porphyr. Phthalocya.* **2011**. 15. 1.
    - Introducing structural flexibility into porphyrin-DNA zipper arrays. Brewer, A.; Siligardi, G.; Neylon, C.; Stulz, E. *Org. Biomol. Chem.* **2011**. 9. 777.
    - Duplex Stabilization and Energy Transfer in Zipper Porphyrin-DNA. Nguyen, T.; Brewer, A.; Stulz, E. *Angew. Chem. Int. Ed.* **2009**. 48. 1974

Signed: ……..

Date: ……..

Acknowledgements

I would like to thank Dr Eugen Stulz for providing me with the opportunity to conduct this research, and for his support and supervision throughout the course of the project, without him none of this would have been possible. I am grateful for all he has done over the last few years.

Thanks are also due to other members of the Stulz research group; Tom Bandy, Jon Burns, Thao Nguyen Nguyen and Dan Singleton. Their advice, support and friendship has been invaluable.

I am greatly appreciative of Rob Johnson and Matt Lacey for the cyclic voltammetry experiments they ran for me, of Dr Fabrice Birembaut for running the Raman spectra, and of Dr Cameron Neylon for collecting and analysing SAXS data.

I would like to thank my parents for their continual support; you have helped me become who I am today. Finally, I would like to thank Franki for her patience, support and understanding, we got there eventually.

Definitions and abbreviations

A	Absorbance
A	Adenosine
AcOH	Acetic acid
AFM	Atomic force microscopy
aq	Aqueous
a.u.	Arbitrary units
br. s	Broad singlet
c	Concentration
C	Cytosine
°C	Degrees centigrade
CD	Circular dichroism
$CDCl_3$	Deuterated chloroform
CD_3OD	Deuterated methanol
CEP-Cl	2-*O*-cyanoethyl-*N*-*N*-di-*iso*-propylchlorophosphoramidite
conc.	Concentrated
CV	Cyclic voltametry
d	Doublet
δ	Chemical shift
dA	2'-Deoxyribose adenosine
dC	2'-Deoxyribose cytosine
DCC	Dicyclohexyl carbodiimide
DCM	Dichloromethane
DDQ	2,3-Dichloro-5,6-dicyanobenzoquinone
DEA	Diethylamine
dG	2'-Deoxyribose guanosine
DIC	Di-*iso*-propyl carbodiimide
DIPEA	Di-*iso*-propylethylamine
DMAP	*N*,*N*-dimethylamino pyridine
DMC	Dimethylcarbonate
DME	1,2-Dimethoxyethane
DMF	*N*,*N*-Dimethylformamide
DMSO	Dimethylsulphoxide
DMT	4-4'-Dimethoxytrityl
DNA	2'-Deoxyribosenucleic acid
DOPC	1,2-dioleoyl-glycero-3-phosphocholine

DOPE	1,2-dioleoyl-glycero-3-phosphoethanolamine
DPV	Differential Pulse Voltammetry
dU	2'-Deoxyuridine
EA	Ethyl acetate
EC	Ethylene carbonate
EDC	1-Ethyl-3-(3-dimethylaminopropyl) carbodiimide
eq.	Equivalent
FDMT	4-(1*H*,1*H*,2*H*,2*H*-perfluorodecane)-4',4''-dimethoxytrityl
Fmoc	9-*H*-Fluoren-9-ylmethoxycarbonyl
G	Guanosine
GC-EI MS	Gas chromatography electron impact mass spectrometry
GC-ESI (neg)	Gas chromatography electrospray mass spectrometry, negative ion detection mode
GC-ESI (pos)	Gas chromatography electrospray mass spectrometry, positive ion detection mode
HOBt	Hydroxybenzotriazole
HR-ESI(neg)	High resolution electrospray mass spectrometry, negative ion detection mode
HR-ESI(pos)	High resolution electrospray mass spectrometry, positive ion detection mode
Hz	Hertz
J_{CF}	Carbon-fluorine coupling constant
J_{HH}	Proton-proton coupling constant
L	Litre
λ	Wavelength
λ_{max}	Maximum wavelength
λ_{em}	Excitation wavelength
λ_{em}	Emissison wavelength
M	Molarity (mol dm^{-3}), or, Mega
m	Milli
m	Multiplet
m	Meta
µ	Micro
MALDI-TOF	Matrix assisted laser desorbsion/ionisation time of flight mass spectrometry
min	Minutes
mol	Mole

MWNT	Multi walled carbon nanotube
m/z	Mass to charge ratio
n	Nano
NMI	*N*-methylimidazole
o	Ortho
pH	$-\log_{10}$ [H]
p	Para
ppm	Parts per million
q	Quartet
quant.	Quantitative
R_f	Retention factor
RBM	Radial breathing mode
Rel. int.	Relative intensity
RNA	Ribosenucleic acid
RPM	Revolutions per minute
RT	Room temperature
s	Singlet
SCE	Saturated Calomel Electrode
SHE	Standard Hydrogen Electrode
SWNT	Single walled carbon nanotube
T	Thymine
t	Triplet
TBAP	Tetrabutylammonium perchlorate
TCA	Trichloroacetic acid
TEA	Triethylamine
TEAA	Triethylammonium acetate
TFA	Trifluoroacetic acid
TLC	Thin layer chromatography
TMPyP	5, 10, 15, 20-tetra (*p*-methylpyridinium)-21*H*, 23*H*-porphyrin tetra tosylate salt
TPP	5, 10, 15, 20-tetraphenyl 21*H*, 23*H*-porphyrin
TPSA	5, 10, 15, 20-tetra(*p*-phenylsulphonic acid) 21*H*, 23*H*-porphyrin tetra sodium salt
U	Uridine
UV-Vis	Ultra violet and visible spectroscopy
ZnTPP	21,23-Zinc (II) 5, 10, 15, 20-tetraphenyl porphyrin

1 – Introduction

1.1 – Porphyrins

Porphyrins are macrocyclic compounds that are prevalent in biological systems; haem[1] and chlorophyll[2] (Figure 1) are porphyrin derived structures that play vital roles in sustaining plant and animal life. Haem is a substituted iron metallated porphyrin[1] responsible for delivering oxygen molecules to all cells of the body. This is achieved by the iron (II) metal in the centre of the macrocycle (ferrous haem) binding to an oxygen molecule adsorbed through the lungs where the O_2 concentration is high and the CO_2 concentration is low. This bound oxygen is then transported around the bloodstream *via* an iron (III) metalled porphyrin (ferric haem), before subsequently being released where it is required in the body, *i.e.* where the O_2 concentration is low and the CO_2 concentration is high, in turn the ferric haem is reduced to ferrous haem and is able to begin the process again. Chlorophyll (Figure 1) is a magnesium metalled porphyrin derivative,[2] where one of the macrocyclic alkenes is reduced to give a structure known as a dihydroporphyrin, or chlorin. Chlorophyll is an essential component of photosystem I[3] and photo system II,[4] the two known mechanisms for photosynthesis in plants, where it absorbs visible light from the sun, creating an electronically excited species, several electron transfer steps ultimately lead to the reduction of NADP (nicotinamide adenine dinucleotide phosphate), which can then reduce atmospheric CO_2 to create sugars.[5] Porphyrins participate in electron transfer reactions in cytochrome P450, one of the enzymes responsible for the oxidation and metabolism of organic compounds such as drug molecules within the body.[6] The photophysical properties of porphyrins are also utilised by nature in light harvesting compounds; the array of bacteriochlorophyll (a substituted porphyrin) formed within the chromosomes of green bacteria is the most efficient light harvesting array known.[7]

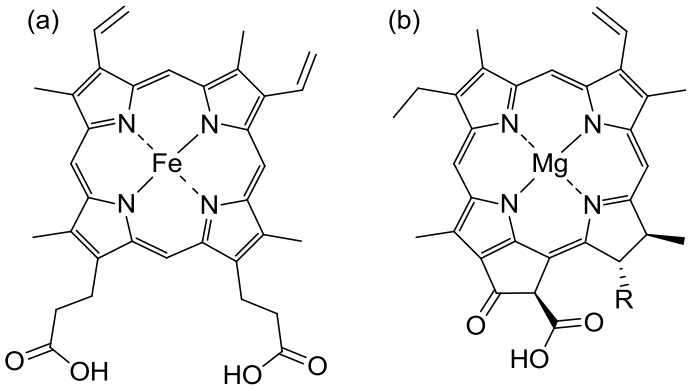

Figure 1. Examples of biological porphyrins, (a) Haem B, and (b) Chlorophyll A

The porphyrin macrocycle is composed of four pyrrolic rings connected *via* the α carbons by methyne bridges, the so called *meso* carbons. The macrocycle includes an eighteen electron aromatic core and an additional 4 π electrons which are involved in two non-aromatic pyrollic double bonds. Through resonance of the aromatic core the two non-aromatic double bonds are included into the aromatic structure of the molecule with the exclusion of the other two β–β carbon double bonds from the aromatic system. Both resonance structures (Figure 2) are equally favoured[8] and rapid inter-conversion results in all the pyrrolic β carbons having identical reactivity and chemical shifts.

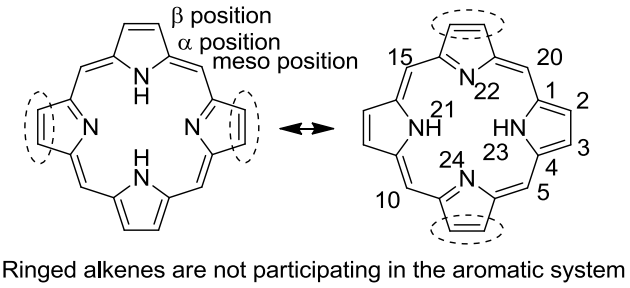

Figure 2. Porphine, the simplest porphyrin as an example of porphyrin naming, numbering and resonance structures.

Porphyrin syntheses may be achieved by a variety of different routes, see - 3.1 – Porphyrin synthesis (page 25) for more detailed discussion. Briefly, synthesis is usually achieved by combining varying ratios of pyrrole, one or more aldehydes and a lewis acid such as boron trifluoride etherate or hydrochloric acid in non protic solvents or proprionic acid as both a lewis acid and the solvent. A varying number of porphyrinogens are formed depending on the number of different aldehydes used in the synthesis. Linear substituted polypyrroles of various lengths are major side products of the synthesis. Oxidation of the porphyrinogens to their respective porphyrins was originally achieved through refluxing in air,[9] using atmospheric oxygen as an oxidising agent. Oxidation by this method limits the functional groups available due to the harsh reaction conditions required, as such oxidation using a benzoquinone based reagent, e.g. 2,3-dichloro-5,6-dicyanobenzoquinone (DDQ) or 2,3,5,6-tetra-chlorobenzoquinone (*p*-chloranil), is now commonly used.

Substituents can be appended to the porphyrin macrocycle at the β position, *meso* position and at the pyrrolic nitrogens (Figure 2). Substitution at the β positions will typically occur prior to forming the macrocycle, as per Sanders *et al.*,[10] however substitution at this position post macrocycle synthesis is also possible.[11] When this approach is used, the reaction occurs with the π electrons in the double bonds outside of the aromatic system due to their

increased nucleophilicity compared to the π electrons in the aromatic system. This approach is less popular than modification of the pyrrole moieties before forming the macrocycle as stereospecific substitution cannot be achieved.

Substitution at the *meso* positions is achieved prior to the porphyrin synthesis by utilising substituted aldehydes in the macrocycle synthesis. The π systems of aromatic substituents at the *meso* positions are discrete from the porphyrin π system due to steric clashes between the aromatic substituents and the hydrogens bonded to the β carbons. This forces aromatic *meso* substituents to adopt an out of plane geometry and hence keeps the π systems discrete, the torsion angle between the plane of the porphyrin and the plane of the aromatic substituent is around 60°.[12]

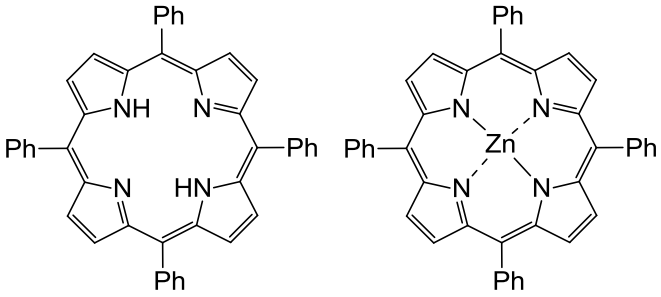

Figure 3. Freebase and zinc metallated tetraphenyl porphyrin

The nitrogen atoms in the centre of the macrocycle may be appended with alkyl substitutions[13] or with a plethora of metal ions (Figure 3) in a variety of molecular geometries, including; square planar (Zn^{2+}, Fe^{2+}),[14] octahedral (Ru^{2+}, Mo^{5+})[14,15] and square pyramidal (Fe^{3+}, Rh^{3+}).[14,16] Small metal ions (Co^{2+}, Cu^{2+}, Fe^{2+}) sit within the plane of the porphyrin and do not distort its structure, larger metal ions (Hf^{4+}, Re^{+})[17], are too big to reside within the 2 Å cavity between the pyrrolic nitrogens and as such, sit above the plane of the ring, distorting the ring's planarity to greater or lesser extents. When porphyrins are metallated with metal ions of sufficient radius and co-ordination number it is possible to form porphyrin-metal-porphyrin sandwich complexes (Zr^{4+}).[18] Due to the direct connection to the conjugated system, metallation of the porphyrin macrocycle affects the photospectrometric properties of the porphyrin molecule.

The absorbance spectra of freebase porphyrins comprise several bands in the visible region; there are two absorbance between 400-430 nm, the so called Soret bands or B-bands these have a molar extinction coefficient in the order of 1 x 10^5 mol^{-1} dm^3 cm^{-1},[19] in solution these two bands coincide and appear as a single peak and is often referred to as a single absorbance, the B-band or Soret band. Separation of the two Soret absorbances occurs when the porphyrins are stacked,[20,21] this may be observed as either a broadening of the signal or as two

discrete absorbances. The intensity of the Soret band is notably larger than those of the smaller Q-band absorbances, these occur between 480-660 nm and have molar extinction coefficients in the order of 1 x 10^4 mol^{-1} dm^3 cm^{-1}.[19]

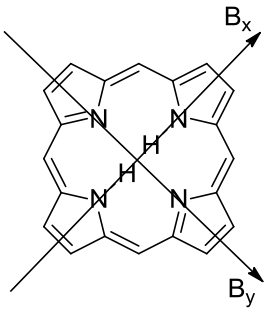

Figure 4. B_x and B_y transitions of porphine

The absorbance spectra of porphyrins has been explained by Martin Gouterman using his four orbital model.[22,23] Due to the presence of the two hydrogen atoms inside the macrocycle, the molecular symmetry is D_{2h} and as such the molecule has two orthogonal dipoles; B_x which lies on the N-H H-N axis, and B_y which is perpendicular to the B_x dipole and lies on the N N axis[22] (Figure 4). The two ground states have quasi-allowed and allowed $\pi \rightarrow \pi^*$ transitions to both the first and second excited states, producing the Q-bands and B-bands respectively. The B_x-B_y energy level split is only ~240 cm^{-1}, typically resulting in the two bands coalescing, however the Q_x-Q_y energy level split is significantly greater, ~3000 cm^{-1}, resulting in discrete Q band absorbances.[22] The Q-band absorbances show further splitting due to excitation to both the ground and the first vibrationally excited states, resulting in four Q band absorbances; $Q_y(1.0)$, $Q_y(0.0)$, $Q_x(1.0)$ and $Q_x(0.0)$ from high to low energy.

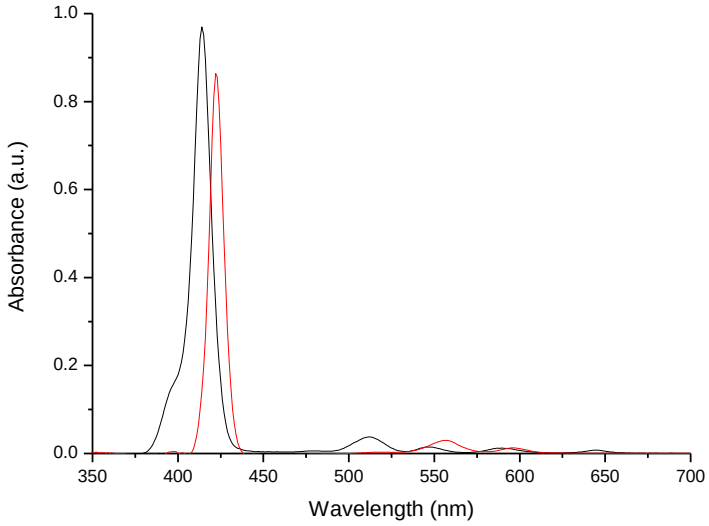

Figure 5. UV-vis of a freebase (black) and zinc metallated (red) porphyrin

When the pyrrolic N-H protons of the porphyrin macrocycle are substituted with a metal the symmetry group of the porphyrin is changed from D_{2h} to D_{4h}. This causes the B_x and B_y transitions become degenerate and as such the absorbance spectra shows a single B band absorbance and only two Q band absorbances; Q (1.0) and Q (0.0).[23]

If the meso position of the porphyrin is appended with a phenyl ring a torsion angle exists between the porphyrin macrocycle and the phenyl substituent; this keeps the porphyrin's π system discrete. As such the unique electronic and photophysical properties of the porphyrin may be probed even if it is bonded to a scaffold such as a nucleobase.

1.2 – 2'-Deoxyribose nucleic acid (DNA)

The structure of 2'-deoxyribose nucleic acid (DNA) was researched by several groups in the early part of the twentieth century with the currently accepted structure being elucidated in 1953 by James Watson and Francis Crick[24] with major crystallographic contributions from Rosalind Franklin, Raymond Gosling and Maurice Wilkins.[25,26] The double stranded helix conformation adopted by DNA has a width of around 20 Å, one helical turn usually incorporates 10.5 base pairs and has a length of around 34 Å, however the dimensions of the helix are subject to a variety of factors including sequence,[27] solvent[28] and salt concentration.[27]

A single strand of DNA consists of three parts; the nucleobase, the sugar ring and the phosphate backbone. Heterocyclic nucleobases are connected at the 1 position of the nucleobase to the 1' position of a 2'-deoxy-D-ribofuranose ring *via* a β glycosidic bond, this is a nucleoside. Nucleosides bonded through the 5' position to a phosphate moiety are called

nucleotides, these nucleotides are the building blocks for the linear polymer that is DNA, wherein the nucleotides are connected *via* phosphodiester linkages.

Natural DNA monomers contain one of four bases; 2'-deoxy adenosine (dA), 2'-deoxy guanidine (dG), 2'-deoxy cytidine (dC) and thymidine (T). 2'-deoxy adenosine and 2'-deoxy guanidine are purine based heterocyclic nucleosides, while 2'-deoxy cytidine and thymidine are pyrimidine based heterocyclic nucleosides. A strand of DNA is teminated at the 5' end in the primary (1°) hydroxyl, while at the 3' end it terminates in a secondary (2°) hydroxyl, this gives the DNA directionality i.e. 3'-ACGT-5' is not the same as 5'-ACGT-3'.

Intermolecular hydrogen bonds between adenosine and thymidine bases, and cytidine and guanidine bases form Watson Crick base pairs and facilitate the formation of duplexes of complimentary sequences (Figure 6). The complimentary single strands of DNA align 'head to tail', the 5' end of one strand aligns with the 3' end of the other and *vice versa*. A-T base pairs form 2 hydrogen bonds with a bonding strength of 15-25 kJ mol^{-1} per base pair, while C-G base pairs share 3 hydrogen bonds with a bonding strength of 25-40 kJ mol^{-1} per base pair.[29,30] G-C rich sequences are more stable than A-T rich sequences of the same length due to the increased number of intermolecular hydrogen bonds and the slight destabilising effect of A-T stacking within the sequence.[31]

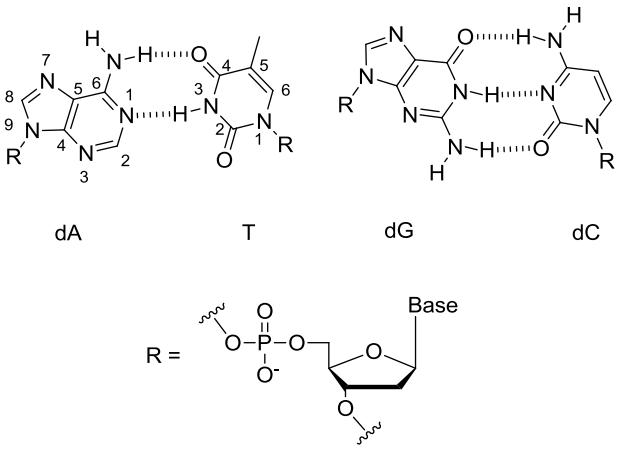

Figure 6. Watson Crick base pairing and numbering of natural nucleotides

The double helix of DNA has two grooves spiralling round its length, the major groove and the minor groove. These grooves are named after their respective sizes, the major groove is 22 Å wide and the minor groove only 12 Å wide.[27] The helical nature of DNA allows it to occur in both right and left handed helices, a right handed helix is one which when observing a section of a duplex, the strand closest to the observer spirals from the top right of the molecule to the bottom left, a left handed helix is the reverse of this i.e. the strand spirals from top left to bottom right.

DNA occurs in many known morphologies, however there are only three major forms; A-form, B-form and Z-form (Figure 7). A-form and B-form DNA are both right handed helices, with the A-form a more compressed helix (11 b.p per helical turn, size ~ 18 Å x 28 Å)[25] than the B-form (10.5 b.p per helical turn, size ~ 20 Å x 34 Å).[24,26] A-form DNA is prevalent in RNA-RNA and chimeric RNA-DNA duplexes, whilst B-form DNA is most commonly found in DNA-DNA duplexes. Z-form DNA is a left handed helix (12 b.p per helical turn, size ~ 18 Å x 45 Å) with little variation in size between the major groove and the minor groove that occurs in high salt concentrations with GC rich sequences.[32]

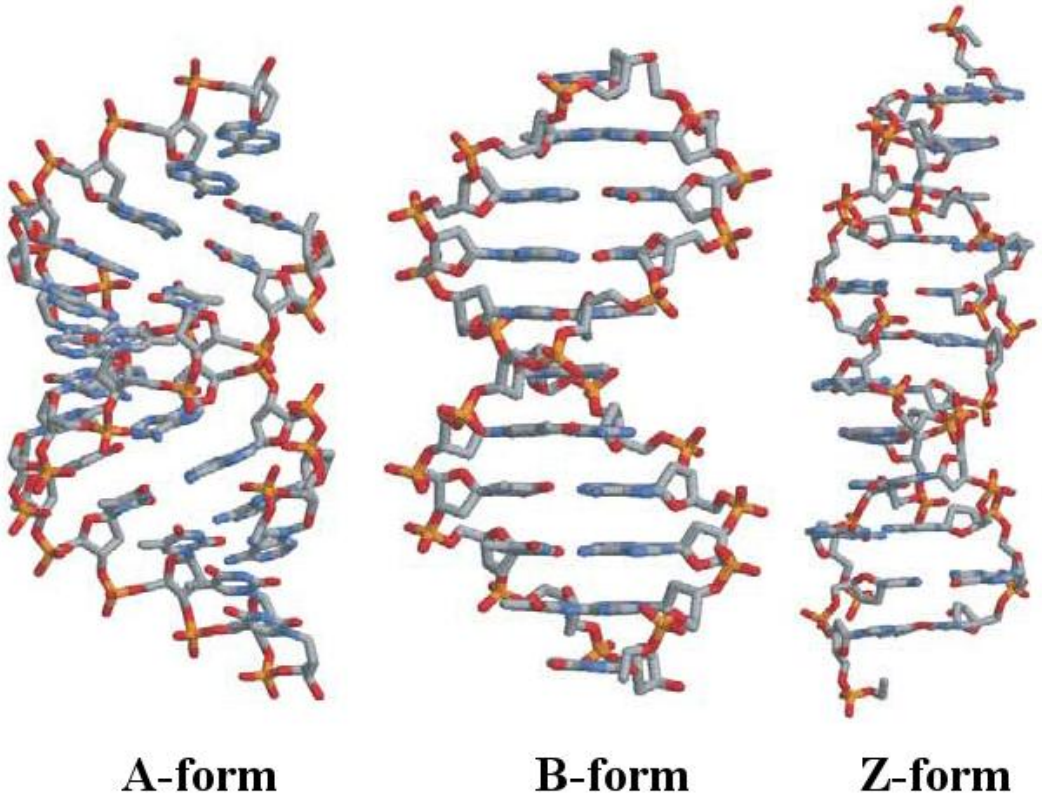

Figure 7. A-form, B-form and Z-form DNA[33]

DNA provides an almost ideal scaffold for supramolecular systems; its properties are very well understood, with sizes, geometries and melting temperatures all able to be predicted with reasonable accuracy. Very specific DNA sequences have been synthesised to create 'DNA origami',[34] that is words or pictures which may be viewed by atomic force microscopy; examples include spelling the acronym 'DNA', a map of the Americas and smiley faces.[35]

Modifications to DNA can be incorporated into site specific locations along the strand, with the building block nature of DNA allowing for very facile fine tuning of the system. Many supramolecular systems would require a very different synthesis route in order to change the

location of one moiety within the system; however by using DNA as a scaffold it is possible to simply change the sequence of bases in the synthesis in order to introduce the desired change, leading to greatly decreased synthesis times.

1.3 – Modification of DNA

Modification to DNA can occur in a variety of positions, these include; base modification, sugar modification, artificial nucleobases and backbone replacement.

Base modification[36] is usually achieved such that it places the substituent into the major groove where it does not perturb the helix to too great an extent, to achieve this pyrimidines are modified at the 5 position. In order for modifications to purine nucleobases to be located in the major groove, the modification would have to be made to the nitrogen in the 7 position. Modified purines nucleobases are therefore usually achieved with the use of the 7-deaza analogue (7-deaza-dG and 7-deaza-dA). Modification at the 8 position of the purine nucleobase avoids the requirement for the 7-deaza analogue, however the substituent is positioned into a more stericaly hindered environment.[36] Modifications are usually incorporated into the monomers *via* palladium cross coupling reactions[37] with the iodinated analogue of the nucleobase. Iodinated analogues are available for all natural nucleosides (Figure 8), however by far the most commonly used is 5-iodo dU since there are no functional groups on the nucleobase that require protection as with the other nucleobases.

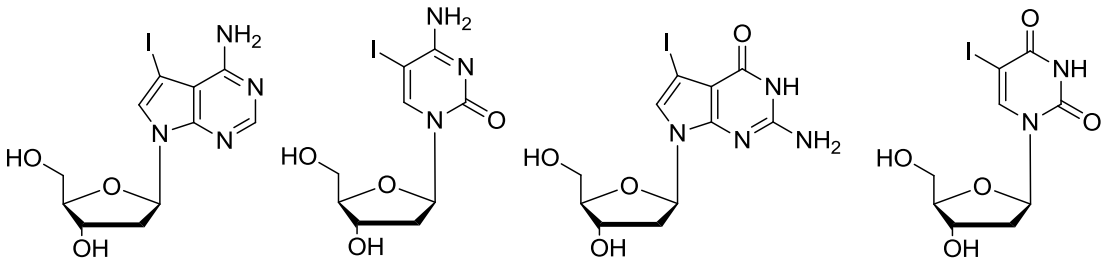

Figure 8. Commercially available iodinated nucleoside analogues

Sugar modifications can be achieved by a few methods, as a terminal modification a 5' hydroxyl or amine (Figure 9a)[38] or the 3' hydroxyl or amine may be appended with a substituent, 5' hydroxyl modifications are not usually problematic since most DNA synthesis is conducted in the 3' to 5' direction. However, 3' modifications require either the modifier to be attached to a universal support and the DNA strand synthesised from there or for the DNA

synthesis to be conducted from 5' to 3' – this route requires more expensive, less reactive and hence less efficient reagents than the 3' to 5' synthesis and as such is not often used.

Modifications may also be made to the sugar ring *via* a 2' hydroxyl[39] (Figure 9b) *i.e.* by incorporating an RNA monomer into the strand, or *via* a thiol (Figure 9c)[40] or 2' amine.[41] Due to the tri-valent nature of the nitrogen molecule, 2' amines allow for either; double bonds between the modification and the nucleoside (Figure 9d),[41] or for the nitrogen to also be bonded to the 4' carbon *via* a methylene unit (Figure 9e)[42] creating an additional 5 membered ring which 'locks' the conformation of the helix into that of B-form DNA – so called locked nucleic acid (LNA).[43] Modifications *via* this route allow not only for terminal modifications but also for modifications within a sequence. Modifications of the sugar cannot be achieved with bulky substituents without perturbing the helix since the modification resides within the helix itself. Aromatic modifications such as the pyrene modification presented by Yamana *et al.*[39] are able to stabilise the duplex through additional π–π interactions.

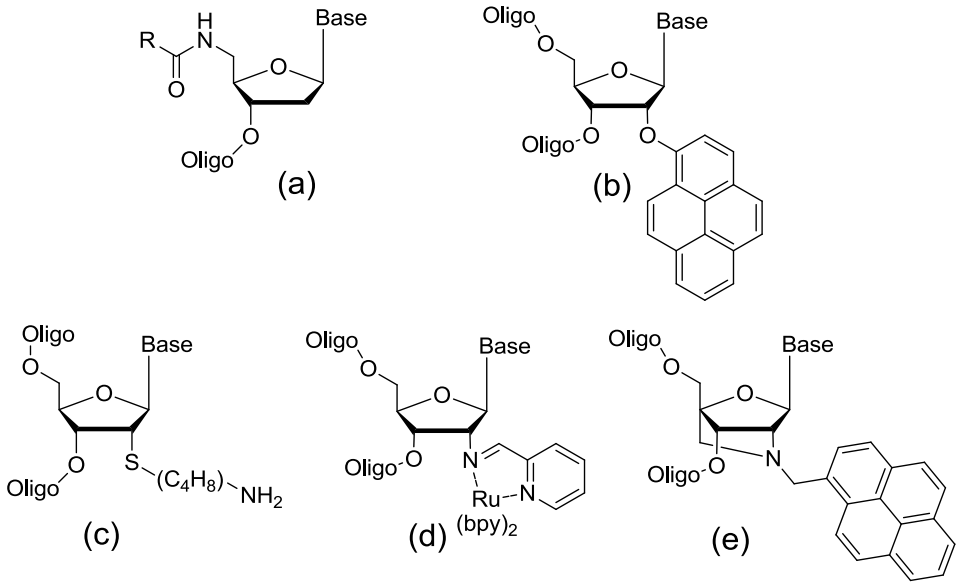

Figure 9. Examples of sugar modification[38,40-42,44]

Artificial nucleobases are organic molecules that replace the natural nucleobase[45,46] (Figure 10), the phosphate backbone and the 2'-deoxy ribose moieties are unchanged – the artificial base is bonded to the sugar *via* the 1' position as per natural DNA. Artificial nucleobases are usually small aromatic molecules which are able to reside within the base stack of the helix, however due to the removal of the natural nucleobase, Watson-Crick base pairing cannot occur at the modified position in a duplex (Figure 10a, b &c), other inter-strand attractive electrostatic forces may be designed into the modified base[47,48] to provide stability of the helix (Figure 10d, e & f). The incorporated artificial nucleobase may have been introduced

to be probed spectroscopically, however, it is also possible to include artificial nuclobases which are of no great interest on their own, but are able to facilitate the site specifically incorporation of metal ions into the helix[47,48] through both dative and covalent bonding. This incorporation of metal ions within the helix creates a 'nanowire' of one atom width (Figure 10e &f).[47,48]

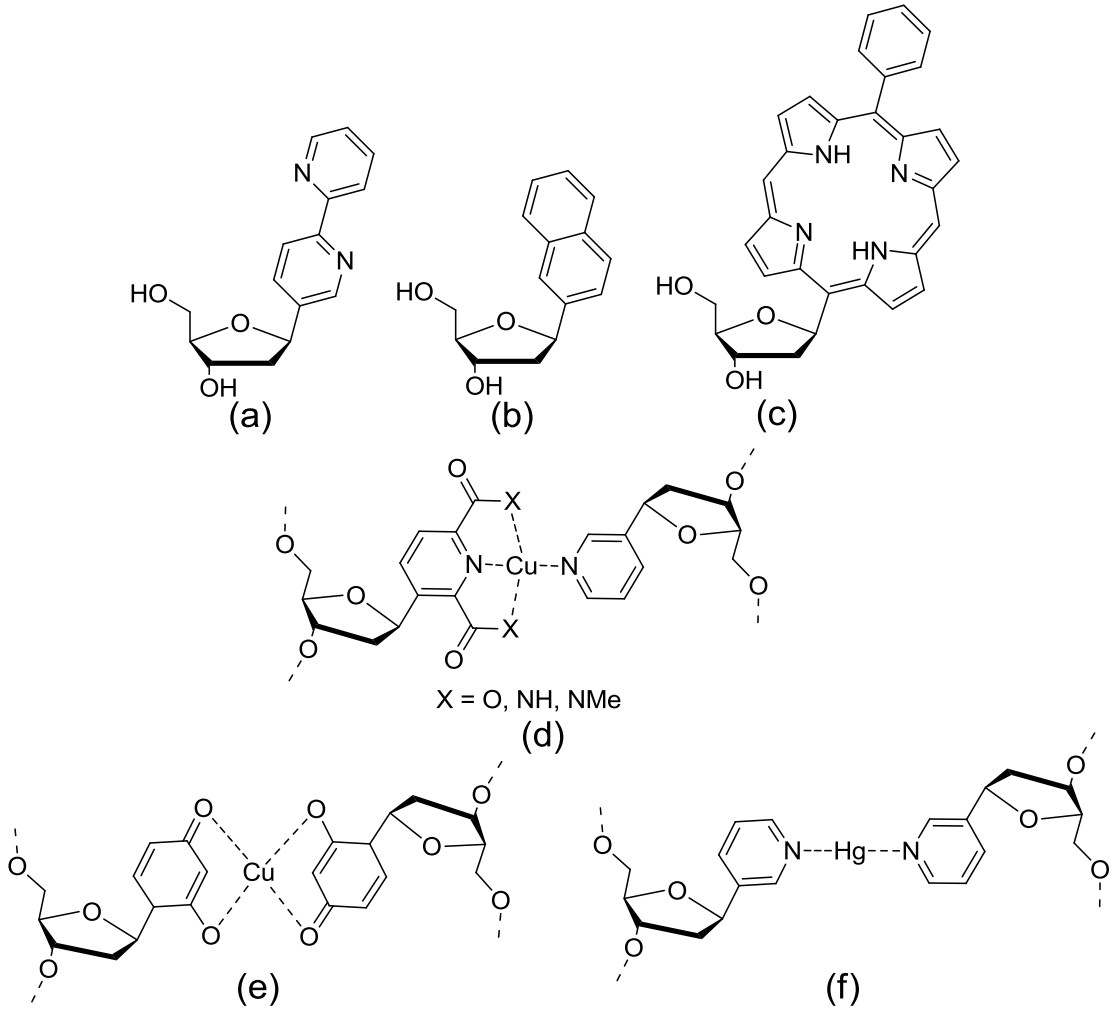

Figure 10. Examples of artificial nucleobases[45-48]

Backbone replacement is the complete removal and replacement of one or more nucleoside with small organic molecules that are bonded to the phosphate backbone (Figure 11). The modification can occur at the end of the strand[49] or mid-sequence.[50] It has been shown that even achiral molecules, such as pyrene,[50] when incorporated as backbone replacements into DNA, are able to form helical structures with induced chirality due to the chiral nature of the DNA. Sheppard *et al.*[51] have demonstrated that it is possibly to covalently bond 3'- and 5'-terminal backbone replacement modifiers together to create longer DNA strands using a complimentary DNA template strand and a metal templated synthesis. The linking of the

strands is achieved through the conversion of two terminal aldehydes into imines linked by an ethylene spacer, this creates a midsequence backbone replacement from the two terminal backbone replacements.

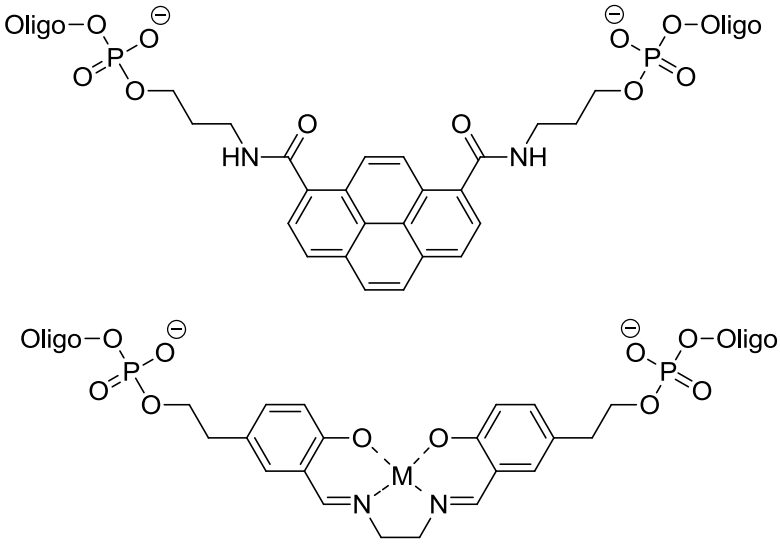

Figure 11. Examples of backbone replacements[50,51]

The inclusion of modifications into DNA often leads to a destabilisation of the duplex, this is commonly observed as a lowering of the duplex's melting temperature (T_m). However, aromatic modifications that are able to π stack (e.g. porphyrins, Figure 12) or small organic molecules that are able to participate in hydrogen bonding are able to offset the degree of destabilisation and with enough interactions between the strands can even stabilise the duplex, leading to an increase in T_m. For example, the incorporation of a single porphyrin modification into a duplex lowers the T_m by ~7 °C, incorporation of multiple porphyrins onto one strand continues to lower the T_m with the degree of destabilisation per porphyrin dropping with subsequent modifications. The decrease in destabilisation per porphyrin levels off at around 4 porphyrin modifications, with a destabilisation of approximately 3 °C per porphyrin.[20,21,52] If however, the modifications are incorporated onto alternate strands in a zipper like fashion, the π-π interactions between the porphyins are no longer intramolecular, but intermolecular; these interactions increase the number of interstrand attractive electrostatic forces and as such are able to impart a net stabilising effect to the duplex despite the multiple modifications appended to it.[21]

Using DNA as a scaffold allows for site specific incorporation of porphyrins, or other small organic molecules, into a 3D framework, however, where the exact orientation and location of the substituents is of less importance a simpler approach to synthesising

supramolecular arrays can be used. Small molecules may be immobilised, through either covalent or non-covalent interactions onto a surface, such as a carbon nanotube molecule.

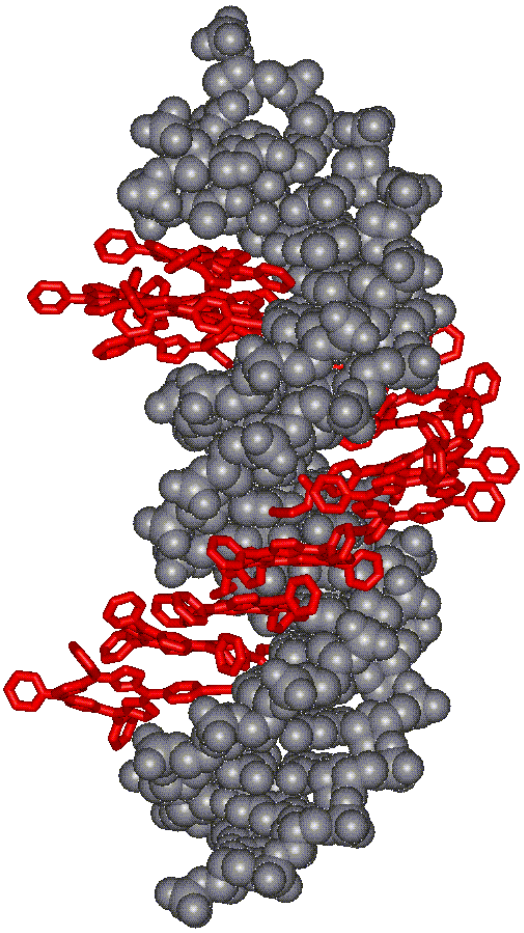

Figure 12. Molecular modelling of zipper-like porphyrin modified DNA

1.4 – Carbon Nanotubes

Carbon nanotubes were first discovered by Iijima[53] in 1991, they are tubular structures consisting entirely of carbon of various diameters and geometries. Carbon nanotubes may be separated into two broad groups (Figure 13); multi walled carbon nanotubes (MWNT) and single walled carbon nanotubes (SWNT). SWNT can be thought of as being a seamless graphene sheet that has been wrapped around on itself to form a hollow tube, the end of the nanotube may or may not be sealed by the carbon lattice. Typical sizes are 2-3 nm in diameter and around 1μm in length,[54] however nanotubes as long as 18.5 cm have previously been reported.[55] The lattices of MWNTs are of a similar structure to those of SWNTs, however, MWNTs consist of two or more individual tubular lattices layers, or one lattice layer rolled

around itself several times.[53] Typically MWNTs have a diameter of 5 nm and are of a similar length as SWNTs, the internal distance between the different carbon lattices is ~3.6 Å.[54]

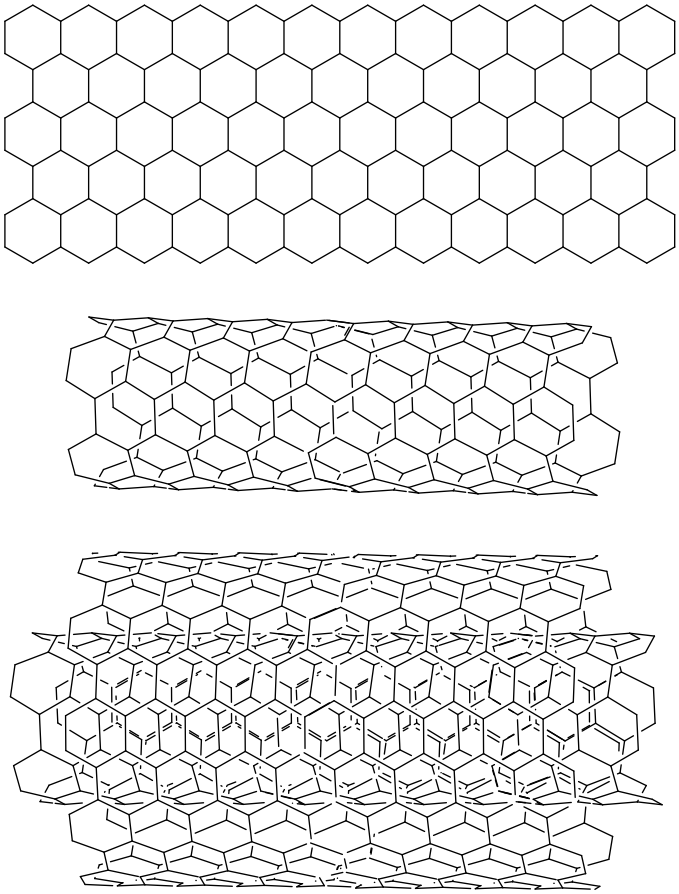

Figure 13. Examples of graphene sheet, single walled carbon nanotube and multiwalled carbon nanotube

Carbon nanotubes are produced by a variety of methods, including; laser ablation of a cobalt and nickle doped carbon target,[56] decomposition of ethylene[57] or methane[55] on molybdenum or iron/molybdenum particles, and high pressure disproportionation of carbon monoxide (HiPCO).[58] Due to the continuous flow of reagents in the HiPCO process, this has become the preferred method for synthesising SWNTs. All of the above methods produce SWNTs of a variety of geometries and sizes, depending on the size of the metal catalyst particle from which the nanotube grew, controlling the catalyst nanoparticle sizes has some effect on controlling the diameter of the resulting nanotubes but not on the geometry of the nanotubes[59].

The orientation of the rows of 6 membered rings within the nanotube lattice can run perpendicular to the length of the nanotube, creating what is known as a zig-zag structure, or they may run at a variety of different angles to the length of the nanotube, resulting in one of numerous chiral configurations or an achiral form known as the armchair structure. The various

structures of nanotubes that it is possible to form may be described with the vectors (*n*, *m*), the vectors describe which carbon atoms would be superimposed if a graphene sheet were to be rolled into a tube (Figure 14). Zig-zag structures are formed when the *m* = 0, armchair structures are produced when *m* = *n* while all other structures are chiral nanotubes.

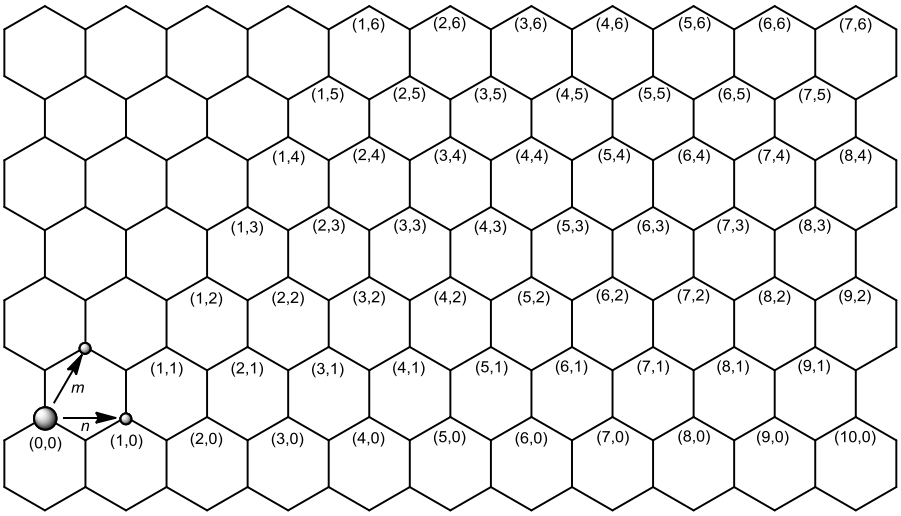

Figure 14. Vector numbering of carbon nanotubes

The differing geometries of SWNTs have differing electronic structures, as a result some carbon nanotubes are metallic while others are semi-conducting. Nanotubes where *n* - *m* = 3*i*, where *i* is an integer, are metallic, for example; (*4*,*1*), (*6*, *3*), (*7*,*1*) and (*9*,*3*) are all metallic nanotubes, all other geometries are semiconducting nanotubes[60]. It is possible to separate the metallic nanotubes from the semiconducting nanotubes[61-63] using a variety of molecules through preferential binding to one type over the other. For applications where the nanotubes are used as supports for covalently bound or non-covalently bound species, a mixture of nanotubes is often used[64-69] since the exact nature of the nanotube is not of major importance.

1.5 – Functionalisation of SWNTs

Functionalisation of single walled carbon nanotubes is possible by a number of different methods, including; covalent bonding of a substrate to the nanotube,[70,71] chemical adsorption to the outside surface of the nanotube,[72,73] and trapping molecules inside the nanotube structure.[74-76]

Covalent attachment of small molecules to single walled carbon nanotubes may be facilitated through a number of methods, including; surface carboxylation and subsequent ester or amide bond formation (Figure 15a);[71,77] reaction with diazonium salts (Figure 15b);[78,79]

reaction of an α-amino acid and an aldehyde (Figure 15c),[80] or; reaction with a nitrile oxide (Figure 15d).[81]

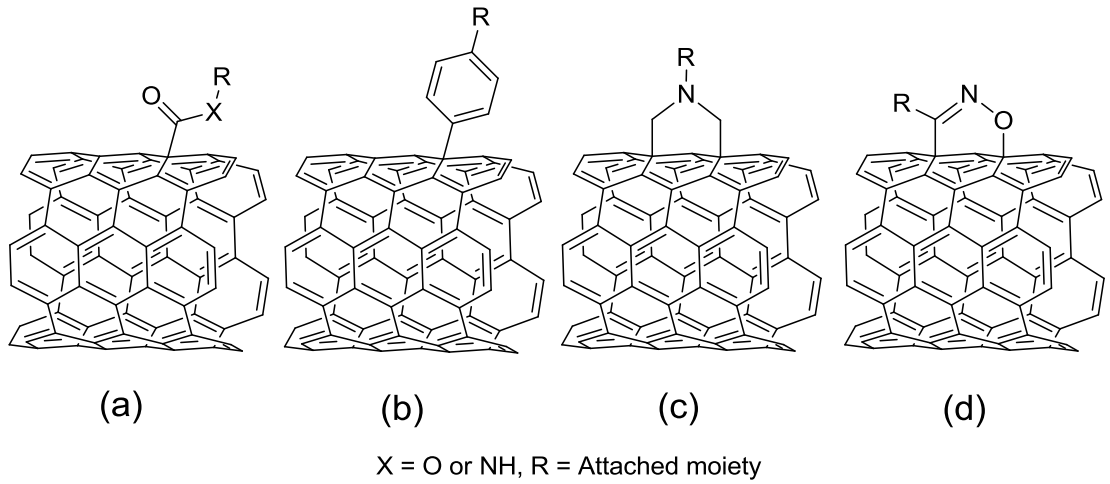

Figure 15. Examples of covalent modifications to SWNTs[71,77,78,81,82]

Numerous organic molecules have been appended to single walled carbon nanotubes (Figure 16) using the aforementioned methods, these include; TTF,[71] ferrocene,[82] phthalocyanines,[78] porphyrins,[83] ruthenium (II) bipyridyl complexes[77] and fluorescein.[84] The covalent attachment of these pendant molecules is achieved in order to study the resulting complexes photophysical or electron transfer properties.

It is also possible to non-covalently bond functional molecules to the surfaces of the single walled carbon nanotubes (Figure 17). It is well documented that polycyclic aromatic molecules adsorb to the surface of carbon nanotubes through π–π interactions and form stable adducts. Compounds adsorbed to the surface of nanotubes include; porphyrins,[85-89] pyrenes,[66,67,69,72] sapphyrins[90] and DNA strands.[73,91-93] As per covalently bound species, these systems are synthesised for their potential applications in light harvesting devices, as photoinduced electron transfer systems, or for solubilising the carbon nanotubes.[88]

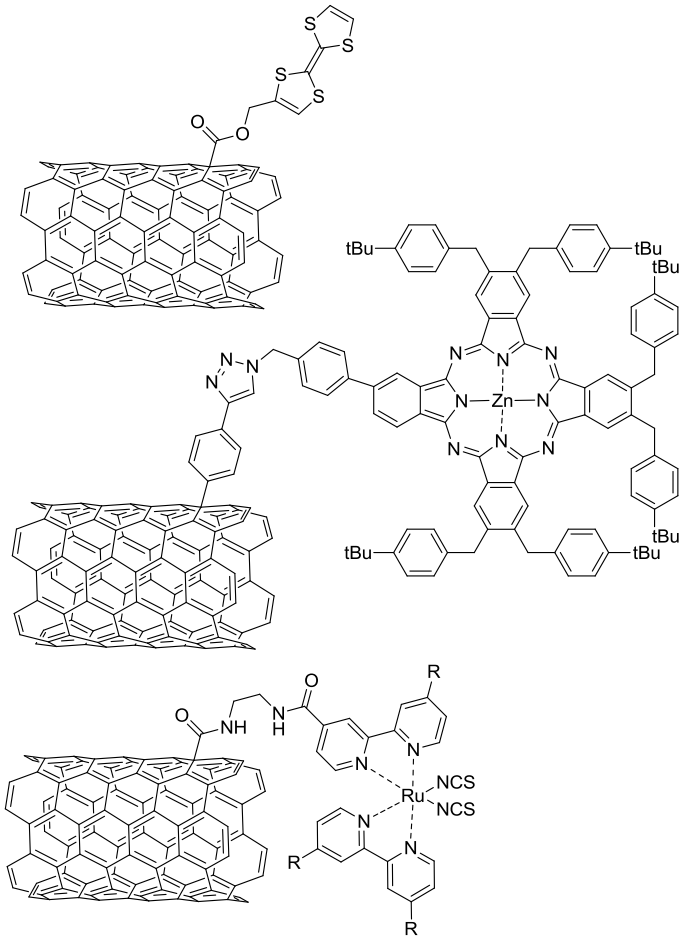

Figure 16. Examples of covalently bound TTF, phthalocyanine and ruthenium (II) bipyridyl modification to SWNTs[71,77,78]

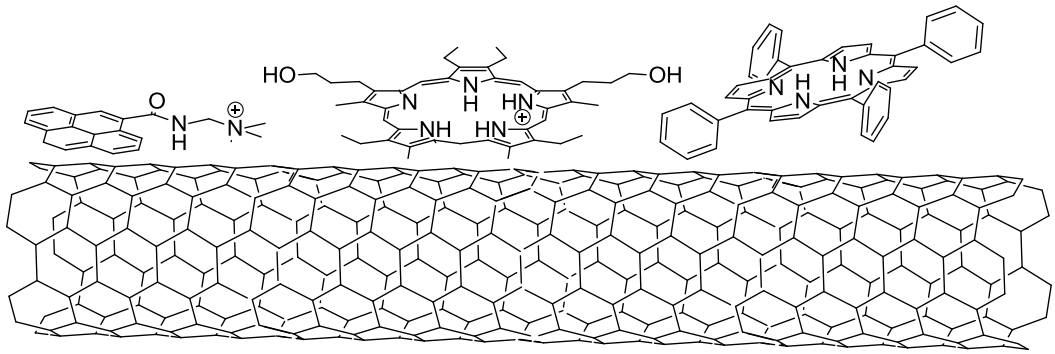

Figure 17. Representation of polyaromatics adsorbed to a SWNT[69,89,90].

Due to the porous nature of single walled carbon nanotubes, small molecules may be sequestered within the walls of the nanotube. Hydrogen[74] and nitrogen[76] gas, and C_{60} fullerenes[75] have been reported to have been stored within the nanotube molecules. This avenue of research is of particular interest for hydrogen storage and for creating storage vessels on a molecular level.

1.6 – Supramolecular porphyrin assemblies

Due to the unique photophysical properties of porphyrins, they are a common feature in supramolecular assemblies. Examples in the literature include covalently attached porphyrin modifications to; isocyanide polymers,[94] DNA oligomers,[21] ethylene glycol or thiophene polymers,[95] butadiyne chains,[96] peptides[97,98], carbon nanotubes[64] and dendrimers.[99] Porphyrin arrays may also be formed though non-covalently interactions. Self assembled porphyrin arrays exist on DNA,[21,100] across lipid bilayers,[101,102] templated on viruses,[103] adsorbed onto carbon nanotubes[87] and self assembled in clover[104] and nanotube[105] arrangements. These arrays are commonly synthesised for light harvesting, photosynthesis mimics and energy or electron transfer purposes.

A multitude of diads,[106-108] triads[106] and tetrads[109] containing porphyrin moieties exist in the literature (Figure 18), with electron transfer between a zinc metallated porphyrin and a freebase porphyrin as a common factor. Other energy transfer steps include; freebase porphyrin to naphthalene diimides[106] and pyromellitimides;[106] fluorescein and rhodamine 110[107] to zinc metallated porphyrin; boron-dipyrrin to zinc porphyrin;[110] and zinc porphyrin to C_{60}.[109,111]

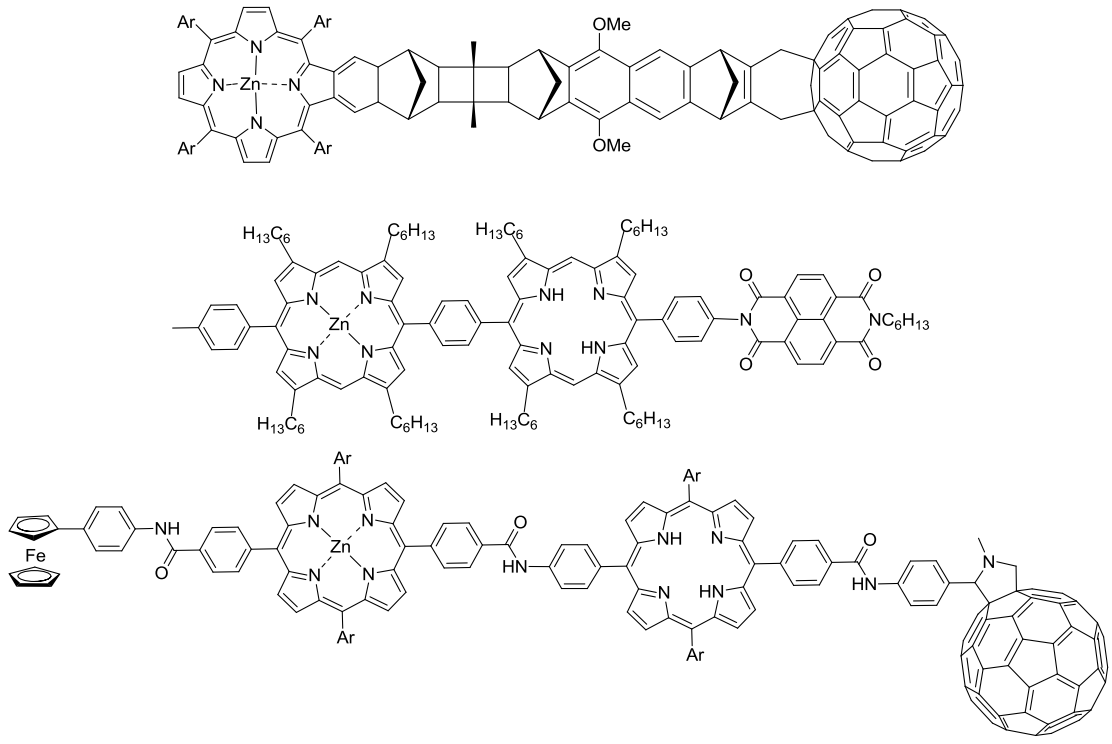

Figure 18. Examples of porphyrin containing diad, triad and tetrads[106,109,111]

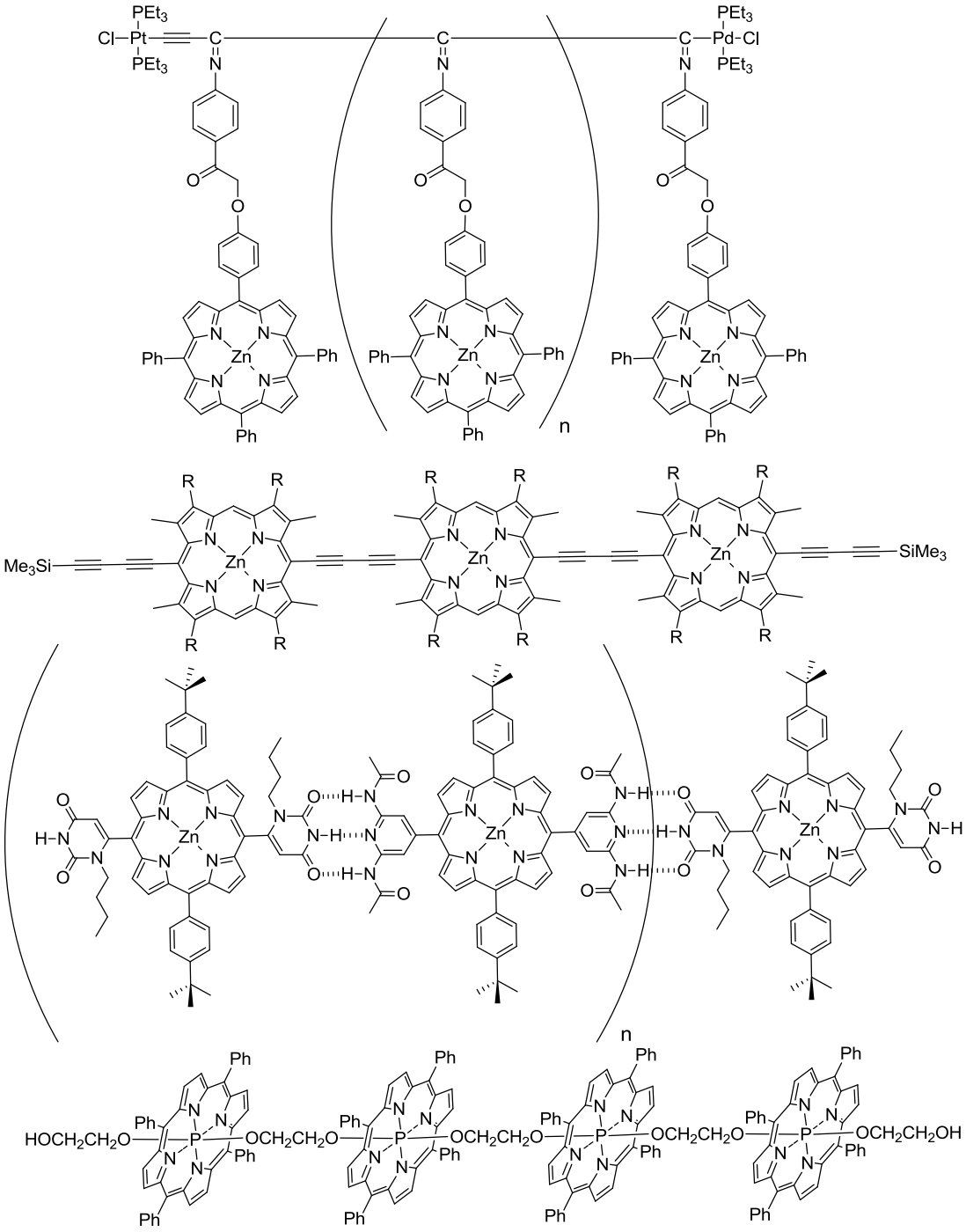

Figure 19. Examples of porphyrin wires[94-96,101]

Porphyrins may also be arranged on a surface,[112] within a matrix[101,102] or incorporated into a supermolecule,[113] such that they form molecular wires that are able to transfer a charge across the array (Figure 19). These arrays may exist as: conjugated, linear supermolecules as per those synthesised by Anderson *et al.*;[114] as a stack of porphyrins bound to a backbone, which interact and hold their structural conformation *via* electrostatic interactions, as per the example synthesised by Majima *et al.*;[94] as a self assembled structure spanning a lipid bilayer, as

demonstrated by Drain;[101] or as a face-to-face stack interconnected by ethyleneglycol or short polythiophene molecules, as synthesised by Segawa *et al.*[95] Although these arrays are very different in structure, the porphyrin moieties within them demonstrate the potential characteristics of a well designed supermolecule, notably; rapid exciton migration,[94,114] high conductance across the system,[113] the transfer of charge over long distances,[115] self assembly[101] and ohmic current-potential (I-V) traces.[95]

1.7 – Porphyrin modified nucleosides, nucleotides and oligomers

A great number of examples of porphyrin modified nucleosides,[116,117] nucleotides[20,21,52,118] and oligomers,[118-121] as well as porphyrins appended with multiple nucleosides,[122,123] exist in the literature (Figure 20). Porphyrin modified uridine and 2'deoxy-uridine have been reported,[117] along with a porphyrin modified guanosine, which has been shown to hydrogen bond with a quinone modified cytidine in solution forming a redox couple.[116] Dinucleosides,[124] dinucleotides[120] and tetranucleotides[119] each containing two porphyrin modified bases have been synthesised, this has lead to the development of modified oligonucleotides synthesised through automated DNA synthesis. An early publication of a porphyrin modified DNA in 1990 reported that the porphyrin was attached to the olignucleotide post-DNA synthesis.[125] Attachment *via* this method meant that the modification was limited in its location to the 5' end of the oligonucleotide strand. Synthesis of modified DNA may now be achieved through automated DNA synthesis with a variety of different porphyrin modifications possible, including; terminal modification at the 5' end,[126] backbone replacement[127] and base modification.[107]

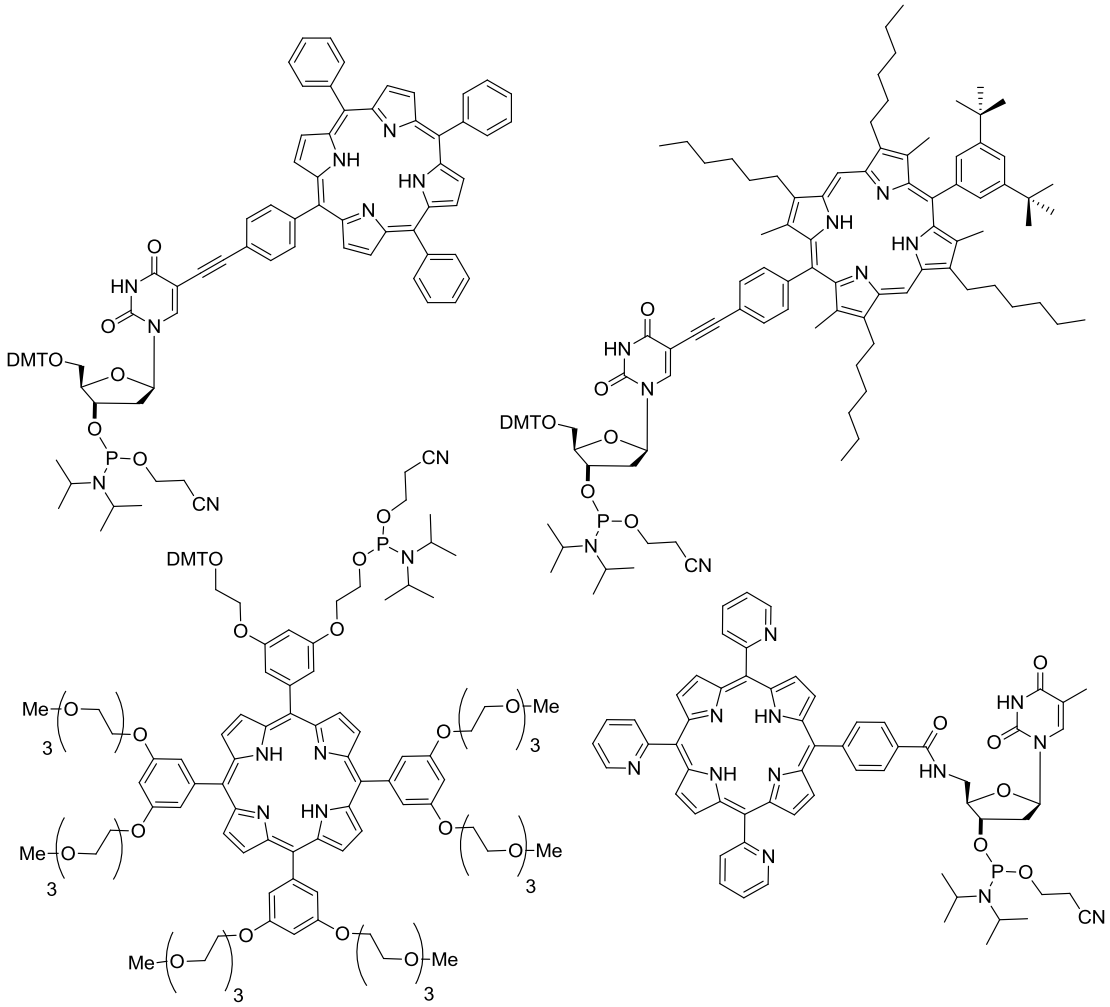

Figure 20. Porphyrin modified nucleosides that have been incorporated into DNA[20,52,126,127]

Broadly speaking three different porphyrin modified nucleobases have been incorporated into DNA; tetraphenyl porphyrins,[20,118,127] diphenyl porphyrins[21,107] and 5,10,15-tripyridyl-20-phenyl porphyrins.[125,126] Where only a single porphyrin modification is present, the spectroscopic behaviour of all the porphyrin modified oligonucleotides is similar, with a single broad absorbance around 420 nm corresponding to the Soret band. However, when additional modifications are added to the oligonucleotides the difference between the tetraphenyl- and diphenyl- porphyrins is pronounced; the absorbance spectra of the diphenyl porphyrin examples show a large broadening of the Soret band, indicative of strong excitonic coupling between the porphyrin moieties.[21,52] No examples of oligonucleotides modified with multiple 5,10,15-tripyridyl-20-phenyl porphyrins exist for comparison. The diphenyl porphyrin used in the aforementioned example has a much greater destabilising effect on the duplex than a tetraphenyl porphyrin,[20,52] this is more than likely due to the pendant hexyl chains attached to the β positions which are required to aid solubility of monomer.

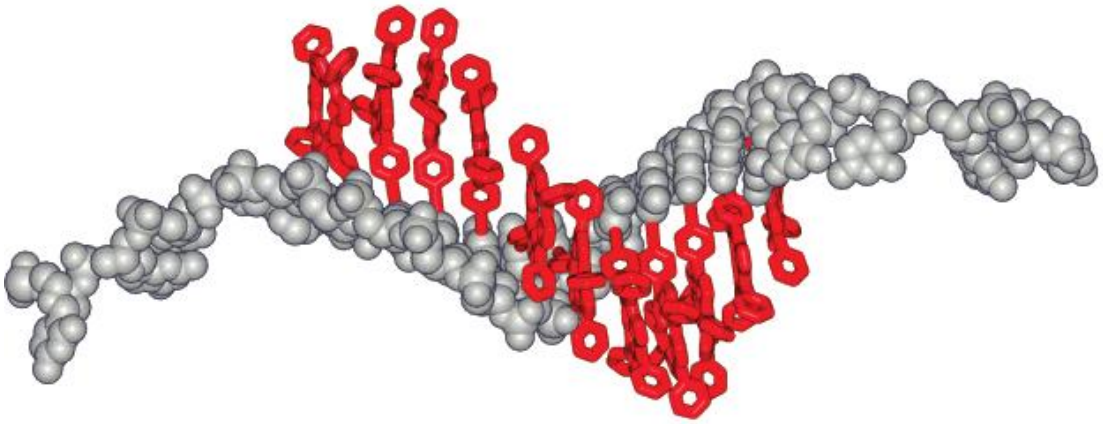

Figure 21. Molecular modelling of a single stranded porphyrin modified oligonucleotide[20]

Oligonucleotides which contain an ever greater number of porphyrin modifications are being reported, the most heavily modified example contains 11 porphyrin modifications on a single strand[20] (Figure 21). It has been shown, but not fully investigated, that the arrangement of the modifications along the oligonucleotide length has a dramatic effect on the stability of the resulting duplex; if all modifications are appended to one stand then the melting temperature of the duplex (T_m) is drastically lowered (ΔT_m = -3 – -21 °C per porphyrin modification[20,52]) depending on the type of porphyrin modification and the number of modified bases included within the sequence. However, if the modifications are arranged in an alternating manner between the strands of the duplex, such that the porphyrins fit together in the major groove in a zipper fashion, then the stability of the duplex should increase provided sufficient number of porphyrin modified bases (>8 modifications) are included within the sequence,[21,118] further research in this area is required to fully understand the origin and extent of these effects.

2 – Objectives

A number of clear objectives were planned for this project from the outset, with several more avenues of research being explored and developed as the project progressed. Firstly, the synthesis of a novel porphyrin modified nucleoside was to be developed, this monomer was to contain a certain degree of structural flexibility across the linking moiety. This flexibility was intended to facilitate the formation of the thermodynamically favoured conformers when incorporated into oligonucleotides.

A number of the novel flexible linked monomers were to be included into an oligonucleotide in a zipper arrangement. The same sequence containing a previously developed rigid linked porphyrin nucleotide and the corresponding unmodified sequence were also to be synthesised for comparison of the photospectrometric properties of the systems. The use of a zipper type system was planned to further the understanding of this arrangement of porphyrin modified DNA.

Probing of the electron transfer properties of an array of porphyrins bound to the DNA scaffold was planned, with the intention of assessing the potential of the porphyrin moieties to be used as a supramolecular wire.

Homo- and hetero-porphyrin single walled carbon nanotube adducts were to be prepared using neutral, tetra-anionic and tetra-cationic porphyrins. These properties of these systems were to be probed to ascertain if the hetero-porphyrin nanotube adducts had differing properties to the homo-porphyrin nanotube systems. Determining the loading of porphyrins on the surface of the nanotubes was to be achieved through desorption of the porphyrins.

Phenomena that may be observed while achieving the objectives listed above were to be duly noted and explored, if resources allowed.

3 – Results and Discussion – Porphyrin DNA

3.1 – Porphyrin synthesis

Porphyrin synthesis has been studied extensively since the first reported synthesis by Fischer and Zeile in 1929;[128] Fischer synthesised dozens of porphyrins (including haem) by cyclising substituted dipyrromethenes in succinic acid melts, with yields of 30 – 50 %. α-substituted dipyrromethenes are synthesised by a condensation reaction between an α-bromo-α'-formylpyrrole and an α-methylpyrrole (β substituents vary depending on the desired porphyrin product), condensation of the dipyrromethene with its corresponding HBr salt forms the porphyrin product (Scheme 1).

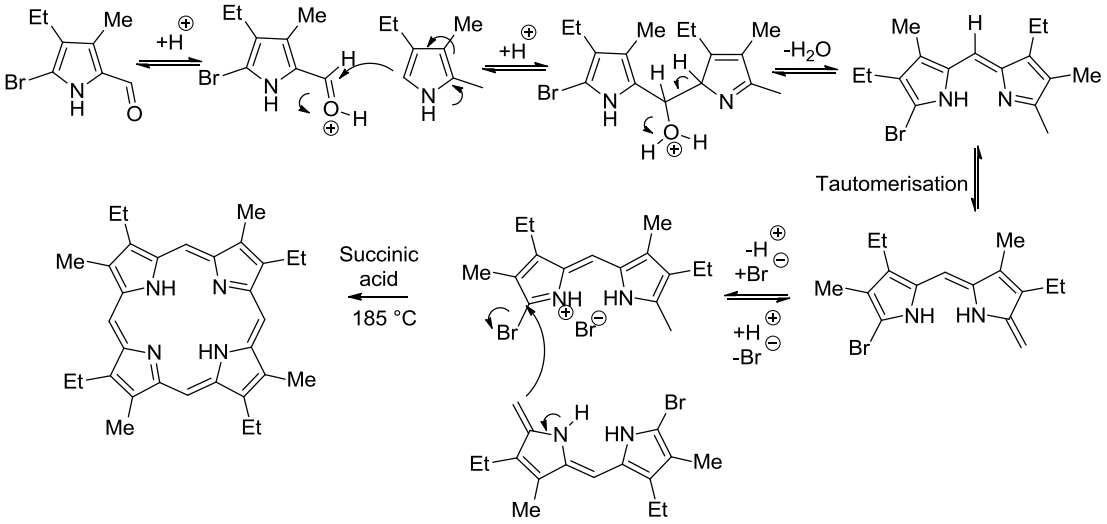

Scheme 1. Synthesis of etioporphyrin *via* the Fischer porphyrin synthesis

Rothemund further developed porphyrin synthesis in the 1930s[129,130] by demonstrating a one pot synthesis with an unstated yield; pyrrole and an aldehyde were dissolved in methanol in a sealed tube before heating to 90 °C, the condensation of the pyrroles with the various aldehydes used allowed for symmetrical substitution at the porphyrin *meso* positions.

Adler and Longo published an improved one pot synthesis[9] of tetra-phenyl porphyrin from pyrrole and benzaldehyde using refluxing propionic acid as the reaction solvent. The use of a Brønsted-Lowry acid in the synthesis activates the aldehyde allowing for a much more facile reaction with the pyrrole nucleophile. Oxidation of the porphyrinogen to the porphyrin occurs due to the reaction vessel being open to air. Using this method Adler and Longo recovered TPP in a 20 % yield.

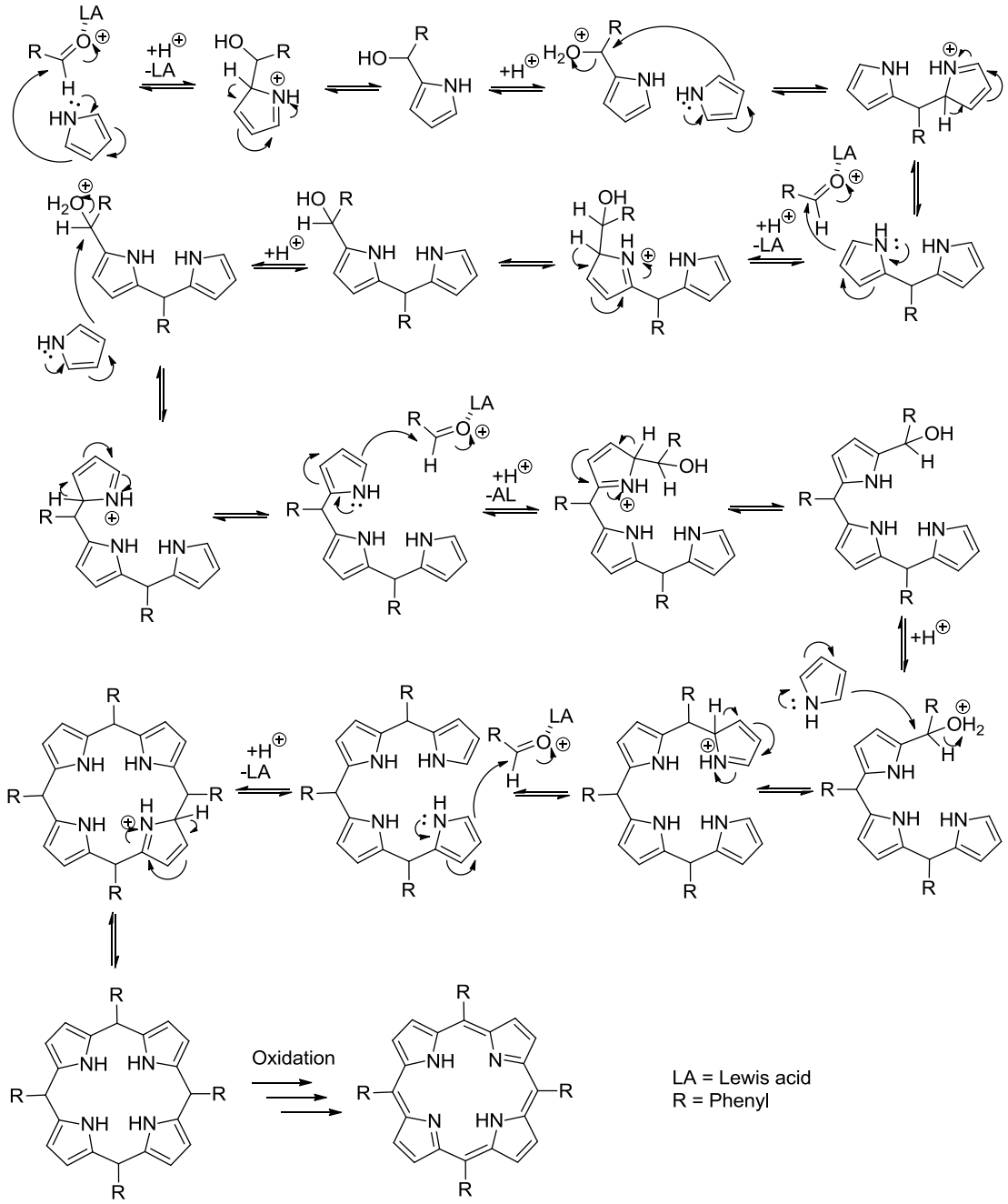

Scheme 2. One pot porphyrin synthesis mechanism

The Adler and Longo synthesis is limited in its application for two reasons, firstly; boiling the reagents in propionic acid (boiling point 141 °C) places limitations on the side groups that may be present on the reagents, secondly; oxidation of the porphyrinogen by molecular oxygen is not the most efficient or reliable method. As such Lindsey *et al.*[131] introduced the use of a Lewis acid, boron trifluoride etherate, or trifluoroacetic acid, in an apolar solvent at room temperature (Scheme 2). The oxidation of the porphyrinogen to the porphyrin was accomplished by the use of a benzoquinone (Scheme 3), either 2,3,5,6-

tetrachlorobenzoquinone (*p*-chloranil) or 2,3-dichloro-5,6-dicyanobenzoquinone (DDQ). This method of synthesising tetra-phenyl porphyrin gave yields of up to 55 %.

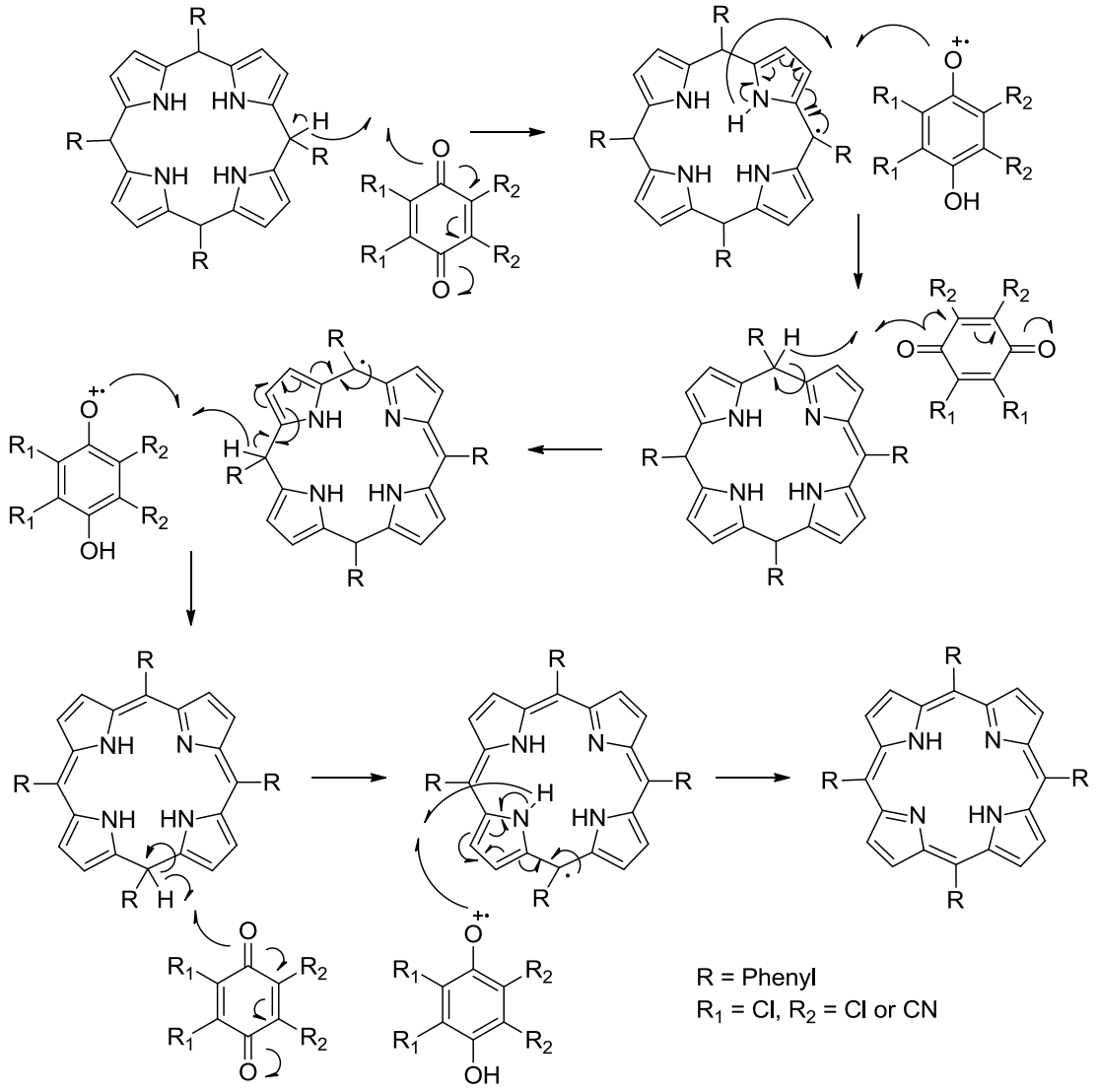

Scheme 3. Mechanism for quinone oxidation of a porphyrinogen

The Lindsey one pot method of porphyrin synthesis is ideal for symmetrical porphyrins, however, asymmetrical porphyrins synthesised *via* this method will be synthesised as a statistical mixture of products. One way to favour the synthesis of a monosubstituted porphyrin is to alter the pyrrole to aldehyde to substituted aldehyde ratios. Previous work by Stulz *et al.*[118] has shown that a 6:6:1 ratio of the components produces primarily the symmetrical porphyrin but with a large proportion of the monosubstituted porphyrin also present. The synthesis of higher substituted porphyrins is negligible by this method.

For substituted porphyrins it was again Lindsey *et al.*[132,133] who provided an elegant solution; a stepwise synthesis of a bilane, a tetramer oligopyrrole. The stepwise synthesis

followed by cyclisation and oxidation gives the product porphyrin with precise control over the position of the substituents in 8 high yielding steps (Scheme 4).

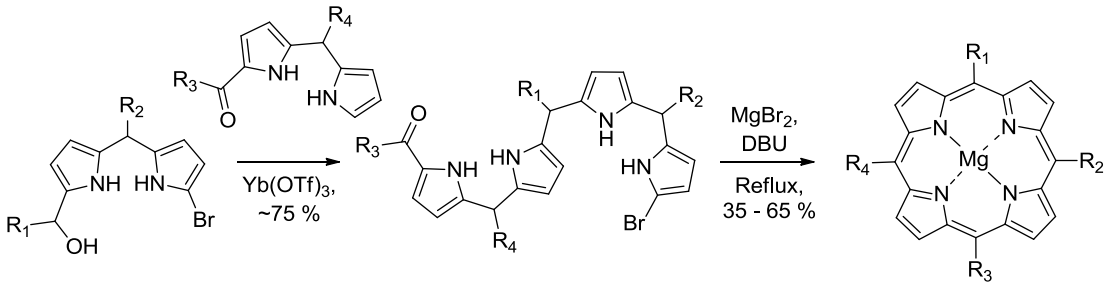

Scheme 4. Example porphyrin synthesis *via* a bilane[133]

A novel flexible linked porphyrin modified nucleoside was to be synthesised and incorporated into duplex DNA. The photophysical properties of the resulting system were to be probed and compared to an analogous sequence containing a previously published rigid linked porphyrin monomer.[20] The potential electron transfer properties of an oligonucleotide containing multiple porphyrin modified nucelobases was to be assessed to ascertain whether porphyrin arrays on DNA scaffolds are viable molecular wires.

3.2 – Synthesis route to acetylene linked porphyrin monomer[20]

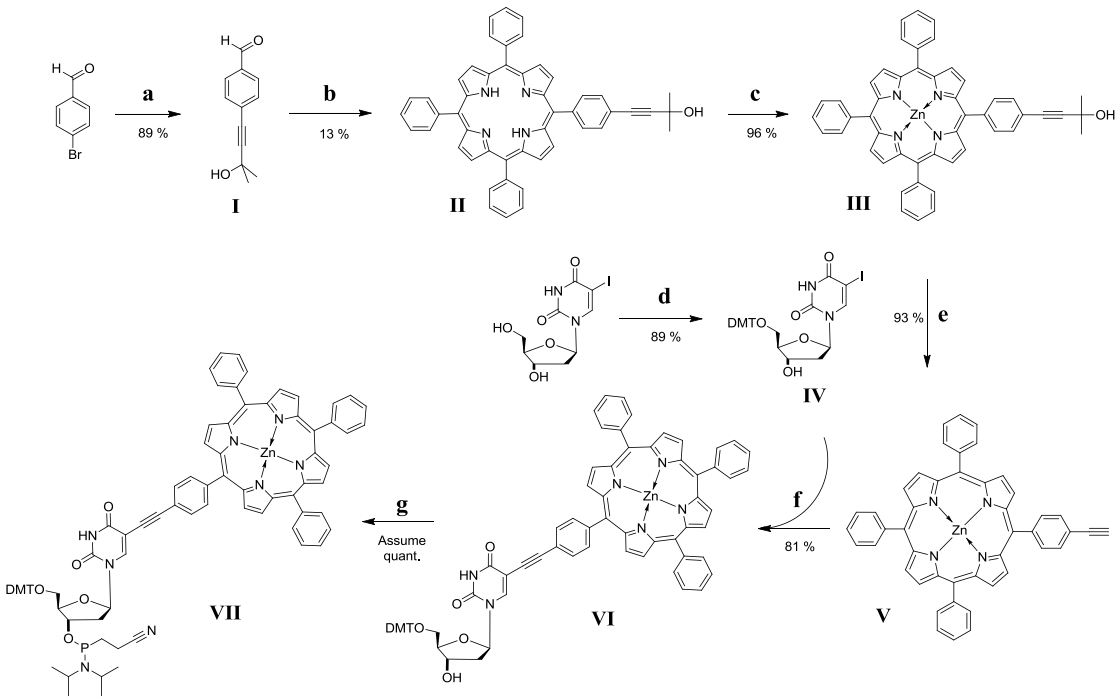

a - 2-hydroxy-2-methyl-but-3-yne, Pd on carbon, CuI, PPh_3, K_2CO_3, 1:1 DME:H_2O 89 % **b** - i) pyrrole, benzaldehyde, $BF_3.Et_2O$, $CHCl_3$ ii) DDQ 13 % **c** - $Zn(OAc)_2.2H_2O$, 8:1 DCM:MeOH, 96 % **d** - 4-4'-dimethoxytrityl chloride, pyridine, 89 % **e** - NaOMe, toluene, reflux, 93 % **f** - 5'-DMT-5-iodo-dU, $Pd(PPh_3)_4$, CuI, TEA, DMF, 81 % **g** - CEP-Cl, DIPEA, DCM, assumed quantitative

Scheme 5. Synthesis route for acetylene linked porphyrin monomer

Synthesis of a rigid linked porphyrin modified nucleoside for use as a control was achieved through adapting the literature procedure.[20] *para*-Bromobenzaldehyde was coupled to 2-hydroxy-2-methyl-but-3-yne *via* a palladium cross coupling reaction (Scheme 5). In this instance the coupling reaction is the Sonogashira coupling, to give the substituted aromatic aldehyde **I** in good yield. Compound **I** was then reacted with pyrrole and benzaldehyde, using boron trifluoride etherate as the catalytic Lewis acid required to promote the condensation of these three molecules. The condensation reactions occur in a statistical manner, forming linear polypyrroles of various lengths, a proportion of which cyclise to form a calyxpyrrole species, the so called porphyrinogens. The only control over which porphyrinogens are formed by this reaction is through the ratios of the substituted aromatic aldehyde, the benzaldehyde and the pyrrole, statistically a ratio of 1:3:4 is required. Previous work, however, has shown that this ratio produces a large proportion of the di- and tri-substituted porphyrinogen, as opposed to the mono-substituted. A greater yield of the mono-substituted porphyinogen may be achieved by using a ratio of 1:6:6 of the substituted aromatic aldehyde to benzaldehyde to pyrrole. This does of course lead to a larger proportion of the unsubstituted tetraphenyl porphyrinogen being

formed, however with both pyrrole and benzaldehyde being commercially available this is an acceptable loss.

All of the condensation reaction occurring are of a reversible nature and as such the mixture of products is continuously changing, when left for too long the reaction tends to form increasing quantities of long chain insoluble polypyrroles. Allowing these reversible reactions to proceed for approximately an hour gives the best recovery of the desired products and at this point the oxidising agent, 2,3-dichloro-5,6-dicyanobenzoquinone (DDQ) is added. This leads the reaction down an irreversible pathway to form a mixure of porphyrins, one of which is the desired product, **II**, and purification of the crude reaction mixture by a series of chromatography columns gives the desired product in 13 % yield.

Zinc metallation of **II** by zinc (II) acetate dihydrate is both facile and high yielding, the purpose of which is to protect the pyrrolic N-H during subsequent reactions. If left unprotected lower yields are obtained when coupling the porphyrin moiety to the nucleobase in a subsequent step. Metallation of the porphyrin appears to be quantitative with the only loss of yield being through purification, which is achieved by simply dissolving the porphyrin in DCM and filtering off the excess zinc acetate dihydrate.

Cleavage of the acetylene's protecting group in **III** is achieved with sodium methoxide in refluxing toluene, the reaction proceeds *via* deprotonation of the alcohol by methoxide and subsequent elimination of acetone to yield the sodium acetylide porphyrin and acetone. Subsequent aqueous workup turns the hemiacetal into acetone and methanol, which may be removed *in vacuo*, and protonates the porphyrin acetylide to give compound **IV** with no need for further purification.

5'-(4'',4'''-dimethoxytrityl)-2'-deoxy-5-iodouridine (**IV**, 5'-DMT-5-iodo-dU) is prepared by a standard S_N1 reaction between the primary 5' hydroxyl of 2'-deoxy-5-iodouridine and 4,4'-dimethoxytrityl chloride (DMT-Cl) in pyridine. The DMT-Cl is added portionwise to the reaction to keep its concentration low such that the slightly more reactive primary hydroxyl of the 5' position will react with it quicker than the less reactive secondary hydroxyl of the 3' position. Addition of the DMT-Cl too quickly often leads to double substitution on the 2'-deoxyribose ring, with both the 3' and 5' hydroxyls being protected. Purification of **IV** is achieved by column chromatography on silica which has been exposed to TEA, failure to basify the terminal siloxy groups leads to cleavage of a some of the DMT protecting groups.

A Sonogashira coupling between 5'-DMT-5-iodo-dU (**IV**) and zinc (II) 5,10,15-triphenyl-20-*p*-ethynylphenyl porphyrin (**V**) gives the acetylene linked porphyrin nucleoside (**VI**) in a reasonable yield of 81 % (Scheme 5). Careful purification by column chromatography on neutralised silica with a reasonably non polar eluent is required due to the similar R_f values of the product and the 5'-DMT-5-iodo-dU staring material (R_f values of 0.48 and 0.45 respectively in 10:1 DCM:MeOH). Often repeated column chromatography is required in order

to recover an acceptable yield of the product; the yield of the reaction is slightly higher than that stated, however it often becomes an uneconomic use of one's time to continue purification for diminishing returns.

Synthesis of the acetylene linked porphyrin phosphoramidite **VII** is only conducted when required due to its instability. The phosphorus (III) centre is required for DNA synthesis, during which it is oxidised to the more thermodynamically stable phosphorus (V) species. Oxidation of the phosphorus can occur in atmospheric conditions with molecular oxygen, the attached porphyrin moiety will speed the oxidation process due to them being excellent converters of molecular triplet oxygen to the more reactive singlet oxygen[134]. The phosphorylation of **VI** is reasonably facile and the reaction typically reaches completion in 2-3 hours; purification of the phosphoramidite, **VII**, may be undertaken by column chromatography under an inert gas with a degassed aprotic eluent, however, this is often not required. Typical purification of the crude product entails removal of the excess CEP-Cl and DIPEA by sequential washes with degassed hexanes. The remaining crude product contains the desired porphyrin nucleotide phosphoramidite, **VII**, and any unreacted porphyrin nucleoside, **VI**, which will not react during DNA synthesis and will simply be washed away once the phosphoramidite has coupled. Due to its sensitivity, characterisation of the porphyrin amidite **VII** is limited to NMR, mass spectrometry and TLC, and the crude product was used immediately in DNA synthesis.

3.3 – Synthesis route to amide linked porphyrin monomer

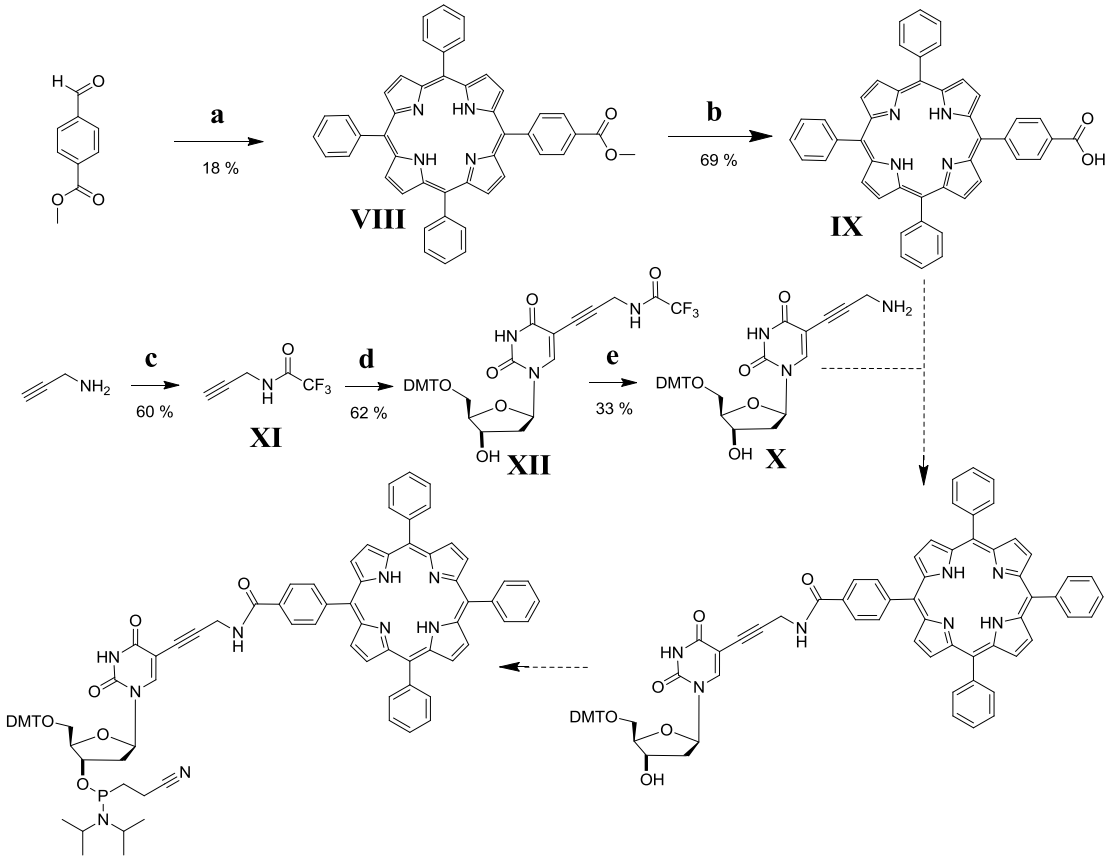

a - i) pyrrole, benzaldehyde, $BF_3.Et_2O$, $CHCl_3$ ii) DDQ 13 % **b** - KOH, pyridine, H_2O, 40 °C, 69 % **c** - ethyl trifluoroacetate, TEA, MeOH, 60 % **d** - **IV**, $Pd(PPh_3)_4$, CuI, TEA, DMF, 62 % **e** - $MeNH_2$, MeOH, H_2O, 33 %

Scheme 6. Synthesis route for amide linked porphyrin monomer

In designing the flexible linker between the nucleobase and the porphyrin, it was decided that a certain degree of ridigity should remain to provide pre-organisation, with the flexibility of the linker being provided by rotation about a small number of bond, as such a propargylamide linker was chosen.

Methyl-4-formylbenzoate was reacted with benzaldehyde and pyrrole in a 1:6:6 ratio as per the synthesis of the acetylene linked porphyrin monomer. The yield of the tetraphenyl methyl ester porphyrin, **VIII**, is consistently higher than that of the protected acetylene porphyrin, typically giving yields of 18 % (Scheme 6). This is due to the –I and –M effects of the methyl ester in the *para* position of the phenyl ring making the aldehyde more electrophillic and hence more reactive to nucleophillic attack by pyrrole. Hydrolysis of the methyl ester, to give **IX**, is achieved with potassium hydroxide in pyridine and water. At room temperature the reaction takes 36 hours to reach completion, however this can be reduced to 18-20 hours by heating to 40 °C. Careful neutralisation is required during the workup since the deprotonated

porphyrin acid is partially water soluble, as is the protonated porphyrin. It is immediately obvious if too much acid has been added to the workup since the protonated porphyrin is bright green compared to the deep purple of the neutral species, this colour change occurs due to a buckling of the porphyin macrocycle which allows the four phenyl rings at the *meso* positions to rotate into the same planarity as the ring, thus greatly extending the molecules conjugation and hence leading to a colour change.

5'-DMT-5-iodo-dU (**IV**) is prepared as has previously been discussed. Initial test Sonogashira couplings to synthesise 5'-DMT-5-propargylamino-dU, **X,** were unsuccessful and it was thought that it was due to the free amine group disrupting the reaction, as such trifluoroacetic propargylamide (**XI**) was prepared. The synthesis of which was achieved by reacting propargylamine with ethyl trifluoroacetate, this reacted in only a moderate yield of 60 %. Coupling of trifluoroacetic propargylamide (**XI**) to 5'-DMT-5-iodo-dU (**IV**), again *via* a Sonogashira coupling[37], gave **XII** in 62 % yield. Here problems arose, cleavage of the trifluoroacetamide of **XII** to liberate the free amine of **X** was not straightforward, a transamination was required for which methanolic ammonia was unsuccessful; methylamine in methanol and water was successful but poor, giving a yield of only 33 %. Further attempts at synthesising **X** directly from 5'-DMT-5-iodo-dU and propargylamine using fresh catalysts were successful, giving the desired product in 73 % yield. As such the synthesis route was revised (Scheme 7).

Several protocols were tested to find an efficient method of coupling **X** and **IX** to make **XIII**; the first method was to form the acid chloride *in situ* from oxalyl chloride, which was then added dropwise to a solution of 5'-DMT-5-propargylamino-dU (**X**), this gave **XIII** in 30% yield. The acid chloride was then synthesised in situ from cyanuric chloride[135], problems arose with various cyanuryl esters forming which were not then converted to the acid chloride. Despite this the reaction of the acid chloride of **IX** with 5'-DMT-5-propargylamino-dU (**X**) proceeded well, giving an overall yield of 51 %. Daniel Singleton of Dr Stulz's research group (University of Southampton) attempted to form **XIII** using PyBrOP, which produced significant quantities of the porphyrin pyrrolidide; EDC which produced significant quantities of the *N*-acylurea side product; and finally using EDC and HOBt which gave the best yields overall. As such **IX** and **X** were coupled using EDC and HOBt, which TLC showed produced several porphyrinic compounds, presumably including the *O*-acyl-*iso*-urea and the *N*-acylurea. Despite several side products **XIII** was synthesised in 80 % yield.

As per the acetylene porphyrin nucleotide phosphoramidite, the amide linked porphyrin nucleotide phosphoramidite, **XIV**, was only synthesised as required. Synthesis and purification techniques were identical to that of the acetylene porphyrin nucleotide phosphoramidite. Due to the sensitivity of the product, characterisation data is limited as the crude product **XIV** was used immediately for DNA synthesis.

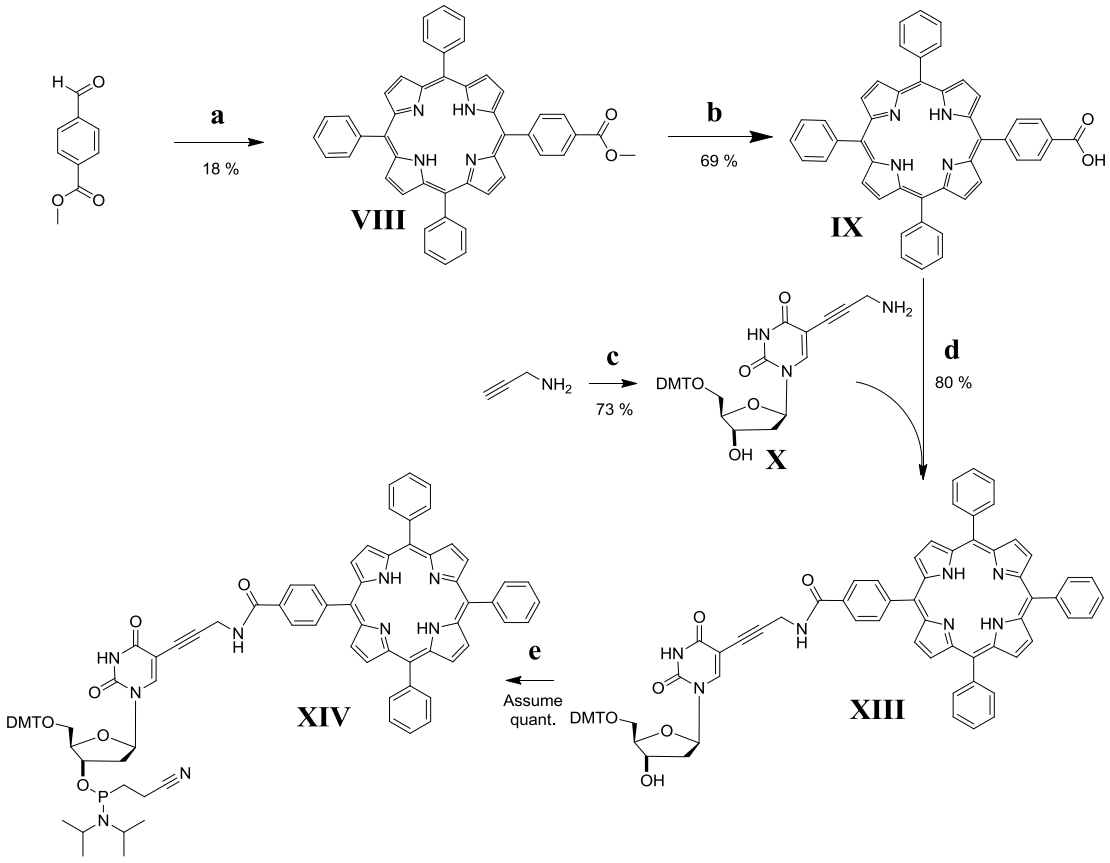

a - i) pyrrole, benzaldehyde, $BF_3.Et_2O$, $CHCl_3$ ii) DDQ 13 % **b** - KOH, pyridine, H_2O, 40 °C, 69 % **c** - **IV**, $Pd(PPh_3)_4$, CuI, TEA, DMF, 73 % **d** - EDC, HOBt, DMAP, DCM, 80 % **e** - CEP-Cl, DIPEA, Assume quantitative

Scheme 7. Final synthesis route for amide linked porphyrin monomer

3.4 – Solid phase DNA synthesis

The most convenient method of synthesising DNA is using solid supported synthesis. A glass bead with known pore sizes (controlled pore glass or CPG), typically 500 Å for small oligomers (<30 bases), is loaded with either the first base of the sequence or with a functional group that allows facile coupling of monomers and cleavage of the product, but is also stable to DNA synthesis conditions (Figure 22).

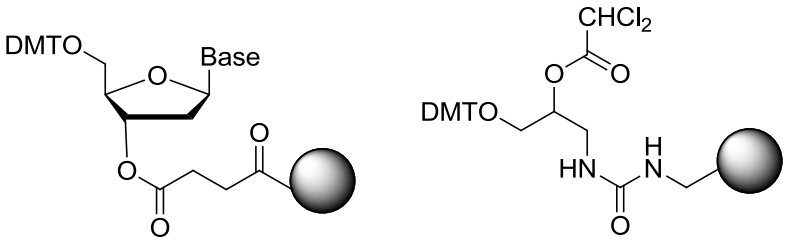

Figure 22. Example nucleoside CPG and universal support CPG

For solid supported DNA synthesis all reagents required are controlled by the DNA synthesizer, the reagents and the CPG columns are kept under an inert atmosphere to avoid oxidation of the phosphoramidite moieties. The required sequences along with reagent volumes, flow rates and reaction times are programmed into the DNA synthesiser which controls the course of the synthesis from that point. The cycle of DNA synthesis comprises four main steps with an acetonitrile wash between them to remove any excess reagents or cleaved small molecules from the CPG column. The four main steps of the synthesis are:

Detritylation – 3 % trichloroacetic acid in DCM is flushed through the CPG column (Scheme 8), cleaving all 5'-DMT protecting groups. This cleavage liberates a vividly orange 4,4'-dimethoxytrityl cation which an inbuilt absorption spectrometer monitors to provide a qualitative measure of the synthesis' success. Observation of this reading allows the user to see if one particular monomer is coupling poorly and adjust the coupling conditions accordingly.

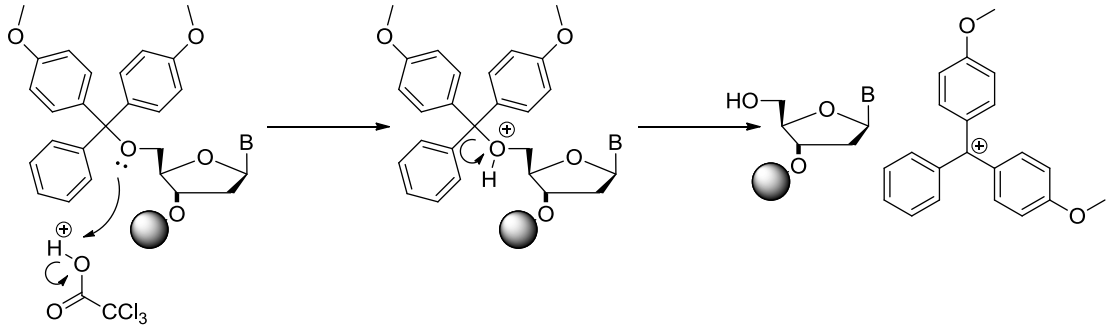

Scheme 8. TCA deprotection mechanism

Activation and coupling – The di-*iso*-propylamino group of the 3'-phosphoramidite is activated through protonation of the tertiary amine by tetrazole followed by substitution of the amine with the tetrazolium anion, this creates a leaving group that may be displaced through nucleophillic attack by the free 5'-hydroxyl of the growing oligonucleotide chain (Scheme 9). An excess of between 2 and 12 equivalents of the activated 3'-phosphoramidite is used to ensure efficient coupling of the free 5'-hydroxyls.

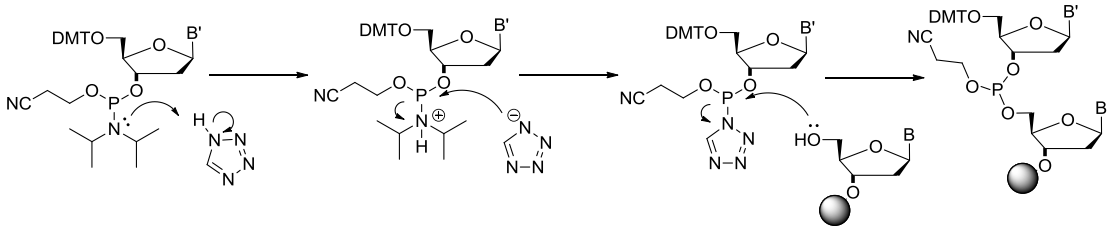

Scheme 9. Activation and coupling mechanism[136]

Capping – Coupling of standard phosphoramidites is usually very efficient with typically around 99 % of the 5'-hydroxyls coupling. The small percentage of uncoupled hydroxyls must be capped (Scheme 10) to ensure they do not react with the next monomer to be introduced, as this would lead to an *n-1* sequence i.e. one base missing in the strand. Capping is achieved with a mixture of *N*-methylimidazole (NMI), acetic anhydride and pyridine; the NMI forms the activated *N*-acetyl-*N'*-methylimidazonium species with the acetic anhydride, efficient acetylation with the 5'-hydroxyl then occurs.[137]

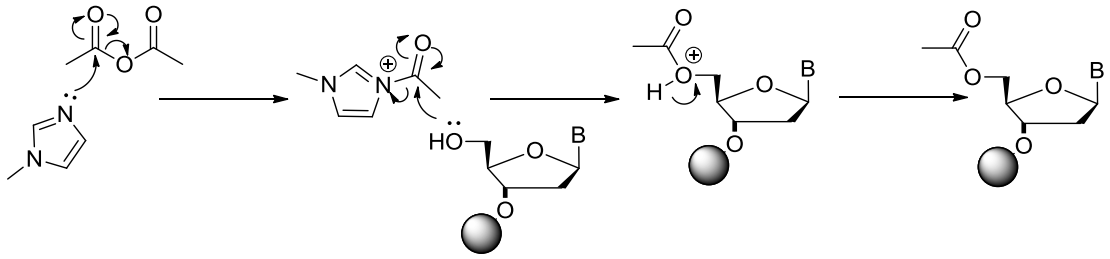

Scheme 10. Capping mechanism

Oxidation – The phosphorous (III) triester is not acid stable and as such must be oxidised to the phosphorous (V) species with iodine, pyridine and water (Scheme 11) prior to continuing the oligonucleotide synthesis. A phosphorus iodine bond is first formed before the iodine is displaced as iodide by water, subsequent deprotonation with pyridine leads to the new phosphorus oxygen double bond and the phosphorus (V) species.

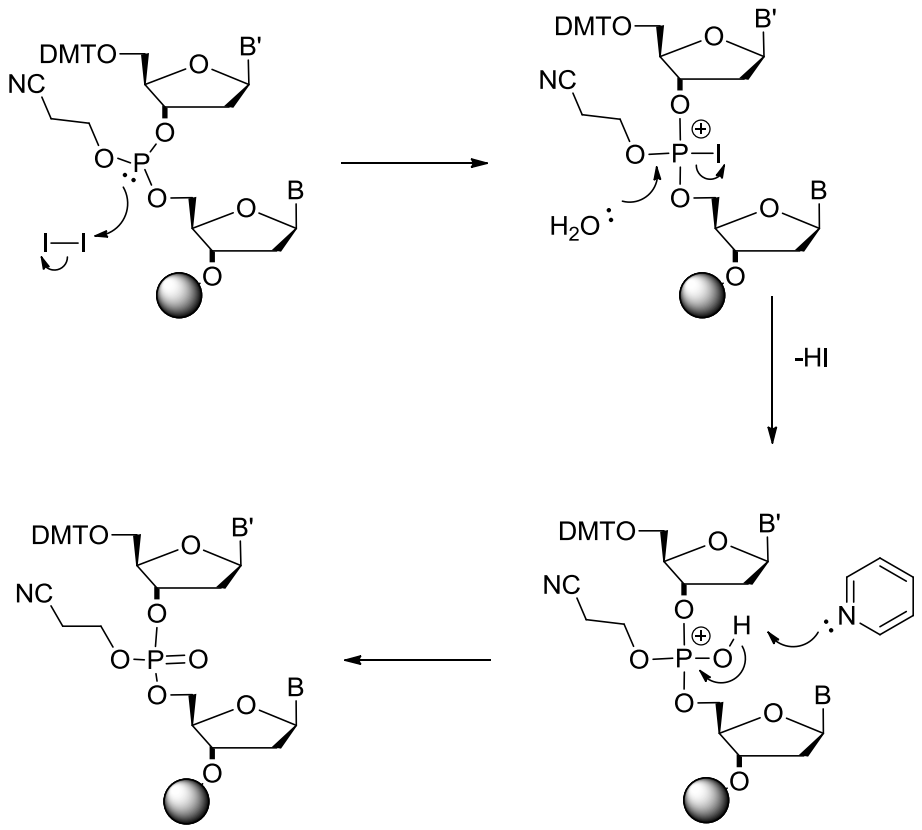

Scheme 11. Oxidation mechanism

These four steps cycle with each new monomer added to the growing oligonucleotide chain as shown in Scheme 12. After the addition of the final monomer in the sequence the synthesis usually stops after the phosphorus oxidation, leaving the 5'-hydroxyl of the final

monomer protected with the DMT protecting group. This protecting group is used to aid purification of the product oligonucleotide.

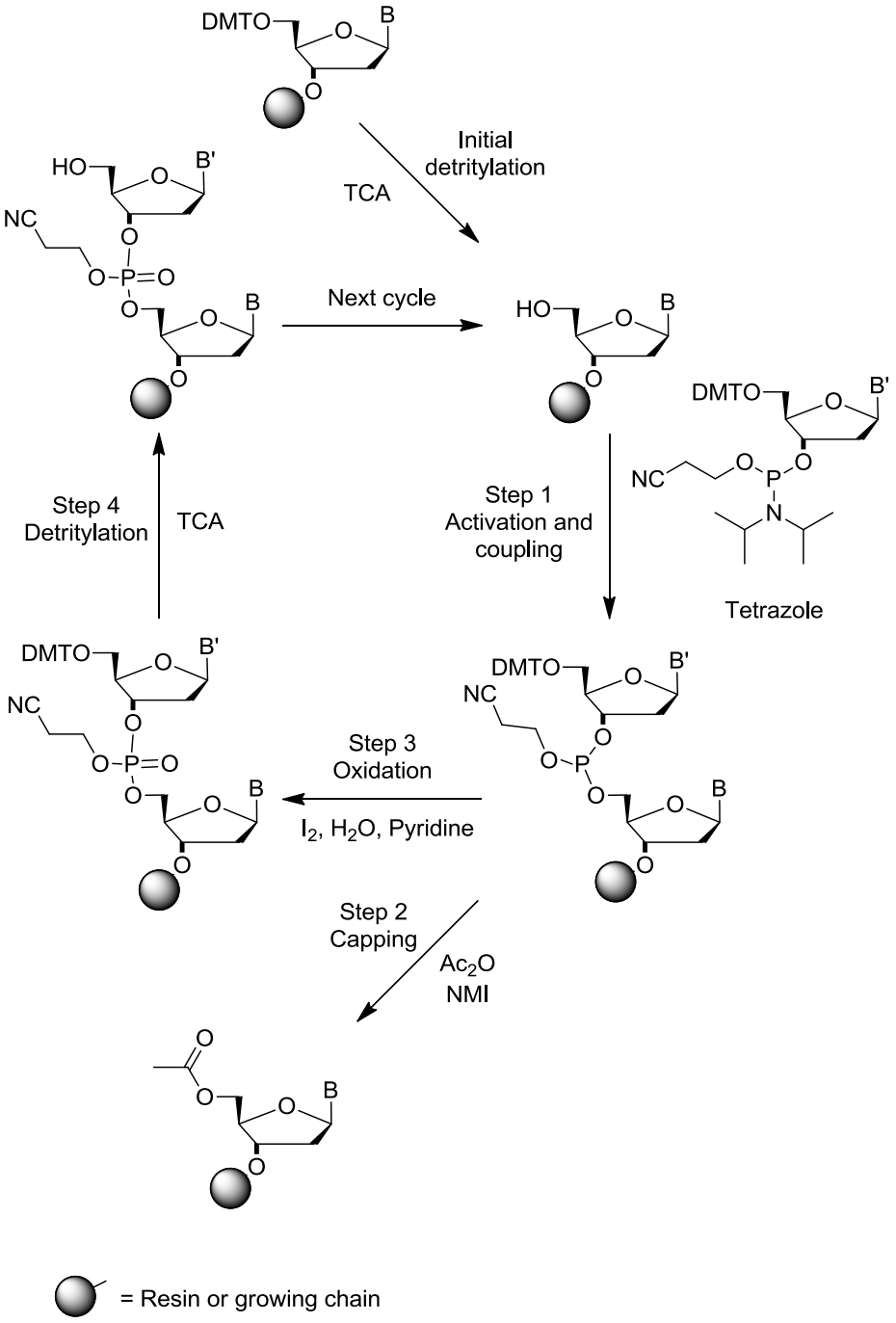

Scheme 12. Overview of solid supported DNA synthesis

3.5 – Purification of DNA

The purification of DNA can be achieved by a few different methods; high pressure liquid chromatography (HPLC) on C-18 modified reverse phase silica is most commonly used. This technique relies on the varying retention times of the different components in the product mixture for separation of the desired product from the failure sequences; through trial and error and after making suitable adjustments to the eluent parameters, baseline separation of the product is often achieved. Once general methods have been established they are often suitable for separating a wide range of oligonucleotides.

Gel electrophoresis of DNA uses a polymer, typically polyacrylamide but sometimes agarose, as a stationary phase through which the oligonucleotides are drawn by applying a potential across the gel. The larger oligonucleotides are retarded more by the polymer and as such travel less distance through the gel. The product DNA can then be recovered from the gel through band excision and elution of the gel portion.

The efficacy of both of the above methods is lowered when the product and/or the contaminants streak through the stationary phase. In the HPLC absorbance trace and in the developed electrophoresis gel this is observed as peak or band broadening, which eventually leads to failure to achieve baseline separation of the components. In these cases the options available are; repeated HPLC or electrophoresis to sequentially remove more and more impurities; a changed of stationary phase and/or eluent, or; affinity chromatography.

Two types of affinity column are commonly used to separate oligonucleotides, the first of which is the PolyPak or GlenPak column, these work by having a stationary phase which has a high affinity for the aromatic DMT protecting group. The crude reaction mixture is loaded onto the column and all components that do not contain the DMT protecting group, i.e. all capped failure sequences and small molecules, are washed off of the column. The desired oligonucleotide that is adsorbed to the column is cleaved from its DMT protecting group by passing 2 % TFA in water through the column, at which point the column in neutralised and the product eluted from it. Purification of standard DNA by this method is quick, inexpensive and efficient, however, the technique relies on the affinity of the stationary phase for the large aromatic DMT protecting group. This affinity is not specific for the DMT unit, the stationary phase has an affinity for any large aromatic group including; MMT, FAM, Cy5 and porphyrins.

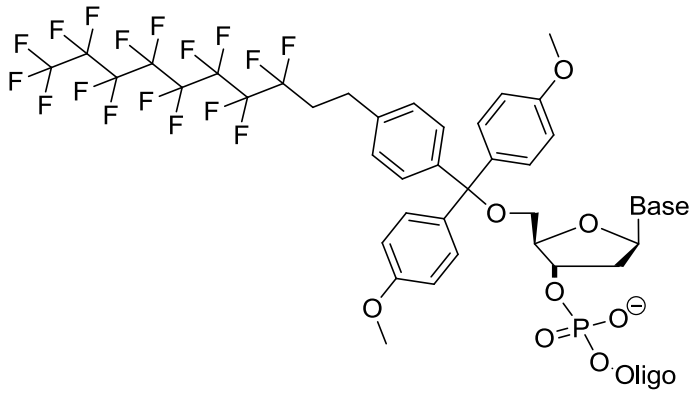

Figure 23. FDMT protected oligonucleotide

The second type of affinity column, FluoroPak type columns, require the last base of the desired sequence to contain a fluorous tag, commonly used are 4-(1*H*,1*H*,2*H*,2*H*-perfluorodecane)-4',4''-dimethoxytrityl (FDMT) tagged monomers (Figure 23). All natural bases are commercially available with an FDMT protected 5'-hydroxyl. The principal of FluoroPak columns is the same as those of GlenPak columns, the stationary phase contains fluorinated organic moieties and as such has an affinity for the FDMT protected product oligonucleotide; this is bound, failure sequences are washed away before cleaving the FDMT group and eluting the product. Purification of DNA by this method is again quick, reasonably priced and very efficient, the down side compared to GlenPak columns is the need to purchase and include a terminal FDMT protected monomer in the DNA synthesis; however this is offset by the greater range of modified oligonucleotides that may be purified by this method. Analytical HPLC of oligonucleotides purified by affinity columns demonstrates their efficacy (Figure 24 & Figure 25).

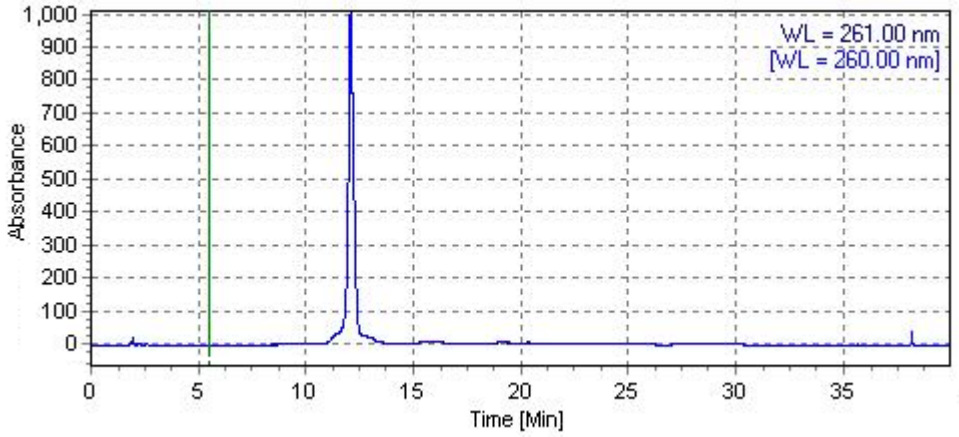

Figure 24. Example HPLC trace of unmodified DNA purified by GlenPak cartridge

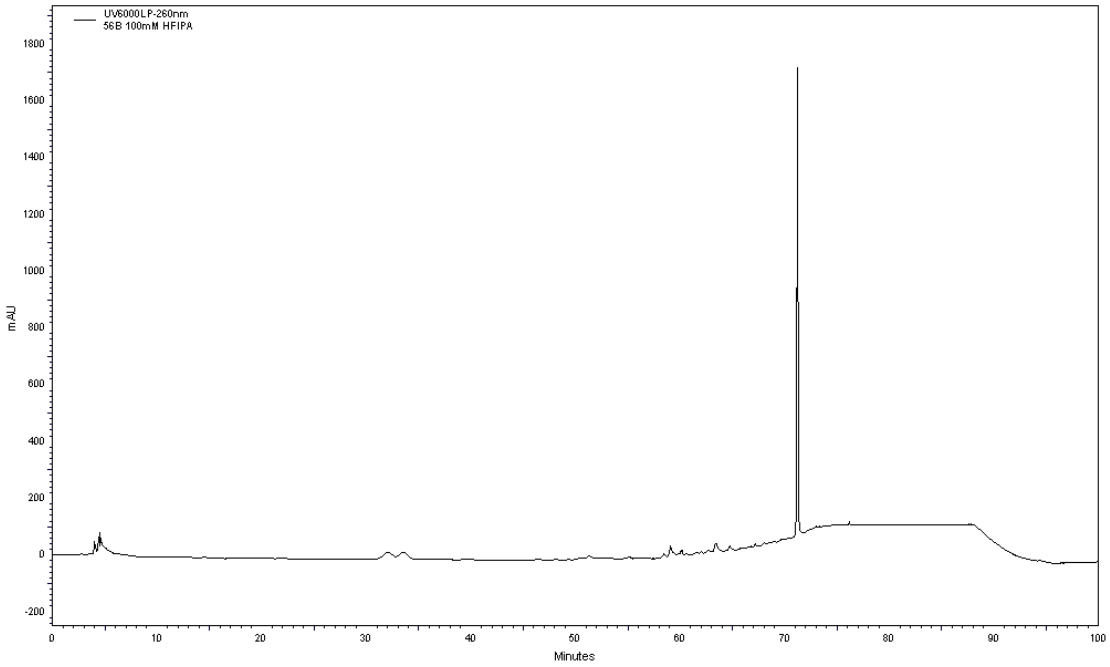

Figure 25. Example HPLC trace of porphyrin modified DNA purified by FluoroPak cartridge

3.6 – General synthesis of porphyrin DNA strands

The two synthesised porphyrin monomers; the acetylene linked porphyrin monomer (**VII**) and the amide linked porphyrin monomer (**XIV**) were incorporated into various single stranded oliomers through solid supported DNA synthesis. The reactivity of the monomers in the DNA synthesiser was comparable to one another, each requiring a concentration of 20 – 30 mM in MeCN:DCM (1:1). Most phosphoramidites are dissolved in MeCN for DNA synthesis, however to increase the monomer concentration a 1:1 mixture of MeCN and DCM was used due to the porphyrins nucleotide not being soluble in MeCN. DCM could not be used on its own since measurement of solvent volume by the DNA synthesiser is unreliable with high vapour pressure solvent. Between 2.5 and 4 equivalents of the porphyrin phosphoramidites were required per coupling; less than 2 equivalents led to very poor coupling efficiencies, while greater than 4 equivalents showed no great improvement in coupling efficiency and as such is simply a waste of the phosphoramidites. Various coupling times between 2 minutes and 12 minutes were tried on different strands, a coupling time of 5 minutes appearing to give the most efficient yields. Systematic studies varying these coupling parameters have not been conducted, the advised coupling conditions given above may not be the optimum conditions; however they work efficiently without too much loss of material.

It should be noted that the acetylene linked porphyrin phosphoramidite (**VII**) is a zinc (II) metallated porphryin, however this is converted back to the freebase porphyrin during the TCA wash to cleave the DMT protecting groups. The UV-vis absorbance spectrum of the

porphyrin modified DNA confirms the presence of the freebase porphryin through there being four Q bands as opposed to the two Q bands of the metallated porphyrin (Figure 26 *c.f.* Figure 5).

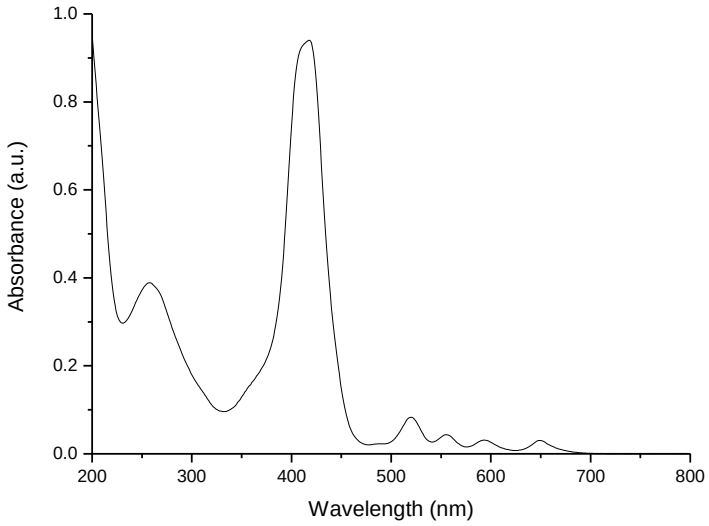

Figure 26. UV-vis of porphyrin modified DNA

The inclusion of a porphyrin monomer into DNA colours the solid support a vivid purple colour, successive additions of porphyrins change the intensity of the colour of the beads very little. The vibrant purple colour of the porphyrin gives a useful visual indicator in all stages of synthesis and handling of porphyrin DNA; from seeing that the modified DNA has been cleaved from the solid support (the support turns colourless and opaque), to observing the purple band of porphyrin modified DNA being captured by and released from the FluoroPak affinity purification columns, to seeing when an aliquot of porphyrin DNA has been completely transferred from one Eppendorf tube to another.

Porphyrins have a tendency to streak on various purification media, unfortunately this property is also passed on to porphyrin modified DNA. All porphyrin DNA strands that will be discussed in this volume have been purified by FluoroPak purification cartridges where the tendency for the DNA to streak is not an issue that hampers its purification. It is possible to purify porphyrin modified DNA on a C18 modified reverse phase HPLC column, however choice of eluent plays a large part in successful purification. Eluting from a buffer of 100 mM triethylammonium acetate, 1% acetonitrile in water to acetonitrile, methanol or ethyl acetate is not particularly successful, injection of the porphyrin DNA leads to streaking through the column with diffuse peaks being detected by the HPLC's absorption spectrometer. Eluting from buffer to THF is significantly more successful, however a gradient from 100 mM 1,1,1,3,3,3-

hexafluoro-*iso*-propanol, 8.4 mM triethylamine in water into methanol gives good resolution of peaks and are a good choice of eluent if preparative or semi-preparative HPLC purification of porphyrin modified DNA is conducted.

Repeated attempts to obtain mass spectrometry of porphyrin modified DNA were made on the strands detailed in this volume, samples were sent both for in house analysis and also to the EPSRC National Mass Spectrometry Centre at Swansea University, none of these attempts were successful. Dr Eugen Stulz, Dr Imenne Bouamaied and Dr ThaoNguyen Nguyen, all of whom have previously synthesised porphyrin modified DNA strands[20,21,120,121] have also repeatedly attempted to obtain mass spectrometry results which have been unsuccessful or vague[52], the exceptions being; porphyrin nucleotide dimers[120] *i.e.* a DNA strand two bases in length; and short sequences (i.e. 6 – 12 bases in length) with only a single porphyrin modification, as shown by other research groups.[126,138] The published mass spectrometry data in these latter papers are only short test sequences, the longer porphyrin modified oligomers (14-mer with one modification and a 39-mer with two modifications) that were actually studied in the papers do not have mass spectrometry data presented, leading to the belief that this group also had problems obtaining mass spectrometry data for longer and multiply modified oligomers.

3.7 – Offset porphyrin modified DNA systems

a 5'-GGC CAT CGT CGC **P**A**P** A**P**A **P**A**P** A**P**A TTA T-3'
b 3'-A GCG A**P**A **P**A**P** A**P**A **P**A**P** AAT ACC GTA TGG-5'

P = porphyrin monomer

Figure 27. Offset porphyrin modified DNA sequence

A modified duplex sequence was designed (Figure 27) to incorporate a zipper like porphyrin modified central section and overhanging single stranded section of DNA, so called 'sticky-ends'. This duplex was designed to be able to test the potential of this system to transport electrons across a lipid bilayer (See - 3.17 – Plans for measuring conductivity, page 82). The system was designed to incorporate a 'zipper' type arrangement of the porphyrins; that is, where the modification are located on alternating strands and on hybridisation the modifications interlock like the teeth of a zip. This arrangement of porphyrin modifications is known to stabilise the duplex through additional inter-strand π-π interactions between the porphyrins moieties; this stabilising effect is not present if all modified bases are located on one strand of the duplex.[20,21,52,118]

3.8 – Synthesis, yield and HPLC of offset porphyrin modified DNA systems

Both the **a** and **b** strands (Figure 27) were synthesised, incorporating either the acetylene linked porphyrin monomer (**VII**), the amide linked porphyrin monomer (**XIV**), or just a thymidine, as such six strands were synthesised.

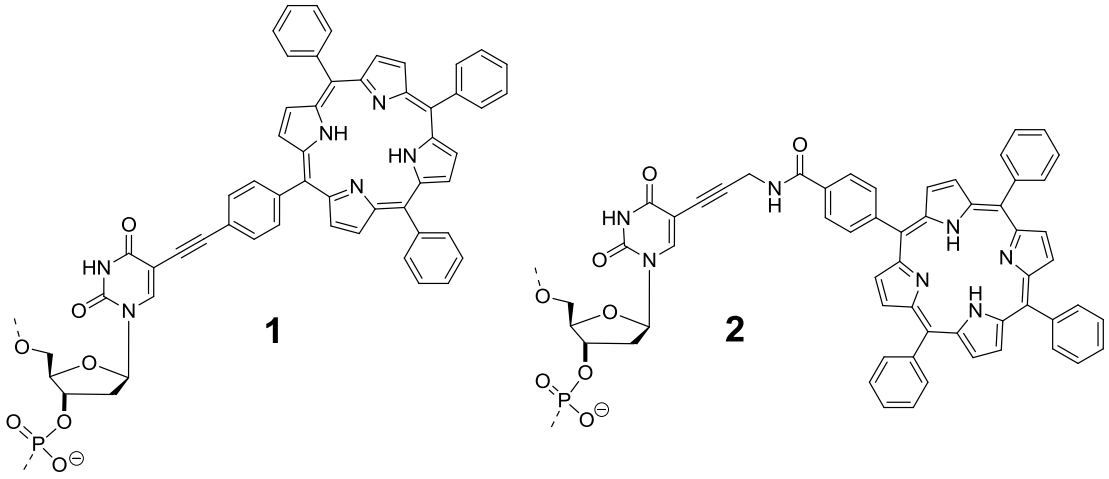

5'-GGC CAT CGT CGC **1**A**1** A**1**A **1**A**1** A**1**A TTA T-3' **3**
3'-A GCG A**1**A **1**A**1** A**1**A **1**A**1** AAT ACC GTA TGG-5' **4**

5'-GGC CAT CGT CGC **2**A**2** A**2**A **2**A**2** A**2**A TTA T-3' **5**
3'-A GCG A**2**A **2**A**2** A**2**A **2**A**2** AAT ACC GTA TGG-5' **6**

5'-GGC CAT CGT CGC TAT ATA TAT ATA TTA T-3' **7**
3'-A GCG ATA TAT ATA TAT AAT ACC GTA TGG-5' **8**

Figure 28. Incorporated porphyrin monomers and synthesised DNA strands

These six strands (Figure 28) allow for the formation of three modified duplexes; where both strands containing the acetylene linked porphyrin monomer (**3•4**); where one strand contains the acetylene linked monomer and the other strand contains the amide linked monomer (**3•6**); and finally, where both strands contain the amide linked monomer (**5•6**). Four duplexes may be formed where only one of the strands contains modified bases; where strand **a** (Figure 27) contains the acetylene linked monomer (**3•8**) or the amide linked monomer (**5•8**); and where strand **b** contains the acetylene linked monomer (**4•7**) or the amide linked monomer (**6•7**). Finally, the completely unmodified duplex (**7•8**) may be formed as a reference to all the modified strands. The yields and HPLC retention times are shown in Table 1.

Strand	Yield (nmoles)	HPLC retention time (min)
3	69	16.52
4	81	16.35
5	218	15.47
6	138	16.52
7	591	12.09
8	486	11.97

Table 1. Yields and HPLC retention times of synthesised oligomers
HPLC conditions: 0.0 min 100 % buffer, 3.0 min 100 % buffer, 25.0 min 100 % THF, 35.0 min 100 % buffer. Buffer – 100 mM TEAA, 1 % MeCN in H_2O. Column – Merck 250 x 4 mm C18 LiChroCART at 55 °C.

The yields of the porphyrin modified strands are notably lower than that of the analogous unmodified strands, at the extreme, nine fold lower. The trityl reading of the DNA synthesiser implied that the couplings of the modified bases were efficient, with no significant drop in coupling efficiency. The modified strands (**3**, **4**, **5** and **6**) do differ from the natural strands (**7** and **8**) at the terminal base; the final base to be coupled to the natural DNA is a 5'-DMT protected nucleoside, whereas the final base of the modified strands is a 5'-FDMT protected nucleotide (Figure 23). Due to the pre-requisite of having a 5' protecting group for affinity purification we have no way of knowing how efficient the coupling of these final 5'-FDMT protected bases were in the syntheses of these strands. It is believed that a poor coupling of the commercially available fluorous tagged nucleotide is a one major contributing factor to the low yields of strands **3**, **4**, **5** and **6**.

Reverse phase HPLC with differing eluent systems was conducted and it was found that of the systems tried, a gradient from 100 mM TEAA, 1 % MeCN in water to THF gave the least streaking of the products. Gradients from the aforementioned buffer to methanol, acetonitrile or ethyl acetate all produced chromatograms where the modified strands streaked through the column. Chromatography was conducted with a column temperature of 55 °C to inhibit the formation of any secondary structures, of which several hairpins structures could form at the poly (AT)/poly (AP) region of the strands.

3.9 – UV-vis of offset porphyrin modified DNA systems

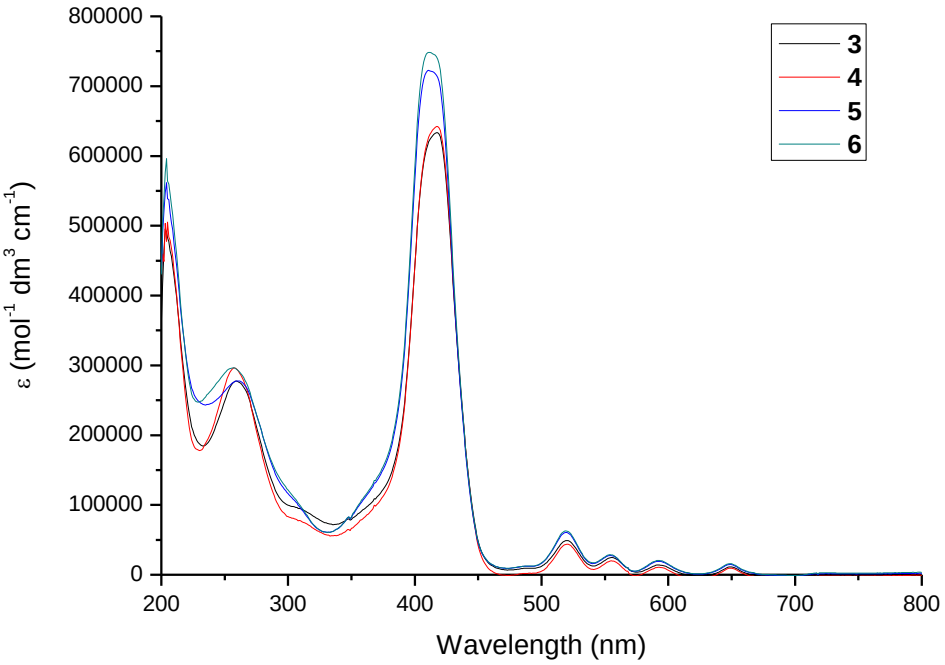

Figure 29. UV-vis of **3**, **4**, **5** and **6** in 100 mM sodium phosphate, 100 mM NaCl, 1 mM Na_2EDTA pH 7.0 at room temperature

The UV-vis spectra of strands **3**, **4**, **5** and **6** at room temperature (Figure 29) all show absorbances at 260 nm due to the DNA bases, large absorbances centred around 415 nm due to the porphyrin soret band and four small absorbances between 500 and 670 nm due to the four freebase porphyrin Q bands. The porphyrin absorbances are due solely to the porphyrin macrocycle, the substituents at the meso positions (*i.e.* the phenyl rings) play no part in the absorbances, with this in mind it can be seen from the ε value of both the soret band and the Q band absorbances that the values for the strands with the longer amide linked porphyrin are notably higher than those strands containing the shorter acetylene linked porphyrin monomer. This is despite the amide linked porphyrin nucleoside (**XIII**) having a lower log ε_{Soret} value (5.49 in methanol) than the acetylene linked porphyrin nucleoside (**VI**), log ε_{Soret} = 5.65 in methanol. This larger ε value for the amide linked monomer can be attributed to less stacking and π-π interactions with other porphyrins and/or the nucleobases.[139] The absorbance maxima of the soret bands also differ slightly between the two porphryin monomers, the strands containing the acetylene linked monomer (**1**) have absorbance maxima at 418 nm, while those containing the amide linked porphryin monomer (**2**) have absorbance maxima at 411 nm. The

absorbance maxima of the Q bands are the same for the two monomers; 520, 555, 592 and 649 nm.

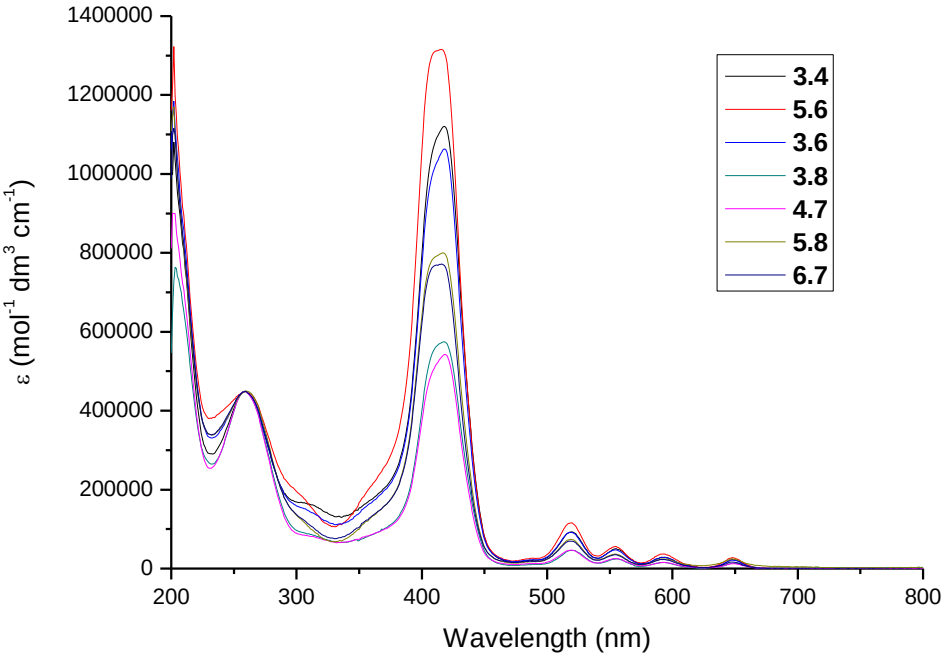

Figure 30. UV-vis of porphyrin modified DNA duplexes in 100 mM sodium phosphate, 100 mM NaCl, 1 mM Na_2EDTA pH 7.0 at room temperature

UV-vis of porphyrin modified duplexes at room temperature (Figure 30) emphasise the difference in ε of the soret band of the two monomers. The duplexes in which only one strand contains porphyrin modified bases show ε values for the Soret band that are comparable to those seen in the UV-vis of single stranded porphyrin modified DNA (Figure 29). The strands containing the acetylene linked porphryin monomer (**3•8** and **4•7**), show a lower ε value than those strands containing the amide linked porphyrin monomer (**5•8** and **6•7**). The ε_{Soret} values of **3•8** and **4•7** are slightly lower than the corresponding porphyrin modified single strands (log ε_{418} ~ 5.81 *c.f.* log ε_{418} ~ 5.74), this slight hypochromicity could imply a favourable organisation of the porphyrins when the duplex with the complimentary unmodified strand is formed.

Duplex **3•4**, where both strands contain the acetylene linked porphyrin monomer, shows an extinction coefficient of the soret band that is twice that of the corresponding duplex where only one strand contains porphyrin modification (**3•8** and **4•7**). This implies that although there may be a small degree of hypochromicity observed for strands **3•8** and **4•7** (15 %), no further hypochromicity is observed with the inclusion of additional porphyrin moieties into the system, i.e. duplex **3•4**.

Duplex **5•6**, where both strands contain the amide linked porphyrin monomer, shows a small degree of hypochromicity (15 %) of the soret band, compared to the corresponding duplexes containing only one modified strand (**5•8** and **6•7**). This is indicative of more efficient stacking of the porphyrin moieties, facilitated by the inclusion of a linker which allows the porphyrin moiety to move in two dimensions with respect to the nucleobase, as well as being able to rotate about the axis of the C(O)-phenyl single bond. Compared to the acetylene linked porphyrin which can rotate about the axis of the linker but is fixed spatially with respect to the nucleobase, this increased conformational freedom allows the porphyrins to align and stack in a more thermodynamically stable conformation, leading to the hypochromicity observed

The hybrid system (**3•6**), where one strand contains the acetylene linked monomer and the other contains the amide linked monomer, shows a larger degree of hypochromicity (21 %) than that observed for duplex **5•6**. The inclusion of two different linkages from the nucleobases to the porphyrins allows for much more efficient stacking of the porphyrins in the major groove. This effect is more pronounced for the hybrid system (**3•6**) than for the duplex **5•6** because the acetylene linker is shorter than the amide linker (3.97 Å and 6.12 Å respectively, measured from nucleobase to the porphyrin phenyl ring after energy minimisation). Thus, all the acetylene linked porphyrin moieties are held closer to the duplex than the amide linked modifications, this facilitates a greater overlap of the porphyrin rings, compared to duplex **5•6** where all of the modification are held at a greater distance outside the major groove.

The peak maximum of **3•4**, **3•8** and **4•7**'s Soret bands remains unchanged (418 nm) compared to their corresponding porphyrin modified single strand, the peak maximum of **5•6**, **5•8** and **6•7**'s Soret bands have been red shifted to 416 nm from 411 nm in their corresponding porphyrin modified single strand. The hybrid system's (**5•8**) Soret band has taken on the appearance of the acetylene linked strands, with a more intense B_x band[140] and a peak maximum at 418 nm. The presence of both the B_x and B_y absorbances can be seen in all duplexes' Soret bands, with their differing intensities due to excitation to varying vibronic levels.[140]

The ε values of the Q bands of all strands mimic the behaviour of the ε values of their respective Soret band, there is also no change in wavelength of the peak maxima; Q band absorbance maxima are at 520, 555, 592 and 649 nm for all duplexes, these are unchanged with respect to the porphyrin modified single strands.

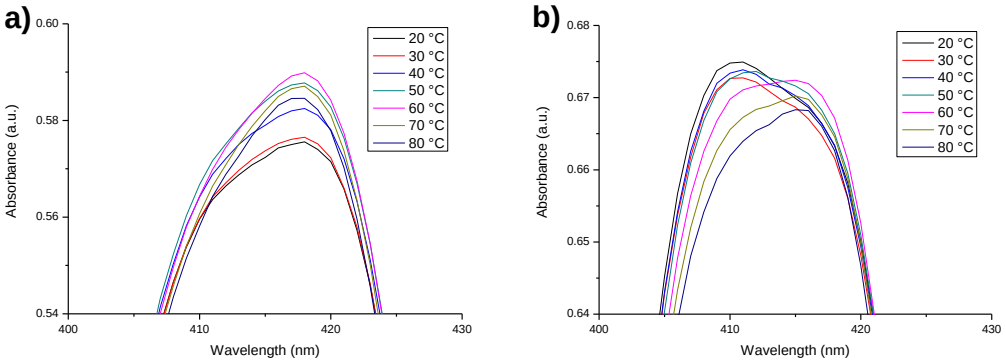

Figure 31. a) Variable temperature UV-vis of an acetylene linked porphyrin containing duplex (**3•4**) b) Variable temperature UV-vis of an amide linked porphyrin containing duplex (**5•6**)

Variable temperature UV-vis (Figure 31) was carried out on all single strands and duplexes in 100 mM sodium phosphate, 100 mM NaCl, 1 mM Na_2EDTA, pH 7.0 in water, several measurements were taken between 25 °C and 80 °C. All strands showed an increase in absorbance of the DNA peak (260 nm) with increasing temperature, as would be expected. The single strands and duplexes that contain the acetylene linked porphyrin monomer (**3**, **4**, **3•4**, **3•6**, **3•8** and **4•7**) all show an increase in absorbance of the Soret band with no change in wavelength of the absorbance maxima. The spectra of the single strands and duplexes which only contain the amide linked porphyrin monomer (**5**, **6**, **5•6**, **5•8** and **6•7**) are not trivial; a decrease in absorbance is observed between 25 °C and 50 °C along with a redshift of 3 nm from 411 nm to 414 nm, at 60 °C the peak absorbance increases and redshifts a further 2 nm to 416 nm, at this point the peak absorbance continues to drop with no further change in wavelength of the absorbance maximum. The net variation in peak intensity of the amide containing strands and duplexes is much lower than the variation in peak intensity of the strands containing the acetylene linked porphyrin monomer. At present it is not known what causes this behaviour. The shifts in peak wavelength and peak intensity of all duplexes are reversible over the time scale of these experiments; measurements were taken with a 5 minute interval between different temperatures.

3.10 – Fluorescence of offset porphyrin modified DNA systems

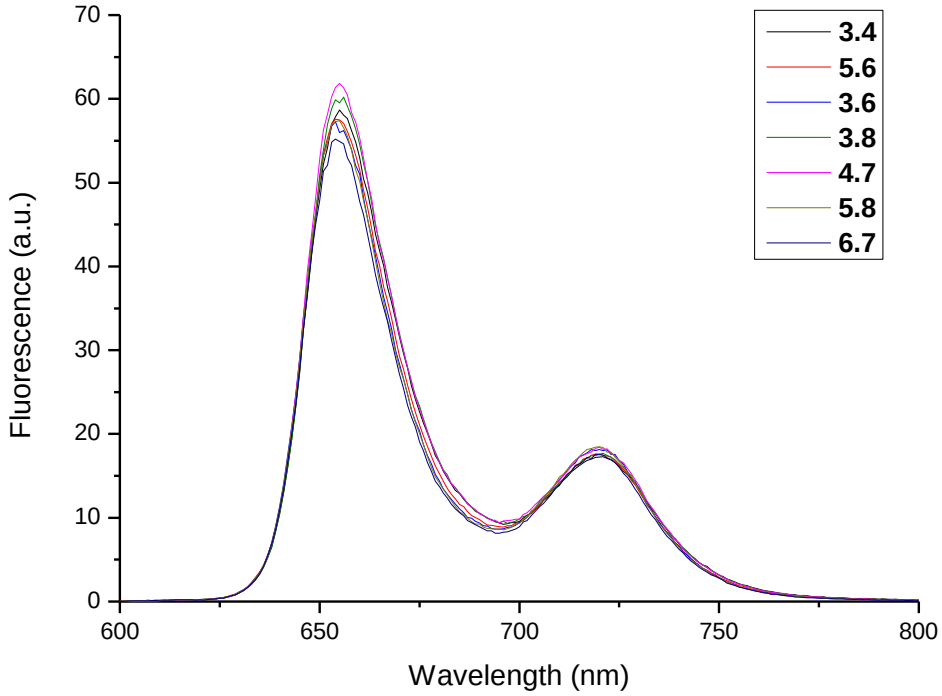

Figure 32. Room temperature fluorescence spectra of porphyrin modified DNA at equal Soret band absorbance, A = 0.48 ± 0.02 in 100 mM sodium phosphate, 100 mM NaCl, 1 mM Na_2EDTA, pH 7.0

Duplex samples of porphyrin modified DNA with equal absorbances of the Soret band were prepared for fluorescence spectroscopy (Figure 32). The fluorescence spectra of all samples are very similar, with maxima at 655 and 720 nm and peak height ratios of 1:0.3. Fluorescence quenching is not observed in any sample. The absence of a peak at ~605 nm should be noted as this indicates that the acetylene linked porphyrin containing samples are no longer zinc metallated, if any zinc metallated porphyrin were still to be present peaks at ~605 and ~650 nm would be observed in the fluorescence spectra.

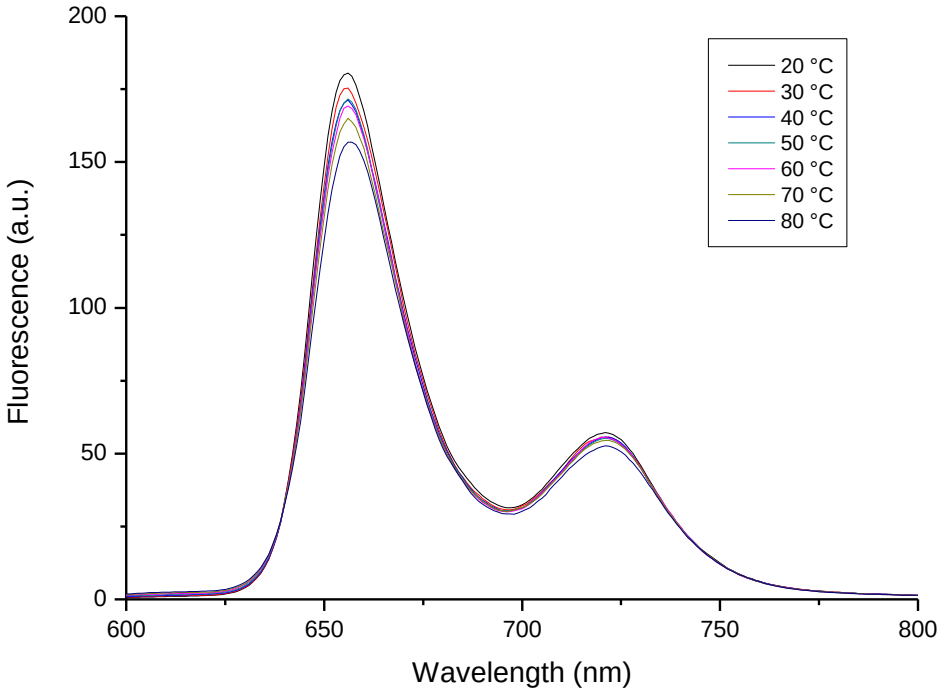

Figure 33. Example of variable temperature fluorescence of porphyrin modified DNA (**3•4**) in 100 mM sodium phosphate, 100 mM NaCl, 1 mM Na_2EDTA, pH 7.0

Variable temperature fluorescence spectra (Figure 33) of duplexes **3•4**, **3•6** and **5•6** were collected, the temperature was increased from 20 °C to 80 °C in 10 °C steps before then lowering the temperature back to 20 °C in 10 °C steps. 5 minute intervals between measurements ensured sample equilibration. The three sets of spectra collected displayed the same changes as one another; a broadly stepwise decrease in fluorescence of both peaks (655 and 720 nm) was observed with increasing temperature, the peak intensities varied only by a small degree, *circa* 10-15 % of the original intensity. The peak ratios remained constant at 1:0.3 over the range of temperatures measured. As the temperature was reduced from 80 °C to 20 °C the fluorescence traces increased to their original intensities. The behaviour exhibited by the duplex systems when heating in 10 °C increments is the reverse of what is observed when the system is heated and cooled slowly (ΔT/min ≤ 1 °C/min), under these conditions the fluorescence intensity increases with increasing temperature by between 25 and 70 % of the original peaks' intensities (see - 3.11 – Transition temperatures of offset porphyrin modified DNA system, page 52). With slow prolonged heating and cooling the samples melt and anneal efficiently, however with quick stepwise heating this mechanism is clearly not occurring, further experimentation in this area would be required in order to propose an alternate mechanism.

3.11 – Transition temperatures of offset porphyrin modified DNA systems

The melting temperature (T_m) of a DNA duplex is generally accepted as a measure of the thermodynamic stability of the duplex,[141] the higher the T_m the more stable the duplex and more energy is required to denature it. The T_m is measured by repeated slow heating and cooling of the duplex (ΔT/min = 1 °C/min) between 20 °C and 80 °C (Table 2), and monitoring the absorbance at 260 nm, i.e. where the nucleobases absorb. When a duplex is heated sufficiently the hydrogen bonds holding the two complimentary strands together are overcome and the strands come apart; it is at this point that a DNA duplex is said to have melted and the T_m is defined as the point at which 50 % of the duplex DNA in solution has dissociated. On melting, the number of stacking interactions between the nucleobases drops rapidly, leading to a hyperchromicity at 260 nm which may be detected by a UV photospectrometer.

	Start Temp (°C)	End Temp (°C)	Rate (ΔT/min)
Ramp 1	20	80	10
Ramp 2	80	20	10
Ramp 3	20	80	1
Ramp 4	80	20	1
Ramp 5	20	80	1
Ramp 6	80	20	1

Table 2. Melting temperature experiment parameters

Repeated measurements were made to obtain T_m values for all duplexes in 100 mM sodium phosphate, 100 mM NaCl, 1 mM Na_2EDTA pH 7.0, however discrete transitions could only be observed for the unmodified duplex (**7•8**, T_m = 47.2 °C). Other strands showed a steady increase in absorbance between 20 °C and 80 °C but without any clear transition from the annealed to the melted duplex, it is possible that the overhanging single stranded ends of the DNA may be causing the lack of a clear transition due to their ability to move spatially without being constrained by complimentary bases. This freedom would allow the bases to stack and unstack with more ease than if hydrogen bonded in a duplex, however, the net degree of stacking in the system decreases with increasing temperature i.e. as the duplex melts and hence the UV melting traces show steadily upwards trending lines.

The solvent system for the UV melting experiments was altered to 9:1 buffer:DMF (buffer = 100 mM sodium phosphate, 100 mM NaCl, 1 mM Na_2EDTA pH 7.0) in the hope that the inclusion of DMF would provide clearer transitions in the UV melting experiments. DMF is

known to disrupt hydrogen bonds[142] and π-π stacking interactions, so it was expected that any melting transitions observed in this solvent would be lower than if they were observed in just buffer.

The melting transition of the unmodified duplex (**7•8**) in 9:1 buffer:DMF was observed at 41.2 °C, 6.0 °C lower than was observed in just buffer. A melting transition for the amide linked porphyrin DNA duplex (**5•6**) was also observed at 45.9 °C, demonstrating that the inclusion of the zipper type porphyrin modifications in this system actually increase the stability of the duplex; presumably though π-π interactions between the porphyrins and hence between the strands. The increase in T_m compared to the unmodified duplex (**7•8**) in the same solvent system is 4.7 °C, therefore the increase in T_m per porphyrin modification is +0.4 °C. This result is very similar to previous finding by Stulz *et al.*,[21] where a different porphyrin zipper DNA system, containing 11 porphyrin modifications was found to stabilise the duplex by +0.5 °C per porphyrin modification. Melting transitions were also observed for both duplexes where only one of the strands was modified with the amide linked porphyrin monomers (**5•8** and **6•7**), rather unexpected these also showed an increase in T_m compared to the unmodified duplex (**7•8**) in the same solvent system. The melting transitions of **5•8** and **6•7** were observed at 46.2 °C and 47.3 °C respectively, these are increases of 5.0 °C and 6.1 °C over that of **7•8**.

Repeated attempts were made to collect melting temperature data in the two solvent systems listed, however no further melting transitions could be observed by this method, often a smooth increase in absorbance with increasing temperature was observed with no obvious transition point, this may be due to the possibility of forming various secondary structures, including hairpins and porphyrin aggregates. On occasions no hyperchromicity with increasing temperature was observed, this does not necessarily imply that no transition has occurred, merely that a transition could not be observed at that wavelength with that technique.[143] As such, fluorescence melting experiments in sodium phosphate buffer were carried out using the same temperature ramps as the UV melting experiments (Table 2). Natural DNA is not fluorescent, so by obtaining a fluorescence melting trace you are observing a different transition, namely the unstacking of the porphyrins, not the unstacking of the nucleobases. Transition temperatures were observed for both the acetylene linked porphyrin DNA system (**3•4**) and for the hybrid system (**3•6**) at 50.8 °C and 51.3 °C respectively. This implies that the DNA duplex is stabilised more, or, since we cannot directly compare this result to the natural DNA duplex, it is at the very least not destabilised as much in the hybrid system (**3•6**) compared to the acetylene linked system (**3•4**). This result is backed up by previous observations (3.9 – UV-vis of offset porphyrin modified DNA system, page 46), where duplex (**3•6**) was shown to have significantly increased levels of inter-porphyrin stacking compared to (**3•4**), hence the higher transition temperature in the fluorescence melting experiments.

Transitions were also observed for all duplexes where only one strand contained modified nucleobases (**3•8**, **4•7**, **5•8** and **6•7**), again, unexpectedly these were all at a higher temperature than for duplexes **3•4** and **3•6**, where both strands contain modified bases. The transitions were observed at 53.3, 51.4, 51.8 and 52.1 °C for **3•8**, **4•7**, **5•8** and **6•7** respectively. Despite repeated attempts, duplex **5•6** did not show a clear transition in this fluorescence melt experiment. As such the measurements were repeated in 9:1 buffer:DMF as per the UV melting experiments.

In 9:1 buffer:DMF the only systems to show clear transition temperatures were the systems where one strand was modified with the amide linked porphyrin monomer (**5•8** and **6•7**), these showed transitions at 48.8 °C and 50.1 °C respectively.

Although not all systems showed clear transitions in one solvent system by one analysis method, enough data was able to be collected to make informed conclusions about the transitions the duplexes are undergoing (Table 3).

System	T_m (°C)		ΔT_m (°C)[d]	ΔT_m per porphyrin (°C)[d]
	Buffer	9:1 Buffer:DMF		
3.4	50.8[c]	n.d.[e]	3.6	0.3
5.6	n.d.[e]	45.9[b]	4.7	0.4
3.6	51.3[c]	n.d.[e]	4.1	0.3
7.8	47.2[b]	41.2[b]	-	0.0
3.8	53.3[c]	n.d.[e]	6.1	1.0
4.7	51.4[c]	n.d.[e]	4.1	0.7
5.8	51.8[c]	48.8[c] 46.2[b]	4.6, 5.0, 7.6	0.8, 1.3, 0.8
6.7	52.1[c]	50.1[c] 47.3[b]	4.9, 6.1, 8.9	0.8, 1.5, 1.0

Table 3. Oligonucleotide transition temperatures

[a] Buffer = 100 mM sodium phosphate, 100 mM NaCl, 1 mM Na_2EDTA pH 7.0. [b] UV melting. [c] Fluorescence melting. [d] Calculated with respect to the unmodified duplex (**7•8**) in the appropriate solvent. [e] No data, no discrete transition was observed.

Transitions were observed for **5•8** (Figure 34) and **6•7** in the same solvent system by both UV melting and fluorescence melting, and were also observed in different solvent systems by the same method (fluorescence melting). The three transitions observed for each duplex were in very good agreement with one another; in 9:1 buffer:DMF both samples showed transitions in the fluorescence melting experiments that were consistently 2.6-2.8 °C higher than the T_m observed by UV melting. As such we may conclude that the transitions observed in the fluorescence melting experiments were caused by the duplex melting. There is a small

difference between the temperature at which the duplexes melt and at which the transition in the fluorescence trace is observed, however this is less than 3 °C and as such the fluorescence melting temperature gives a good representation of the duplexes' T_m values.

With this in mind it can be seen that the zipper duplexes (**3•4**, **3•6** and **5•6**) have similar degrees of stabilisation per porphyrin modification; between +0.3 and +0.4 °C per porphyrin. Interestingly the duplexes where only one strand contains modified bases seems to give a marginally larger degree of stability to the duplex than when both strands are modified. The origin of this stabilisation is thought to be a hydrophobic effect. It also appears that the melting temperatures of the porphyrin modified oligomers are affected less by the presence of DMF than the natural DNA; **5•8** and **6•7** show differences of 3.0 °C and 2.0 °C respectively between their transitions in buffer and 9:1 buffer:DMF, compared to a difference of 6.0 °C for the unmodified duplex (**7•8**). A hysteresis of between 3 and 5 °C is observed between the melting and annealing transitions of the porphyrin modified DNA, indicating that the kinetics of melting and annealing are different, the hysteresis of the corresponding unmodified duplex (**7•8**) is 1 °C and as such the melting and annealing processes of the modified duplexes are different from those of the unmodified duplex also.

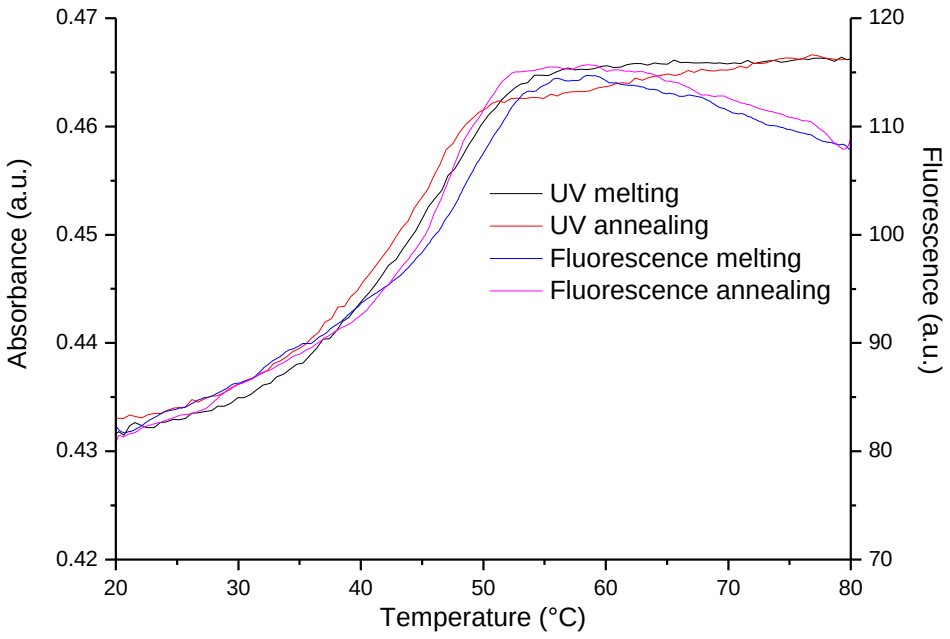

Figure 34. Example of UV and fluorescence melting traces of the same strand (**5•8**)

3.12 – Circular dichroism (CD)

Optically active chiral molecules absorb left and right circularly polarised light to differing levels depending on the wavelength of the irradiating light. This differential absorption of circularly polarised light about a UV-vis absorption band is known as the Cotton effect[144]. Circular dichroism (CD) spectroscopy measures this difference in absorbance of circularly polarised light as a function of wavelength. The sign and magnitude of the CD trace depends on a number of conditions, including; the chirality of the molecule and excitonic coupling[19]. Achiral molecules that would otherwise be optically inactive by CD spectroscopy (but are active by UV-vis spectroscopy) can show Cotton effects through induced chirality, due to the chiral environment in which it is held. Due to the sensitivity of CD to detect the environment in which a probed molecule is held, and its ability to detect inter- and intra-molecular interactions, it is a valuable tool for elucidating; protein structures[145]; the interactions of chromophores in light harvesting systems[146] and the absolute configuration of chiral organic molecules[144].

CD, being a form of absorbance spectroscopy, requires the absorbance of the sample to be kept within the linear region of the Beer-Lambert law, that is to say $A \leq 1.5$ a.u. Berova *et al.*[144] recommend an absorbance of ~0.8 a.u. for the peak of interest. As such when collecting spectra of the offset porphryin modified DNA systems, the DNA absorbance and the Soret band absorbances were treated independently, with two samples of different concentrations being measured, due to the large difference in the relative absorbances of these two peaks. Unless otherwise stated, samples were measured over a 1 cm pathlength with concentrations of the order of 2.5-4.5 μM, data is collected as θ (mdeg) but converted to $\Delta\varepsilon$ (mol^{-1} dm^{-3} cm^{-1}) (see - 7 – General Experimental Details, page 125) to allow comparison of the different concentration samples required in order to keep the absorbance at an optimum.

3.13 – Circular dichroism (CD) of offset porphyrin modified DNA systems

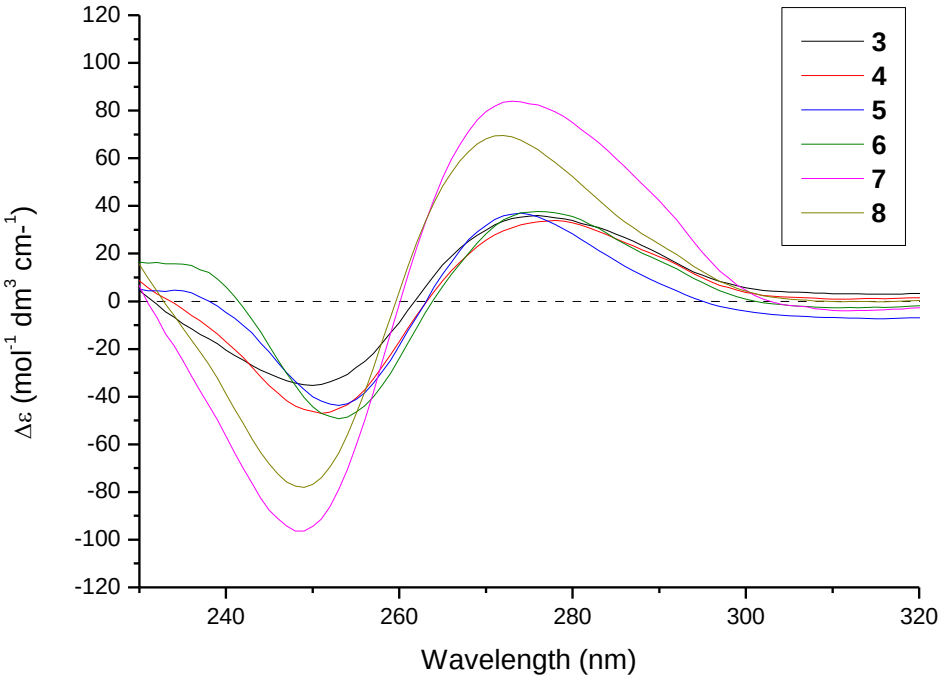

Figure 35. 230 – 320 nm CD spectra of single stranded porphyrin modified and natural DNA in 100 mM sodium phosphate, 100 mM NaCl, 1 mM Na_2EDTA, pH 7.0 at room temperature

Natural single stranded DNA (**7** and **8**) shows peaks at +271/-249/+219 nm, as would be expected.[147] Acetylene linked porphyrin modified single stranded DNA (**3** and **4**) shows a similar trace (Figure 35), with slight shifts in peak positions (+276/-250/+218 nm) and a lowering of peak intensities. Single strands containing the amide linked monomer (**5** and **6**) show a different trace shape, with peaks at +276/-253/+235/+218 nm, again the peak intensities are lower than those of the unmodified single strands. The CD traces of **5** and **6** suggest that they exist in a different conformation to the random coil that the single stranded DNA adopts. This may be due to stacking of the porphyrin moieties along the length of the strand, as per the molecular modelling of Stulz *et al.*[20] The lowering in intensity of the traces may be due to a disruption of the excitonic coupling of the nucleobases caused by the presence of the porphyrin modifications.

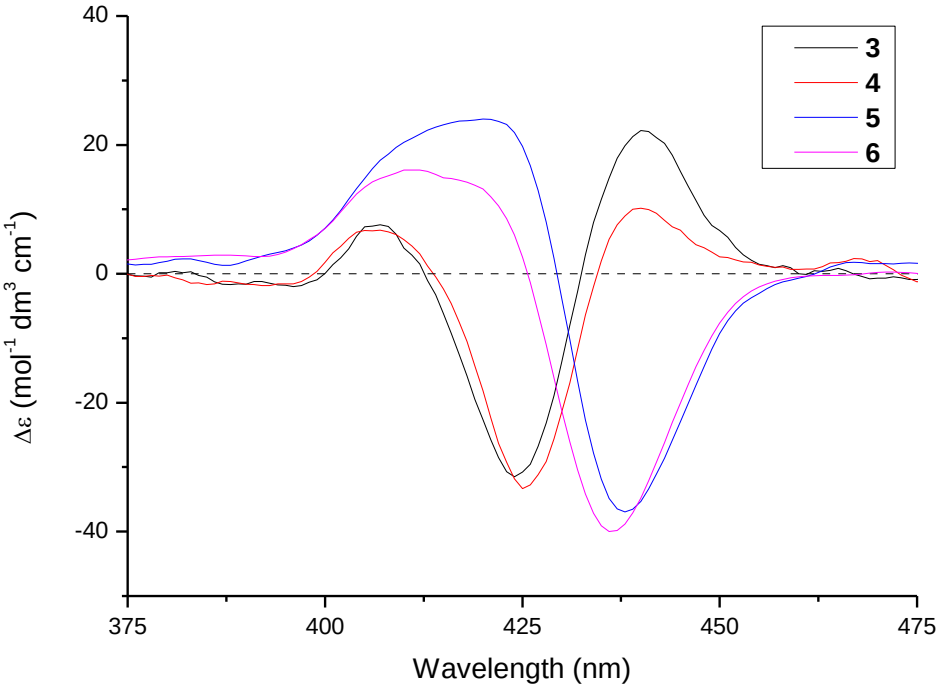

Figure 36. 375 – 475 nm CD spectra of single stranded porphyrin modified and natural DNA in 100 mM sodium phosphate, 100 mM NaCl, 1 mM Na_2EDTA, pH 7.0 at room temperature

Natural DNA does not have any absorbances in the visible region and as such cannot show a Cotton effect in the CD, measurements in this region show a flat line at $\Delta\varepsilon = 0$. For this reason the traces of **7** and **8** in Figure 36 have been omitted for clarity.

The CD spectra of porphyrin modified single strands (**3**, **4**, **5** and **6**) shows excitonic coupling[19,148] of the Soret bands between the porphyrins (Figure 36); porphyrins are known to show excitonic coupling at distances of up to 50 Å.[149] The spectra of the strands containing the acetylene linked porphyrin (**3** and **4**) both show a trisignate with very little difference in the peak positions; +440/-426/+406 nm and +440/-425/+406 nm for **3** and **4** respectively. These trisignates indicate that the acetylene linked monomers must be considered as circular oscillators,[150] i.e. the B_x and B_y transitions[151] (see - 1.1 – Porphyrins, page 1) are discrete and both contribute to the excitonic coupling of the system. The discrete nature of the transitions is due to the short, inflexible acetylene linker between the oligonucleotide and the porphryin which restricts the porphryins' conformation with respect to the other porphyrins attached to the oligonucleotide.

Strands **5** and **6** show simpler bisignate traces with comparable intensities to those of strands **3** and **4**, peak maxima are found at -438/+420 nm and -436/+411 nm for **5** and **6** respectively. The simpler bisignate traces indicate that the amide linked monomer in strands **5**

and **6** can be assumed to be linear oscillators,[150] *i.e.* the B_x and B_y transitions are not discrete and may be treated as a simple dipole across the porphyrin moiety. This simpler situation arises due to the conformational flexibility that the longer amide containing linker affords to the porphyrins.

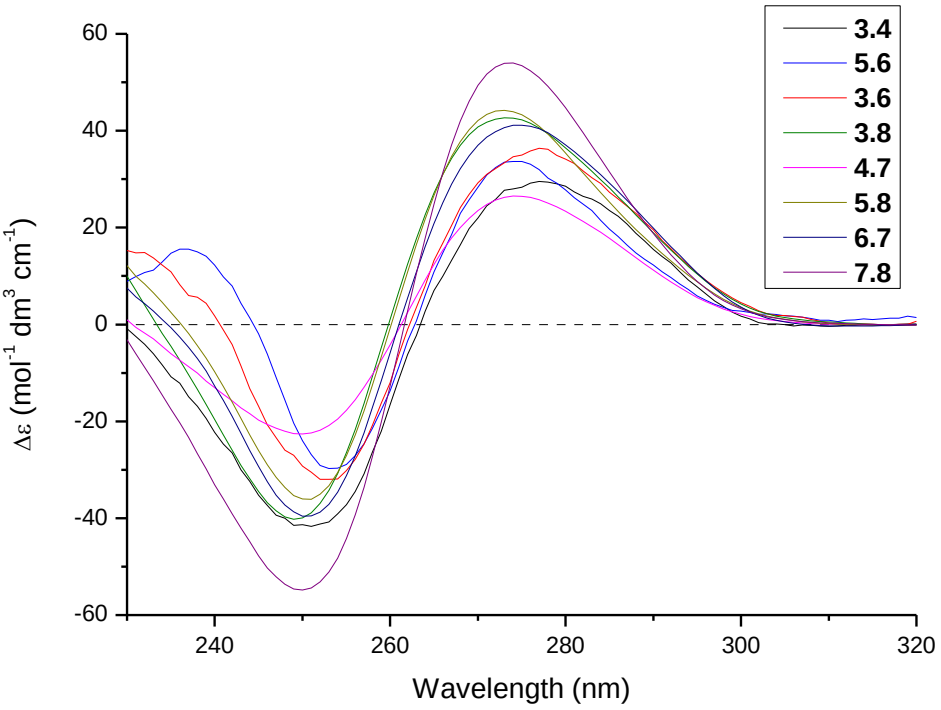

Figure 37. 230 – 320 nm CD spectra of duplex porphyrin modified and natural DNA in 100 mM sodium phosphate, 100 mM NaCl, 1 mM Na_2EDTA, pH 7.0 at room temperature

The natural DNA duplex (**7•8**), duplexes where both strands are modified (**3•4**, **5•6**, **3•6**) and also duplexes where only one strand contains modified bases (**3•8**, **4•7**, **5•8** and **6•7**) all show a bisignate indicating the formation of B-DNA[152,153] (Figure 37). This indicates that the porphyrin modifications do not drastically alter the ability of the sequence to form a duplex and that the conformation of the resulting duplex is the same as that of the unmodified duplex. There are small variations in peak intensities and peak positions between the different systems, with all bisignate peaks between +275 (± 2)/-251 (± 2) nm. However, this indicates that the inclusion of up to twelve porphyrins into the major groove over a length of 12 bases does not alter the conformation of the duplex.

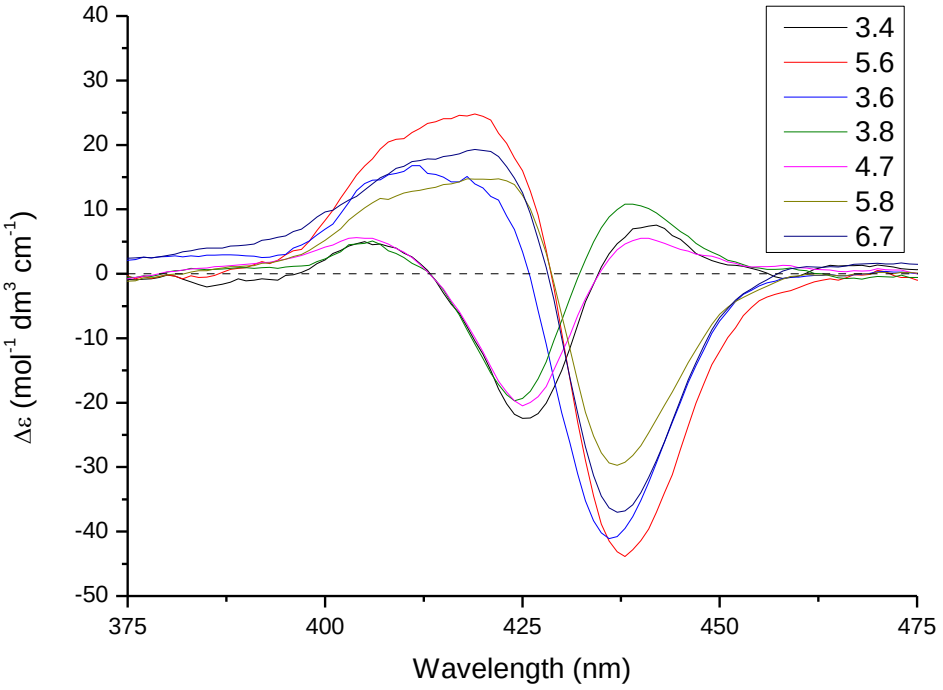

Figure 38. 375 – 475 nm CD spectra of duplex porphyrin modified and natural DNA in 100 mM sodium phosphate, 100 mM NaCl, 1 mM Na_2EDTA, pH 7.0 at room temperature

Porphyrin modified duplexes (**3•8**, **4•7**, **5•8** and **6•7**) where only one strand contains porphyrin modified bases show similar behaviour to their corresponding modified single stranded systems (**3**, **4**, **5** and **6**, Figure 38), generally with very little change in peak positions (±1 nm), the exception being **6•7** where the maxima of the very broad positive peak has shifted by 8 nm. There is a slight decrease in peak intensity compared to the single stranded systems which may be caused by a number of factors; the porphryins being held slightly further away from one another, since the intensity of the excitonic coupling between chromophores is inversely proportional to the distance squared;[148] slight changes in the Soret band extinction co-efficient on duplex hybridisation;[154] or, changes in the relative orientation of the porphryins.[155] Of these strands, those containing the acetylene linked monomer (**3•8** and **4•7**) are behaving as circular oscillators, as per the corresponding single strands (**3** and **4**), peak maxima are found at +439/-424/+406 nm and +441/-425/+404 nm for **3•8** and **4•7** respectively. The duplexes with one strand containing the amide linked porphryin monomer (**5•8** and **6•7**) are again behaving as linear oscillators, as per their corresponding single strands (**5** and **6**) with peak maxima at -437/+419 nm for both **5•8** and **6•7**.

The duplex where both strands contain the acetylene linked porphyrin monomer (**3•4**) shows a CD trace that is very similar to both the corresponding single strands (**3** and **4**) and to

the duplexes **3•8** and **4•7** where only one strand contains modified bases. The porphryins behave as circular oscillators with peak maxima are found at +441/-426/+406 nm and peak intensities are comparable to those of **3•8** and **4•7** and as such are slightly lower than the corresponding single strands (**3** and **4**). This would suggest that the orientation of the porphryins with respect to the duplex is the same in **3•4**, **3•8** and **4•7**.

The CD trace of duplex **5•6**, where both strands contain the amide linked porphyrin monomer, is very similar to those of the corresponding duplex where only one strand contains modified bases (**5•8** and **6•7**) and to one of the corresponding single strands (**5**), with peak maxima at -438/+419 nm. The peak maxima differ slightly from **6** at the broad, almost flat topped, positive peak at +411 nm. Duplex **5•6** shows the porphyrin modifications to behave as linear oscillators, similar to the corresponding single strands and the duplexes incorporating one modified strand. The peak intensities of **5•6** are comparable to those of the corresponding single strands (**5** and **6**) but larger than those of **5•8** and **6•7**. It would appear that the orientation of the porphryins in **5•6** is similar to their orientation in both the corresponding single strands (**5** and **6**) and the duplexes with one modified strand (**5•8** and **6•7**). The factors varying the peak intensities are the same as described above, but one possible explanation would be that in the single stranded systems (**5** and **6**) the porphryins are free to orientate themselves close to one another leading to the larger peak intensities, when hybridised with an unmodified single strand (**5•8** and **6•7**) the porphryins are forced further away from each other resulting in the drop in peak intensites, however when hybridised with the complimentary porphyrin containing strand the inter-porphryin distance decreases and as such the peak intensities increase again. Further experimentation would be required to validate or refute any possible theories.

The CD trace of **3•6** superficially appears like that of the duplex containing the amide linked porphyrins (**5•6**), the trace shows the porphyrins to be behaving as linear oscillators as per **5•6** but the peak maxima are slightly shifted (-436/+412 nm). The characteristics of the curve are more akin to those duplexes that contain the amide linked porphryin monomer as opposed to those containing the acetylene linked monomer.

Comparing the three duplex systems where both strands contain modified bases (**3•4**, **5•6** and **3•6**), it is evident that there are three different conformations present, however it is not possible to explicitly state what conformations these systems exist as without significant further experimentation.

3.14 –Metallation and analysis of offset porphyrin modified DNA systems

The porphyrin macrocycle can be metallated with a variety of metals, some with reasonable ease (e.g. zinc) while others require more forcing conditions (e.g. platinum). There are very few metals that have not been incorporated into the porphyrin macrocycle, as the 'periodic table of metallated porphyrins'[14] demonstrates.

Small quantities (~5 nmoles) of porphyrin modified single stranded DNA, containing either the acetylene linked monomer (**3**) or the amide linked monomer (**5**) were metallated with zinc, cobalt or copper by heating the DNA in solution with a vast excess of the metal (II) acetate. Unbound metal ions were then chelated with EDTA before purification with a GlenPak column, being affinity columns they act like a mini chromatography column and allow the excess bound metal ions to be eluted with 'salt wash' (5 % acetonitrile, 100 mg mL^{-1} sodium chloride in water) before the metallated DNA is eluted with an acetonitrile and water mixture (1:1).

Duplexes where one strand contains metallated porphyrin modification and the other strand contains freebase porphryin modifications were prepared by heating to 80 °C (60 °C for Zn metallated strands due to possible thermal demetallation) for 5 minutes and then allowing to cool to room temperature.

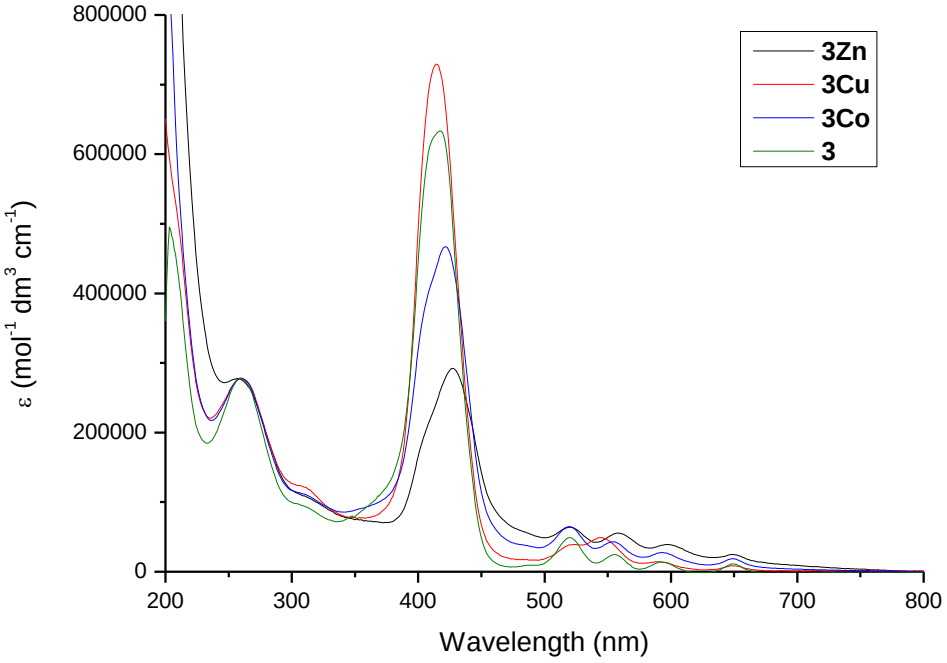

Figure 39. 200 – 800 nm UV-vis spectra of metallated and free base **3** in 100 mM sodium phosphate, 100 mM NaCl, 1 mM Na_2EDTA, pH 7.0 at room temperature

The inclusion of a metal into the porphyrin macrocycle has a marked affect on both the Soret band and the Q band absorbances as shown in Figure 39. Zinc (II) metallation of the acetylene linked porphyrin strand **3** gives **3Zn**, the metallation leads to a dramatic drop in the ε value for the Soret band (log ε_{426} = 5.46 *c.f.* log ε_{418} = 5.83 for **3**) and a shift in the peak maxima from 418 nm to 426 nm. The changes to the Q bands are more subtle, with slight shifts in peak position to 520, 558, 598 and 649 nm from 520, 557, 594 and 651 nm. Copper metallation (**3Cu**) causes an increase in the extinction coefficient of the Soret band (log ε_{414} = 5.86) with a shift in peak position to 414 nm, the change in the Q bands is more marked than for **3Zn**, with peak maxima at 525, 544, 590 and 648 nm. Cobalt metallation (**3Co**) leads to a decrease in the Soret band extinction coefficient (log ε_{422} = 5.44) and a shift in peak maximum to 422 nm. The changes to the Q bands are minimal, with peak maxima located at 519, 554, 593 and 649 nm. The metallation of the porphyrin does not affect the absorbance of the oligonucleotide at 260 nm.

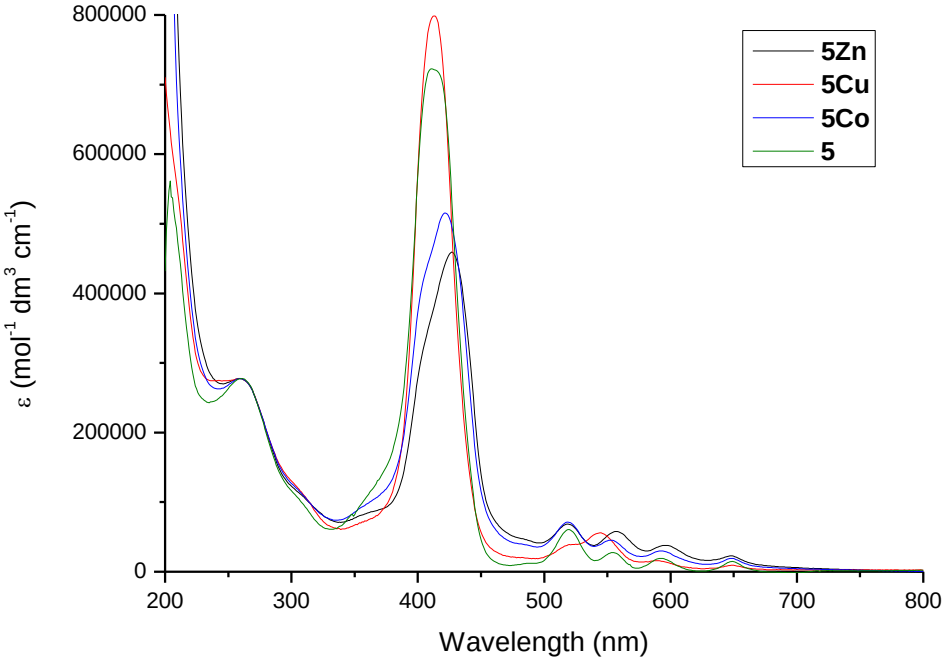

Figure 40. 200 – 800 nm UV-vis spectra of metallated and free base **5** in 100 mM sodium phosphate, 100 mM NaCl, 1 mM Na_2EDTA, pH 7.0 at room temperature

Zinc (II) metallation of the amide linked porphyrin strand **5** gives **5Zn** (Figure 40), again this zinc metallation leads to a drop in the ε value of the Soret band (log ε_{427} = 5.49 *c.f.* log ε_{419} = 5.80 for **5**), the peak maximum again shifts by 8 nm from 419 nm to 427 nm. Slight shifts in peak position of the Q bands are observed, with peak maxima at 519, 557, 596 and 647 nm, shifted from 520, 557, 594 and 651 nm. Copper metallation of the amide linked porphyrin containing strand (**5Cu**) shows the same characteristics as that of **3Cu**, namely an increase in the extinction coefficient of the Soret band (log ε_{414} = 5.58) with a shift in peak position to 414 nm, again, the change in the Q bands is quite pronounced with peak maxima at 525, 544, 590 and 648 nm. Cobalt metallation (**5Co**) leads to a decrease in the Soret band extinction coefficient (log ε_{422} = 5.44) and a shift in peak maximum to 422 nm, identical to that of **3Co**. The Q bands are also identical to those of **3Co**, with peak maxima located at 519, 554, 593 and 649 nm. As per metallation of strand **3**, the absorbance at 260 nm is unaffected by metallation of the porphyrin macrocycle. Interestingly the four orbital model proposed by Martin Gouterman in 1959[22] which explains the absorbance spectra of the porphyrin macrocycle would suggest that metallated porphyrins should only have 2 Q bands due to the increase in symmetry (D_{4h} from D_{2h}), however all **3M** and **5M** have 4 Q bands. We believe that the presence of the four Q bands is due to the inclusion of the porphyrin macrocycles into a chiral environment (the

major groove of the DNA), hence the D_{2h} point group does not accurately represent the oligonucleotide bound macrocycle and four discrete Q band transitions are possible.

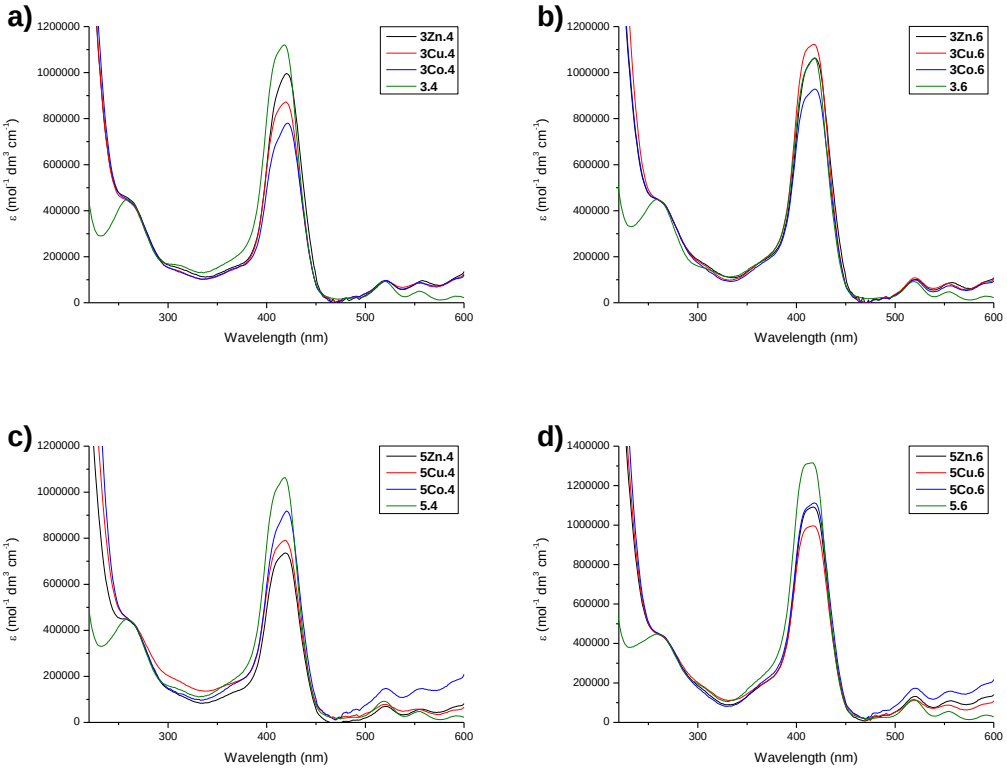

Figure 41. 220 – 600 nm absorbance spectra of a) **3M•4** b) **3M•6** c) **5M•4** and d) **5M•6** duplexes, in 100 mM sodium phosphate, 100 mM NaCl, 1 mM Na_2EDTA, pH 7.0 at room temperature

Duplexes **3M•4**, where both strands contain the acetylene linked monomer, show a redshift of the Soret peak maximum from 417 nm to 420 nm for all metallated strands (Figure 41a). Duplexes **3M•6** and **5M•4**, where one strand contains the acetylene linked monomer and the other the amide linked monomer, do not show any shift of the Soret peak maximum (419 nm, Figure 41b & c). Duplex **5M•6** shows a small redshift of the Soret peak maximum from 416 nm to 417 nm for **5Zn•6** and **5Cu•6** and 418 nm for **5Co•6** (Figure 41d). Decreases in ε values for the Soret band are observed for all strands except **3Zn•6** and **3Cu•6**, the exact change in ε appears to be specific to the individual duplexes, with differing metal and linker combinations giving different ε values.

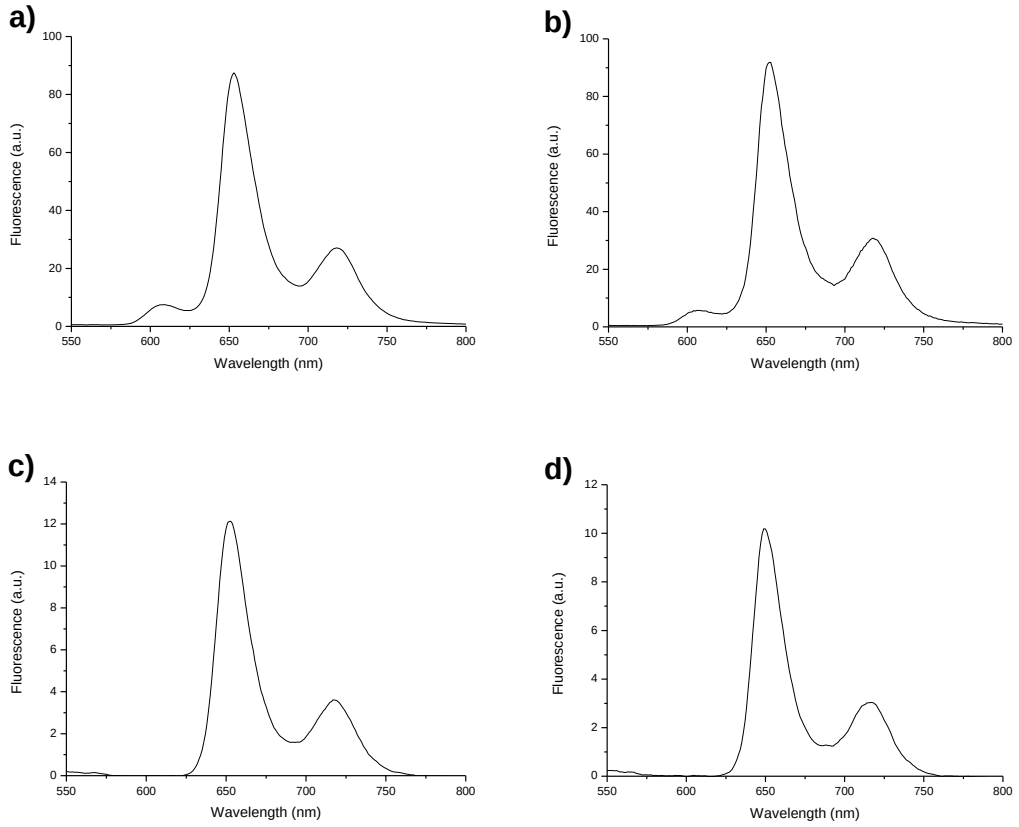

Figure 42. 550 – 800 nm fluorescence spectra of a) **3Zn** *c* = 2.09 µM b) **5Zn** *c* = 2.32 µM c) **3Cu** *c* = 1.34 µM and d) **5Cu** *c* = 0.83 µM, in 100 mM sodium phosphate, 100 mM NaCl, 1 mM Na_2EDTA, pH 7.0 at room temperature, with excitation at the Soret band maxima

Emission spectra were collected of **3Zn**, **5Zn**, **3Cu** and **5Cu** (Figure 42) in 100 mM sodium phosphate, 100 mM sodium chloride, 1 mM disodium EDTA, pH 7.0 by exciting the samples at their respective Soret band maxima. No emission spectra were recorded for **3Co** or **5Co** as they showed no fluorescence activity. The fluorescence spectra presented do not show emission peaks where they might be expected (~610 nm and 660 nm) and the spectra of the copper metallated strands closely resembles those of the freebase strands, however, both the soret band of the UV-vis absorbance spectra and the CD spectra (see - Figure 39, Figure 40 and Figure 43) clearly show metallation of the samples. The appearance of the spectra may be due to inter-porphyrin interactions (e.g. excitonic coupling) caused by the spatial arrangement of the porphyrins on the DNA strands.

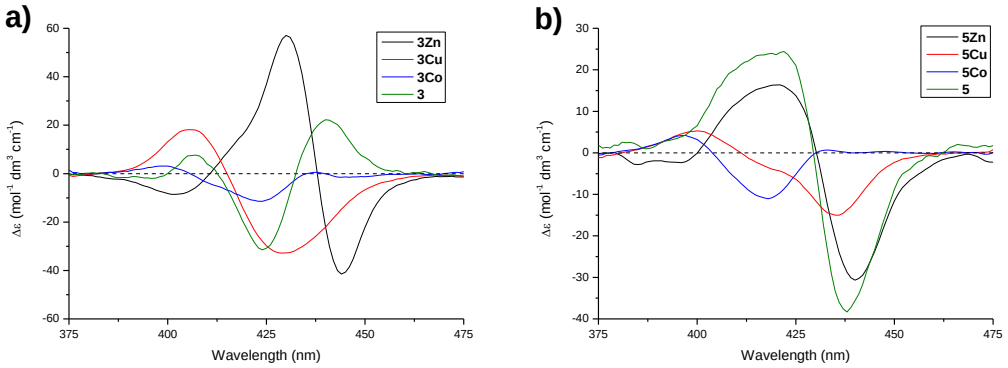

Figure 43. 375 – 475 nm CD spectra of a) **3M** and b) **5M** single strands in 100 mM sodium phosphate, 100 mM NaCl, 1 mM Na_2EDTA, pH 7.0 at room temperature

Metallation of strand **3** leads to dramatically different circular dichroism (Figure 43a), the spectrum of **3** shows a +/-/+ trisignate with maxima at +440/-426/+406 nm. The spectrum of the zinc metallated strand (**3Zn**) shows a trisignate at -444/+430/-402 nm, copper metallation (**3Cu**) leads to a -429/+405 nm bisignate and cobalt metallation (**3Co**) leads to a -424/+399 bisignate.

The circular dichroism spectrum of **5** shows a -/+ bisignate with peak maxima at -438/+422 nm, zinc metallation of this strand (**5Zn**) also shows a -/+ bisignate but with shifted peak maxima (-440/+420 nm, Figure 43b). The copper metallated analogue (**5Cu**) shows a complex bisignate with maxima at -435/+400 nm, however it appears that an additional may be present at -416 nm. Cobalt metallation (**5Co**) shows a -/+ bisignate with peak maxima at -418/+396 nm.

It is clear that metallation of the porphyrin moieties in strands **3** and **5** leads to a significant change in their excitonic coupling, due to the difference in the circular dichroism traces this technique provides a useful tool for determining the metallation state of the porphryins in strands **3** and **5**, which UV-vis alone would be unable to do.

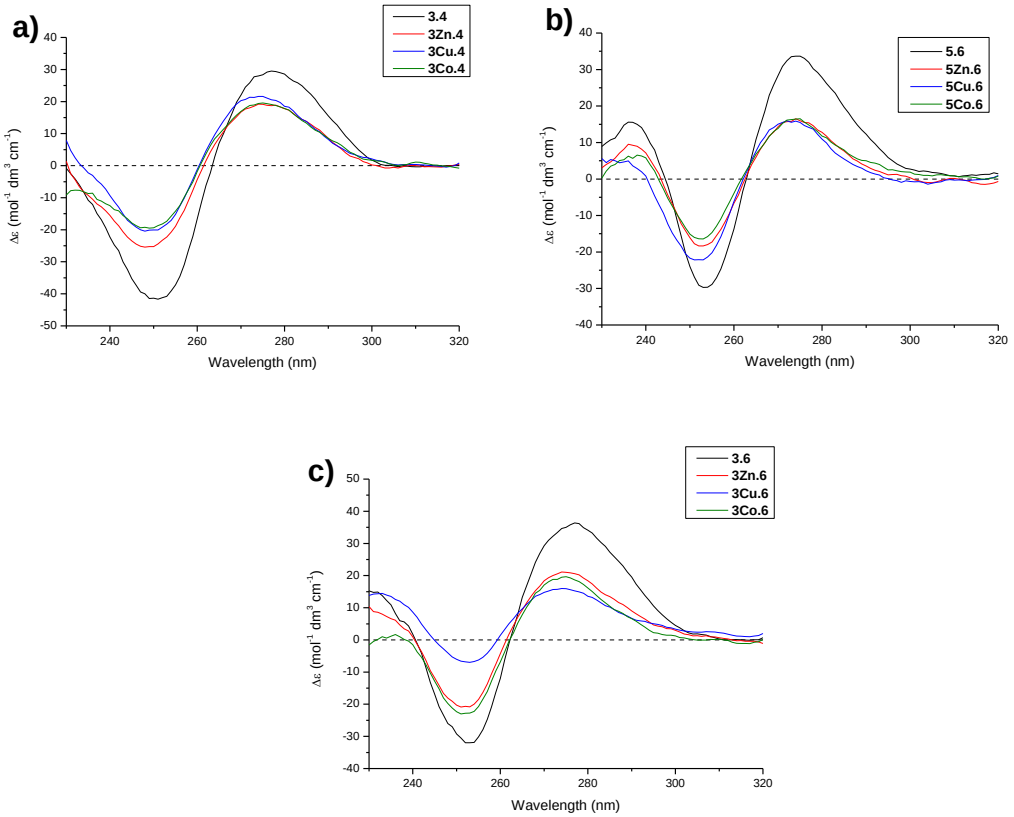

Figure 44. 230 – 320 nm CD spectra of a) **3M•4** b) **5M•6** and c) **3M•6** duplexes in 100 mM sodium phosphate, 100 mM NaCl, 1 mM Na_2EDTA, pH 7.0 at room temperature

Circular dichroism of metallated porphyrin modified duplexes was conducted (Figure 44), this showed that systems where one strand contains metallated porphyrin modification and the other strand contains freebase porphyrin modifications will readily form B-DNA duplexes. The peak maxima of the metallated porphyrin containing duplexes are shifted by less than 2 nanometres, peaks are found at +275/-249, +273/-252 and +275/-252 for **3M•4**, **5M•6** and **3M•6** respectively, shifted from +277/-251, +274/-253 and +277/-253 for **3•4**, **5•6** and **3•6** respectively.

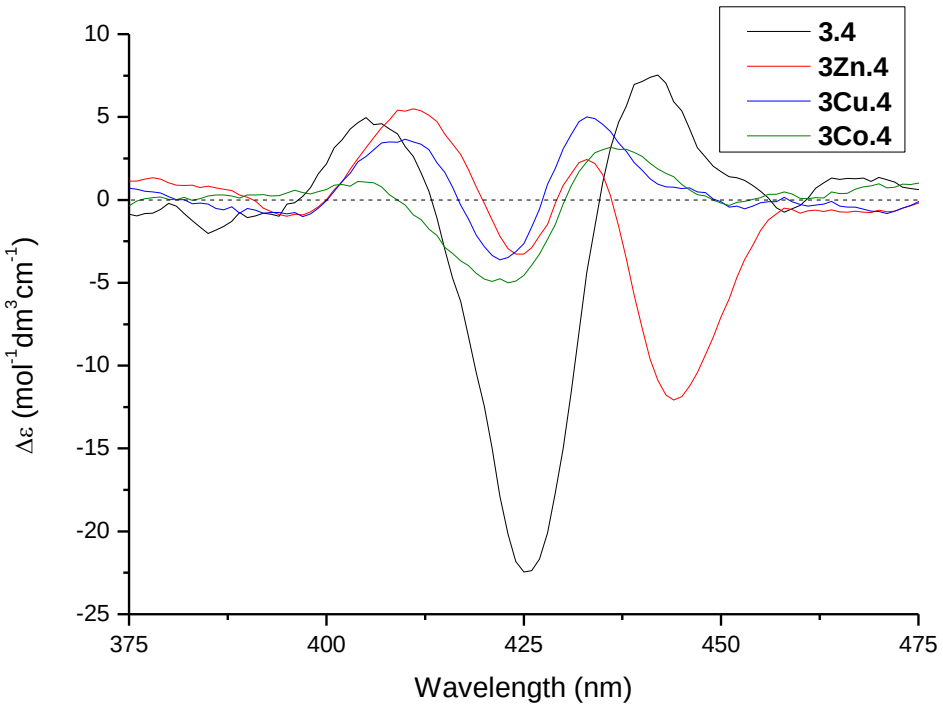

Figure 45. 375 – 475 nm CD spectra of **3M•4** duplexes in 100 mM sodium phosphate, 100 mM NaCl, 1 mM Na_2EDTA, pH 7.0 at room temperature

The Soret bands of the porphyrins bonded to duplex **3•4** appear to be particularly sensitive to metallation (Figure 45), the change in the observed spectra is much more pronounced when measuring CD as opposed to UV-vis absorbsion. Cobalt and copper metallation of the duplexes retains the +/-/+ trisignate, albeit with shifts in peak positions and decreases in peak intensity, as has been mentioned previously (See - 3.13 – Circular dichroism (CD) of offset porphyrin modified DNA system, page 57) there are a number of factors that impact on peak intensity of CD spectra, so it is not possibly to pin point the cause of the drop in peak intensity upon metallation of this duplex. The peak maxima are found at +436/-423/+405 and +433/-422/+410 nm for **3Co•4** and **3Cu•4** respectively. The inclusion of zinc ions into this system shows a marked change in the CD trace, the +/-/+ trisignate of **3•4** becomes a -/+/-/+ tetrasignate with peak maxima located at -444/+433/-425/+411 nm. As has previously been discussed, the CD spectra of **3•4** shows significant excitonic coupling with multiple interactions, the porphyrins in **3•4** behave as linear oscillators and as such both the B_x and B_y transitions contribute to the spectrum as a superposition of signals. As CD is phase sensitive.slight changes to these interactions (i.e. through zinc metallation of the porphyrin macrocycle) leads to very pronounced changes to the CD spectrum.

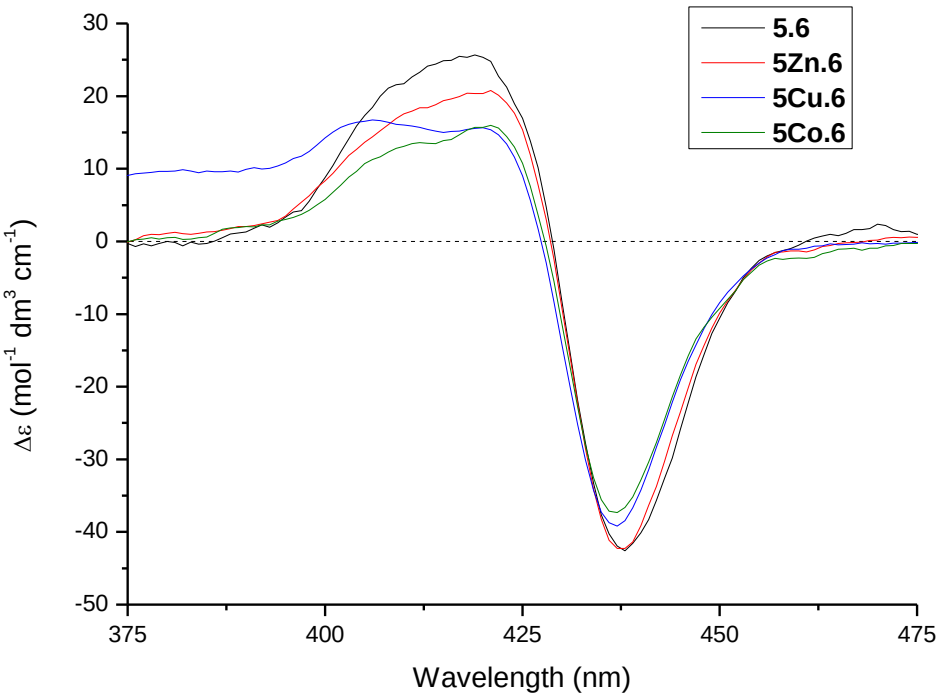

Figure 46. 375 – 475 nm CD spectra of **5M•6** duplexes in 100 mM sodium phosphate, 100 mM NaCl, 1 mM Na_2EDTA, pH 7.0 at room temperature

5M•6 duplexes appear to be much less sensitive to metallation that those of **3M•4** (Figure 46). The CD trace of **5Zn•6** retains the -/+ bisignate profile of the freebase parent duplex (**5•6**). **5Cu•6** and **5Co•6** show similar traces to **5•6** but with the presence of a new shoulder/peak between 400 and 410 nm, giving a -/+/+ trisignate. This 'new' peak is not obvious for **5Zn•6** or **5•6**, however the positive peaks in the spectra are quite broad which may be masking the presence of this signal. Peak maxima are located at -438/+421, -437/+419/+406 and -437/+421/+412 nm for **5Zn•6**, **5Cu•6** and **5Co•6** respectively.

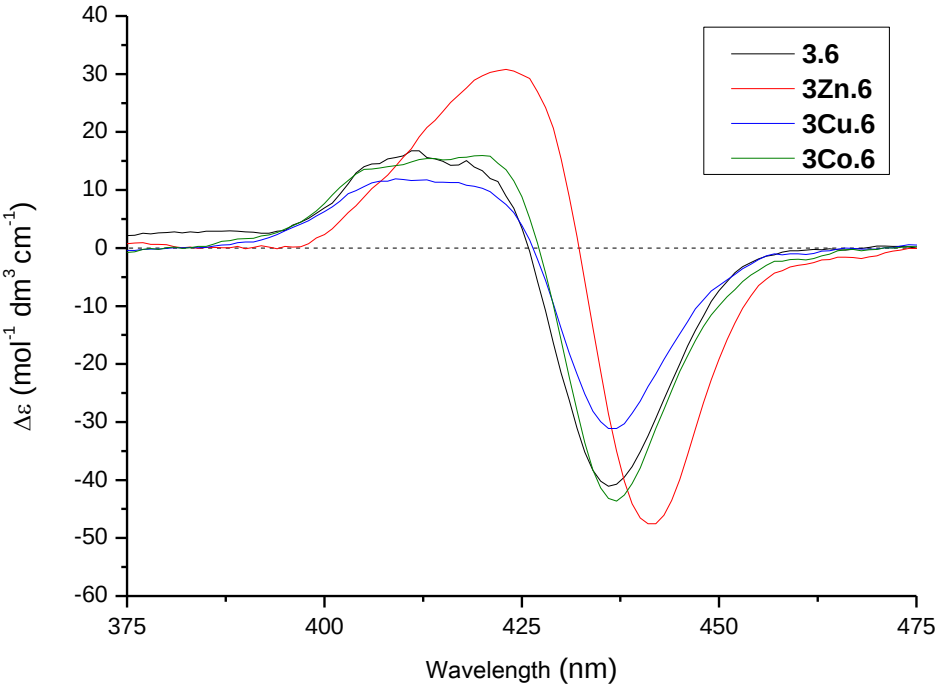

Figure 47. 375 – 475 nm CD spectra of **3M•6** duplexes in 100 mM sodium phosphate, 100 mM NaCl, 1 mM Na_2EDTA, pH 7.0 at room temperature

All **3M•6** duplexes retain the -/+ bisignate character of the parent duplex (**3•6**) with no appearance of new peaks (Figure 47). A pronounced change in the CD trace is observed for **3Zn•6**, showing both an increase in peak intensity and also a redshift of both peak maxima to -441/+423 nm, showing that this duplex system is very sensitive to zinc metallation. Other **3M•6** duplexes show smaller changes in the CD spectra, with comparable peak intensities to those of the parent duplex (**3•6**) and peak maxima at -437/+410 and -437/+420 for **3Cu•6** and **3Co•6** respectively.

The sensitivity of the CD responses of the porphryin modified oligonucleotides to metallation varies across the systems and varies with the metal that is chelated. Duplex **3•4** shows the highest sensitivity to metallation, with significant changes of the CD traces for all three metal ions inserted. Duplex **5•6** shows subtle but detectable changes in the CD traces upon copper and cobalt metallation, but lacks definitive changes to the spectrum upon zinc metallation. Duplex **3•6** appears to be the least sensitive across the range of metals tested, with changes in the CD spectum only being observed on zinc metallation.

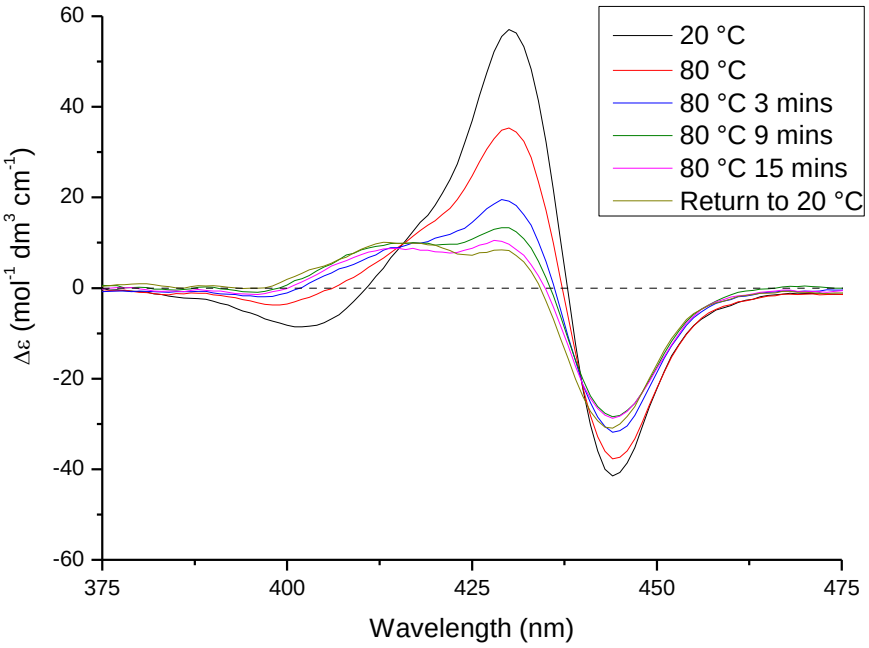

Figure 48. 375 – 475 nm CD spectra of **3Zn** in 100 mM sodium phosphate, 100 mM NaCl, 1 mM Na_2EDTA, pH 7.0 heating and holding at 80 °C and returning to 20 °C

On heating to 80 °C, the CD spectrum of single stranded zinc metallated acetylene linked porphyrin DNA (**3Zn**) was observed to change rapidly (Figure 48). The spectra continue to change on heating, eventually stabilising after a period of 15 minutes and showing no further change after up to an hour at 80 °C, this behaviour was not observed when heating **3Co** or **3Cu**. Heating **3Zn** cause the -/+/- trisignate with peak maxima at -444/+430/-402 nm to adopt a -/+/+ trisignate with peak maxima at -444/+429/+413 nm. All traces share an isochroic point at 415 nm, indicating that there are two species within the sample. The change in the CD traces appear to take on some of the characteristics of the corresponding freebase strand (**3**), which has peak maxima at +440/-426/+406 nm. The chelated zinc ion is reasonably labile despite the tetradentate nature of the porphyrin macrocycle and it is thought that partial demetallation of **3Zn** is occurring on heating.

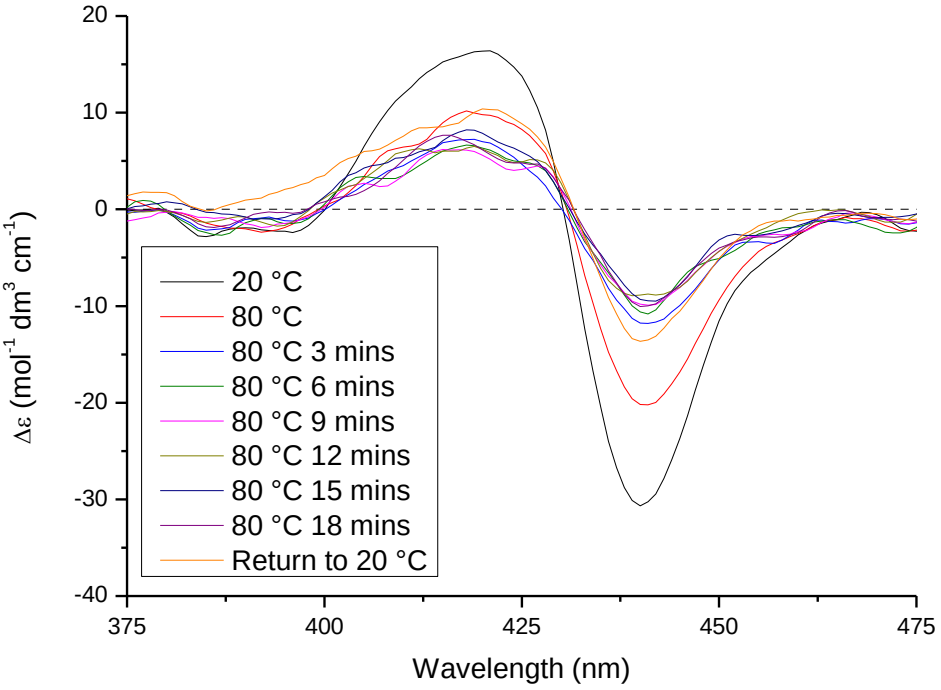

Figure 49. 375 – 475 nm CD spectra of **5Zn** in 100 mM sodium phosphate, 100 mM NaCl, 1 mM Na_2EDTA, pH 7.0 at 20 °C, heating and holding at 80 °C and returning to 20 °C

The same experiment was conducted with **5Zn** (Figure 49), on heating to 80 °C the -/+ bisignate (peak maxima located at -440/+420 nm) decreases in peak intensity about an isochoric at 430 nm for the first 6 minutes, at which point no further change in CD is observed over a 1 hour period. On cooling back to 20 °C the CD trace does increase marginally in peak intensity however it does not reach the level at which it started. Again suggesting that partial demetallation of the strand has occurred on heating.

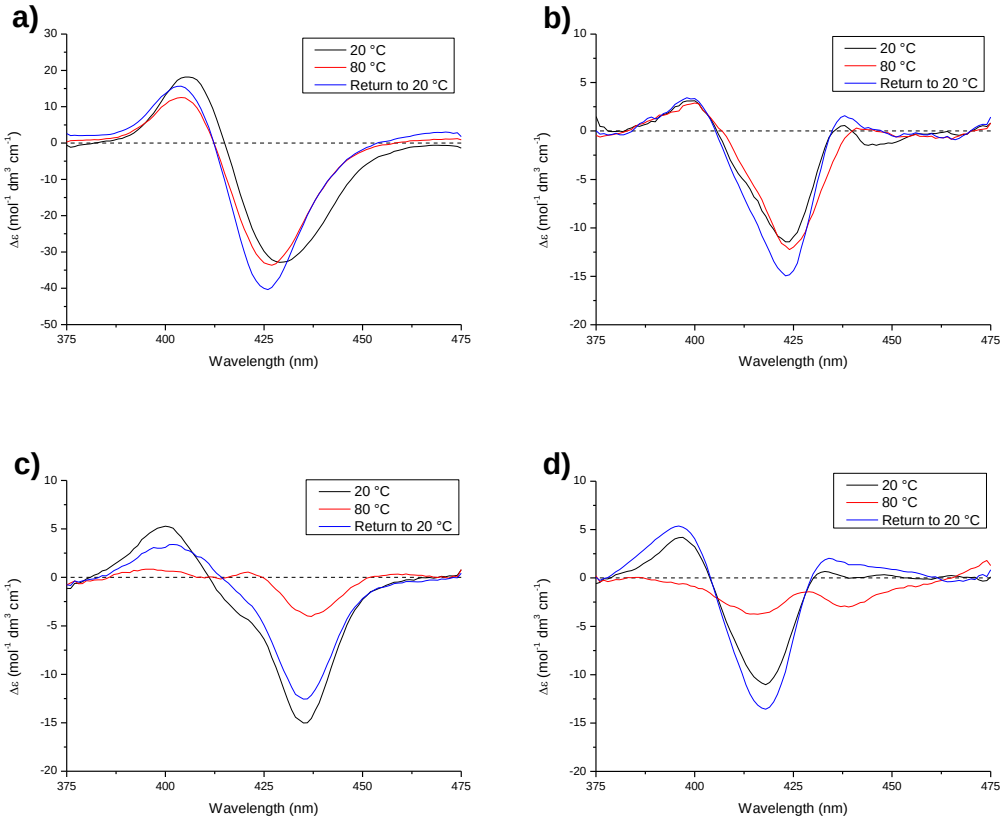

Figure 50. 375 – 475 nm CD spectra of a) **3Cu** b) **3Co** c) **5Cu** and d) **5Co** in 100 mM sodium phosphate, 100 mM NaCl, 1 mM Na_2EDTA, pH 7.0 at 20 °C, 80 °C and returning to 20 °C after 5 minutes

Circular dichroism spectra were collected for strands **3Cu**, **3Co**, **5Cu** and **5Co** at 20 °C before heating to 80 °C and holding for 5 minutes to thermally equilibrate the samples, at which point a additional spectra were collected and the samples cooled back to 20 °C, again the samples were equilibrated for 5 minutes before collecting the second spectra at 20 °C (Figure 50).

3Cu and **3Co** showed little change in the CD spectra on heating and cooling, with peak positions shifting by 3 nm or less, peaks maxima are located at -428/+403 ± 2 nm and +439/-423/+399 ± 2 nm for **3Cu** and **3Co** respectively. Small changes in the peak intensity were observed, the largest of which occurred for the negative peak after cooling back to 20 °C where an increase in peak intensity of ~25 % was observed. Since the profile of the traces did not change on heating and cooling it can be noted that the conformation of the porphryin modified duplex is largely the same and that dematallation has not occurred. The increase in peak intensity is likely due to small changes in stacking of the porphyrins, resulting in changes in the peak intensity, since peak intensity is proportional to the distance squared[148].

5Cu and **5Co** showed a marked change in circular dichroism spectra on heating to 80 °C, the -/+ bisignate of **5Cu** (-435/+401 nm) becomes a simple negative peak at -437 nm, while the -/+ bisignate of **5Co** (-418/+397 nm) becomes a -/- trace with peak maxima at -439/-416 nm. These traces show a large change in the excitonic coupling of the porphyrins on heating which is not observed for the analogous strands containing the shorter acetylene linker (**3Cu** and **3Co**). The longer amide linker combined with the additional rotational freedom about the methylene unit allows the porphryin modified oligonucleotides (**5Cu** and **5Co**) to adopt significantly different conformations when heated to 80 °C compared to those present at 20 °C. On cooling back to 20 °C both **5Cu** and **5Co** show very similar circular dichroism traces to those recorded before heating, as such no significant conformational changes occur on heating and cooling using the parameters listed above. No demetallation is observed for **5Cu** or **5Co**, demonstrating the thermal stability of the copper and cobalt ions within the porphryin macrocycle for both the acetylene linked monomer (**1**) and the amide linked monomer (**2**).

3.15 – Molecular modelling of offset porphyrin modified DNA systems

Molecular modelling of duplexes **3•4**, **5•6** and **3•6** was conducted using Schrodinger's MacroModel, classical mechanical modelling parameters were applied to the systems, i.e. equilibrium bond lengths applied, atoms treated as points in a three dimentional framework with atom sizes governed by the van der Waals radii, electrostatic and torsional forces are minimised to the local minimum. Various energy minimisation forcefields are available for use within the MacroModel package, each of which is optimised for a specific set of molecule e.g. oligonucleotides and proteins (AMBER), small molecules (MM2/MM3) or aromatic molecules (QCFF/PI). It was decided that the best choice of minimising parameters for the molecules of interest would be the Assisted Model Building with Energy Refinement (AMBER) forcefield. Molecular Dynamics (MD) would provide more accurate data on these systems, however in a personal communication, Dr Charles Laughton (School of Pharmacy, University of Nottingham, UK) suggested that a years work would be required to acquire MD simulations on these systems. This was seen as being as an excessive and unnecessary step and as such was not conducted.

For clarity the overhanging single stranded ends to the duplexes were omitted from the modelling and only the central fully hybridised portion of the strands was included. All structures were minimised until the potential energy gradient reached 10^{-2}, this was reached after over ~15,000 iterations. All models were started from the same initial DNA structure (B type DNA) in water.

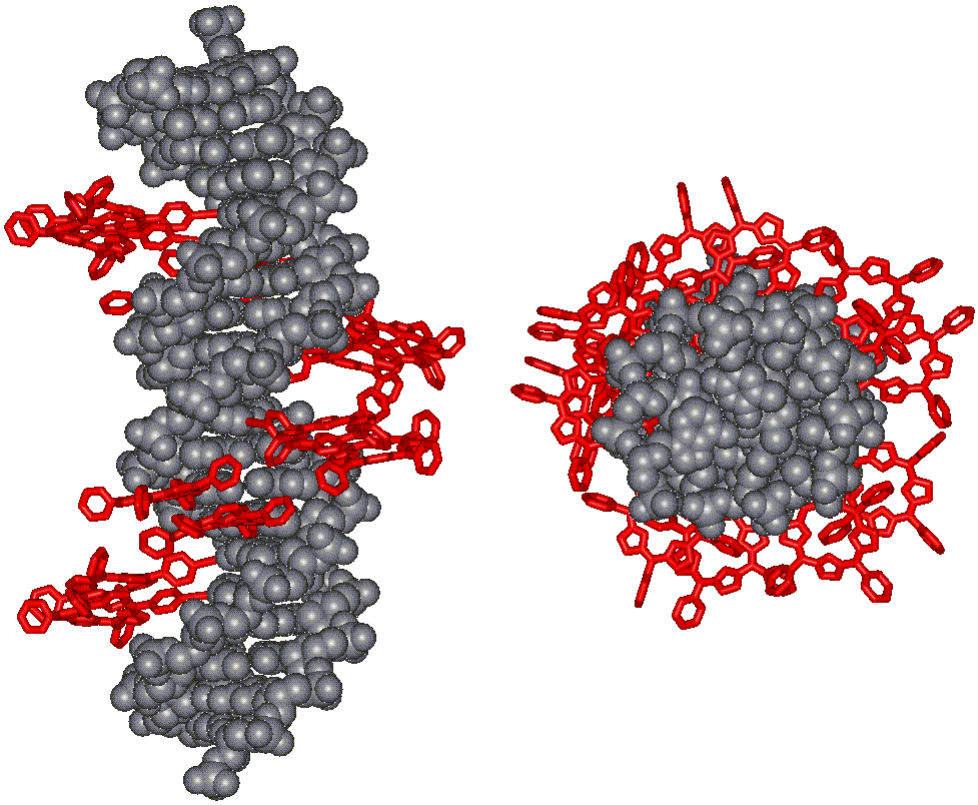

Figure 51. Molecular modelling of **3•4** with overhanging single stranded ends and protons omitted for clarity

Molecular modelling of **3•4** (Figure 51) shows the acetylene linked porphyrin substituents stacking in a pairwise fashion within the major groove of the oligonucleotide. Stacking in this arrangement arises from the rigid linkers being both inflexible and of the same length as one another which leads to two interlinked offset helices of porphrins and gives the appearance of a zig-zag arrangement of the porphryrins as you move along the successive base pairs of the helix. The closest inter-porphyrin distances of this model are 4.3 Å and 6.5 Å with the plane of the porphyrin rings at 71° to the helical axis.

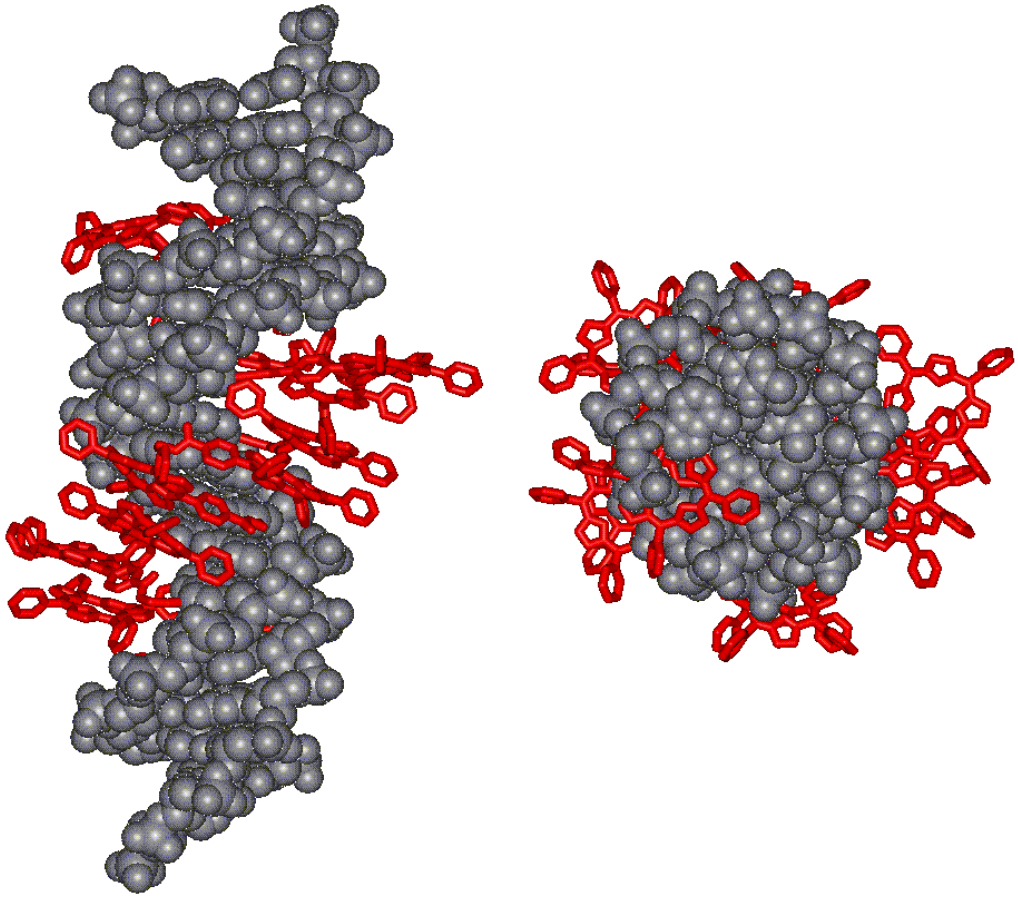

Figure 52. Molecular modelling of **5•6** with overhanging single stranded ends and protons omitted for clarity

The conformational flexibility afforded to the porphyrins in **5•6** by the longer, less rigid amide containing linker allows them to adopt a different stacking arrangement within the major groove (Figure 52). The stacking of the macrocycles is still in a pairwise manner with closest inter-porphyrin distances of 4.4 Å and 7.9 Å, however the orientation of the plane of the porphyrin rings is very different to those in **3•4**, with an angle of 110° between the plane of the porphryin rings and the helical axis.

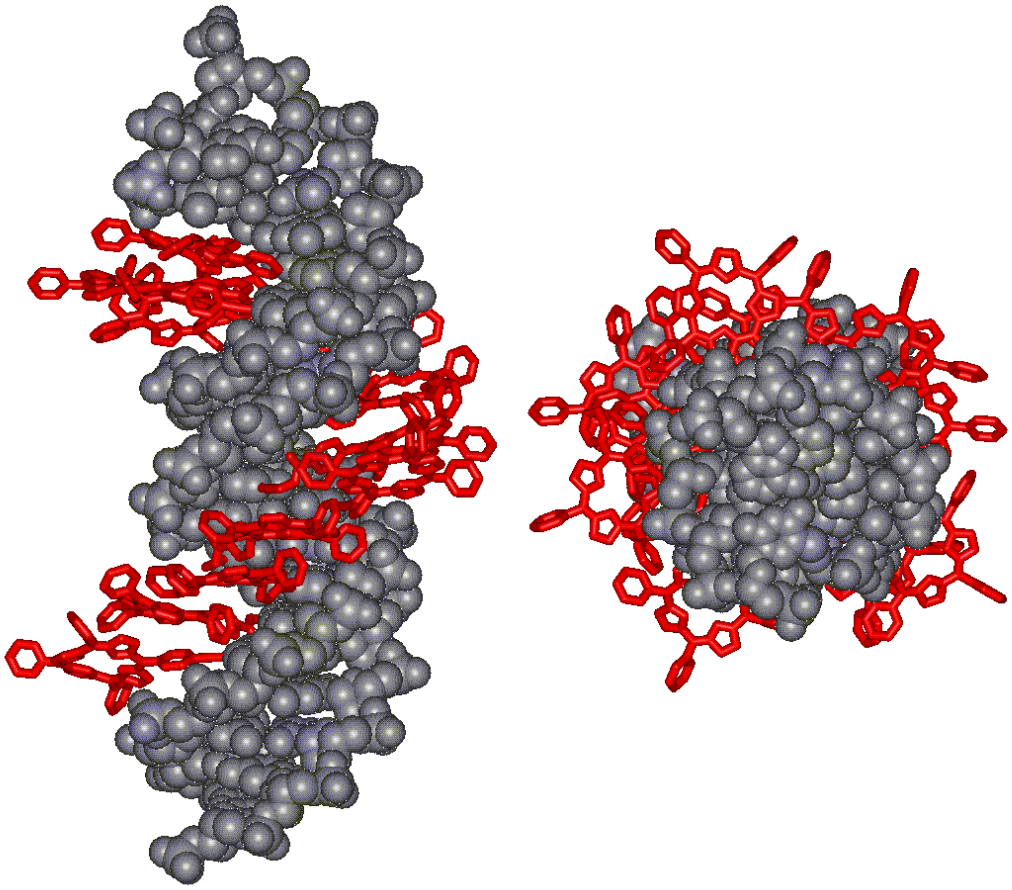

Figure 53. Molecular modelling of **3•6** with overhanging single stranded ends and protons omitted for clarity

Modelling of the hybrid system (**3•6**), where one strand contains the rigid acetylene linker and the other contains the longer, more flexible amide containing linker, shows the porphyrin moieties to stack within the major groove in a much more regular fashion (Figure 53). The pairwise stacking in **3•6** is much less pronounced than it is in **3•4** or **5•6**, with inter-porphyrin distances of 4.5 Å and 5.5 Å and the plane of the porphyrin macrocycles at 94° to the helical axis.

The molecular modelling of **3•4**, **5•6** and **3•6** all show the B type DNA duplex to be stable under the modelling parameters, the porphyrins do not significantly perturb the structure of the duplex but stack in the major groove of the DNA and adopt three very different spatial arrangements within the groove. These observations have all been discussed previously and are backed up by the acquired UV-vis, fluorescence and circular dichroism data of the duplexes (see - 3.9 – UV-vis of offset porphyrin modified DNA system, page 46, 3.10 – Fluorescence of offset porphyrin modified DNA system, page 50 and 3.13 – Circular dichroism (CD) of offset porphyrin modified DNA system, page 57). As such, it is believed that the predicted models are

more than just 'intelligent pictures' and reflect with at least some accuracy the structures adopted by the synthesised oligonucleotides.

3.16 – Aggregation of 5•6 at high concentrations

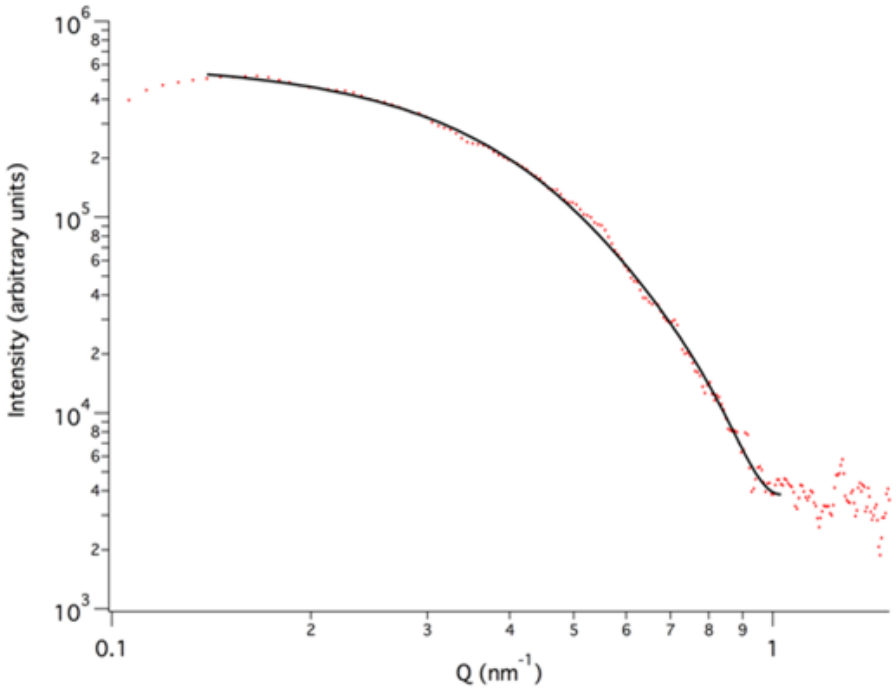

Figure 54. SAXS measurements of **5•6** at 50 μM in 100 mM sodium phosphate, 100 mM sodium chloride, 1 mM Na_2EDTA pH 7.0

Aggregation of the porphyrin modified DNA in solution at high concentrations has previously been observed[155] so a 50 μM sample of **5•6** in 100 mM sodium phosphate, 100 mM sodium chloride, 1 mM Na_2EDTA pH 7.0 was sent for measurement by Small Angle X-ray Scattering (SAXS, Figure 54). SAXS measurements were recorded and analysed by Dr Cameron Neylon of the Rutherford Appleton Laboratory (Didcot, UK).

Various elongated geometric shapes were found to fit the observed data, the simplest of which was a cylinder of radius 3.9 nm and a length of 13 nm. Measurements of the molecular model of **5•6** suggest that the duplex has a width of 1.7 nm and an overall length of 10.5 nm, as such the most probable system that satisfies these dimensions is an aggregation of between two and four duplexes held side-by-side caused by the hydrophobic effect of the porphyrins (Figure 55). Solubility is not affected by this aggregation, there was no precipitation of the DNA and no light scattering was observed in the SAXS experiment.

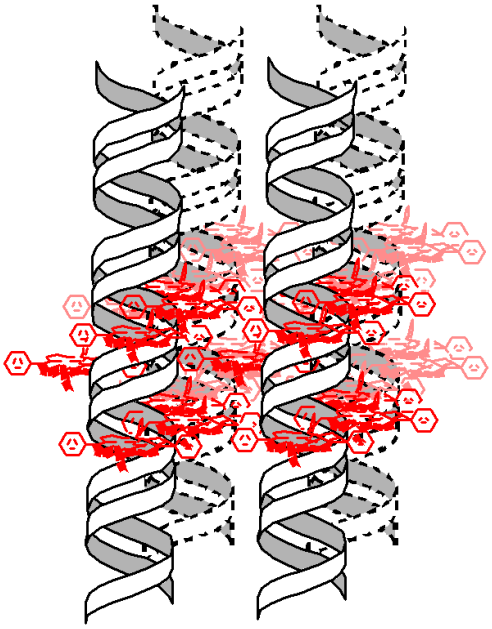

Figure 55. Proposed structure of the aggregates of **5•6** at high concentration (50 μM)

Circular dichroism and absorbance spectra of **5•6** at 1 μM and 56 μM were recorded (Figure 56a); both spectroscopic techniques showed marked differences in the spectra between the high and low concentration samples. As has previously been discussed the CD of the low concentration sample shows a -/+ bisignate with maxima at -438/+419 nm, while the spectrum of the high concentration sample (Figure 56a) shows a +/-/+ trisignate with peak maxima at +454/-437/+416 nm. The peak intensities are also increased in the high concentration sample, this may be due to the increase in close proximity porphyrin macrocycles allowing for more facile excitonic coupling.

The absorption spectra (Figure 56b & c) show that there is a red-shift in the absorption maximum from 411 nm to 419 nm, there is a hypochromicity of the Soret band in the higher concentration sample, demonstrated by the significant decrease of the Soret band's ε value. Serial dilution of a sample of **5•6** (Figure 56d) from 45.4 μM down to 1.0 μM in 100 mM sodium phosphate, 100 mM sodium chloride, 1 mM Na_2EDTA pH 7.0, suggests that aggregation of this sample occurs above a concentration of 33 μM and as such will not affect any of the previous solution phase spectroscopic measurements, all of which were conducted with solution of the order of 1-5 μM.

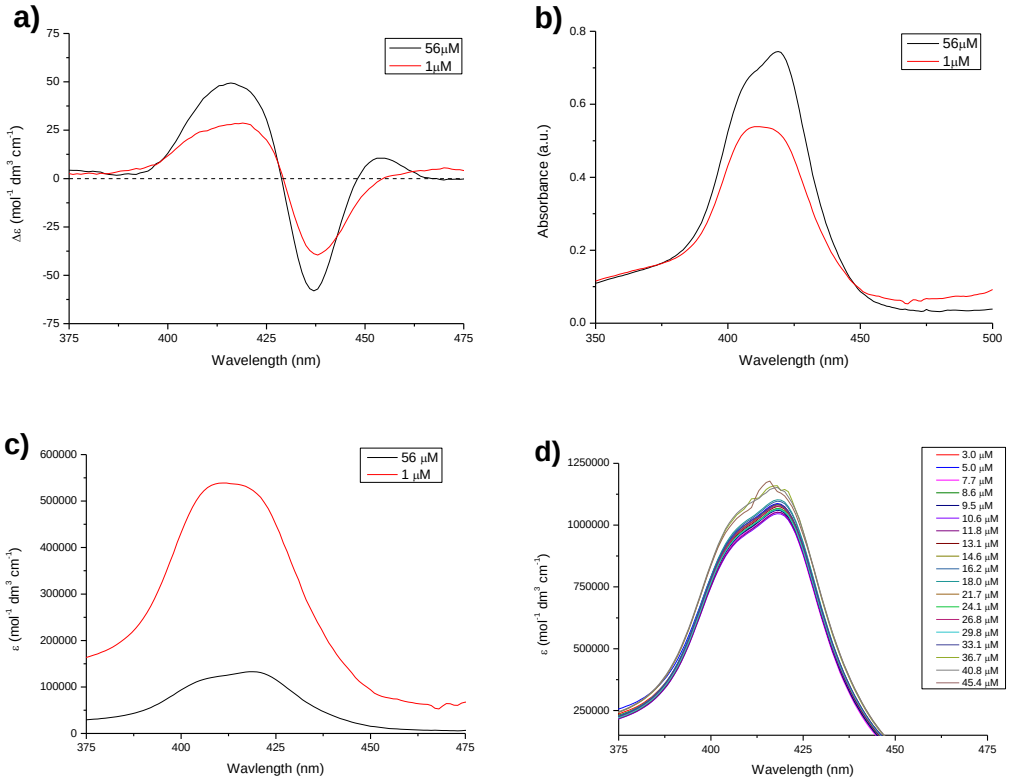

Figure 56. a) 375 – 475 nm CD spectra of **5•6** b) and c) 375 – 475 nm absorption spectra of in **5•6**. d) 375 – 475 nm absorption spectra of a serial dilution of **5•6**. All spectra measured in 100 mM sodium phosphate, 100 mM NaCl, 1 mM Na_2EDTA, pH 7.0 at room temperatu

3.17 – Plans for measuring conductivity

Prof. Hywel Morgan, Dr Maurits de Planque and Dr Sara Aghdaei (University of Southampton) developed a 'lab on a chip' system capable of forming lipid bilayers between two droplets on a surface,[156,157] using this apparatus it is possible to pass a current across the resulting lipid bilayer. The offset porphyrin modified DNA systems (page 43) were designed to have their potential as a supramolecular wire assessed using this apparatus; each of the strands would be dissolved into an unstable vesicle, made of lipids (Figure 57) such as 1,2-dioleoyl-sn-glycero-3-phosphatidylcholine (DOPC) and 1,2-dioleoyl-sn-glycero-3-phosphoethanolamine (DOPE). The dissolution into an organic environment was to be facilitated through the exchange the backbone counterions with tetra-*n*-butyl ammonium ions.

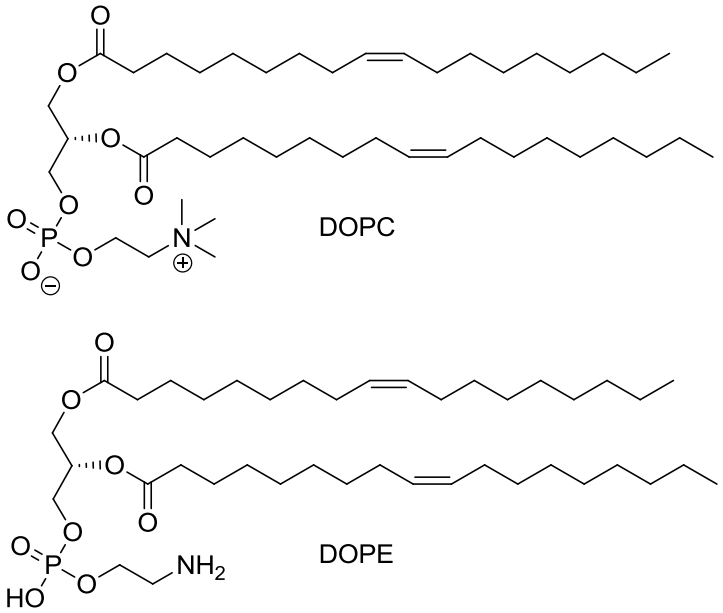

Figure 57. Structures of DOPC and DOPE lipids

The porphyrin modified section of the oligomer strands, being hydrophobic, should reside at least partially within the lipid monolayer due to the hydrophobic effect, the hydrophilic unmodified section of DNA would reside in the aqueous centre of the vesicle. The two vesicles, containing the two complimentary strands would then be driven together on the chip and due to their unstable nature will form a lipid bilayer at their interface (Figure 58). Hybridisation of the duplex at this interface would occur, allowing electronic probing of the system.

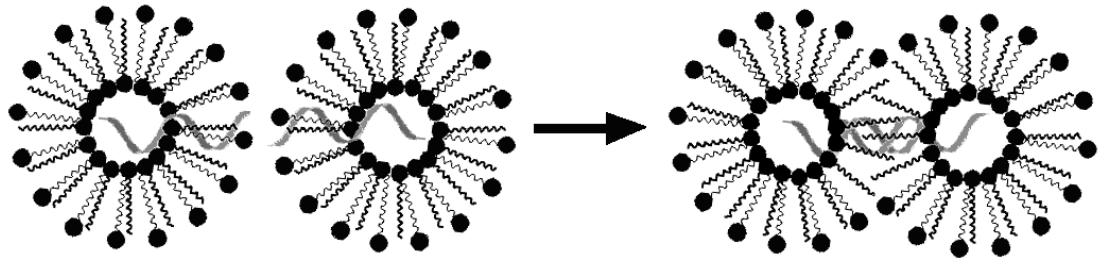

Figure 58. Schematic of lipid bilayer formation

Due to the limited availability of the apparatus and of the expertise required to utilise it, it was not possible to conduct this experiment. Alternate method of probing other porphyrin modified DNA's electron carrying properties were sought, the method decided upon was to tether porphyrin modified DNA to a gold electrode using thiol modifiers at one end of the strand and to incorporate an electrochemical marker at the other end of the strand. Multiple reports of electrochemical analysis of DNA using this method exist in the literature[158-160] using a variety of redox markers, including; ferrocene,[160] methylene blue,[158] anthraquinone[161] and pyrrolo-quinoline-quinone[159] to name a few.

3.18 – Ferrocene modified oligonucleotides for use as electrochemical markers

The synthesis and electrochemistry of ferrocenyl modified nucleotides and ferrocene phosphoramidites are well documented in the scientific literature,[162-167] however, there are also reports of decomposition of the ferricenium cation ($FeCp_2^+$) through nucleophillic attack[168] by hydroxyl, chloride and bromide ions in aqueous media and degradation of the ferrocene redox marker through repeated cyclic voltammetry scans.[169] The synthesis of an amide linked ferrocenyl modified nucleobase was previously published by Grinstaff *et al.*[162] Utilising an alternative synthesis route this target molecule could be synthesised in two steps from the previously synthesised propargylamino-dU (**X**). Due to the quantity of literature detailing the use of ferrocene as an efficient redox marker for oligonucleotides, it was decided that the synthesis of a ferrocene monomer and subsequent incorporation into DNA (**9**, Figure 59) could provide a rapidly accessible solution that was worthwhile trying.

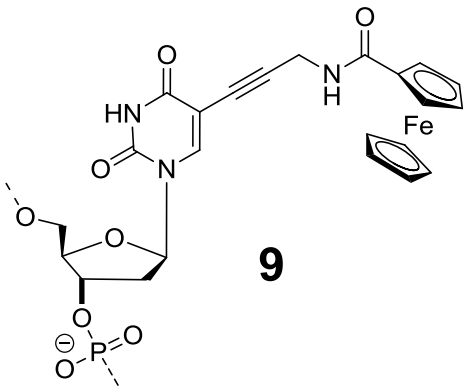

9

Figure 59. Incorporated ferrocene monomer

3.19 – Synthesis route to ferrocene modified nucleotide monomer

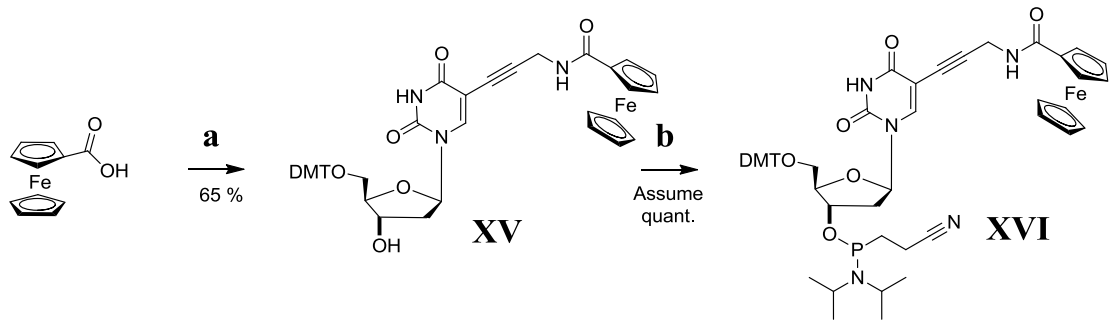

a - **X**, EDC, HOBt, DMAP, DCM, 65 % **b** - CEP-Cl, DIPEA, Assume quantitative

Scheme 13. Synthesis route for ferrocene modified nucleotide monomer

Ferrocene carboxylic acid and 5'-DMT-5-propargylamino-dU (**X**) were coupled using the standard peptide coupling reagents, EDC and HOBt, the reaction proceeded with a moderate yield of 65 % (Scheme 13). Several products were formed during the reaction, however purification was straightforward, requiring a single silica chromatography column.

The ferrocene modified nucleotide amidite (**XVI**), as with other phosphoamidites, was not prepared until required. Synthesis of **XVI** was straightforward, with the reaction reaching completion within a few hours, generally purification was as per the porphyrin phosphoramidites (**VII** and **XIV**), that is simply washing away the excess CEP-Cl and DIPEA with hexanes and using the crude material for DNA synthesis. However, due to the more stable nature of the ferrocene modified nucleotide amidite (**XVI**) compared to porphyrin phosphoramidites (**VII** and **XIV**) due to the absence of a porphyrin moiety, column chromatography was performed and characterisation of **XVI** achieved. Column chromatography was not successful in removing all traces of CEP-Cl and as such an accurate yield can not be stated for this reaction, neither can accurate concentrations be stated for the UV-Vis and fluorescence data; relative peak intensity is stated in absence of log ε values. ^{1}H NMR and ^{13}C{^{1}H} NMR confirmed the presence of excess CEP-Cl in the product after column chromatography. Washing the crude product with hexanes as per the usual phosphoamidite purification prior to column chromatography would have allowed the collection of data of the pure product.

3.20 – Synthesis of ferrocene modified oligonucleotides

The ferrocene monomer (**XVI**) was prepared immediately before use and was dissolved in 1:1 DCM:MeCN to a concentration of 100 mM and test couplings of this phosphoramidite solution were coupled over 5 minutes and 10 minutes coupling time on a 1 mmole scale; both couplings used 11.20 equivalents of the ferrocene monomer. The same sequence was used for both test couplings (Figure 60).

3' – ACT TAG **F**GA ACC GAT – 5' **10**

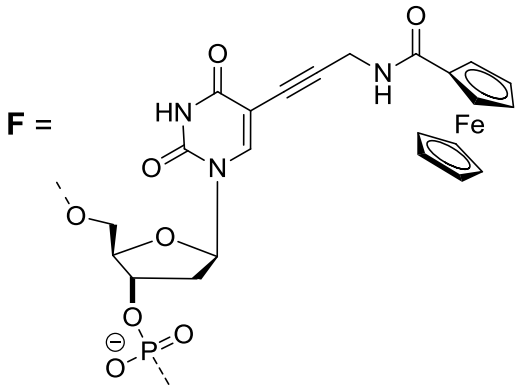

Figure 60. Ferrocenyl DNA test sequence

Coupling the ferrocene monomer (**XVI**) over 5 minutes gave a yield of 347 nmoles, while a 10 minute coupling gave a yield of 446 nmoles, mass spectrometry confirmed the presence of the desired product with no evidence of degradation or side products.

Having demonstrated that the ferrocene monomer couples with sufficient efficiency and that no degradation of the product occurs either during the synthesis or the purification of the strands, a much more heavily modified duplex was planned (Figure 61).

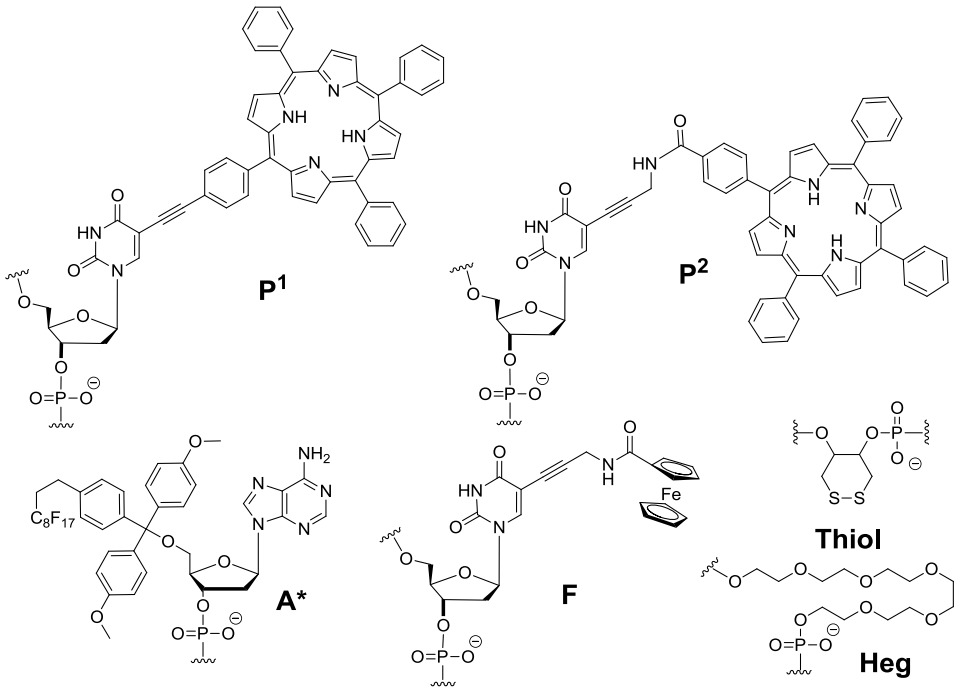

3' – (**Thiol Heg**)$_3$ **P^1**A**P^1** A**P^1**A **P^1**A**P^1** A**F**C GCT AC**A*** – 5' **11**

5' – **A*P^2**A **P^2**A**P^2** A**P^2**A **P^2**AG CGA TGT – 3' **12**

Figure 61. Synthesised porphyrin, ferrocene and thiol modified strands and incorporated monomers

The synthesis of strand **11** (Figure 61) requires the use of a universal support to which the commercially available cyclic dithiol phosphoramidite (**Thiol**) and hexa-ethylene glycol phosphoramidite (**Heg**) were coupled. The manufacturer's recommendation for efficient incorporation of multiple cyclic dithiol molecules is that the monomers should be alternated with hexa-ethylene glycol linked monomers. The thiol and the heg linkers are incorporated following the manufacturer's recommended coupling protocols and are included to allow for facile adsorption of the duplex to a gold electrode.

Duplex **11•12** was designed to incorporate 10 porphyrin modified nucleobases in a zipper formation, spanning approximately one helical turn of the duplex (~3.4 nm). The porphyrins are located immediately after the thiol and heg linkers in order to hold the porphyrin 'wire' as close to the surface as possible. The previously described ferrocene modified nucleobase (**F**) is located immediately after the porphyrin modifications and is incorporated onto the strand that is bound to the surface to allow for electrochemical probing of both the surface bound single strand and the surface bound duplex. Strands **11** and **12** both terminate at the 5' end with a fluorous tagged adenosine monomer to allow for facile purification of the strands.

The syntheses of strands **11** and **12** were very low yielding, with only 8 and 12 nmoles of the target strand synthesised respectively. The trityl measurements made by the DNA

synthesiser during the synthesis of strand **11** showed that the initial coupling of the commercial cyclic dithiol monomer to the universal support was poor. Unusually, the trityl reading of strand **12** showed a relatively poor coupling efficiency of the amide linked porphyrin monomer (~80 % coupling efficiency). Due to the scarcity of material the strands were characterised by UV-vis and fluorescence spectroscopy only before sending to Robert Johnson (Prof. Phil Bartlett's group, University of Southampton, UK) for preliminary cyclic voltammetry measurements.

Strand **11** was dissolved in 10 mM Tris buffer (pH 7.2) and adsorbed onto a 1 mm diameter gold disc electrode before cyclic voltammetry measurements were collected. The CV spectra of strand **11** did not show any redox peaks at all, simply a double layer capacitance. Since no redox activity was detected electrochemical desorption of the DNA[170] from the surface was ruled out, two possible situations may have occurred; the DNA did not functionalise the surface, or, the ferrocene moiety has degraded.

Steel *et al.*[171] developed a method using chronocoulometric response curves to quantifying the coverage of DNA on adsorbed to a gold surface. Their technique relies on the measurement of the charge built up on the electrode surface with and without the presence of ruthenium hexamine, a redox marker known to bind quantitatively to the olignucleotide's phosphate groups *via* electrostatic attractions.[172] The difference in the charge built up allows the number density of the redox marker, and hence the DNA, to be worked out. Typical values are of the order of 1-10 x 10^{12} molecules cm^{-2}. Robert Johnson (Prof. Phil Bartlett's group, University of Southampton, UK) determined the surface density of strand **11** on the measured gold electrode to be 1.3 x 10^{12} molecules cm^{-2}. As such it can be concluded that strand **11** binds to the gold electrode surface as would be expected and the reason for not observing any redox activity is due to decomposition of the ferrocene moiety. As has previously been discussed this was always a possibility.

An additional ferrocene modified strand (**11a** and **11b**) with cyclic di-thiol and hexa-ethylene glycol monomers was synthesised in order to test the suitability of the ferrocene monomer to act as a redox couple. Once again the coupling of the commercially obtained cyclic di-thiol monomer onto the universal support was very poor, resulting in a low yielding synthesis (37 nmoles from a 1 μmole synthesis), mass spectrometry could not confirm the presence of the desired product and cyclic voltammetry did not show any redox active species. At this point it was decided that an alternative redox active probe should be synthesised.

3.21 – Ruthenium *tris*-bipyridyl modified nucleotides for use as electrochemical markers

Various examples of different ruthenium *tris*-bipyridyl modified oligonucleotides exist in the literature, including; 5'-terminal modifiers,[173] 5'-amino modifiers,[174] 7-modified C7-deaza-dC[175] and 5-modified dU.[175,176] These are synthesised for both their spectroscopic and electrochemical properties. The ruthenium *tris*-bipyridyl monomers exhibit a number of favourable properties for these applications; they are fluorescent with high quantum yields,[177] the three bidentate ligands are stable and resilient to ligand exchange[173,177] and the ruthenium centre shows reversible electrochemical behaviour.[176]

It was decided to synthesise a previously published ruthenium *tris*-bipyridyl modified nucleotide monomer[176] but *via* a different synthetic route. Grinstaff *et al*. protect the 3'- and 5'-hydroxyls with benzoyl protecting groups, before cleaving them and reprotecting the 5'-hydroxyl with a DMT protecting group. These steps were to be omitted in the proposed synthesis of the monomer (Figure 62).

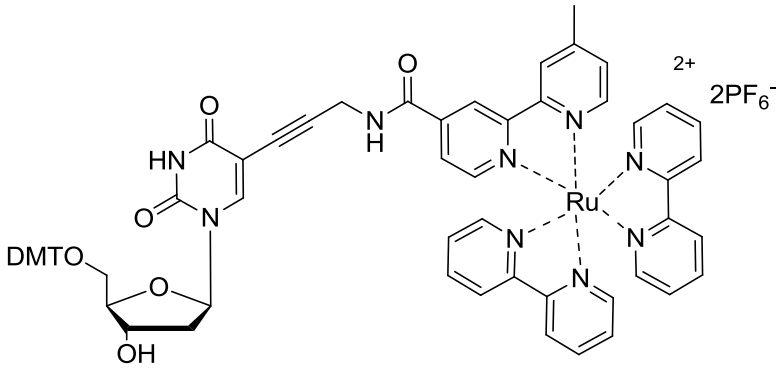

Figure 62. Ruthenium *tris*-bipyridyl monomer

3.22 – Synthesis route to ruthenium *tris*-bipyridyl modified nucleotide monomer

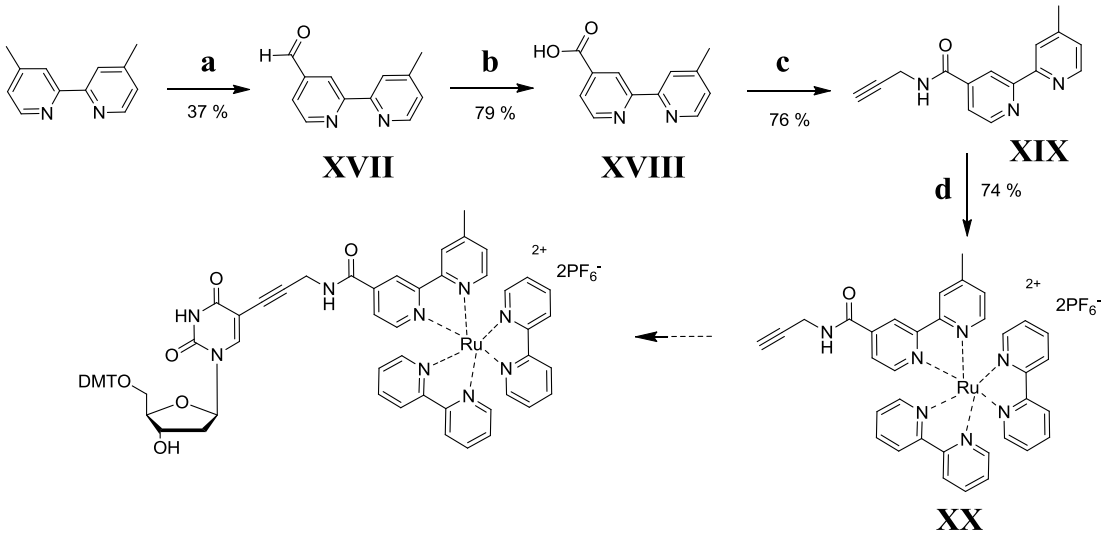

a - SeO2, dioxane, 125 °C, 37 % **b -** $AgNO_3$, NaOH, ethanol, H_2O, 79 % **c -** propargylamine, DCC, HOBt, DIPEA, DMF, 76 % **d -** i) $Ru(bpy)_2Cl_2$, EtOH, H_2O, reflux, ii) KPF_6 74 %

Scheme 14. Synthesis route for ruthenium tris-bipyridyl modified nucleotide monomer

4,4'-dimethyl-2-2'-bipyridyl-4'-carboxaldehyde (**XVII**) was prepared *via* a selenium (IV) oxidation of 4,4'-dimethyl-2-2'-bipyridine as per literature methods[176] (Scheme 14), chromatography is not required to purify **XVII** due to a well thought out work up procedure. Hot filtration removes selenium byproducts, basic extractions remove any 4,4'-dimethyl-2-2'-bipyridyl-4'-carboxylic acid side product, sodium metabisulphite extractions take the product (**XVII**) into the aqueous phase as the aldehyde bisulphite, adjusting the pH of this aqueous solution to pH 10 and extraction into DCM isolates the product in 37 % yield.

4,4'-dimethyl-2-2'-bipyridyl-4'-carboxylic acid (**XVIII**) was formed by an oxidation of **XVII** with silver nitrate and sodium hydroxide as per literature methods[176]. The insoluble silver (I) oxide side product was filtered off and purification of the product was achieved by basic extractions, followed by re-acidification, allowing the product, **XVIII**, to precipitate with a yield of 79 %.

Three methods of synthesising **XIX** were tried; PyBrOP gave the product in 34 % yield requiring purification by column chromatography; DIC and HOBt gave the product in 39 % yield requiring purification by column chromatography and crystallisation to remove the last traces of the *N*-acylurea side product; lastly DCC and HOBt gave the product in 76 % yield, requiring purification by column chromatography.

Ruthenium (IV) (*N*-(prop-2-ynyl)-4-methyl-2-2'-bipyridyl-4'-carboxamide) $(bipy)_2$ *bis*-hexafluorophosphate salt (**XX**) was prepared by refluxing **XIX** with ruthenium *bis*-bipyridyl-*bis*-chloride overnight, the product precipitates after the introduction of potassium hexafluorophosphate to the reaction mixture and is recovered in 74 % yield.

At this point in the synthesis problems were encountered: **XX** was coupled with 5'-DMT-5-iodo-dU (**IV**) *via* a Sonogashira coupling, however the resulting ruthenium *tris*-bipyridyl nucleoside monomer could not be isolated. The product and the unreacted starting material (**XX**) would not move off of the baseline of a TLC plate without the introduction of a salt into the eluent; acetonitrile, saturated aqueous potassium nitrate and water were used in ratios between 20:1:3 and 50:1:3 which caused the ruthenium compounds to streak through the column, giving no resolution at all. A change in synthetic route was introduced at this point, changing the hexafluorophosphate counterions for nitrate counterions (Scheme 15).

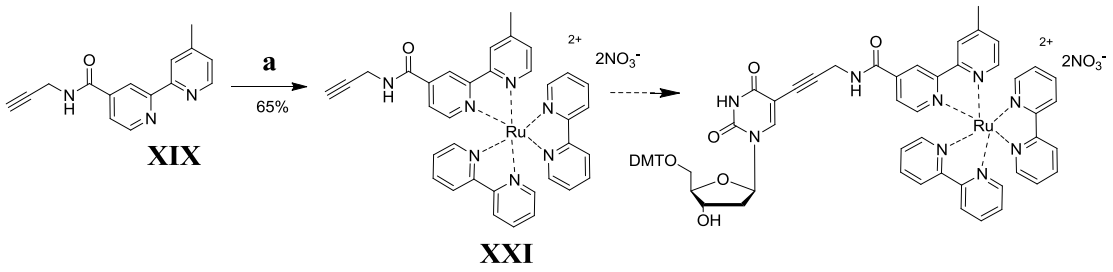

a - i) $Ru(bpy)_2Cl_2$, EtOH, H_2O, reflux, ii) KNO_3, 65 %

Scheme 15. Synthesis route for ruthenium tris-bipyridyl modified nucleotide monomer

The synthesis of **XXI** (Scheme 15) was performed analogous to that of **XX** but with the addition of potassium nitrate to the reaction mixture as opposed to potassium hexafluorophosphate. Purification was conducted by column chromatography on silica using a 20:1:3 mixture of acetonitrile:saturated potassium nitrate:water as the eluent to give **XXI** in 65 % yield. All ruthenium salts that are purified using this solvent system require concentrating *in vacuo* and then redissolving in an apolar solvent that the compound is most soluble in, typically DCM, followed by filtration to remove the potassium nitrate from the product.

Repeated attempts to couple 5'-DMT-5'-iodo-dU (**IV**) to **XXI** were made, NMR suggested the ruthenium *tris*-bipyridyl modified monomer was present in the crude product mixture, however could not be isolated as a pure product. A test coupling of **XXI** to 5'-iodo-dU was tried with the intention of protecting with the 4-4'-dimethoxytrityl group after coupling (Scheme 16).

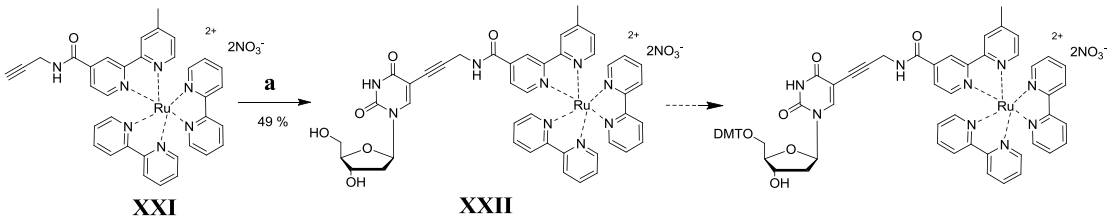

a - 5-iodo-dU, $Pd(PPh_3)_4$, CuI, TEA, DMF, 49 %

Scheme 16. Synthesis route for ruthenium tris-bipyridyl modified nucleotide monomer

XXI was coupled to 5-iodo-dU to give **XXII** in a modest 49 % yield (Scheme 16). Two attempts were made to DMT protect **XXII**; firstly one equivalent of DMT-Cl was added to the reaction mixture in pyridine as per usual, when no reaction occurred the number of equivalents was successively increased to 40 equivalents, no reaction occurred within a 7 days; secondly, due to the S_N1 nature of the reaction, a weakly co-ordinating counterion, silver triflate, was added in an attempt to promote the disassociation of the DMT group from the attached chlorine, but up to 2 equivalents had no affect on the reaction. The unprotected ruthenium *tris*-bipyridyl monomer (**XXII**) could not be DMT protected.

Another modification was made to the synthetic route, this time an attempt to couple the ruthenium *tris*-bipyridyl moiety to the nucleoside *via* an amide coupling was made (Scheme 17).

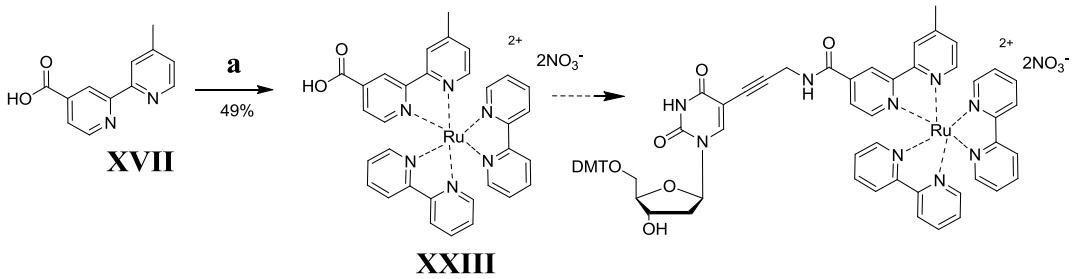

a - i) $Ru(bpy)_2Cl_2$, EtOH, H_2O, reflux, ii) KNO_3, 49 %

Scheme 17. Synthesis route for ruthenium tris-bipyridyl modified nucleotide monomer

XXIII (Scheme 17) was synthesised as per the previous ruthenium tris-bipyridyl compounds by refluxing in ethanol and water to give the desired product in 49 % yield. DCC and HOBt were used to couple **XXIII** and **X**; TLC showed the presence of what is believed to be the desired product; an orange spot, indicative of a ruthenium *tris*-bipyridyl species, which on dipping into anisaldehyde solution became vibrantly orange, indicative of the cleavage of the DMT protecting group liberating the highly coloured aromatic DMT cation, and on heating after dipping into anisaldehyde turns dark blue/black, indicative of a sugar moiety. After partial purification of the reaction mixture MALDI-ToF in positive ion mode showed peaks at mass

890.5 Da – the detritylated monomer minus both counterions, and 1192.7 – the tritylated product minus both counterions. Once again only the detritylated adduct could be isolated, it was found that with every chromatography column run more and more product lost the 4-4'-dimethoxytrityl protecting group. It is thought that the very mildly acidic solution of potassium nitrate (pH 6.2) in water used in the eluent, when combined with the siloxy groups of the silica stationary phase, was sufficient to cleave the DMT protecting group. Triethylamine was added to the eluent in order to prevent this, however deprotection was still observed. No further attempts to synthesise the ruthenium *tris*-bipyridyl monomer were attempted. Future attempts by this synthesis route may be more successful using alternate counterions, e.g. perchlorate, thereby avoiding the use of potassium nitrate solutions in eluents for column chromatography. Another contributing factor for not pursuing the use of the ruthenium *tris*-bipyridyl monomer as a redox marker was the high potentials required to oxidise and reduce the ruthenium centre. The cyclic voltammetry of compound **XX** was measured by Robert Johnson (Prof. Phil Bartlett's group, University of Southampton, UK) and shown to have oxidation and reduction peaks at 1.146 V and 1.013 V vs SCE respectively (Figure 63). Cycling to these potentials could result in charge transfer through the DNA leading to oxidative damage,[178] electrochemical desorption of the oligonucleotide from the electrode surface[170,179] or an unfavourable conformation of the oligonucleotides on the gold surface[180] due to attractive forces on the anionic backbone.

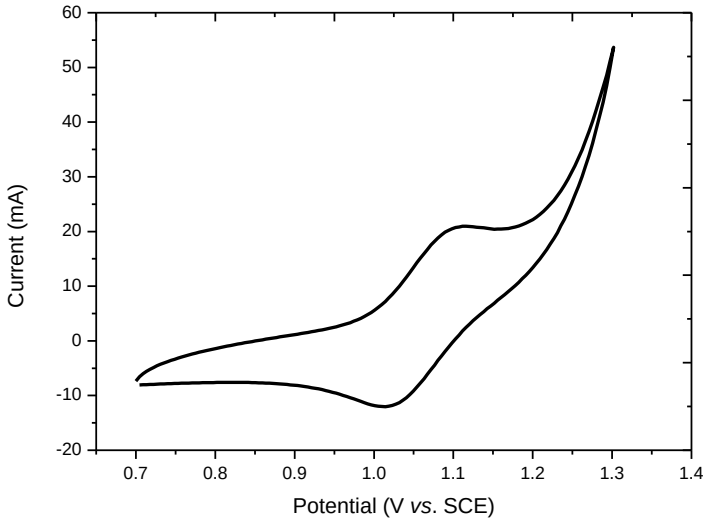

Figure 63. Cyclic voltammetry of **XX** *vs.* SCE

3.23 – Naphthalene diimide modified oligonucleotides

Naphthalene diimide moieties (Figure 64) are often used in charge transfer reactions. Several examples exist[106,181,182] of charge transfer diads and triads, with electron movement from a freebase porphyrin to a naphthalene diimide for the diad species, and from a zinc metallated porphyrin to a freebase porphyrin to a naphthalene diimide for the triads (Figure 64); lifetimes of these charge separated systems have been measured up to 80 μs.[106] The naphthalene diimide moiety has proved itself to be an ideal replacement for an ubiquinone when mimicking photosynthesis,[183] with a favourable reduction potential and minimal spectral overlap with the zinc porphyrin. Naphthalene diimides have also found use as semiconductors in field effect transistors (FET)[184] and as such a naphthalene diimide modified nucleotide was a tempting molecule to explore, especially if combined with a porphyrin modified nucleotide within an oligonucleotide strand, leading to the formation of a unidirectional charge transfer system.

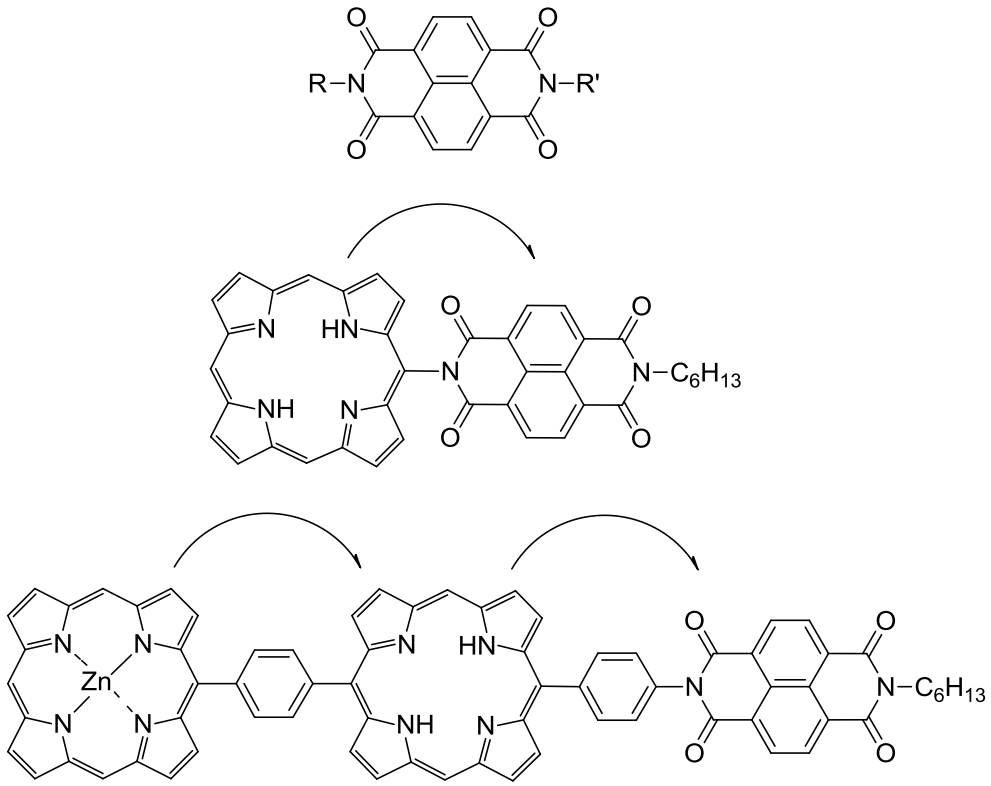

Figure 64. Naphthalene diimide structure with example diad and triad structures[176]

3.24 – Synthesis route to naphthalene diimide modified nucleotide monomer

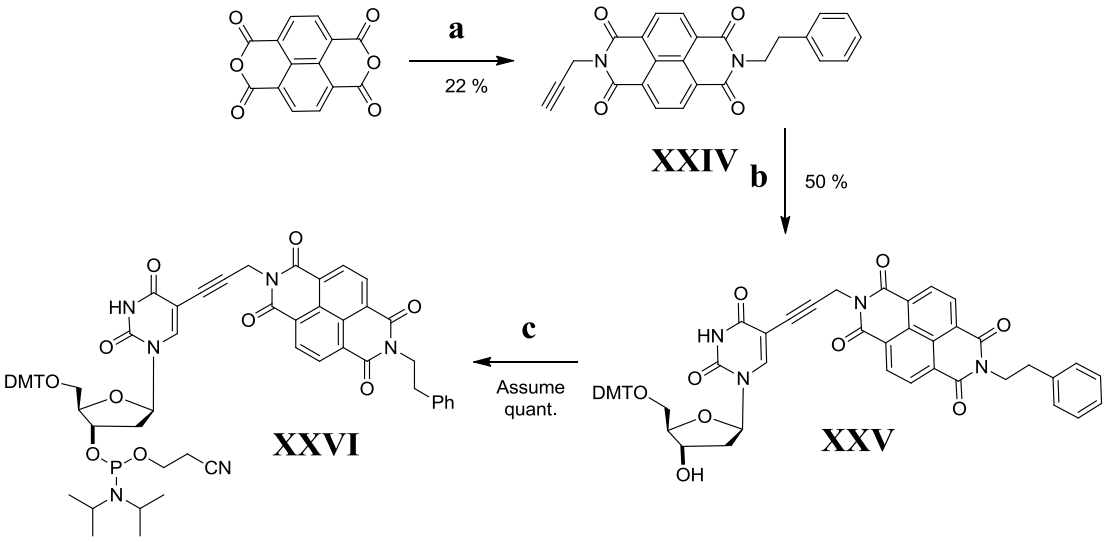

a - propargylamine, phenylethylamine, DMF, 120 °C, 22 % **b -** IV, $Pd(PPh_3)_4$, CuI, TEA, DMF, 50 % **c -** CEP-Cl, DIPEA, Assume quantitative

Scheme 18. Synthesis route for naphthalene diimide modified nucleotide monomer

Naphthalene-1,4,5,8-tetracarboxylate dianhydride, propargylamine and phenylethylamine were heated to 120 °C in DMF to form a statistical mixture of three naphthalene diimides, *N-N'-bis*-(prop-2-yne)-naphthalene diimide, *N-N'-bis*-(ethylbenzene)-naphthalene diimide and the desired product, *N*-(prop-2-yne)-*N'*-(ethylbenzene)-naphthalene diimide (**XXIV**, Scheme 18). Phenylethylamine was chosen as the second primary amine in the synthesis of **XXIV** over a smaller primary amine, such as methylamine, in the hope that it would increase solubility of the product and would aid resolution between the three naphthalene diimides formed. With regards to the former, it was a successful choice, with regards to the latter it was the wrong choice. The three naphthalene diimides synthesised have very similar R_f values in a variety of solvent systems, with *N-N'-bis*-(prop-2-yne)-naphthalene diimide having the highest R_f and *N-N'-bis*-(ethylbenzene)-naphthalene diimide the lowest. As such a yield of 22 % of the desired product (**XXIV**) was achieved after purification by six chromatography columns.

Coupling of the naphthalene diimide **XXIV** to 5'-DMT-5-iodo-dU (**IV**) *via* a Sonogashira coupling to give the naphthalene diimide modified nucleoside **XXV** proceeded with a moderate yield of 50 %.

The phosphitylation of **XXV** was only performed when required, with the reaction proceeding comparatively slowly and requiring additional portions of CEP-Cl and DIPEA

added to the reaction mixture in order for it to reach completion. Purification of **XXVI** was performed by washing with hexanes before using the crude product immediately in DNA synthesis, as such the product was not fully characterised.

3.25 – Synthesis of naphthalene diimide modified oligonucleotides

Naphthalene diimide modified nucleotide phosphoramidite (**XXVI**) was synthesised immediately prior to use and a 50 mM solution in 1:1 DCM:MeCN was used for DNA synthesis with a coupling time of 5 minutes. Two naphthalene diimide containing oligonucleotides were synthesised, **13** and **14** (Figure 65), containing one and two naphthalene diimide modified bases (**N**) respectively.

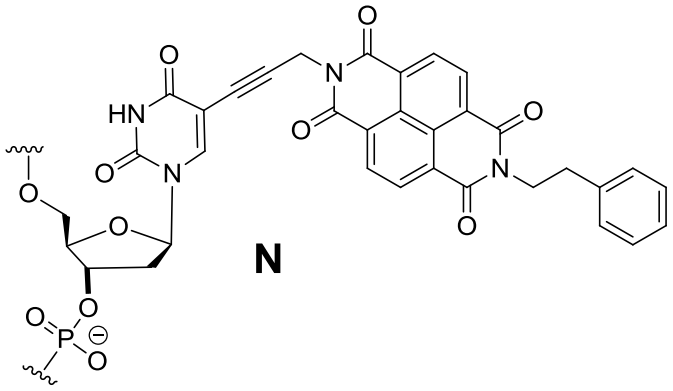

N

3' – ACT TAG TGA **N**CC GAG CAG TC – 5' **13**
3' – ACT TAG TGA **N**C**N** GAG CAG TC – 5' **14**

Figure 65. Synthesised naphthalene diimide modified strands and the incorporated monomer, **N**

UV-vis spectroscopy of strands **13** and **14** did not show any absorbances except for that of the nucleobases at 260 nm, which is not unexpected due to the weakly absorbing nature of the naphthalene diimide modified nucleobase. UV-vis measurements of **XXV** show the naphthalene diimide moiety to have absorbances with log ε values on the order of 3.3 and 3.6. In order to collect fluorescence data for naphthalene diimide modified nucleoside **XXV** it was necessary to increase the concentration by several orders of magnitude from the sample used for UV-vis analysis (from 0.11 mM to 12.7 mM) due to the low quantum yields of naphthalene diimides (~0.002),[185] consequently no fluorescence of strands **13** and **14** was observed. Mass spectrometry was unable to confirm the presence of the desired strands.

It was decided that further exploration of naphthalene diimide modified stands would only be conducted when the electron transfer processes could be measured as this was not yet available.

3.26 – Anthraquinone modified oligonucleotides

Multiple examples of anthraquinone modified oligonucleotides exist, with modifications to the nucleobase,[161,186,187] 2'-*O*-modifications to the ribose ring[188-190] and both 3'- and 5'-terminal modifiers[191-193] being reported in the literature. The anthraquinone moiety provides a stable, easily modified, pH dependent, 2 electron redox probe (Figure 66) that has been used for a variety of different systems, including; detection of duplex hybridisation,[189] detection of electrochemically induced duplex melting[191] and stabilisation of triplex forming oligonucleotides.[192]

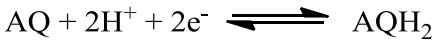

Figure 66. Electrochemical redox reaction of anthraquinone

The redox potentials of the anthraquinone moiety are pH dependent, with a nearly linear relationship between pH 4.0 and pH 10.0, the peak maxima shift to more negative potentials in higher pH solutions by approximately 60 mV per pH unit.[188]

The inclusion of a terminal anthraquinone monomer into an oligonucleotide increases the stability of the resulting duplex or triplex formed through end capping.[192,193] 2'-*O*-modified anthraquinone monomers naturally position the anthraquinone moieties within the duplex and as such intercalation leads to a significant increase in duplex stability.[190]

A stabilisation of the duplex can also be achieved by the inclusion of an anthraquinone modified nucleobase linked *via* a short chain (Figure 67a); intercalation of the anthraquinone occurs through base inversion, as demonstrated by Gothelf *et al*. through mismatch studies.[161] If the linker between the nucleobase and the anthraquinone moiety is sufficiently long (Figure 67b), base inversion and intercalation no longer occurs and a small decrease in the duplex stability (3-5 °C) is observed,[186] however despite the small destabilisation of the duplex there does not appear to be any significant perturbation to the overall conformation, and the duplex continues to form B-type DNA despite the inclusion of the anthraquinone moiety.[186]

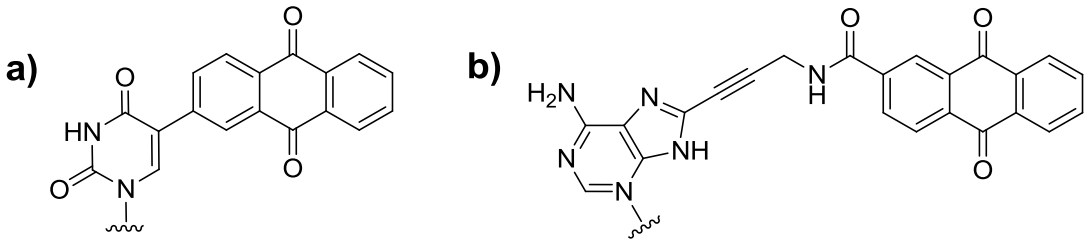

Figure 67. a) Intercalating anthraquinone monomer[161] b) Non-intercalating anthraquinone monomer[186].

In order to ensure the anthraquinone moieties incorporated into the planned DNA systems were located in the major groove of the double helix, it was decided that a modified nucleobase with a long amide containing linker as per the amide linked porphyrin monomer (**2**) and analogous to the anthraquinone-dA monomer used by Grinstaff *et al.*[186] (Figure 67b) was required (monomer **Q**, Figure 68).

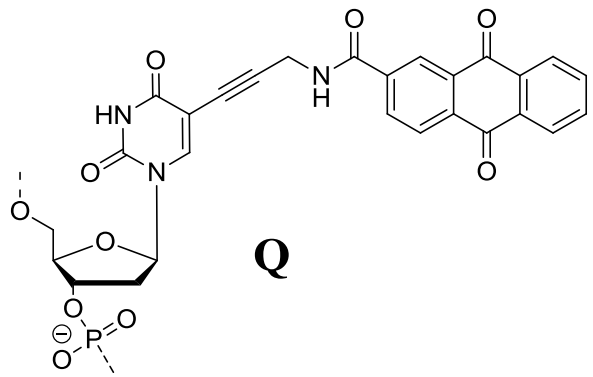

Figure 68. Anthraquinone monomer **Q**

3.27 – Synthesis route to anthraquinone modified nucleotide monomer

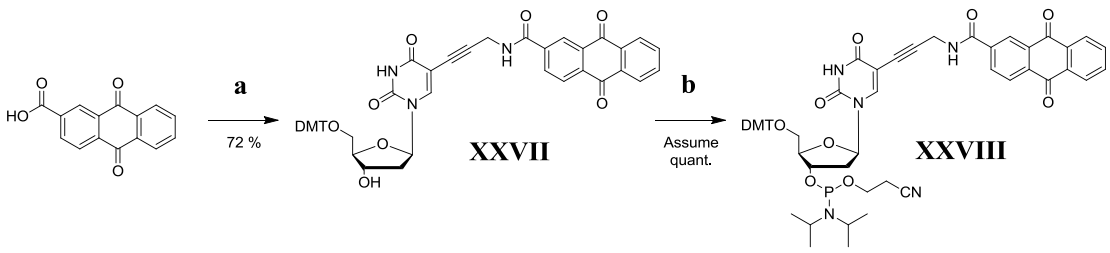

a - X, DCC, HOBt, DIPEA, DMF, 72 % **b** - CEP-Cl, DIPEA, Assume quantitative

Scheme 19. Synthesis route for anthraquinone modified nucleotide monomer

Anthraquinone-2-carboxylic acid was coupled to 5'-DMT-5-propargylamino-dU (**X**) using DCC and HOBt to give **XXVII** in 72 % yield (Scheme 19). Cyclic voltammetry of **XXVII** in 50 % DMSO/50 % 1.0 M NaCl 10 mM Tris (pH 7.2) with a sweep rate of 100 mV s^{-1} showed clear reduction and oxidation peaks at -479 mV and -524 mV vs SCE (Figure 69).

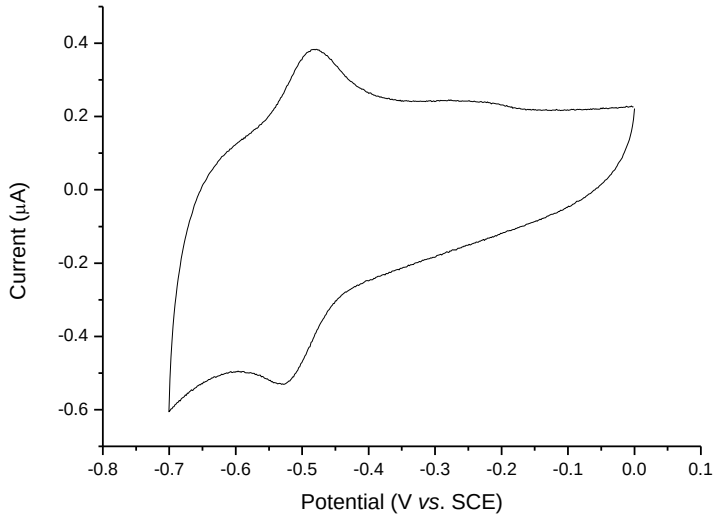

Figure 69. Cyclic voltammetry of **XXVII** *vs.* SCE

Anthraquinone modified nucleotide monomer (**XXVIII**) was only synthesised as required, the synthesis of which was achieved quickly, with the reaction reaching completion in 2 hours. Purification was achieved by precipitating the product and washing with hexanes. Full characterisation of the product was not attempted due to the instability of the P(III) centre, however gas chromatography electrospray ionisation mass spectrometry in positive ion mode

showed a peak an *m/z* = 1040.8, corresponding to the $[M+Na]^+$ ion. **XXVIII** was used immediately for DNA synthesis.

3.28 – Synthesis of anthraquinone modified oligonucleotides

Since various anthraquinone modified nucleobase phosphoramidites are known to couple well during DNA synthesis, no test strands were synthesised. During the synthesis of strands **15** and **17** (Figure 70) the anthraquine modified nucleobase phosphoramidite (**XXVIII**) was prepared as a 30.5 mM solution in DCM and MeCN (1:1) and coupled over 5 minutes which gave a good coupling efficiency.

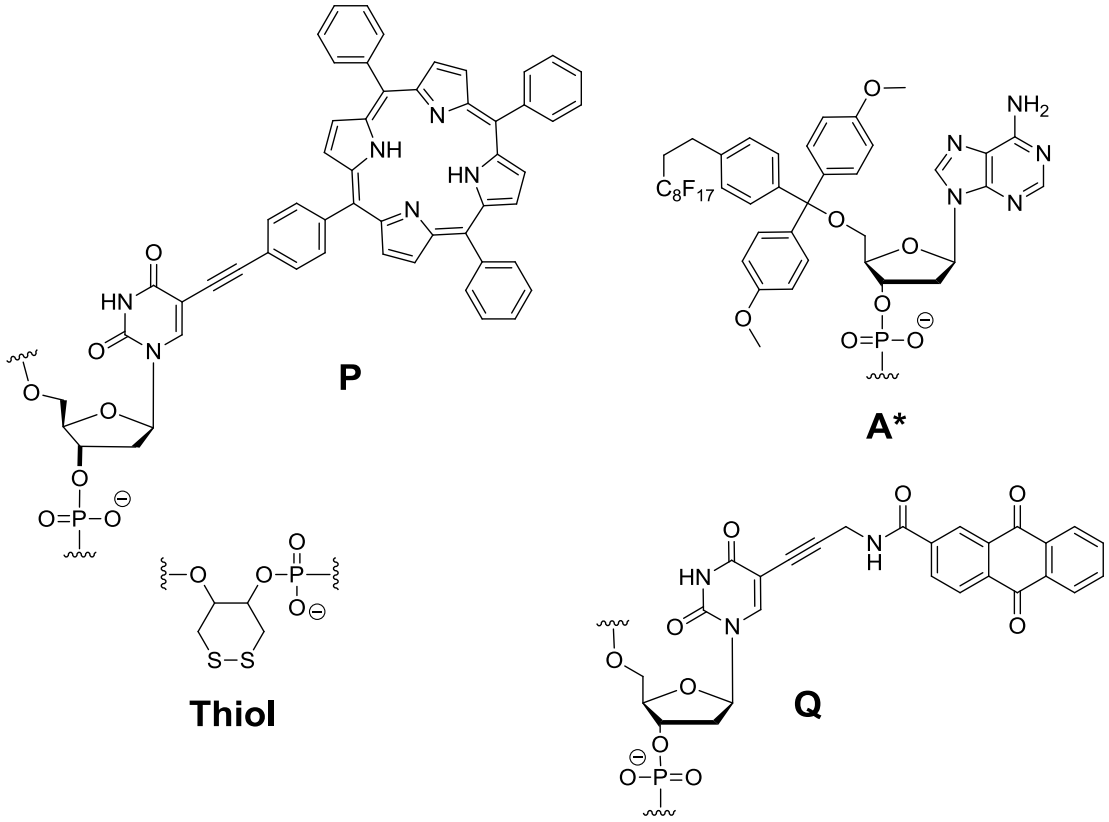

3' - **Thiol** **P**A**P** A**P**A **P**A**P** A**Q**C GCT AC**A*** - 5'	**15**
5' - **A*P**A **P**A**P** A**P**A **P**AG CGA TGT - 3'	**16**
3' - **Thiol** TAT ATA TAT A**Q**C GCT AC**A*** - 5'	**17**
5' - ATA TAT ATA TAG CGA TGT - 3'	**18**

Figure 70. Synthesised porphyrin, anthraquinone and thiol modified strands and incorporated monomers

Synthesised strands were characterised by UV-vis and fluorescence spectroscopy and by HPLC analysis. Mass spectrometry was not conducted on the strands due to the presence of

the porphyrin moieties for reasons previously discussed (see - 3.6 – General synthesis of porphyrin DNA strands, page 41). DNA strands were then passed to Robert Johnson (Prof. Phil Bartlett's group, University of Southampton, UK) to conduct cyclic voltammetry experiments.

Electrochemical measurements were conducted on clean 1 mm diameter gold disc electrodes (synthesised in house), the electrode surface was functionalised by immersing in a 1 μM solution of the thiolated DNA strand in 10 mM Tris buffer (pH 7.2), 1 M sodium chloride for 24 hours. Data were collected in the aforementioned buffer using a three electrode setup with a platinum counter electrode and an SCE reference electrode.

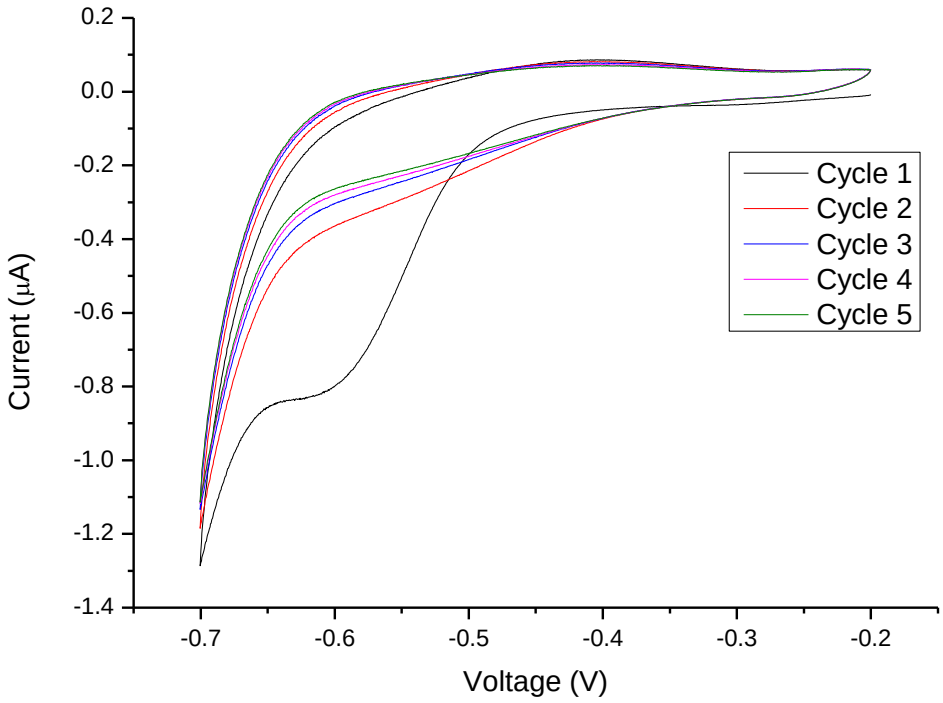

Figure 71. Surface bound cyclic voltammetry of strand **17**, in 10 mM Tris buffer (pH 7.2), 1 M sodium chloride with a scan rate of 100 mV s^{-1}

Figure 71 shows the data collected for surface bound cyclic voltammetry for single strand **17**, the data is reproducible. Data collection started at a potential of -0.2 V and was cycled to -0.7 V. On the first cycle a reduction peak at -0.614 V is present, with the presence of an ill-defined oxidation peak at -0.415 V but the integral of this possible oxidation peak is not sufficiently large enough to correspond to a complete re-oxidation of the anthraquinone moieties. On further cycles both the reduction peak and the possible oxidation peak reduce in magnitude and by the third cycle they are no longer recognisable as redox peaks. Due to a plethora of literature on the redox activity of anthraquinone species[161,188,189,191,194] it is fair to

conclude that the observed data is not showing irreversible reduction, but that it is showing the surface bound species being desorbed from the gold electrode surface. Electrochemical desorption of thiolated DNA from gold electrodes has previously been observed,[170,179] albeit at marginally more negative potentials (-0.85 V vs. SCE).

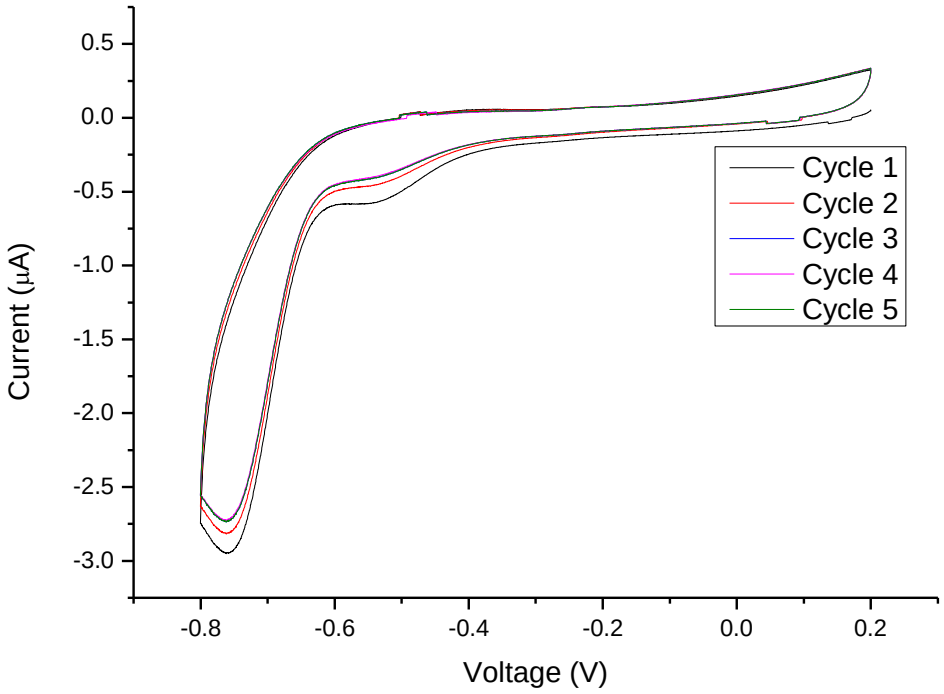

Figure 72. Surface bound cyclic voltammetry of strand **15**, in 10 mM Tris buffer (pH 7.2), 1 M sodium chloride with a scan rate of 100 mV s^{-1}

The cyclic voltammetry of single strand **15** (Figure 72) also shows a desorption of the anthraquinone and porphyrin modified oligonucleotide strands, again the potential across the cell was cycled between -0.2 V and -0.7 V and a reduction peak at -0.534 V was observed for the first cycle. This peak decreased in magnitude over further cycles. The corresponding oxidation peak (-0.380 V) is again very small and reducing in magnitude with repeated cycling.

Unfortunately due to the desorption of the oligonucleotides and hence the inability to collect multiple scans at various scan speeds, quantitative analysis of the data following the Laviron procedure[195], and thus obtaining kinetic data on the electron transfer rate, cannot be obtained on these systems. However, qualitatively we can state that the inclusion of the porphyrin substituents between the electrode surface and the anthraquinone in strand **15** allow for faster electron transport to the anthraquinone redox marker. This is evident from the smaller separation of the reduction and oxidation peaks of strand **15** compared to strand **17** (154 mV vs

199 mV respectively). This suggests that the porphyrin moieties are aiding the transport of electrons between the electrode surface and the redox marker and hence are behaving as a supramolecular wire along the length of the modified section of the olignucleotide (~3.4 nm).

Hybridisation of the above strands with the complementary strand was achieved by standard methods; porphyrin and anthraquinone containing duplex **15•16** and the anthraquinone containing reference duplex **17•18** were formed.

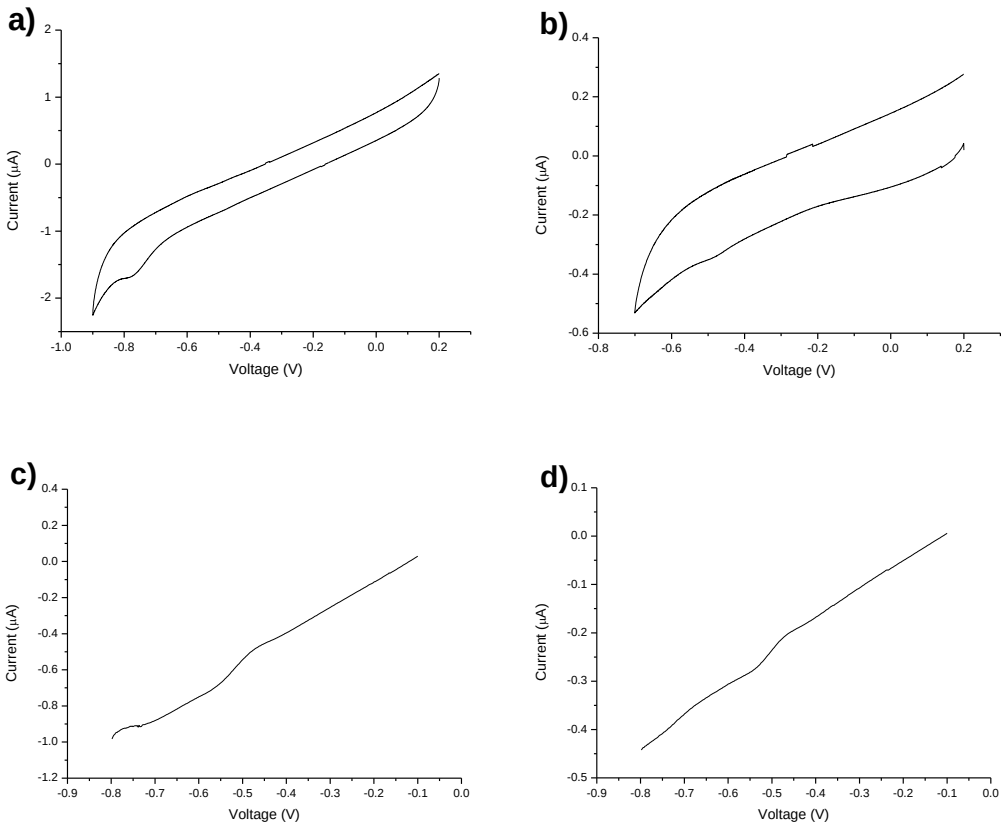

Figure 73. a) CV of **15•16**, b) CV of **17•18**, c) DPV of **15•16** and d) DPV of **17•18** in 10 mM Tris buffer (pH 7.2), 1 M sodium chloride with a scan rate of 100 mV s^{-1}

Cyclic voltammetry of these duplexes did not show the expected redox peaks (Figure 73a & b), sample **17•18** simply showed a double layer capacitance, while sample **15•16** showed a small reduction peak at a much more negative potential (-0.78 V *vs.* SCE), there was no corresponding oxidation peak, the origin of this reduction peak is uncertain however since it is not seen in the corresponding reference strand (**17•18**) it may be a reduction of the porphyrin moieties. Scans with differential pulse voltammetry (DPV, Figure 73c & d), an electrochemical technique able to detect much lower concentration samples due to a lower charging current effect, showed a very low surface coverage of the duplexes and hence revealed why they CV was not able to detect any redox peaks.

As there is no linker between the DNA duplex and the terminal cyclic di-thiol modifier, it is thought that hybridisation of the duplex provides a steric hindrance to the end of the duplex that is sufficient to prevent facile adsorption onto the gold surface. The inclusion of a hexa-ethylene glycol linkeage as per the ferrocene modified oligonucleotide (**11**) was omitted due to its previously observed low coupling yields (see – 3.20 – Synthesis of ferrocene modified oligonucleotides, page 86). The inclusion of a linker such as hexa-ethylene glycol would provide sufficient distance between the cyclic dithiol modifier and the oligonucleotide to allow for facile surface adsorption[191], this in turn would allow for cyclic voltammetry to be conducted at variable scan rates and thus deduce an electron transfer rate for the system.

4 – Concluding Remarks – Porphyrin DNA

The synthesis of porphyrin modified nucleotides, their characterisation and subsequent site specific incorporation into duplex DNA has been presented. Two different porphyrin modified nucleotides have been studied with differing behaviours observed in both the monomeric state and when incorporated in an oligomer. The porphyrins, when incorporated into the duplex in a zipper fashion, impart a large degree of stabilisation to the duplex with little disruption to the overall structure of the B-form DNA. Both porphyrin monomers show similar degrees of duplex stabilisation. Metallation of the porphyrins with zinc, copper and cobalt has been achieved post DNA synthesis; zinc metallated porphyrins have been shown by CD to be thermally unstable. CD has proved to be a valuable tool in analysis of and identification of the different porphyrins modified systems. Molecular modelling of three of the systems has shown three very different spatial conformations; details of these predictions had previously been confirmed by photospectrometric means. At high concentrations porphyrin modified oligonucleotides have been shown to aggregate into clusters of 2-4 duplexes in a side by side manner, aggregation is not observed at concentrations normally used for analysis.

The synthesis of a ferrocene modified nucleotide and its inclusion into oligomeric DNA has been presented with the aim of utilising it as a redox marker, electrochemical analysis has shown the ferrocene monomer to be unstable and hence unsuitable for this purpose.

The synthesis of a ruthenium *tris*-bipyridyl modified nucleotide was attempted by a variety of routes, all ultimately unsuccessful due to the loss of the DMT protecting group.

The synthesis of a naphthalene diimide modified nucleotide and its incorporation into oligomeric DNA has been presented, subsequent electron transfer studies with this monomer were postponed to concentrate on other aspects of the project.

The synthesis of an anthraquinone modified nucleotide and its incorporation into DNA alongside porphyrin modification has been discussed. Electrochemical analysis has been conducted on these systems, which show the porphyrin modified single strand to act as a ‘molecular wire’. Analysis of the modified duplexes was unsuccessful due to steric hindrance of the terminal cyclic di-thiol modifier causing problems in attachment of the duplex to the gold electrodes.

5 – Results and Discussion – Porphyrin-SWNTs

5.1 – Porphyrin modified single walled carbon nanotubes

Porphyrins have previously been attached to single walled carbon nanotubes for use as donor-acceptor complexes,[67,69] photovoltaic devices[196,197] and field effect transistors.[198] Modification of the SWNTs with the porphyrin moieties is possible through covalent[64,65,196] and non-covalent[88,89,198,199] bonding interactions with the sp^2 carbon atoms of the nanotube. Non-covalent attachment of the porphyrins to the SWNT through π–π interactions is favourable since it preserves the electronic structure of the nanotubes.[89] Porphyrin adsorbed single walled carbon nanotubes have been shown to exhibit interaction between the π systems, manifesting itself as a broadening and redshift of the porphyrin Soret band[89] in the absorption spectrum and a quenching of the porphyrin fluorescence.[89] A Dexter type electron exchange mechanism, has been reported as the mode of interaction between the two species.[199]

Porphyrin adsorbed nanotubes have previously been synthesised with neutral,[88,89,200] anionic[69,197,201] and cationic[69,197] porphyrins, however, no research has been conducted on hetero-porphyrin systems i.e. systems containing more than one porphyrin species. These systems, particularly a mixed charge system is of interest due to potential aggregation of the porphyrins as a 1:1 salt on the nanotubes' surfaces (Figure 74), this may display some interesting photophysical and electron transfer properties.

Homo- and hetero-porphyrin single walled carbon nanotube adducts were to be synthesised and their photophysical properties measured to ascertain whether hetero-porphyrin nanotube adducts differ significantly from the homo-porphyrin systems. The loading of the porphyrins on the nanotubes surfaces was also to be determined.

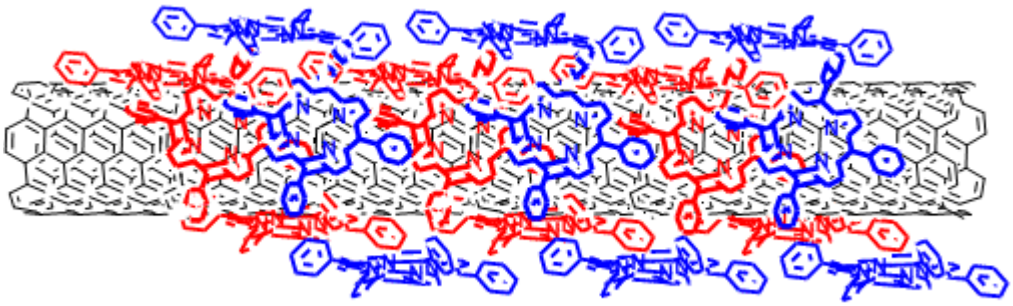

Figure 74. Schematic representation of porphyrins adsorbed onto a SWNT

5.2 – Synthesis of porphyrin adsorbed single walled carbon nanotubes

Using a standard method (see - 8.2 – General method for preparation of porphyrin adsorbed nanotubes, page 130) porphyrins were adsorbed onto the surface of single walled carbon nanotubes (SWNT). Three homo-porphyrin and three hetero-porphyrin carbon nanotube systems were synthesised. The porphyrins used in this study (Figure 75) were 5,10,15,20-tetraphenyl porphyrin (TPP), the tetra sodium salt of 5,10,15,20-(phenyl-*p*-sulphonic acid) porphyrin (TPSA) and the tetra tosylate salt of 5,10,15,20-(4'-*N*-methyl pyridinium) porphyrin (TMPyP).

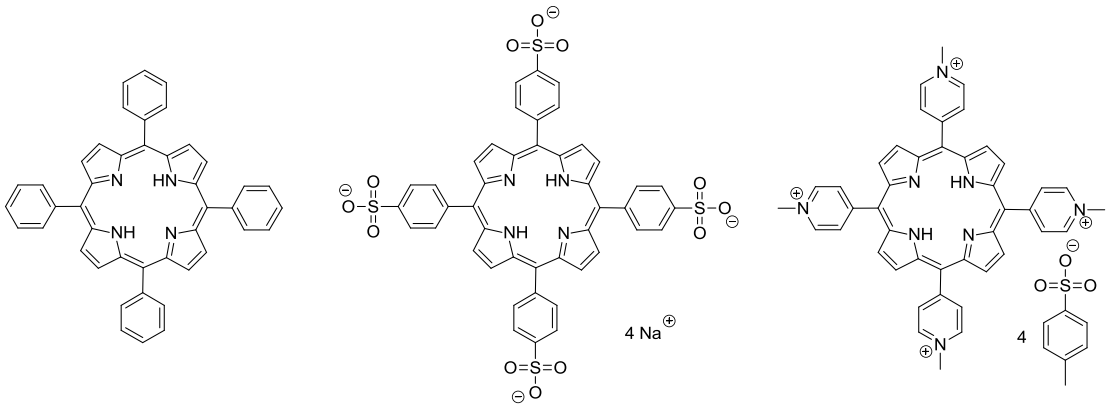

Figure 75. Porphyrins used to synthesise porphyrin adsorbed carbon nanotubes

Nakashima *et al.*[202] published a method for the removal of any residual iron carbonyl catalyst from carbon nanotubes synthesised by the HiPCO process[58] (High Pressure Carbon Monoxide) involving heating in air and sonication in strong acid before neutralising, washing and drying. This process was reproduced and the carbon nanotubes thoroughly dried under high vacuum before use. To synthesise the porphyrin modified carbon nanotubes, purified single walled carbon nanotubes (1 mg) and porphyrin(s) (2 mg) were suspended/dissolved in DMF and stirred rapidly for 24 hours before sonicating in an ultrasonic bath for two hours. The samples were centrifuged for one hour and the excess unbound porphyrins decanted off, the sample was topped up with DMF before sonicating (2 minutes) and centrifugation (1 hour) again. This washing process was repeated three times to ensure removal of all unbound porphyrins before drying the samples thoroughly under high vacuum. The systems synthesised along with their associated names are shown in Table 4.

Loaded Porphyrin(s)	Nomenclature
TPP	**i**-SWNT
TPSA	**ii**-SWNT
TMPyP	**iii**-SWNT
TPP / TPSA	**i/ii**-SWNT
TPP / TMPyP	**i/iii**-SWNT
TPSA / TMPyP	**ii/iii**-SWNT

Table 4. Synthesised porphyrin SWNT adducts

5.3 – Absorption and fluorescence analysis of porphyrin-SWNT adducts

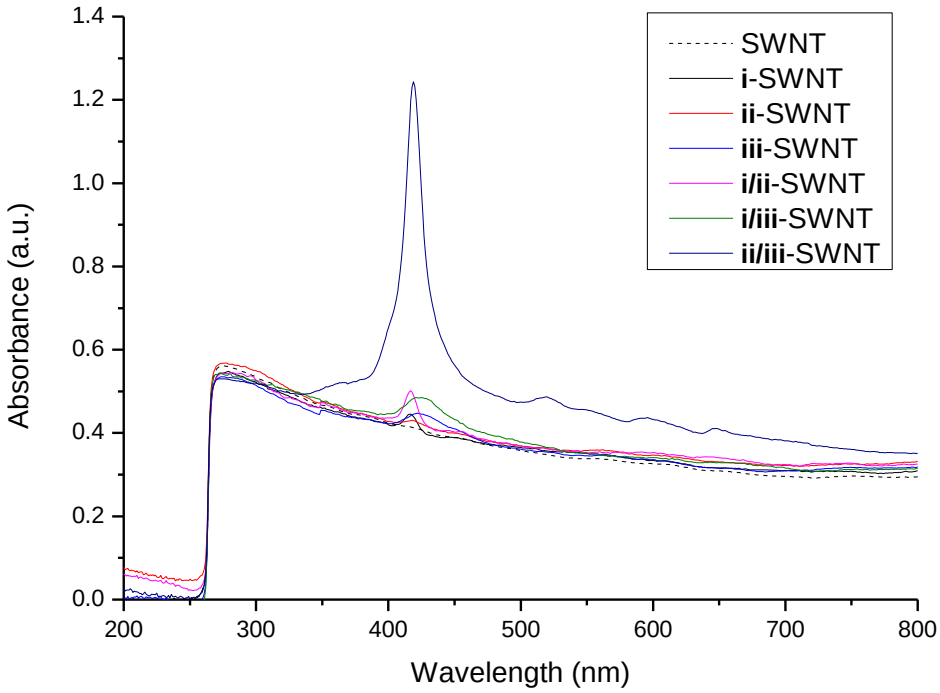

Figure 76. 200 – 800 nm UV-vis of porphyrin-SWNT adducts in DMF at equal nanotube concentration c = 0.3 mg ml^{-1}

UV-vis analysis of the suspended porphyrin-SWNT adducts at equal nanotube concentration (0.3 mg ml^{-1}, Figure 76) show the carbon nanotubes to scatter light at wavelengths longer that 260 nm. The spectra showed the characteristic freebase porphyrin absorbance bands

(Soret band/B band at ~420 nm and four Q bands between 500 and 675 nm) above the background scattering of the carbon nanotubes. Shouldering of the Soret band towards the longer wavelengths may be observed, indicative of π–π stacking of the porphyrin moieties[19,203,204]. A pronounced difference in the amplitude of the Soret band absorption was observed, with most samples show an absorbance of the same order of magnitude as each other, however, the mixed charge system (**ii/iii**-SWNT) shows a greatly increased Soret band absorbance, with peak maxima an order of magnitude larger than the other samples. This may be explained by; a hyperchromicity of the porphyrin absorbances of **ii/iii**-SWNT, or; a hypochromicity of the porphyrin absorbances of all other samples, or; a greater loading of the porphyrins on the carbon nanotube surface. The most probable explanation is the latter, since the tetra-anionic porphyrin (**ii**) and tetra-cationic porphyrin (**iii**) would be able to form porphyrin-porphyrin salt dimers on the surface of the SWNT. TPSA (**ii**) and tin metallated TMPyP have previously been shown to form stable supramolecular aggregates.[204,205]

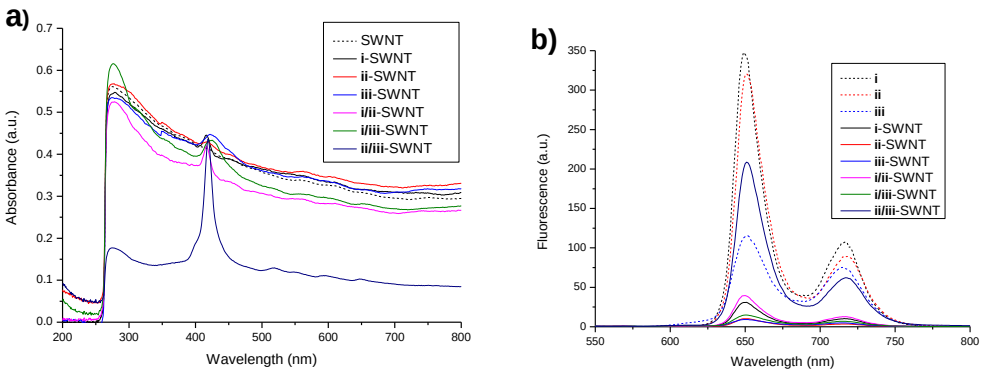

Figure 77. a) 200 – 800 nm UV-Vis of porphyrin-SWNT adducts at equal absorbance, A_{Soret} = 0.435 ± 0.015 in DMF, and b) 550 – 800 nm fluorescence spectra of porphyrin-SWNT adducts and porphyrins at equal absorbance, A_{Soret} = 0.435 ± 0.015 in DMF

UV-vis samples were diluted such that the absorbance of the Soret bands were equal (A_{Soret} = 0.435 ± 0.015, Figure 77*a*), these samples were then used for fluorescence spectroscopy analysis (Figure 77b). All samples show the characteristic porphyrin fluorescence with no significant shift in peak maxima (651 nm and 715 nm). Again most of the porphyrin-SWNT adducts showed fluorescence spectra of similar amplitude, however, as per the UV-vis results the mixed charge system (**ii/iii**-SWNT) shows a greatly increased spectral intensity. The samples' emissions are generally quenched with respect to the parent porphyrins in solution, an observation that has previously been observed for homo-porphyrin modified single walled carbon nanotubes,[89,198] it is thought that the quenching arises due to electron exchange *via* a Dexter type mechanism.[199]

5.4 – Atomic force microscopy (AFM) of porphyrin-SWNT adducts

Atomic force microscopy (AFM) of the porphyrin-SWNT adducts was conducted on oxidised silicon wafers (Figure 78) that were first cleaned by sonication in *iso*-propyl alcohol. In order to obtain images of the porphyrin-SWNT adduct containing the tetra-anionic TPSA porphyrin (**ii**-SWNT), the oxidised silicon substrate first required passivation with a nickel (II) chloride solution due to electrostatic repulsion of the terminal siloxy groups. Without surface pacification excessive bundling of the sample was visible with the naked eye and no clear AFM images could be obtained.

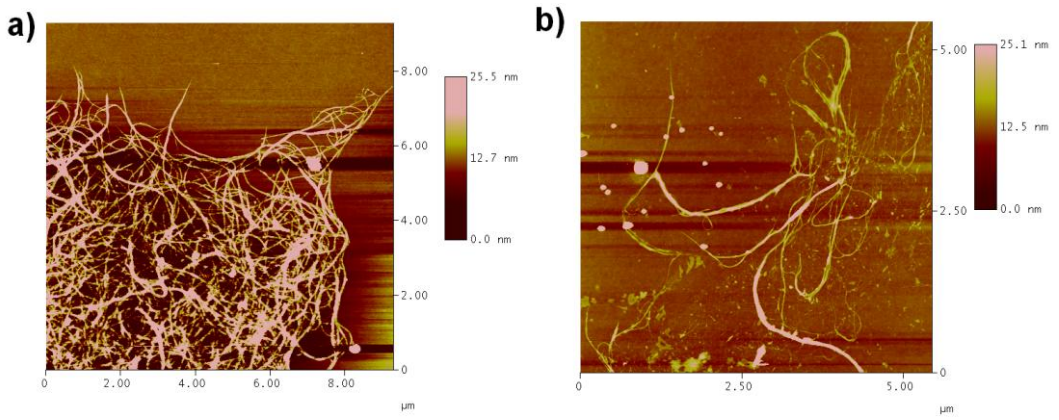

Figure 78. Example AFM images of porphyrin-SWNT adducts a) **i**/**ii**-SWNT b) **ii**/**iii**-SWNT

AFM samples were prepared by spin coating a suspension of the porphyrin-SWNT adduct in DMF onto the oxidised silicon substrate before drying under a flow of nitrogen at room temperature.

All porphyrin-SWNT samples showed bundling of the samples to a greater or lesser extent, however all samples showed areas where individual nanotubes were exposed to allow section analysis of the sample and hence the diameter of the porphyrin-SWNT adducts to be obtained. Section analyses were conducted on a variety of different nanotubes within the sample and the mean diameter calculated, the mean diameter of the unmodified single walled carbon nanotubes was measured to be 1.462 nm. All porphyrin-SWNT adducts showed an increased mean diameter, ranging from 1.672 nm (**ii/iii**-SWNT) to 2.194 nm (**i**-SWNT) which is consistent with adsorption of porphyrin moieties to the nanotube surfaces and comparable to previous measurements of porphyrin adsorbed single walled carbon nanotubes.[88,89]

5.5 – Resonance Raman spectroscopy of porphyrin-SWNT adducts

Resonance Raman spectroscopy of the porphyrin-SWNT adducts was conducted by Dr Fabrice Birembaut (Prof. Andrea Russel's group, University of Southampton, UK). Carbon nanotubes show various peaks in the resonant Raman spectra according to different stretches,[206] one of which corresponds to a radial expansion of the nanotubes, the so called 'radial breathing modes'[207] at wavelengths shorter than 280 nm. The radial breathing mode peaks comprise a number of different peaks relating to different nanotube diameters, the relation between the resonance Raman peak and the diameter is shown in Figure 79:

$$\omega\ (cm^{-1}) = 223.75 / d\ (nm)$$

Figure 79. Radial breathing mode relationship between absorption peak and diameter[207]

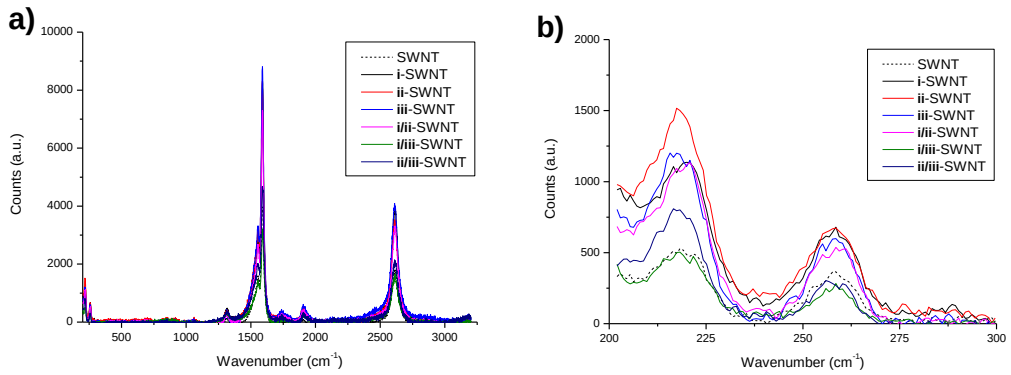

Figure 80. a) 200 – 800 cm^{-1} overview of the resonance Raman spectra of porphyrin-SWNT adducts, and b) Radial breathing modes of the porphyrin-SWNT adducts

It was hoped that observation of the radial breathing modes of unmodified single walled carbon nanotubes and porphyrin-SWNT adducts would show a shift in peak maxima, no such shift was observed (Figure 80). The resonance Raman spectra of both unmodified single walled carbon nanotubes and the porphyrin-SWNT adducts are largely similar; some changes in peak intensity are observed which is thought to be an effect due to residual solvent in some samples, no other significant changes in the spectra are observed. All spectra show the characteristic peaks corresponding to single walled carbon nanotubes; radial breathing modes (200-275 cm^{-1}), D band (1250-1350 cm^{-1}), G band (1450-1650 cm^{-1}), 2nd order modes (1700-2000 cm^{-1}) and G' band (2500-2750 cm^{-1}).[208] Due to instrument limitations measurements could not be taken below 202 cm^{-1} and as such only two of the radial breathing modes could be observed at 259

cm^{-1} and 217 cm^{-1}, corresponding to nanotube diameters of 0.86 nm and 1.03 nm respectively (see Figure 79). From previous mean diameter measurements by AFM, it is expected that several more radial breathing modes for these samples exist below 200 wavenumbers.

5.6 – Determining porphyrin loading of the porphyrin-SWNT adducts

Various reports of porphyrin modified single walled nanotubes exist in the literature,[66,85,86,209] however no attempts to quantify their loading have yet been reported. Due to perturbations of the porphyrin Soret band, direct analysis of the UV-vis spectra of the porphyrin-SWNT adducts cannot be relied upon to provide accurate loading levels and an alternative method was sought. The desorption of porphyrins from single walled carbon nanotubes to aid the separation of metallic and semi-conducting nanotubes has previously been reported,[63] an adaptation of this method was used to desorb the porphyrins and UV-vis analysis was used to quantify the porphyrins removed.

The porphyrin-SWNT adducts were sequentially stirred in toluene, 10:1 toluene:DMF and finally glacial acetic acid for 7 days in each solvent system. The removed porphyrins were quantitatively analysed by UV-vis spectroscopy and a suspension of a sample of the stripped nanotubes was also analysed; each time showing the presence of further porphyrins adsorbed to the nanotubes' surfaces and hence indicating incomplete desorption from the nanotubes. This observation is contrary to the results observed by Li *et al.*[63] who observed complete removal of a substituted porphyrin moiety (5,10,15,20-tetra(*p*-hexadecyloxyphenyl) porphyrin) from the single walled carbon nanotubes after stirring in acetic acid.

The quantitative UV-vis analysis of the desorbed porphyrins (Table 5) showed relative loading levels that would not be expected from the previously obtained UV-vis data of the porphyrin-SWNT adducts (see - 8.3 – UV-Vis of porphyrin-SWNT adducts at equal concentration, page 132). All homo-porphyrin-SWNT adducts (**i**-SWNT, **ii**-SWNT and **iii**-SWNT) and **i/iii**-SWNT showed comparable loading levels while **ii/iii**-SWNT showed a loading level that was several times higher. This is consistent with the UV-vis spectra of the porphyrin-SWNT adducts, however, sample **i/ii**-SWNT shows a loading level approximately five times larger than that of **ii/iii**-SWNT. This would not be expected based on the previous data. Since UV-vis analysis of the stripped nanotubes still showed the presence of porphyrin absorbances it was concluded that preferential desorption of at least one of the porphyrins was occurring.

Porphyrin-SWNT adduct	Porphyrin	nmoles desorbed from 1 mg sample with:			Total (nmoles mg^{-1})
		Toluene	Toluene/DMF	Acetic acid	
i-SWNT	**i**	0.19	0.085	0.16	0.43
ii-SWNT	**i**	0.15	0.013	0.034	0.20
iii-SWNT	**iii**	0.22	0.10	0.067	0.39
i/ii-SWNT	**i**	3.7	0.28	0.15	6.4
	ii	2.0	0.19	0.14	
i/iii-SWNT	**i**	0.13	0.057	0.022	0.48
	iii	0.096	0.14	0.037	
ii/iii-SWNT	**ii**	0.016	0.21	0.052	1.2
	iii	0.017	0.67	0.081	

Table 5. Nanomoles of porphyrin sequentially desorbed from porphyrin-SWNT adducts (2 significant figures)

Further desorption experiments were conducted on freshly prepared porphyrin-SWNT adducts by stirring rapidly in DMSO (Table 6). Desorption of porphyrins **i** (TPP) and **iii** (TMPyP) with DMSO is much more facile, with approximately a 10 fold increase in the amount of porphyrins desorbed from the nanotube samples. However, removal of porphyrin **ii** (TPSA) with DMSO shows similar results for sample **ii**-SWNT to those obtained by desorbing with toluene, toluene/DMF and acetic acid.

Deconvolution of the UV-vis spectra of the desorbed porphyrins for sample **ii/iii**-SWNT shows a large proportion of porphyrin **iii** (TMPyP) with only a small amount of porphyrin **ii** (TPSA) being desorbed by DMSO. Mixtures of cationic and anionic porphyrins usually form 1:1 complexes,[210,211] deconvolution of the UV-vis data for sample **ii/iii**-SWNT after sequential stripping with toluene, toluene/DMF and acetic acid also show proportions of porphyrins **ii** and **iii** to be approximately equal for all of the aforementioned solvent. This data suggests that a 1:1 complex of porphyrins **ii** and **iii** is present in sample **ii/iii**-SWNT but that desorption of porphyrin **ii** (TPSA) with DMSO is not favourable, hence observing a large proportion of porphyrin **iii** (TMPyP) when stripping sample **ii/iii**-SWNT with DMSO. Alternatively, it is possible that the loading of the tetra-anionic porphyrin **ii** (TPSA) is low due to electrostatic repulsions with the π system of the carbon nanotube and that sample **ii/iii**-SWNT does not form a 1:1 complex on the nanotubes' surfaces, further experimentation is required to ascertain if a 1:1 complex between porphyrin **ii** and **iii** is formed in sample **ii/iii**-SWNT.

Porphyrin-SWNT adduct	Porphyrin	nmoles stripped with DMSO	Total (nmoles mg^{-1})	Minimum loading (nmoles mg^{-1})
i-SWNT	**i**	18	18	18
ii-SWNT	**ii**	0.23	0.23	0.23
iii-SWNT	**iii**	3.0	3.0	3.0
i/ii-SWNT	**i**	0.064	0.27	6.44
	ii	0.20		
i/iii-SWNT	**i**	5.8	11	11
	iii	5.1		
ii/iii-SWNT	**ii**	15.0	270.0	270.0
	iii	260.0		

Table 6. Nanomoles of porphyrin desorbed from porphyrin-SWNT adducts with DMSO and minimum loading levels of the porphyrin-SWNT adducts (2 significant figures)

As per the sequential desorption experiment, the UV-vis analysis of a suspension of the stripped porphyrin-SWNT adducts showed incomplete desorption, showing that the porphyrins form strong π–π interactions with the carbon nanotube surfaces and hence complete desorption is not favoured. It is possible that the desorption experiments are removing the outer layers of adsorbed porphyrins i.e. those that would be most weakly bound to the surface, leaving the porphyrins closest to the surface of the nanotubes still adsorbed.

Although absolute loading data of the porphyrins has not been obtained, a minimum loading level can be stated for each porphyrin-SWNT adduct (Table 6). The loading levels of most porphyrin-SWNT samples are comparable at approximately 5-20 nmoles of porphyrin adsorbed per milligram of carbon nanotube, with the exceptions of; **ii**-SWNT which shows a low absorbance in the UV-vis analysis of the porphyrin-SWNT adducts (Figure 76) and low loading levels in both desorption experiments, and; sample **ii/iii**-SWNT which shows a significantly higher absorbances and fluorescence and also high loading levels in both desorption experiments. The relative loading levels of the different sampled as observed by desorption are broadly comparable to the relative loading levels as seen in the UV-vis spectra of the porphyrin-SWNT adducts (Figure 76), suggesting that although hypochromicity may be occurring in the UV-vis spectra such that quantitative analysis of it would not be valid, it is not significant enough to invalidate qualitative interpretation of the data.

5.7 – Elemental analysis of porphyrin-SWNT adducts

Samples of porphyrin-SWNT adducts were dried *in vacuo* for several days before submitting for elemental analysis (MEDAC Ltd, Egham, UK) in order to obtain additional data that may aid elucidation of the porphyrin loading levels. A 'blank' sample of single walled carbon nanotubes that had been treated exactly the same as the porphyrins-SWNT adducts i.e. by stirring in DMF, sonicating, centrifuging, decanting and drying *in vacuo* was also included in order to provide a reference sample.

Name	% composition		Elemental ratio		Carbon atoms in SWNT per porphyrin molecule	nmoles of porphyrin per mg of carbon	Comments
	C	N	C	N			
SWNT	79.89	0.00	6.65	0.00			
i-SWNT	78.01	1.80	6.5	0.13	158.18	527	
ii-SWNT	71.30	1.63	5.94	0.12	160.06	521	
iii-SWNT	75.23	1.87	6.26	0.13	313.23	266	
i/ii-SWNT	73.20	2.27	6.09	0.16	108.25	770	Assuming 100% **i**
					108.25	770	Assuming 100% **ii**
i/iii-SWNT	76.71	2.05	6.39	0.15	126.40	659	Assuming 100% **i**
					268.80	310	Assuming 100% **iii**
ii/iii-SWNT	66.19	6.06	5.51	0.43	7.26	11478	Assuming 100% **ii**
					30.52	2730	Assuming 100% **iii**
					65.77*	1267*	Assuming 1:1 salt of **ii**:**iii** * = per porphyrin dimer.

Table 7. Elemental analysis results of porphyrin-SWNT adducts

The results (Table 7) for the 'blank' sample of single walled carbon nanotubes showed the sample to contain only 79.89 % carbon and 1.27 % hydrogen, the remaining 18.84 % elemental composition is unknown, possibly containing residual hydrogen chloride and/or water from the purification steps[202] (see – 8.1 – Purification of single walled carbon nanotubes, page 130). However, the nitrogen content present in the sample was measured to be 0.00 % (measured to 2 decimal places) and therefore all DMF had been successfully removed by prolonged storage under high vacuum.

Since the only difference between the 'blank' SWNT sample and the porphyrin-SWNT adducts was the inclusion of porphyrins when stirring the sample in DMF, it is assumed that the nitrogen content of all the porphyrin-SWNT adducts originates from the porphyrins, since the 'blank' SWNT sample measured 0.00 % nitrogen after the same manipulation and drying processes.

The data received from MEDAC Ltd for the homo porphyrin-SWNT adducts (**i**-SWNT, **ii**-SWNT and **iii**-SWNT) was converted to empirical formulae and multiplied through to give relative elemental ratios such that the chemical formula of the adsorbed porphyrin could be subtracted and hence reveal what part of the elemental ratio was due to the carbon nanotubes themselves. This allowed us to state that per porphyrin molecule there are *x* number of carbon atoms which are due to the carbon nanotubes, manipulation of this data gives the number of porphyrin molecules per milligram of carbon nanotube. The same method was used to calculate data for the hetero porphyrin-SWNT adducts (**i/ii**-SWNT, **i/iii**-SWNT and **ii/iii**-SWNT), however in these cases without knowing the relative ratios of the porphyrins adsorbed, one must assume 100 % coverage of one porphyrin or the other in order to provide the extreme limits of loading. The principle assumption of this data manipulation is that there are no other molecules other than porphyrins and carbon nanotubes present in the samples.

Working through the data for sample **i**-SWNT shows a theoretical loading of 527 nmoles (0.32 mg) of porphyrin **i** per milligram of carbon nanotubes, sample **ii**-SWNT shows a theoretical loading of 521 nmoles (0.53 mg) of porphyrin **ii** per milligram of carbon nanotube, while sample **iii**-SWNT shows a theoretical loading of 266 nmoles (0.36 mg) of porphyrin **iii** per milligram of carbon nanotubes. These theoretical loading levels are significantly higher than those observed by quantitative UV-vis spectroscopy through desorption of porphyrins.

Sample **i/ii**-SWNT shows a theoretical loading level of 770 nmoles of porphyrin per milligram of carbon nanotube whether assuming the sample is loaded entirely with porphyrin **i** or porphyrin **ii**, what does change between the two extremes is the mass of porphyrin loading, this correspond to 0.47 mg and 0.94 mg for porphyrin **i** and porphyrin **ii** respectively.

Sample **i/iii**-SWNT shows a theoretical loading level of 659 nmoles (0.40 mg) of porphyrin per milligram of carbon nanotube assuming it is completely loaded with porphyrin **i** and a loading level of 310 nmoles (0.42 mg) per milligram of carbon nanotube assuming it is completely loaded with porphyrin **iii**.

Lastly, sample **ii/iii**-SWNT shows significantly higher theoretical loading levels than all other samples which is consistent with previous observations, however, closer inspection reveals the numbers to be nonsensical, the theoretical loading level implied by the elemental analysis suggests that there is more porphyrin in the sample than was mixed with the carbon nanotubes to start with. The lowest theoretical loading level suggested (that of the 1:1 dimer) would require 3.0 mg of porphyrin to have been mixed with the carbon nanotubes to start with

and for all of it to have been adsorbed, neither of which is true. As such, the assumption that the nitrogen content of the samples is due solely to the porphyrins is flawed. However, we have seen from the 'blank' carbon nanotube sample, which underwent the same processes as the loaded porphyrin-SWNT adducts before being sent for elemental analysis, that no nitrogen content was detected. From these observations it is thought that the adsorption of multiple layers of porphyrins onto the surface of the carbon nanotubes creates a framework within which DMF solvent molecules are able to reside, much like the inclusion of solvent molecules within a crystal structure. This observation does not render the elemental analysis data redundant; it is still useful for qualitative rather than quantitative analysis.

Looking solely at the percentage composition of the samples in Table 7 it can be observed that the 'blank' carbon nanotube sample has the highest percentage composition of carbon (79.89 %), as would be expected. The inclusion of porphyrins to the carbon nanotubes introduces a variety of different atoms to the sample, one of which was measured in the elemental analysis (nitrogen), but several others were not measured (sulphur, oxygen, sodium). The inclusion of these non-carbon atoms will lower the carbon percentage composition of the sample, as is observed for every porphyrin-SWNT adduct. Of the three porphyrins used in this study the one containing the highest percentage of 'non-carbon' atoms is porphyrin **ii** (TPSA, $C_{44}H_{26}N_4Na_4O_{12}S_4$), the elemental analysis shows that samples containing porphyrin **ii** have a much lower carbon percentage composition than the other samples, 71.30 %, 73.20 % and 66.19 % for **ii**-SWNT, **i/ii**-SWNT and **ii/iii**-SWNT respectively. The final figure is the most interesting, sample **ii/iii**-SWNT which showed a significantly higher UV-vis absorbance of the Soret band, a significantly higher fluorescence and also a significantly higher minimum loading level from desorbing the porphyrins, shows a significantly lower carbon percentage composition (66.19 %) and a significantly higher nitrogen percentage composition (6.06 %). For all samples except **ii/iii**-SWNT the nitrogen content has been very similar, between 1.6 and 2.3 %, however, sample **ii/iii**-SWNT shows a nitrogen percentage composition that is between 2.7-3.7 times higher than the rest of the samples. The only possible sources of this nitrogen content are the porphyrins and the DMF solvent in which they were dissolved when synthesising the porphyrin-SWNT adducts. So, unless the porphyrins are creating a highly porous framework on the carbon nanotube surface for the DMF to reside within, which is highly unlikely and there is a plethora of evidence to demonstrate that porphyrins interact with one another *via* face to face (*H* aggregate) or offset face to face (*J* aggregate) stacking interactions,[19,104,105,203] then it follows that the increased inclusion of solvent must be due to the increased levels of porphyrins on the surfaces of the carbon nanotubes. It is highly likely that there is a large inclusion of solvent in all of the synthesised porphyrin-SWNT adducts, although the theoretical loading levels suggested by the elemental analysis are not impossible for most samples, they are quite improbable for several reasons; visual inspection of the porphyrins washed away on synthesis of

the porphyrin-SWNT adducts, visual inspection of the porphyrin-SWNT adducts, photospectrometric analysis of the samples and finally, the desorption experiments.

5.8 – Cyclic voltammetry of porphyrin-SWNT adducts

Cyclic voltammetry may be used as a quantitative analysis method; the integral of the redox peaks corresponds to a charge, which in turn corresponds to a number of electrons transferred. Assuming that complete oxidation or reduction of the sample occurs, it is possible to use this information to deduce the number of molecules responsible for that particular redox peak.

Porphyrin-SWNT samples were given to Matthew Lacey (Prof. John Owen's research group, University of Southampton, UK) to obtain cyclic voltammetry measurements on. The samples were individually ground with acetylene black and PTFE in approximately 30:60:10 ratios, electrodes were created by rolling this mixture into a sheet approximately 80 μm thick and punching 1 cm diameter discs out. These disc electrodes were dried under high vacuum overnight before transferring to a glove box for assembly in an electrochemical cell (Figure 81) using an elemental lithium anode.

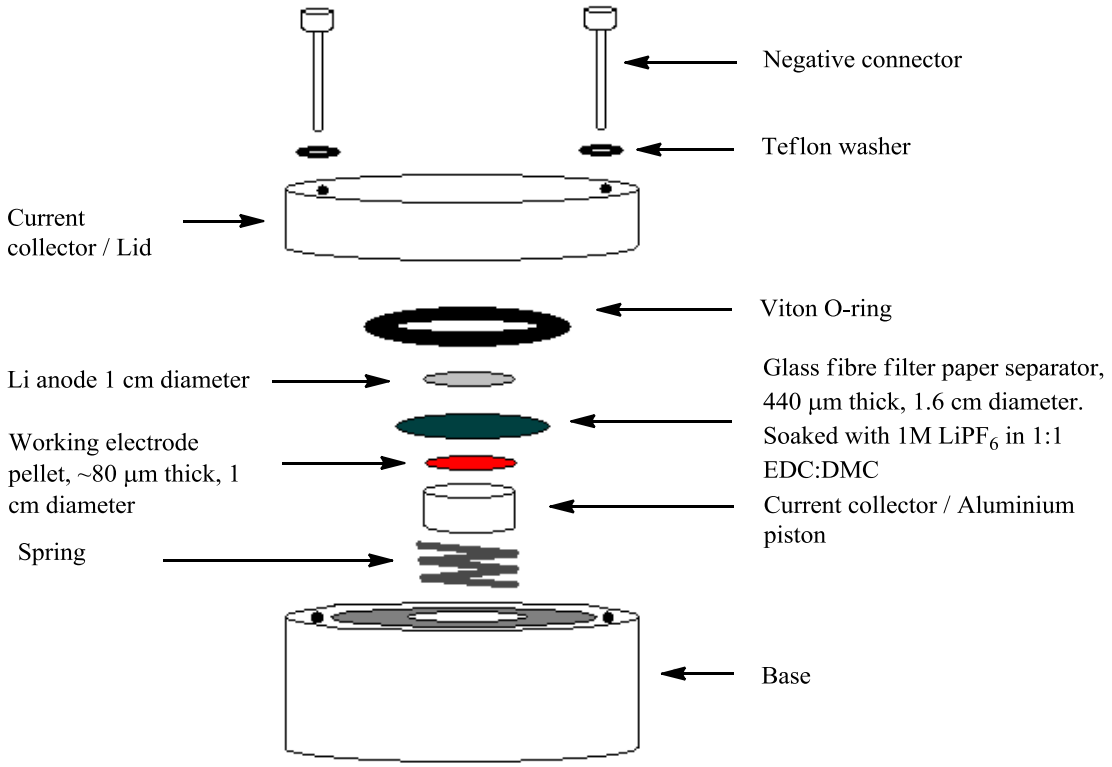

Figure 81. Schematic of an electrochemical cell for cyclic voltammetry of porphyrin-SWNT adducts

All samples showed double layer capacitance at all scan rates, fast scan rates failed to reveal any redox peaks for any of the samples. Data collection was at 0.2 mV s^{-1} with a collection time of approximately 48 hours. Redox peaks are observed through the double layer capacitance for **ii**-SWNT and **ii/iii**-SWNT only. Slow scan rates (<10 mV s^{-1}) are required in order to resolve the peaks as anything more than vague humps. The peaks of the 2/3-SWNT are more clearly resolved than those of **ii**-SWNT. The data was normalised for the exact mass of the porphyrin-SWNT within each sample (Figure 82).

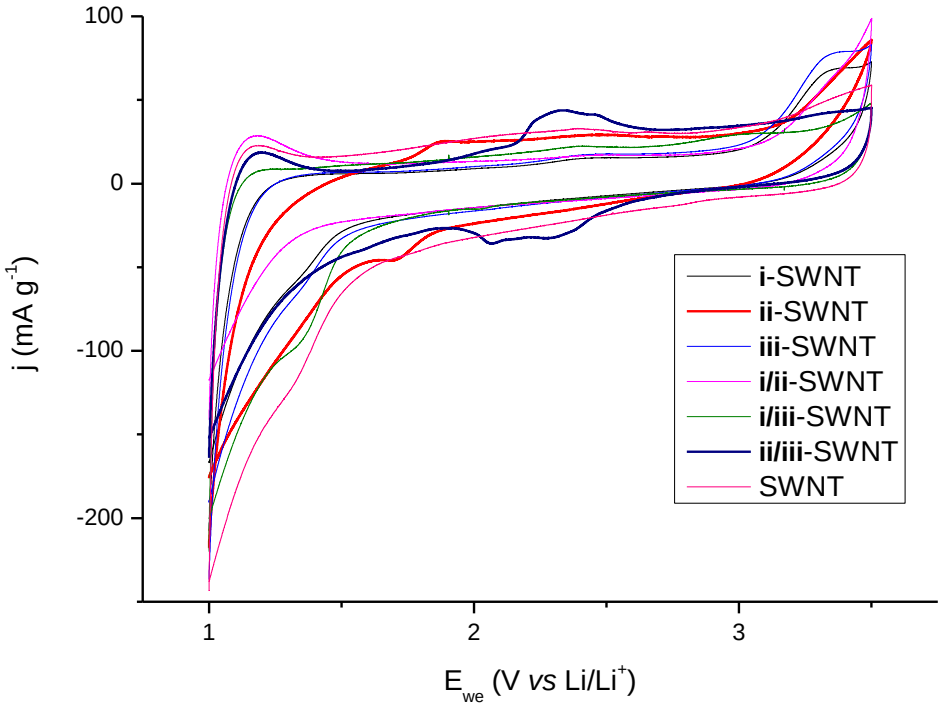

Figure 82. Cyclic voltammetry of porphyrin-SWNT adducts normalised for mass. Traces showing redox peaks are in bold

ii-SWNT shows a single reduction peak (Figure 82) and a single oxidation peak at 1.72 and 1.88 V *vs.* Li/Li^+ respectively (Li/Li^+ potentials are at -3.040 V *vs.* SHE). **ii/iii**-SWNT shows two reduction peaks that merge together (2.30 V and 2.07 V *vs.* Li/Li^+) and a broad oxidation signal that only shows one clear peak maxima (2.33 V *vs.* Li/Li^+). These signals are in reasonable agreement with the reduction peaks observed by Zhao *et al.*[85] of TPP adsorbed to a carbon nanotube surface (-0.7 V *vs.* SCE, equivalent to -2.58 V *vs.* Li/Li^+). Integration of the redox peaks for sample **ii**-SWNT show the porphyrin loading on the surface of the nanotubes to be 30-40 nmoles mg^{-1}, this result is higher than minimum loading level shown by desorption of the porphyrins from the surface, as would be expected since UV-vis analysis of the desorbed porphyrin-SWNT adducts showed that the desorption was incomplete.

Similar data processing of the redox peaks for sample **ii/iii**-SWNT show the porphyrin loading to be 230-240 nmoles per milligram, this is in good agreement with the results observed by desorption of the porphyrins from the nanotubes' surfaces (270 nmoles mg^{-1}). Quantitative analysis of the individual reduction peaks is not possible due to the proximity of the peak maxima to each other, however, qualitatively the areas encompassed by the peaks appear approximately equal. This implies that there are equal proportions of the two porphyrins within the sample, as would be expected for a 1:1 binary salt system. This backs up the observations made during the desorption experiments (see – 8.15 – General method for the sequential stripping of porphyrin adsorbed nanotubes, page 143).

No other porphyrin-SWNT adducts showed any clear redox peaks, it is thought that the reason for this is due to low loading levels and/or broad redox peaks not allowing the signals to be observed above the double layer capacitance of the carbon nanotubes and acetylene black bulking agent.

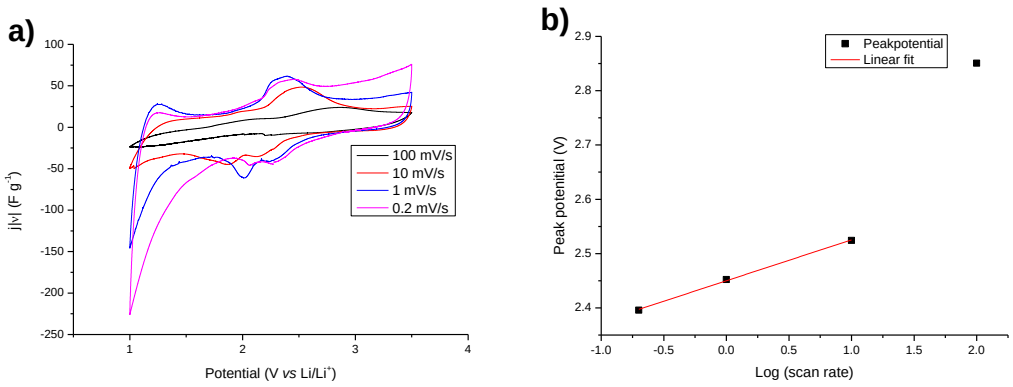

Figure 83. a) Cyclic voltammetry of **ii/iii**-SWNT, normalised for scan rate. b) Plot of oxidation peak potential versus natural logarithm of the scan rate

The cyclic voltammagrams of **ii/iii**-SWNT were normalised for the scan speed (Figure 83a), the peak current scales with the scan rate, indicative of a surface bound species[212,213] and in good agreement with previously observed cyclic voltammetry of a porphyrin adsorbed nanotube species.[85] The peak potential of the oxidation peaks were plotted against the natural logarithm of the scan speed (Figure 83b), a linear relationship is observed at the slow scan speeds (the outlying point corresponds to a comparatively fast scan speed of 100 mV s^{-1}) indicative of slow electron transfer kinetics of the surface bound species.

6 – Concluding Remarks – Porphyrin-SWNT adducts

The synthesis and analysis of homo- and hetero-porphyrin adsorbed single walled carbon nanotubes has been presented. Both neutral and charged porphyrins have been adsorbed to the surfaces in a variety of systems, one of which being a mixed charge system (**ii/iii**-SWNT). Attempts to ascertain the loading of the porphyrins on the surface of the carbon nanotubes were made by a variety of different methods, results suggest that all systems bar **ii/iii**-SWNT have a similar surface loading of the order of around 30 nmoles mg^{-1} of carbon nanotube, while the mixed charge system (**ii/iii**-SWNT) forms a 1:1 salt and shows a surface loading several times higher, around 230 nmoles mg^{-1} of carbon nanotube. Elemental analysis suggests that DMF solvent molecules are trapped within the porphyrin stacks on the surface of the carbon nanotubes.

7 – General Experimental Details

Suppliers

Chemicals were supplied by Fisher, Sigma Aldrich, Apollo, Fluka, Acros, Link, SAFC, Glen Research and Berry and Associates and used as received. DNA purification columns were supplied by Glen Research and Berry and Associates. Spin filters were supplied by Costar. Ultrafiltration units were supplied by Millipore. Nylon filtration membranes were supplied by Supelco. Desalting columns were supplied by GE Healthcare.

Column Chromatography and TLC

Column chromatography was conducted using silica gel (Kieselgel 60), silica gel type H and/or basic alumina (50-200μm, Brockmann activity I). Size exclusion chromatography was carried out on lipophilic sephadex beads (pore size 25-100μm). TLC was carried out on Merck aluminium backed sheets of silica gel 60 F254 or aluminium backed sheets of alumina 60 F254. TLC plates were visualised using UV light (254 nm and 365 nm), phosphomolybdic acid (10 % in ethanol), iodine on silica, potassium permanganate in water, anisaldehyde in ethanol, ninhydrin in acetone, mary's reagent (4,4'-bis-(dimethylamino)benzhydrol) in acetone, dinitrophenyl hydrazine in ethanol and/or ferric chloride in methanol. Retention factors (R_f) are given with the relevant eluent.

NMR spectroscopy

NMR spectroscopy was conducted at 25 °C using Bruker Advance DPX-300 and Advance DPX-400 machines at ^{1}H frequencies of 300.130 and 400.132 MHz respectively, using 5 mm diameter NMR tubes (Wilmad Lab Glass 507-PP-8). Raw data was subjected to a zero fill (64K points), a Lorentzian-Gaussian window function with line broadening of 0.15 – 0.3 Hz or 1.0 – 2.0 Hz, a first order Fourier transformation and phase correction as required. Chemical shifts (δ) for ^{1}H and $^{13}C\{^{1}H\}$ NMR are given relative to residual non-deuterated solvent, chemical shifts (δ) for $^{19}F\{^{1}H\}$, and $^{32}P\{^{1}H\}$ NMR are given relative to an external reference of $CFCl_3$ and 85% H_3PO_4 in H_2O respectively. Coupling constants (J) are given in Hertz (Hz).

Mass Spectrometry

Low resolution electrospray mass spectrometry was conducted using a Walters ZMD. High resolution electrospray mass spectrometry was conducted using an LTQ Orbitrap XL at the EPSRC National Mass Spectrometry Service Centre, Swansea. MALDI-TOF was conducted using a ThermoBioAnalysis Dynamo using a *p*-nitroaniline matrix and internally referenced against 5,10,15,20-tetraphenyl porphyrin (Mw – 614.25) and 2,8,12,18-tetrahexyl-3,7,13,17-tetramethyl-5,15-di(*p*-(3-hydroxy-3-methyl but-2-ynyl)phenyl porphyrin (Mw – 1082.88) or using a Micromass TOFSpec2E using external calibrants of terfenadine, bradykinin, angiotensin 1, substance P, renin substrate and ACTH clip for masses under 5000 Da, for larger molecules a range of oligonucleotides ranging from 5000 to 15000 Da are used.

UV-visible spectroscopy

UV-Vis spectroscopy was carried out on a Varian Cary 50 Bio or Varian Cary 300 Bio spectrophotometers using quartz cells (supplied by Hellma and Starna) with 1 mm or 1 cm path lengths. DNA melting profiles were collected at 260 nm as an average of at least two melting and annealing cycles. Heating and cooling cycles were controlled using a Varian Cary Temperature Controller and peltier system with a Varian Cary Series II Temperature Probe.

Fluorescence spectroscopy

Fluorescence spectroscopy was conducted on a Perkin Elmer LS50B or Varian Cary Eclipse spectrometers using quartz cells (supplied by Hellma and Starna), excitation for fluorescence melting experiments was at the sample's λ_{max}, and transitions temperatures were collected as an average of at least two melting and annealing cycles. Heating and cooling cycles were controlled using a Varian Cary Temperature Controller and peltier system with a Varian Cary Series II Temperature Probe

Circular Dichroism

Circular dichroism spectroscopy was carried out on an Applied Photophysics Chirascan spectrometer (150 W Xe arc) in quartz cells (Hellma) with a pathlength of 1 cm or 100 µm. Spectra were collected with a 1 nm step size, 1 nm bandwidth, integration time of 4 seconds per point. Molar $\Delta\varepsilon$ was calculated as follows:

$$\text{mdeg} = 32{,}980 \cdot \Delta A$$

$$\text{Molar } \Delta\varepsilon = \Delta A / c \cdot L = \text{mdeg} / 32{,}980 \cdot c \cdot L$$

A = Absorbance (a.u.); c = Concentration (mol dm^{-3}); L = Pathlength (cm)

High Pressure Liquid Chromatography

HPLC was carried out on a Varian Galaxie system using a C18 endcapped, reverse phase Merck LiChroCART 4 x 250 mm column. Eluents used were 100 mM TEAA 1% MeCN aqueous buffer, MeCN and MeOH. Buffer solutions were filtered through a Supelco Nylon 66 Membrane filter (0.45 µm pore size) before use. Flow rates were set to 1 mL min^{-1}. Eluent gradients varied and are stated with the relevant data.

DNA synthesis

DNA synthesis was carried out on an Applied Biosystems Expedite machine using 500 Å pore CPG beads. Deblocking steps used 3% TCA in DCM solution, activation steps use 0.1 M 'Activator 42' (5-(*bis*-3,5-trifluoromethylphenyl)-1*H*-tetrazole) in MeCN, capping steps used acetic anhydride in THF (Cap A) and pyridine and NMI in THF (Cap B), oxidizing steps used 0.02M iodine, pyridine and water in THF, washing steps used MeCN. All syntheses were performed as a 'DMT-on' synthesis to aid purification protocols. Cleavage of cyano ethyl groups at the end of the synthesis is achieved using 20% v/v DEA in MeCN. Standard synthesis protocols were used, coupling times used varied between 30 seconds and 10 minutes, depending on the phosphoramidite used.

Atomic Force Microscopy

AFM was conducted on a Veeco Metrology Multimode AFM microscope in tapping mode using NanoWorld Paintprobe FM-W tips. Surfaces used were either oxidised silicon or mica. Samples were either spin coated using a Speciality Coating Systems Inc. Spincoater Model PG700 or were dropped on the surface and allowed to air dry.

Raman Spectroscopy

Raman spectroscopy was carried out using a Renishaw 2000 series using a 633 nm excitation laser and equipped with a Leica microscopy with 5X lens.

Cyclic voltammetry

Cyclic voltammetry of porphyrin-SWNT systems was carried out thin film (< 100 μm) working electrode pellets using a Bio-Logic Instruments – Princeton Applied Research VMP2 in the range of 1.0 – 3.5 V vs. Li/Li^+ with a 1M $LiPF_6$ in 1:1 EC:DMC electrolyte at scan rates between 100 and 0.2 mV sec^{-1}. All other cylcic voltammetry was carried out on an Eco Chimie microAutolab III, measurements in solution were conducted with a glassy carbon working electrode, thiolated DNA samples were measured after adsorption to gold electrodes. Platinum counter electrodes were used in all measurements.

Infrared spectroscopy

Infra red spectra were collected using a Thermo Electron Corporation Nicolet 380 FT-IR, spectra were obtained of samples in the solid state between 500 and 40`00 cm^{-1}.

Small Angle X-ray Scattering

SAXS data was collected on an Anton Parr SAXess instrument with a slit geometry source with 1.54 Å x-ray radiation. Samples data was collected for 12 hours, buffer background was collected for 12 hours.

Melting point

Melting points were acquired in soda glass capillary tubes using an Electrothermal Engineering 9100 machine.

Centrifugation

Centrifugation was achieved using a Technico mini, Eppendorf 5415D or Thermo electron corporation Heraeus Biofuge Primo centrifuge.

Drying DNA samples

DNA samples were dried using an Eppendorf Concentrator 5301 using the appropriate setting for the solvent at room temperature.

Thermomixing

Agitation of samples (with or without heating) was done using either an Eppendorf Thermomixer Compact or Eppendorf Thermomixer Comfort.

Dispensing

Micropippetting was conducted using Gilson Pipetman, Sororex Acura 825 or Fisherbrand micropipettes. Microsyringing was conducted using Hamilton, SGE or Sanitex microsyringes.

Sonication

Sonication was conducted using a Fisherbrand 37 kHz, 120 W ultrasonic bath.

8 – Experimental

8.1 – Purification of single walled carbon nanotubes

As per Nakashima *et al.*,[202] single walled carbon nanotubes (25.0 mg) were heated to 225 °C overnight, cooled (RT) and conc. hydrochloric acid (15 mL) added. The resulting suspension was sonicated for 15 minutes, filtered through a glass sinter and washed with copious saturated sodium bicarbonate solution (~ 600 mL). Carbon nanotubes were dried *in vacuo* for 4 hours before heating to 50 °C overnight.

8.2 – General method for preparation of porphyrin adsorbed nanotubes

Single wall nanotubes (1.0 mg) and porphyrin(s) (TPP synthesised in house, TPSA and TMPyP supplied by Sigma 2.0 mg total) were stirred vigorously in DMF (10 mL) for 24 hours, the suspension was sonicated for 2 hours, centrifuged (10,000 rpm) for one hour, the solvent decanted off and replaced with fresh DMF (10 mL). Sonication, centrifugation and washing were repeated three times. Samples synthesised are outlined in Figure 84 and Table 8.

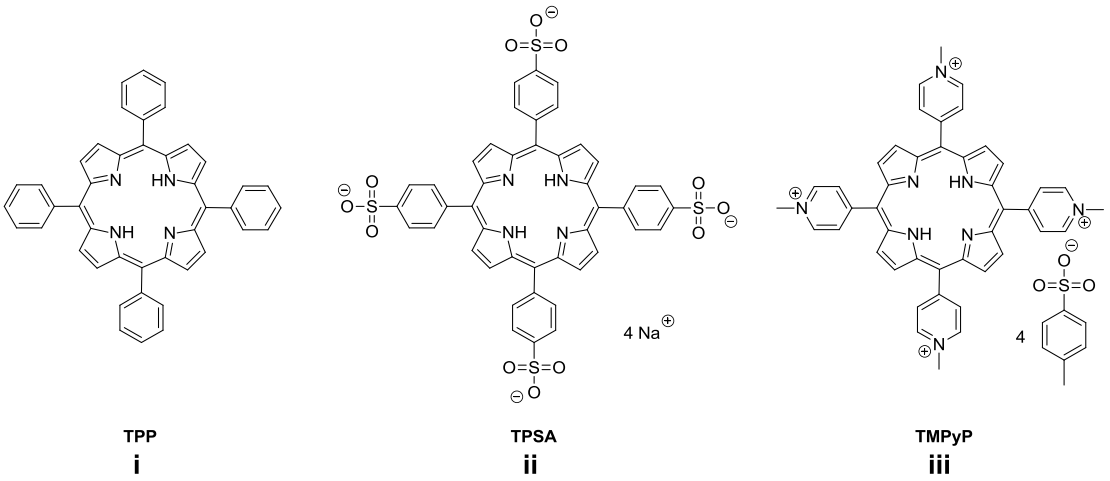

Figure 84. Porphyrins used in synthesising porphyrin SWNT adducts

Loaded Porphyrin(s)	Nomenclature
TPP	**i**-SWNT
TPSA	**ii**-SWNT
TMPyP	**iii**-SWNT
TPP / TPSA	**i / ii**-SWNT
TPP / TMPyP	**I / iii**-SWNT
TPSA / TMPyP	**ii / iii**-SWNT

Table 8. Nomeclature of synthesised porphyrin SWNT adducts

8.3 – UV-Vis of porphyrin-SWNT adducts at equal concentration

Porphyrin-SWNT samples (0.3 mg) were suspended in DMF (1 mL) in 1 cm pathlength quartz cuvettes.

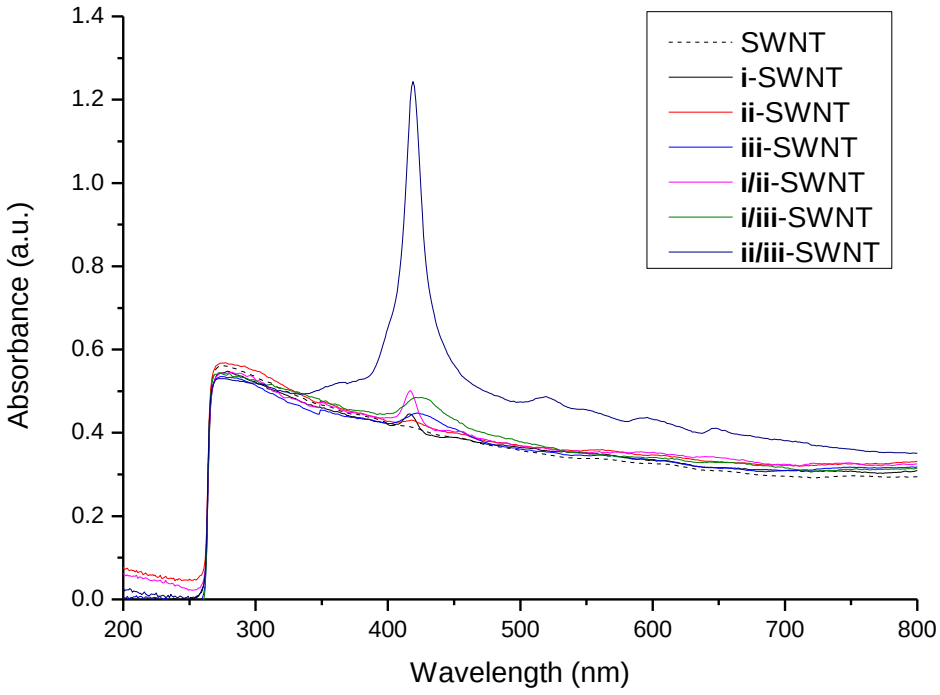

Figure 85. UV-Vis spectra of porphyrin-SWNT adducts at equal concentration (0.3 mg ml^{-1}) in DMF

Sample	λ_{max} (nm)	A_{max} (a.u.)
i-SWNT	417	0.45
ii-SWNT	418	0.43
iii-SWNT	422	0.45
i/ii-SWNT	417	0.50
i/iii-SWNT	424	0.48
ii/iii-SWNT	419	1.23

Table 9. Absorbance maxima of porphyrin-SWNT adducts at equal concentration

8.4 – UV-Vis of porphyrin-SWNT adducts at equal porphyrin absorbance

Porphyrin-SWNT samples were suspended in DMF (1 mL) in 1 cm pathlength quartz cuvettes.

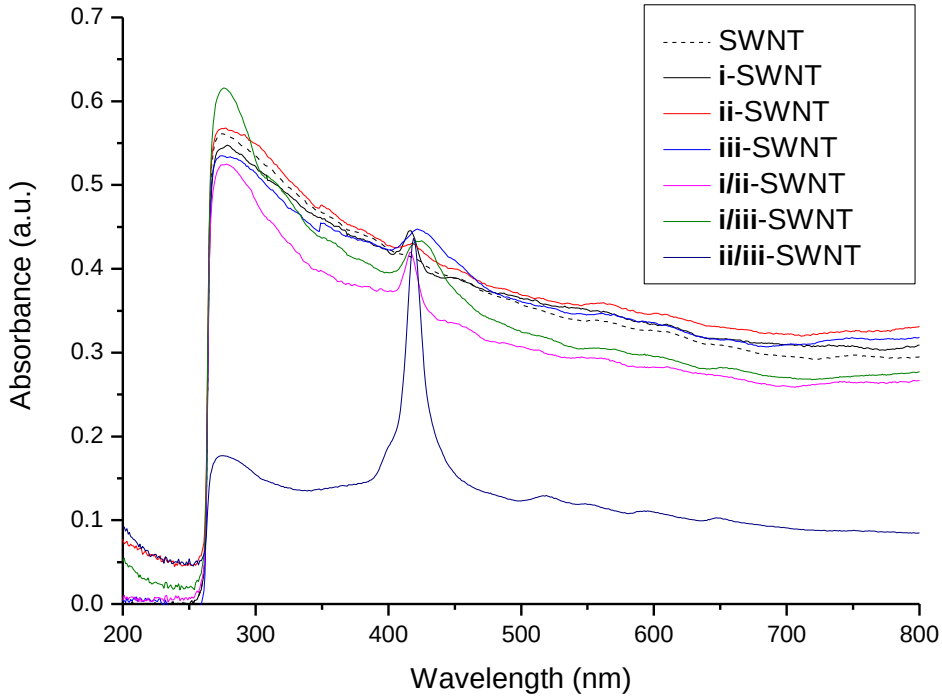

Figure 86. UV-Vis spectra of porphyrin-SWNT adducts at equal absorbance (A = 0.435 ± 0.015 a.u.) in DMF

Sample	λ_{max} (nm)	A_{max} (a.u.)
i-SWNT	417	0.45
ii-SWNT	418	0.43
iii-SWNT	422	0.45
i/ii-SWNT	417	0.42
i/iii-SWNT	424	0.44
ii/iii-SWNT	419	0.44

Table 10. Absorbance maxima of porphyrin-SWNT adducts at equal absorbance

8.5 – Fluorescence spectroscopy of porphyrin-SWNT adducts at equal porphyrin absorbance

Porphyrin-SWNT adducts were excited at their respective porphyrin λ_{max} with a 5 nm excitation and 5 nm emission slit width in 1 cm pathlength quartz cuvettes.

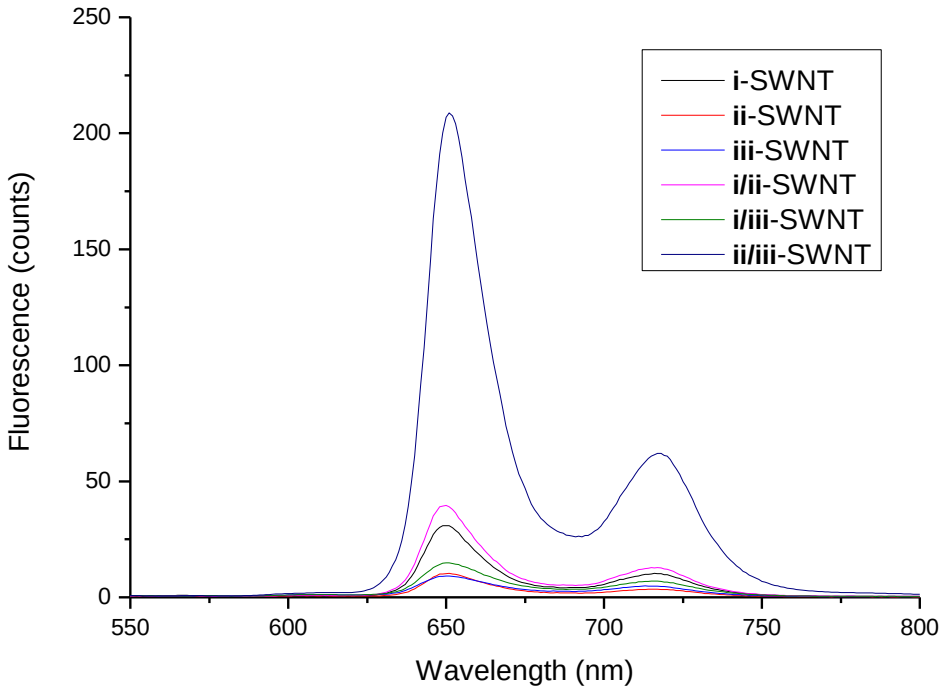

Figure 87. Fluorescence spectra of porphyrin-SWNT adducts at equal absorbance (A = 0.435 ± 0.015 a.u.) in DMF

Sample	λ_{ex} (nm)	λ_{em} (nm) (Rel. Int.)
i-SWNT	417	651 (1.00), 716 (0.33)
ii-SWNT	418	651 (1.00), 717 (0.35)
iii-SWNT	422	650 (1.00), 715 (0.53)
i/ii-SWNT	417	650 (1.00), 717 (0.33)
i/iii-SWNT	424	650 (1.00), 716 (0.47)
ii/iii-SWNT	419	651 (1.00), 717 (0.30)

Table 11. Emission maxima of porphyrin-SWNT adducts at equal absorbance.

8.6 – Raman spectroscopy of porphyrin-SWNT adducts

Porphyrin-SWNT adducts (0.15 mg) were dried *in vacuo* for 4 days prior to conducting Raman spectroscopy. Samples were excited using a 633 nm laser.

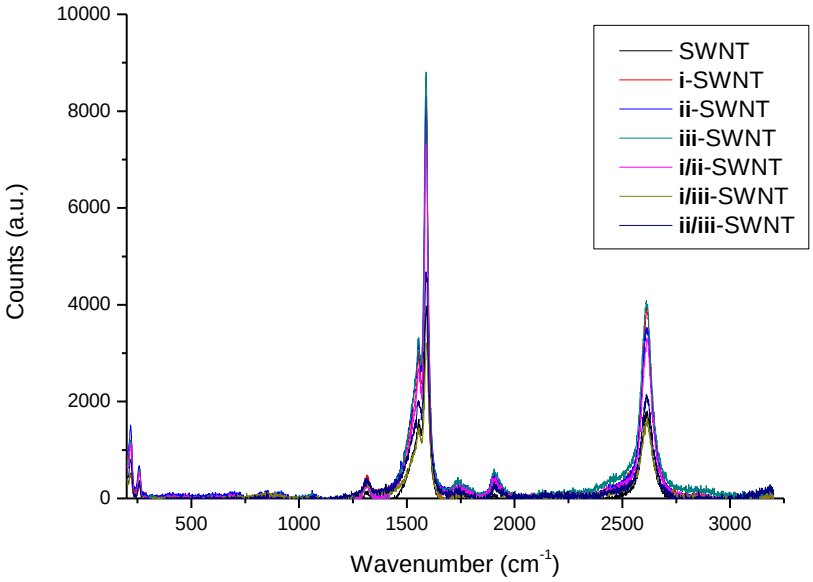

Figure 88. Raman spectra of porphyrin-SWNT adducts

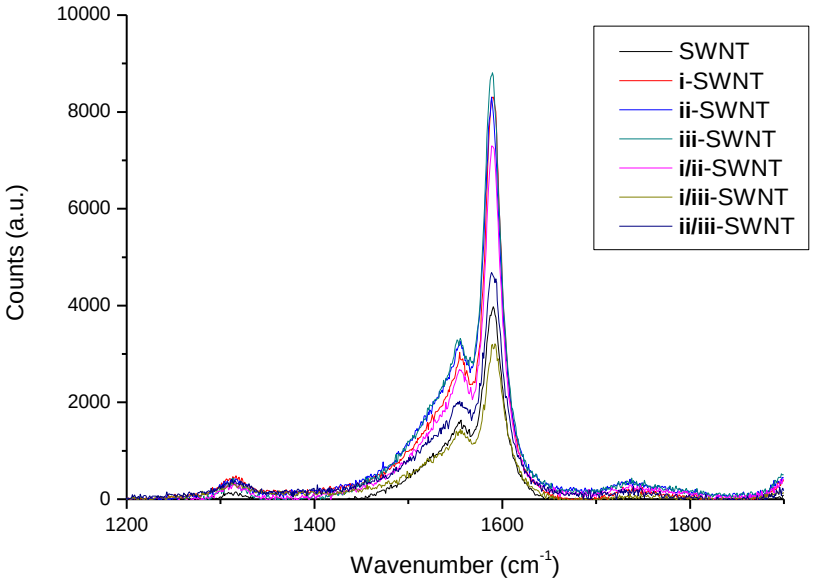

Figure 89. Raman spectra of porphyrin-SWNT adducts, detailing the tangential G bands

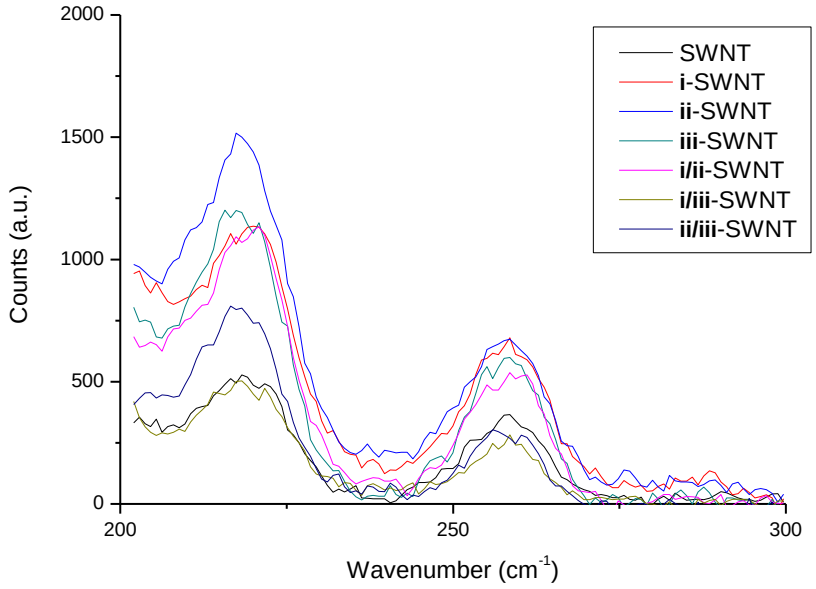

Figure 90. Raman spectra of porphyrin-SWNT adducts, detailing the radial breathing modes of the SWNTs

8.7 – Preparation of AFM samples

Oxidised silicon wafers were sonicated in *iso*-propyl alcohol and dried under nitrogen prior to use. Porphyrin-SWNT samples in DMF were spin coated onto the wafers using the parameters shown in Table 12. Samples were dried at room temperature prior to imaging.

Time (seconds)	Speed (rpm)
0	700
10	700
13	900
33	900
36	1200
56	1200
57	0

Table 12. Spin coating parameters

8.8 – AFM of i-SWNT adducts on oxidised silicon

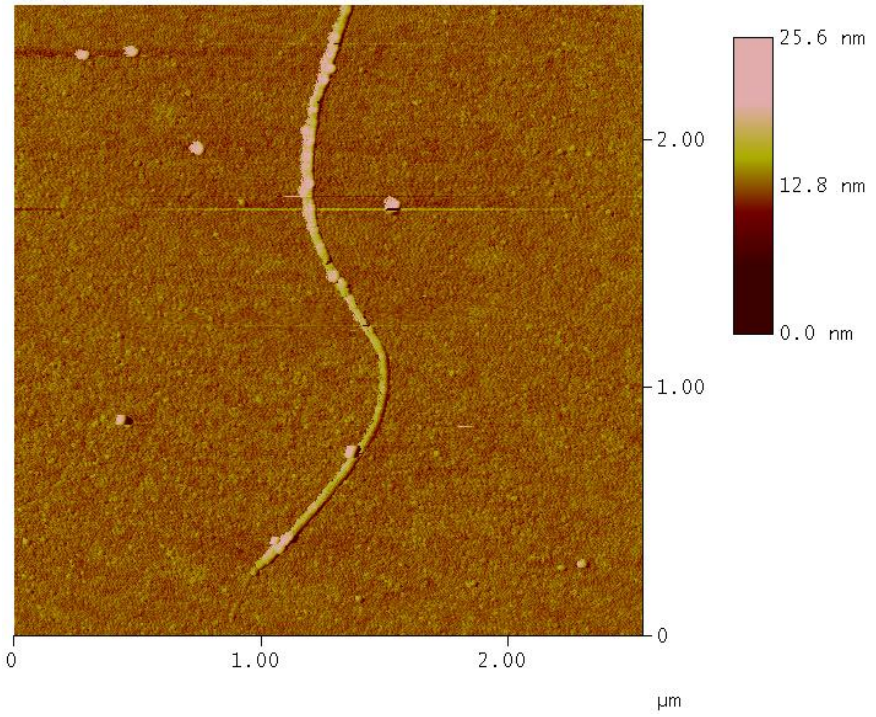

Figure 91. Example AFM image of **i**-SWNT

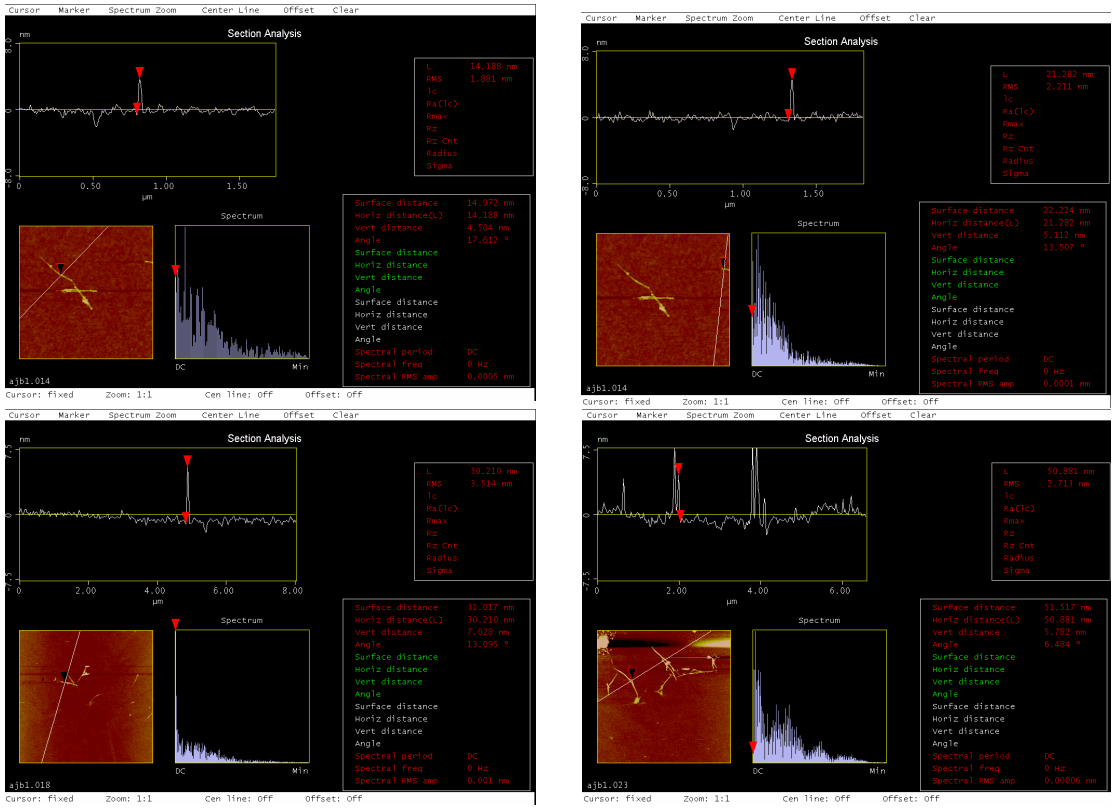

Figure 92. Example AFM images and height profiles of **i**-SWNT

8.9 – AFM of ii-SWNT adducts on oxidised silicon

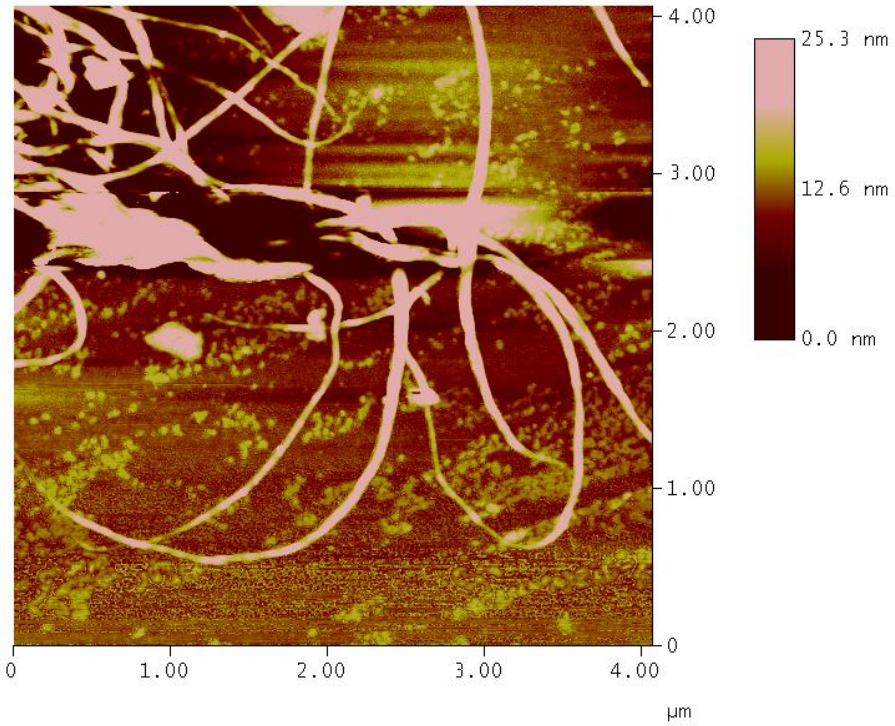

Figure 93. Example AFM image **ii**-SWNT

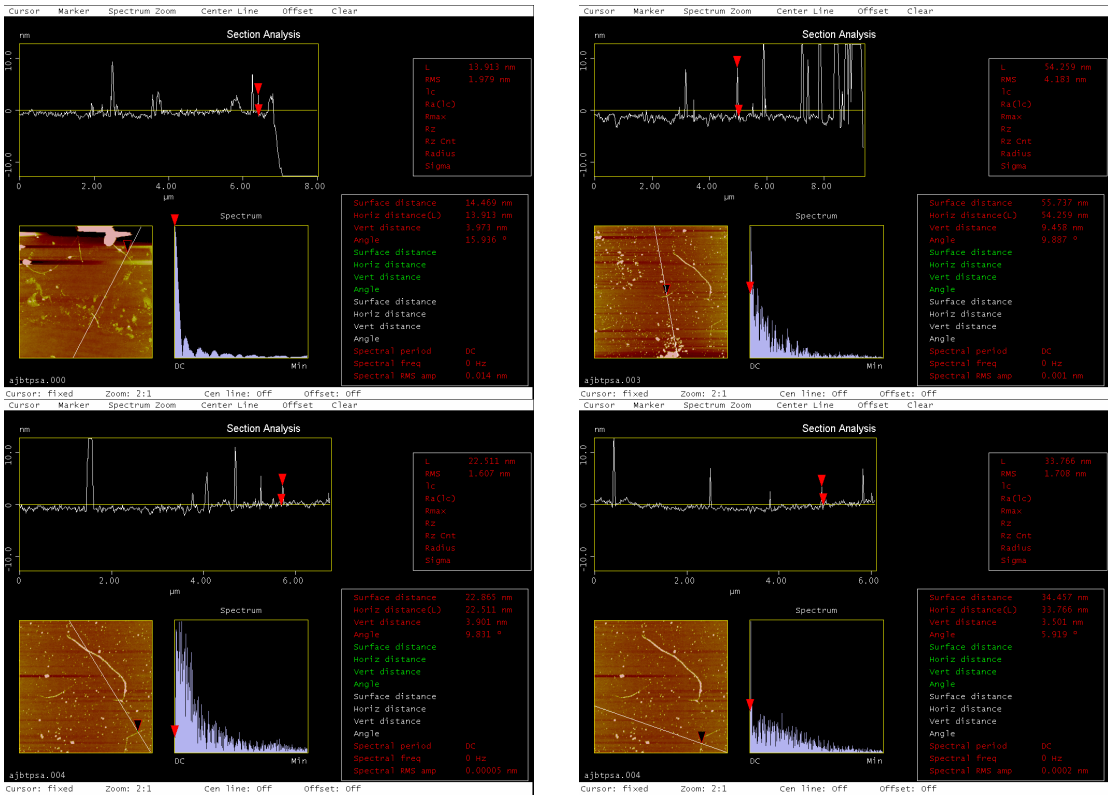

Figure 94. Example AFM images and height profiles of **ii**-SWNT

8.10 – AFM of iii-SWNT adducts on oxidised silicon

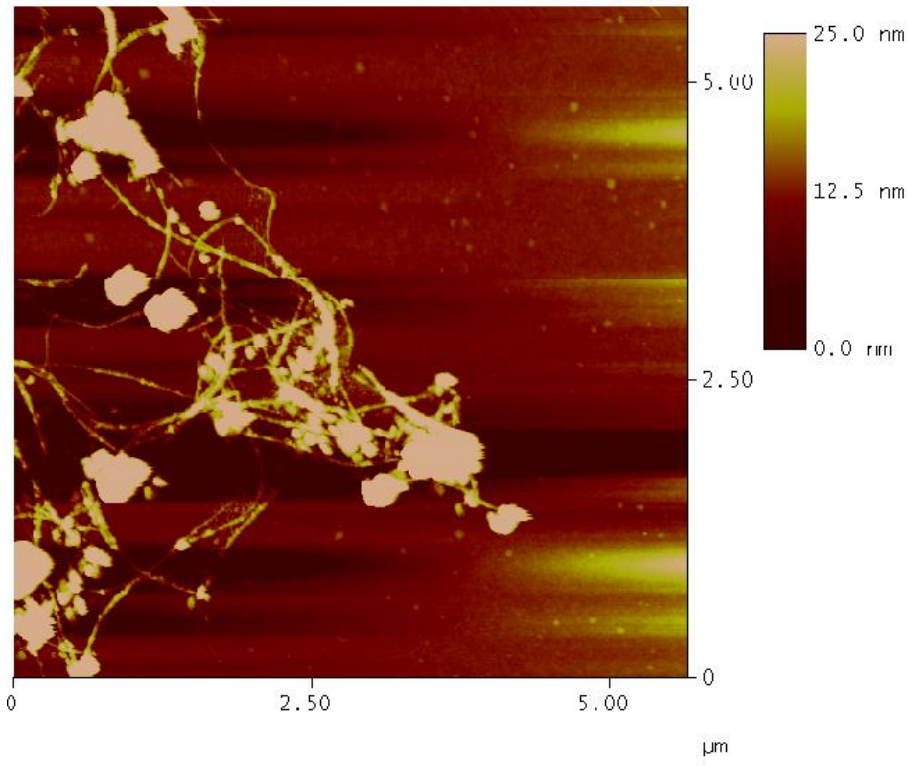

Figure 95. Example AFM images **iii**-SWNT

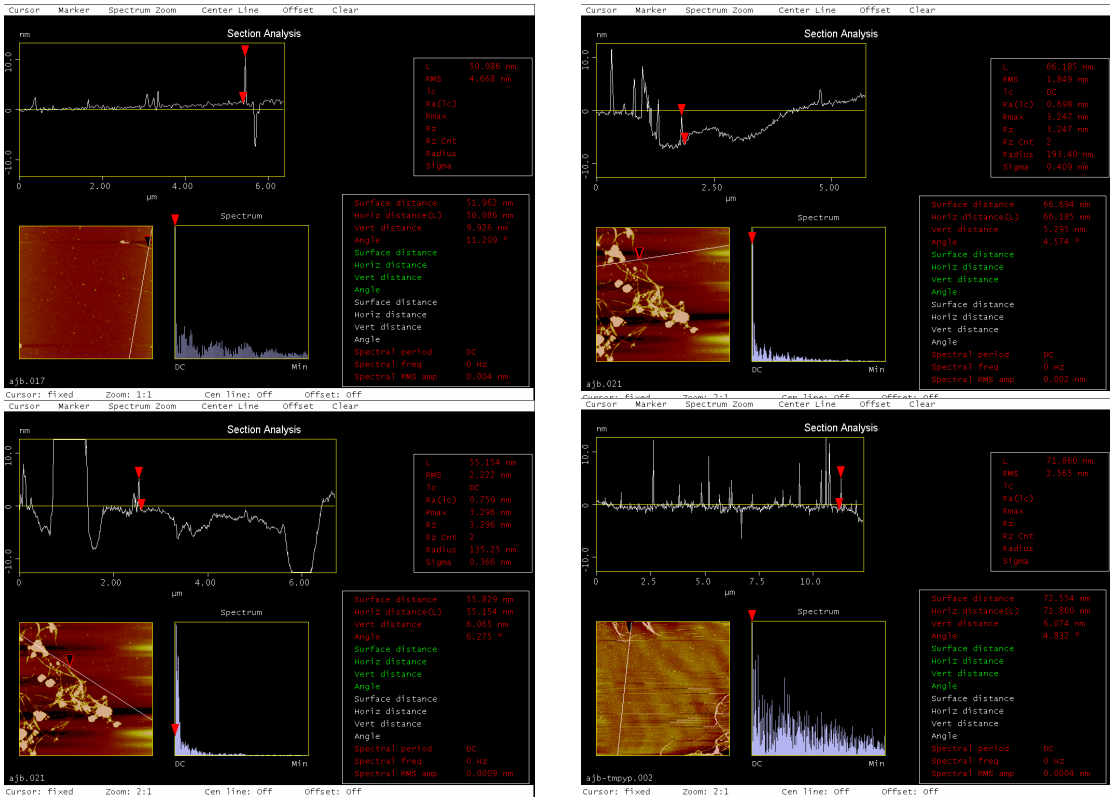

Figure 96. Example AFM images and height profiles of **iii**-SWNT

8.11 – AFM of i/ii-SWNT adducts on oxidised silicon

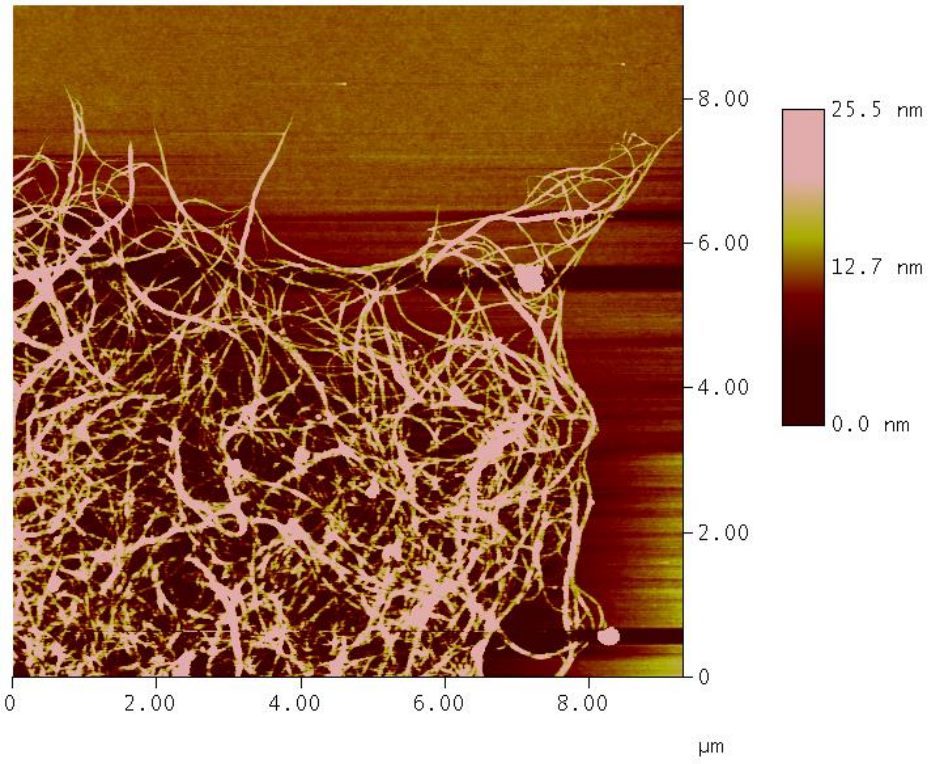

Figure 97. Example AFM images of **i/ii**-SWNT

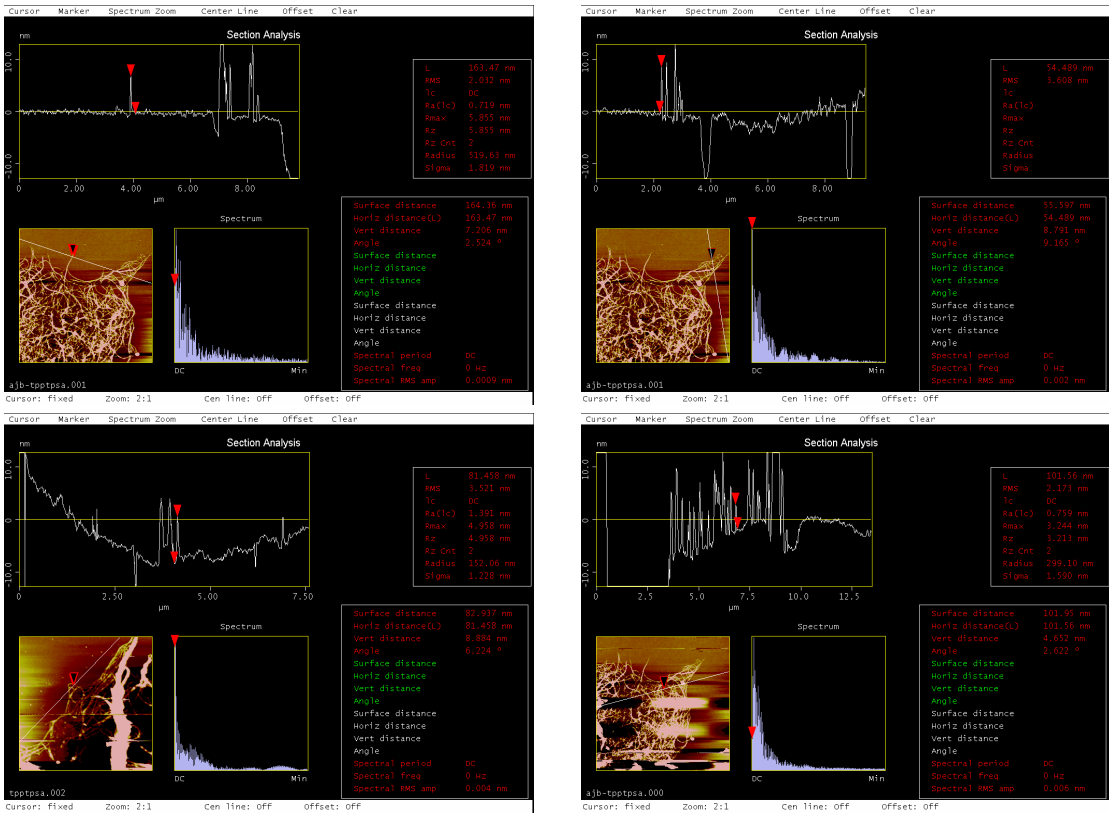

Figure 98. Example AFM images and height profiles of **i/ii**-SWNT

8.12 – AFM of i/iii-SWNT adducts on oxidised silicon

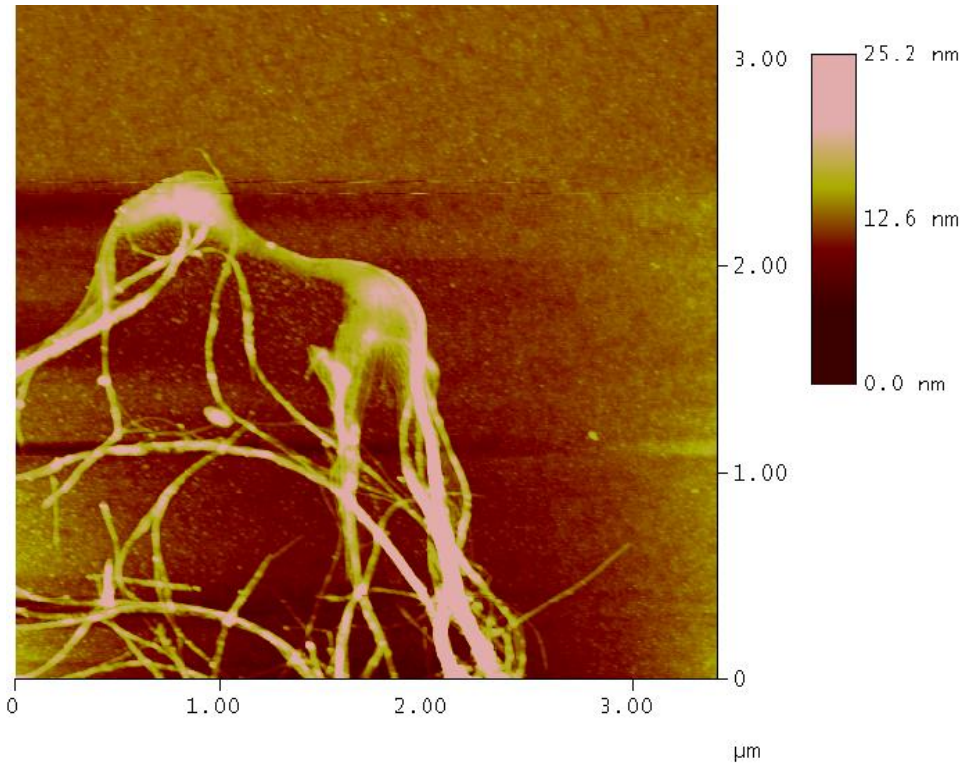

Figure 99. Example AFM images of **i/iii**-SWNT

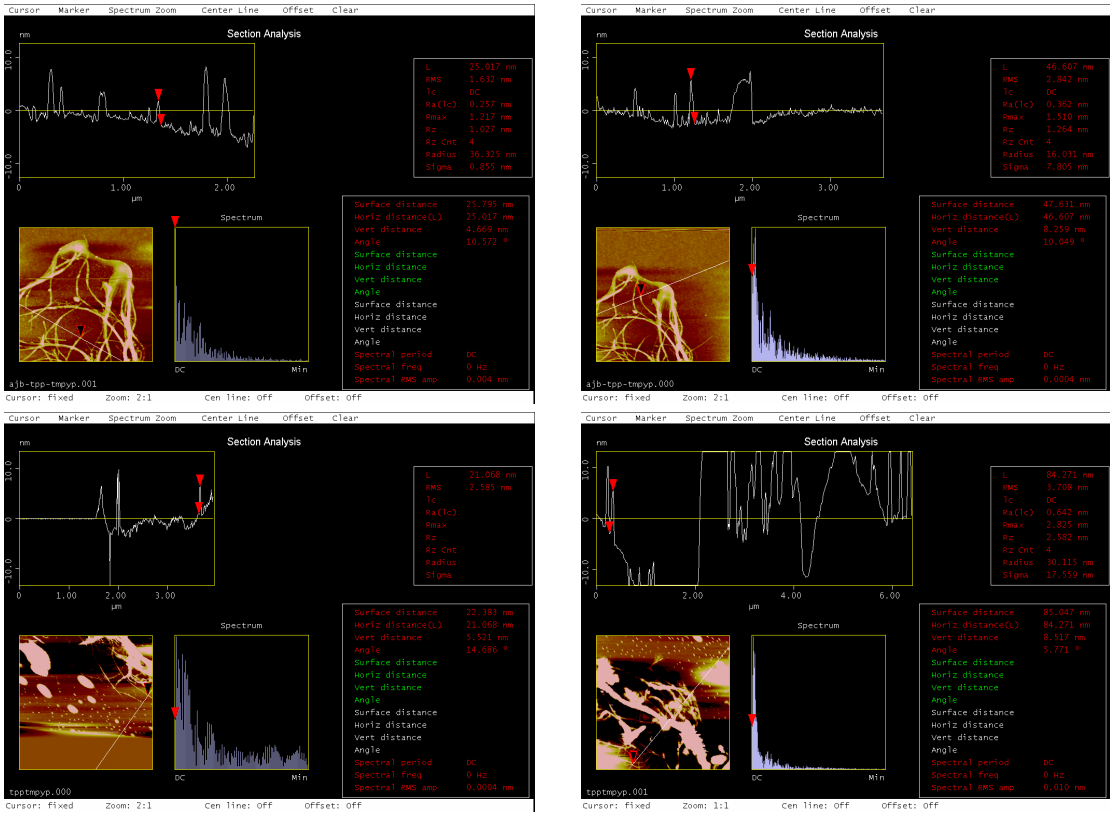

Figure 100. Example AFM images and height profiles of **i/iii**-SWNT

8.13 – AFM of ii/iii-SWNT adducts on oxidised silicon

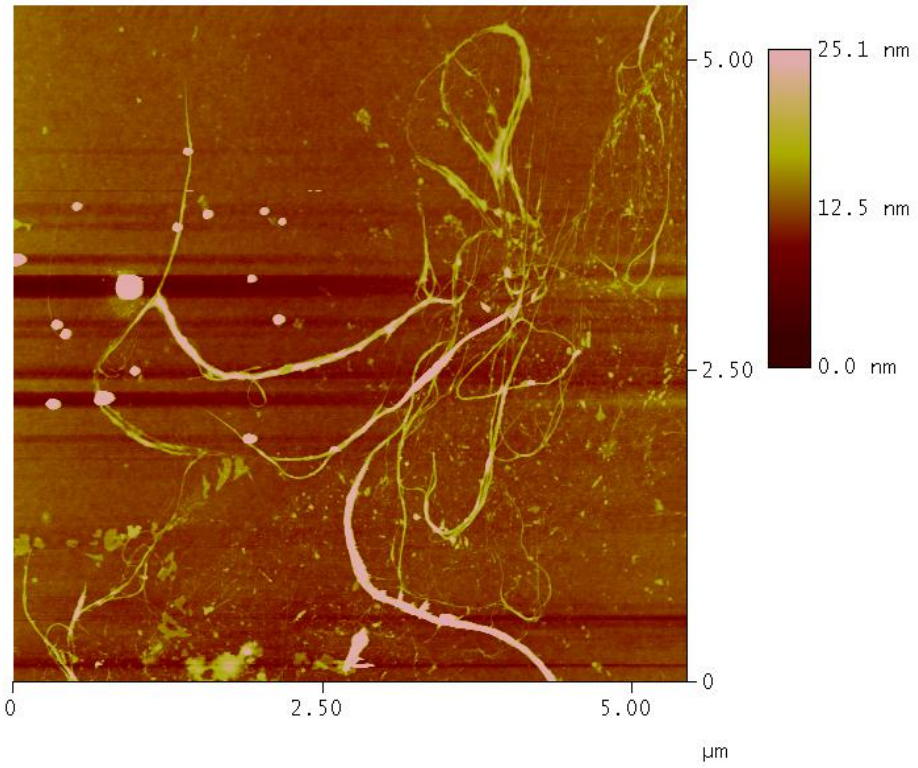

Figure 101. Example AFM images of **ii/iii**-SWNT

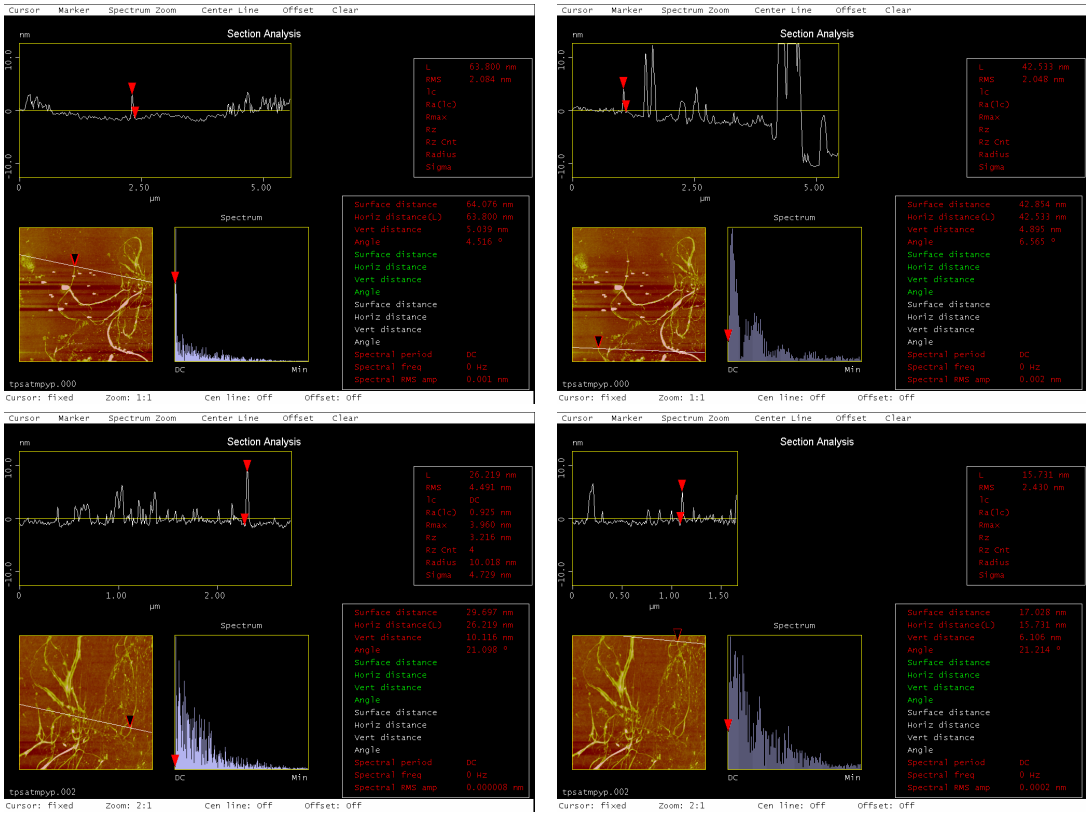

Figure 102. Example AFM images and height profiles of **ii/iii**-SWNT

8.14 – Mean diameter of porphyrin-SWNT adducts

Sample	Mean individual diameter by AFM (nm)
SWNT	1.462
i-SWNT	2.194
ii-SWNT	1.748
iii-SWNT	2.067
i/ii-SWNT	2.154
i/iii-SWNT	1.695
ii/iii-SWNT	1.672

Table 13. Mean diameter of individual porphyrin-SWNT adducts

Sample	Mean bundle diameter by AFM (nm)
SWNT	2.716
i-SWNT	7.295
ii-SWNT	9.627
iii-SWNT	7.945
i/ii-SWNT	10.876
i/iii-SWNT	7.401
ii/iii-SWNT	7.137

Table 14. Mean diameter of bundles of porphyrin-SWNT adducts

8.15 – General method for the sequential stripping of porphyrin adsorbed nanotubes

Porphyrin-SWNT (1.0 mg) samples were dried *in vacuo*, suspended in toluene (30 mL) and stirred (1,200 rpm) for 7 days. The suspension was centrifuged (10,000 rpm, 2 hours) and the solvent decanted. The solvent was concentrated *in vacuo* and the remaining residue was redissolved into DMF (1 mL) for UV-Vis analysis. The remaining porphyrin-SWNT samples were re-suspended into toluene:DMF (10:1, 11 mL) and stirred (1,200 rpm) for 7 days, centrifuged (10,000 rpm, 2 hours), the solvent decanted and concentrated *in vacuo*. The residue was redissolved in DMF (1 mL) and analysed by UV-Vis. The porphyrin-SWNT adducts were re-susupended in glacial acetic acid (10 mL) and stirred (1,200 rpm) for 5 days. The suspension was centrifuged (13,200 rpm, 5 hours), the solvent decanted, concentrated *in vacuo* and the residue redissolved in DMF (1 mL) for UV-Vis studies.

8.16 – Stripping of porphyrin-SWNT adducts with toluene

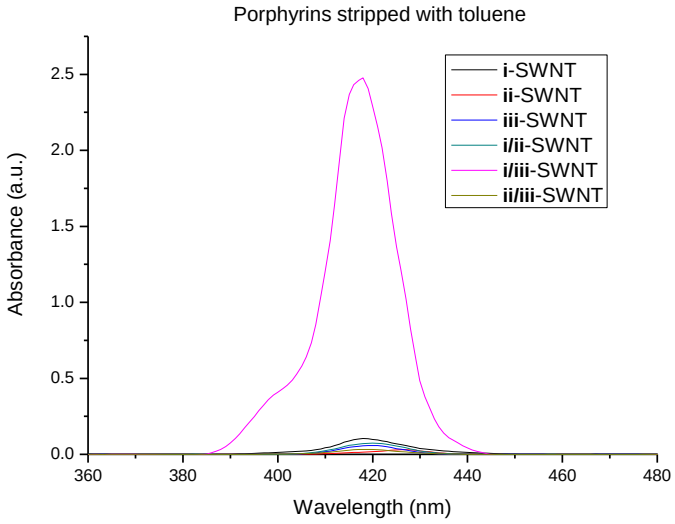

Figure 103. UV-Vis of porphyrins stripped with toluene

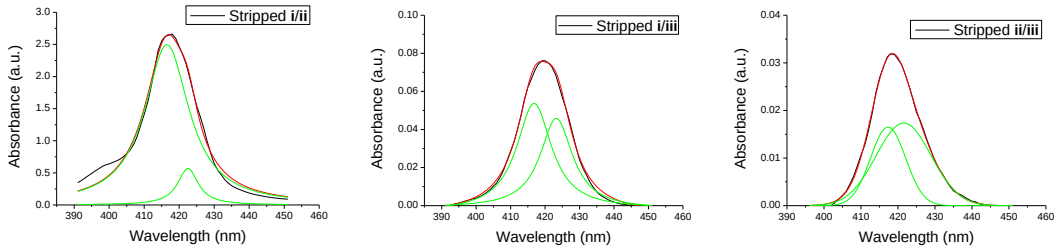

Figure 104. Deconvolution of mixed porphyrin UV-Vis spectra. Black line – Collected spectra; Red line – Fitted curve; Green lines – Deconvoluted spectra.

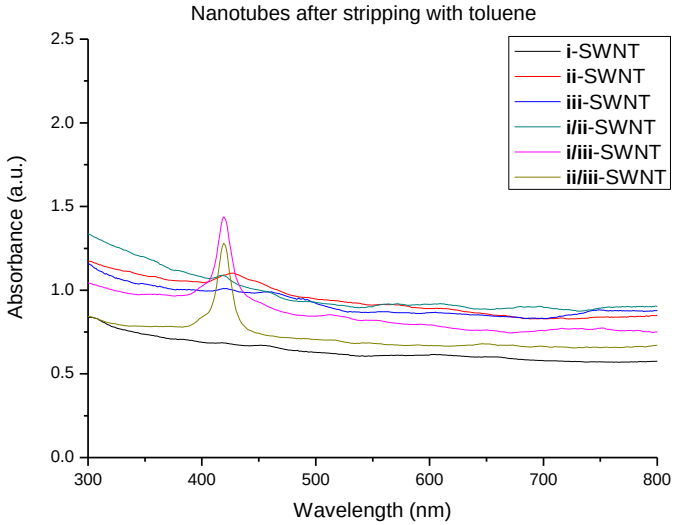

Figure 105. Porphyrin-SWNT adducts after stripping with toluene

8.17 – Stripping of porphyrin-SWNT adducts with toluene:DMF (10:1)

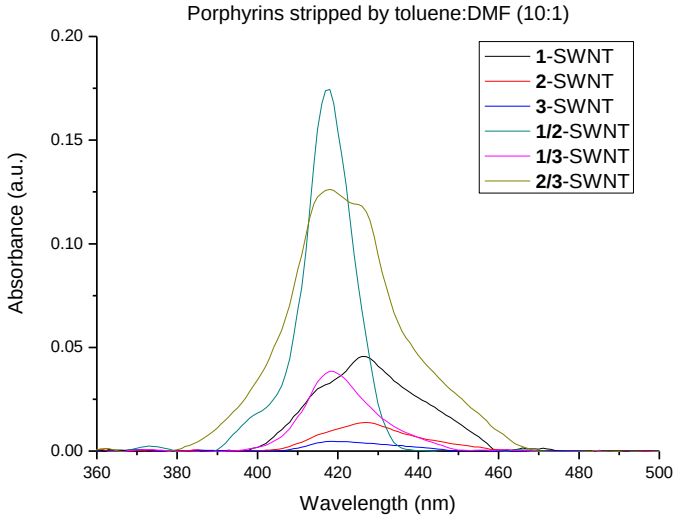

Figure 106. UV-Vis of porphyrins stripped with toluene:DMF (10:1)

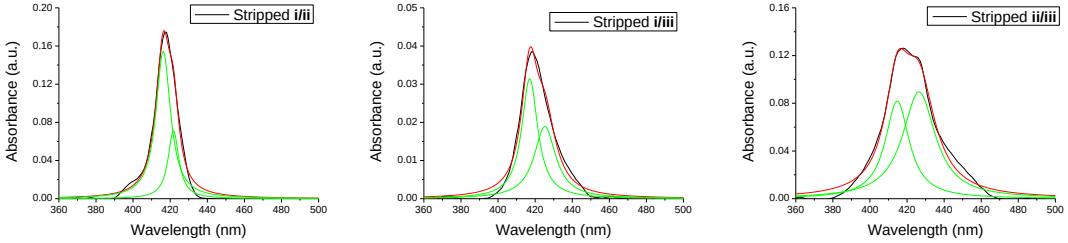

Figure 107. Deconvolution of mixed porphyrin UV-Vis spectra. Black line – Collected spectra; Red line – Fitted curve; Green lines – Deconvoluted spectra.

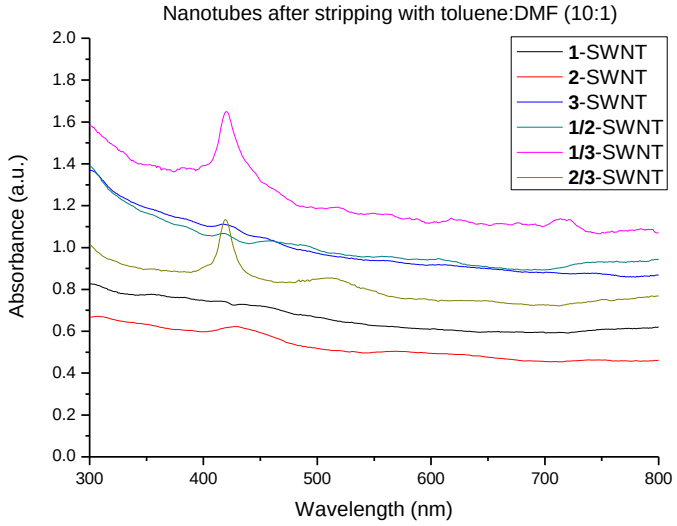

Figure 108. Porphyrin-SWNT adducts after stripping with toluene:DMF (10:1)

8.18 – Minimum loading level of porphyrin-SWNT adducts

The UV-Vis spectra of the porphyrin Soret bands of the mixed porphyrin species stripped from the porphyrin-SWNT adducts were deconvoluted using OriginPro 7.5. Gaussian curves were assumed for both components of the mixed peak.

Porphyrin-SWNT complex	ε	Moles by UV-vis after stripping with:						nmol total	
		Toluene		Toluene/DMF		Acetic acid			
		absorbance	nmoles	absorbance	nmoles	absorbance	moles		
TPP **i**	544000	0.103	0.19	0.046	0.085	0.087	0.16	0.43	0.43
TPSA **ii**	383000	0.059	0.15	0.005	0.013	0.013	0.034	0.20	0.20
TMPyP **iii**	135000	0.03	0.22	0.014	0.10	0.009	0.067	0.39	0.39
TPP(TPSA) **i/ii**	544000	2.009	3.7	0.154	0.28	0.079	0.15	4.12	6.44
(TPP)**TPSA i/ii**	383000	0.765	2.0	0.071	0.19	0.052	0.14	2.32	
TPP(TMPyP) **i/iii**	544000	0.068	0.13	0.031	0.057	0.012	0.022	0.20	0.48
(TPP)**TMPyP i/iii**	135000	0.013	0.096	0.019	0.14	0.005	0.037	0.27	
TPSA(TMPyP) **ii/iii**	383000	0.016	0.042	0.082	0.21	0.02	0.052	0.31	1.18
(TPSA)**TMPyP ii/iii**	135000	0.017	0.13	0.09	0.67	0.011	0.081	0.87	

Table 15. Loading of porphyrin-SWNT adducts as deduced by UV-Vis

8.19 – General method for the stripping of porphyrin adsorbed nanotubes with DMSO

Porphyrin-SWNT adducts (1.0 mg) were stirred (12,000 rpm) in DMSO (30 mL) for 7 days. The sample was centrifuged (10,000 rpm, 90 minutes), the solvent decanted and dried *in vacuo*. UV-vis spectroscopy was used to analyse both the dried dissolved material and the stripped porphyrin-SWNT sample.

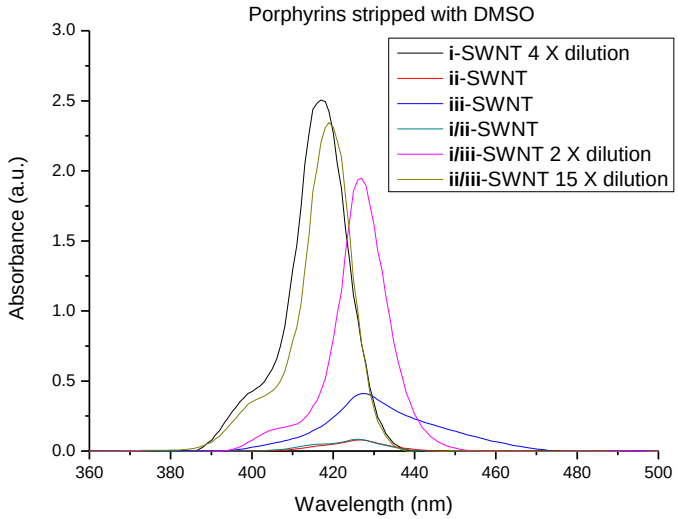

Figure 109. UV-Vis of porphyrins stripped with DMSO

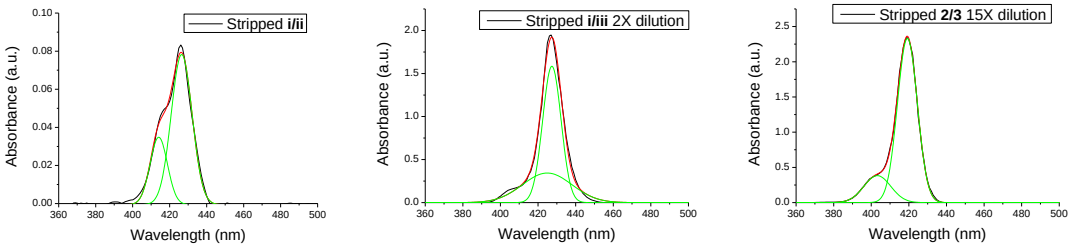

Figure 110. Deconvolution of mixed porphyrin UV-Vis spectra. Black line – Collected spectra; Red line – Fitted curve; Green lines – Deconvoluted spectra

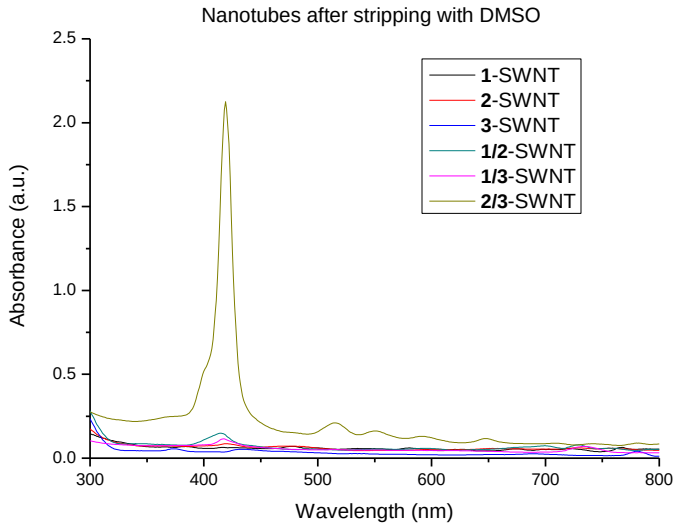

Figure 111. Porphyrin-SWNT adducts after stripping with DMSO

Porphyrin-SWNT complex	ε	Moles by UV-vis after stripping with:			
		DMSO		nmol total	
		absorbance	nmoles		
TPP **i**	544000	10	18.4	18.38	18.38
TSPP **ii**	383000	0.089	0.23	0.23	0.23
TMPyP **iii**	135000	0.411	3.0	3.0	3.0
TPP(TSPP) **i/ii**	544000	0.035	0.064	0.064	0.27
(TPP)**TSPP ii/ii**	383000	0.078	0.20	0.20	
TPP(TMPyP) **i/iii**	544000	3.16	5.8	5.8	10.89
(TPP)**TMPyP i/iii**	135000	0.688	5.1	5.1	
TSPP(TMPyP) **ii/iii**	383000	5.76	15	15	270
(TSPP)**TMPyP ii/iii**	135000	34.485	255	255	

Table 16. Loading of porphyrin-SWNT adducts as deduced by UV-Vis

The UV-Vis spectra of the porphyrin Soret bands of the mixed porphyrin species stripped from the porphyrin-SWNT adducts were deconvoluted using OriginPro 7.5. Gaussian curves were assumed for both components of the mixed peak.

8.20 – Preparation of electrochemical cells of porphyrin-SWNT complexes

Sample preparation and acquisition of cyclic voltammograms was performed in collaboration with Matthew Lacey of Prof. John Owen's research group (University of Southampton) in the following manner.

Porphyrin-SWNT complex was ground with acetylene black and granular PTFE in an approximate 30:60:10 ratio, exact ratios were noted for each sample. The ground sample mixture was sandwiched between aluminium foil and rolled through sequentially smaller press apertures until the desired pellet thickness was obtained (~80 μm). Pellets were formed by punching 1 cm diameter disks out of the sample sheet, pellets were dried *in vacuo* before being transferred to a glove box and assembled into an electrochemical cell for measurement, as per the diagram below.

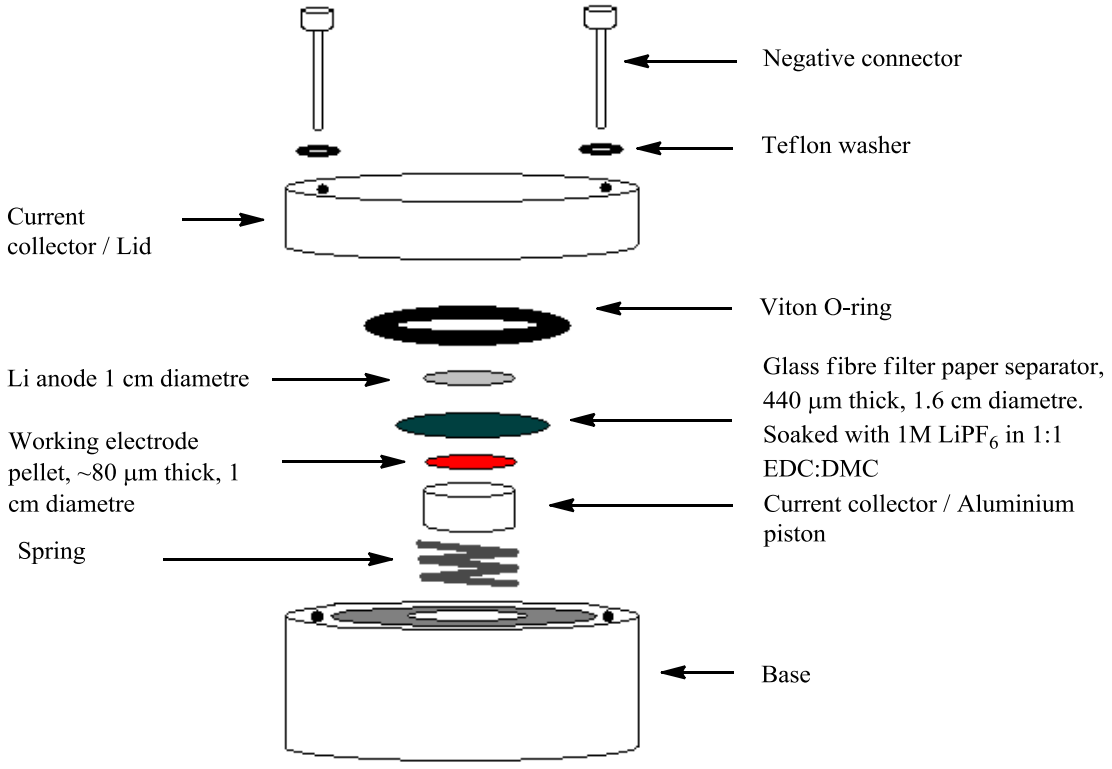

Figure 112. Schematic of a solid state electrochemical cell

8.21 – Cyclic voltammetry of porphyrin-SWNT adducts

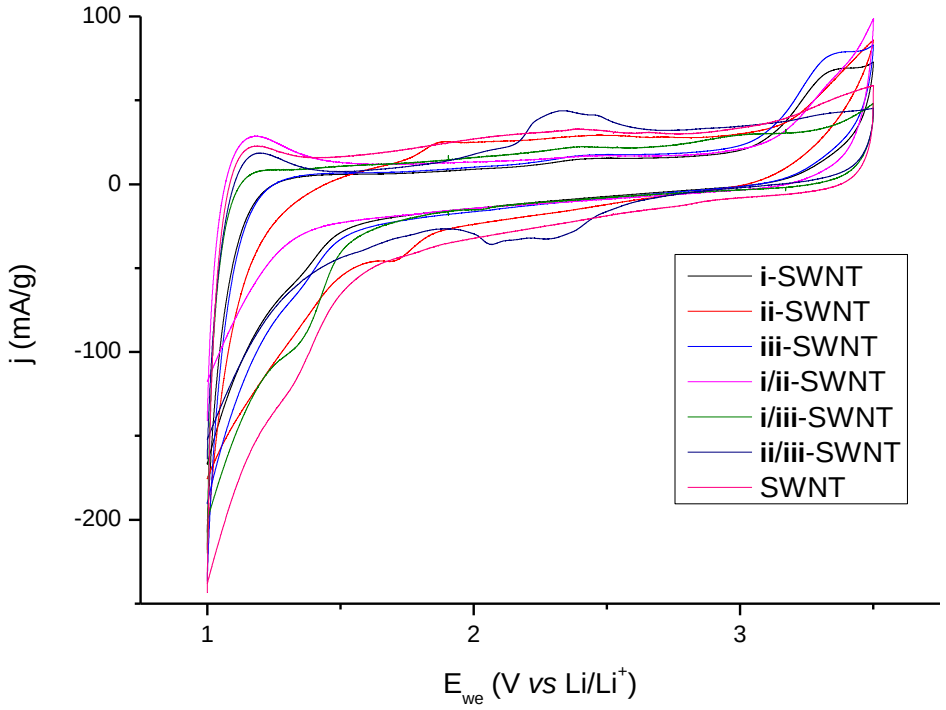

Figure 113. Cyclic voltammogram of porphyrin-SWNT adducts, sweep rate 0.2 mV s^{-1}, potentials *vs* Li/Li^+, current normalised for pellet percentage composition of sample

Sample	Pellet mass (mg)	Pellet % by mass		
		Sample	Acetylene Black	PTFE
i-SWNT	3.22	31.52	61.71	6.77
ii-SWNT	3.68	29.06	66.17	4.76
iii-SWNT	2.96	30.05	60.46	9.49
i/ii-SWNT	2.80	27.88	64.13	7.99
i/iii-SWNT	3.74	28.93	62.81	8.26
ii/iii-SWNT	3.67	29.91	64.79	5.28

Table 17. Exact percentage compositions of porphyrin-SWNT adduct pellets for cyclic voltammetry

8.22 – Cyclic voltammetry of ii-SWNT

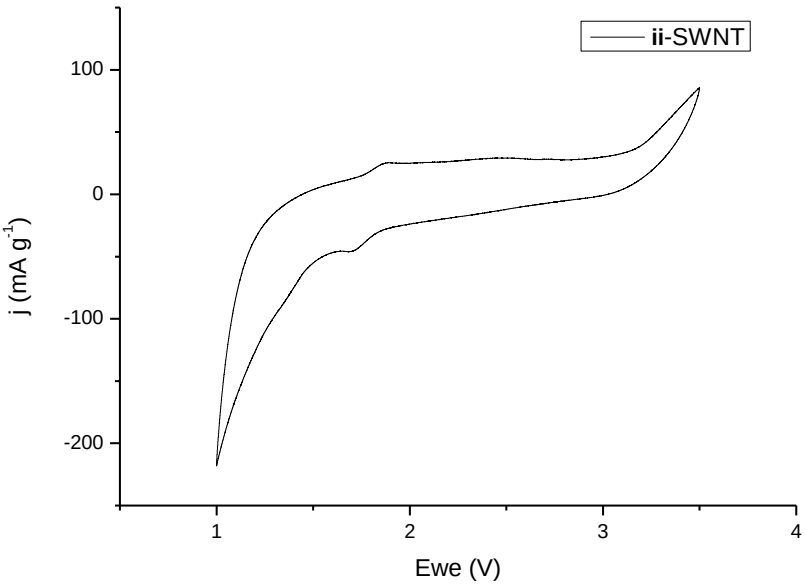

Figure 114. Solid state cyclic voltammogram of **ii**-SWNT

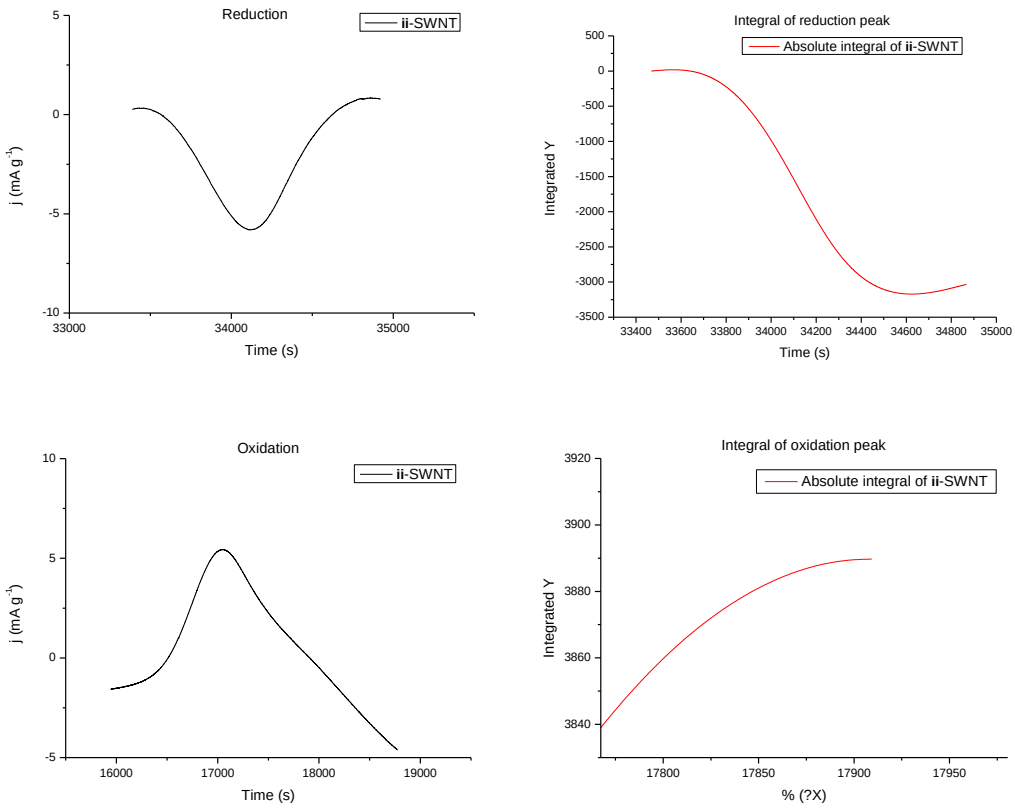

Figure 115. Integration of peaks of the cyclic voltammagram of **ii**-SWNT

Reduction peak integral = 3171 mAs g^{-1} = 3.171 As g^{-1} = 3.171 C g^{-1}

3.174 C g^{-1} / 96485.34 C mol^{-1} = 3.29 x 10^{-5} mol g^{-1} = 32.9 nmoles mg^{-1}

Oxidation peak integral = 3889 mAs g^{-1} = 3.889 As g^{-1} = 3.889 C g^{-1}

3.889 C g^{-1} / 96485.34 C mol^{-1} = 4.031 x 10^{-5} = 40.3 nmoles mg^{-1}

8.23 – Cyclic voltammetry of ii/iii-SWNT

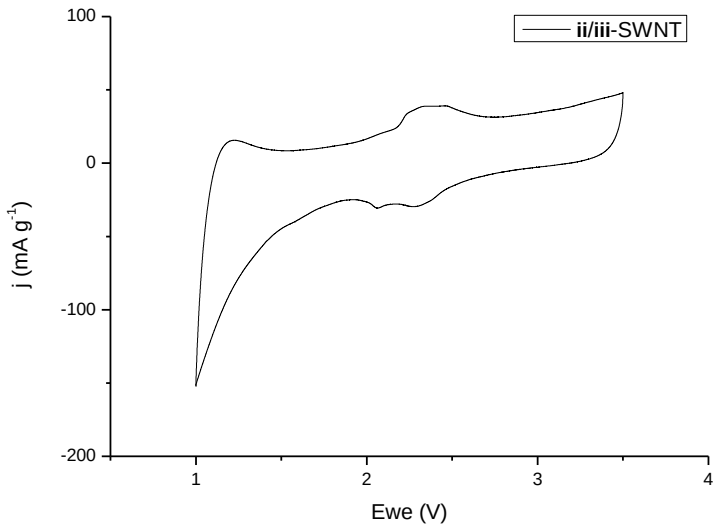

Figure 116. Solid state cyclic voltammogram of **ii/iii**-SWNT

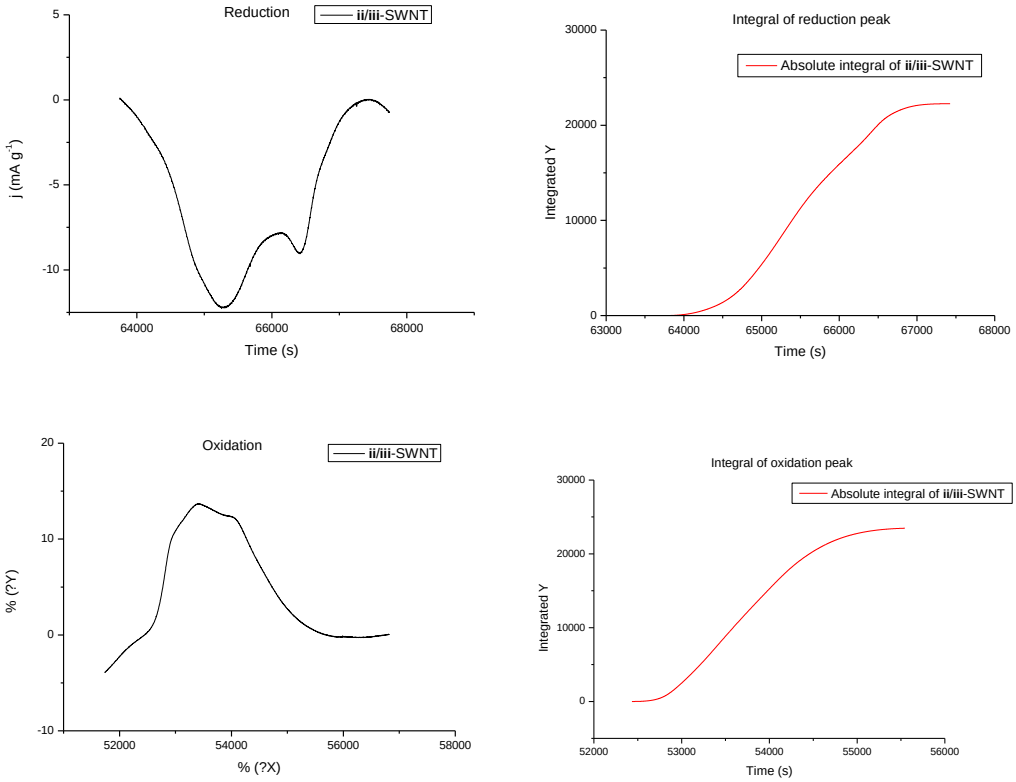

Figure 117. Integration of peaks of the cyclic voltammagram of **ii/iii**-SWNT

Reduction peak integral = 22261 mAs g^{-1} = 22.261 As g^{-1} = 22.261 C g^{-1}

22.261 C g^{-1} / 96485.34 C mol^{-1} = 2.31 x 10^{-4} mol g^{-1} = 231 nmoles mg^{-1}

Oxidation peak integral = 23475 mAs g^{-1} = 23.475 As g^{-1} = 23.475 C g^{-1}

23.475 C g^{-1} / 96485.34 C mol^{-1} = 2.43 x 10^{-4} = 243 nmoles mg^{-1}

8.24 – Cyclic voltammetry with varying scan rates of ii/iii-SWNT

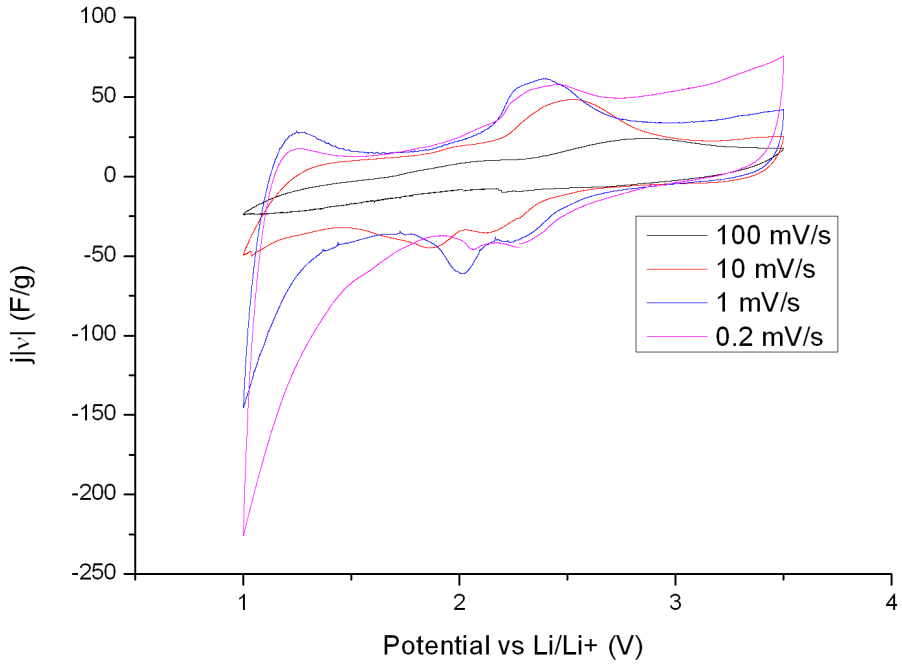

Figure 118. Cyclic voltammogram of **ii/iii**-SWNT with differing sweep rates

Peak oxidation potentials from Figure 118 were plotted versus the natural log of their respective scan rate in order to demonstrate slow electron transfer kinetics.

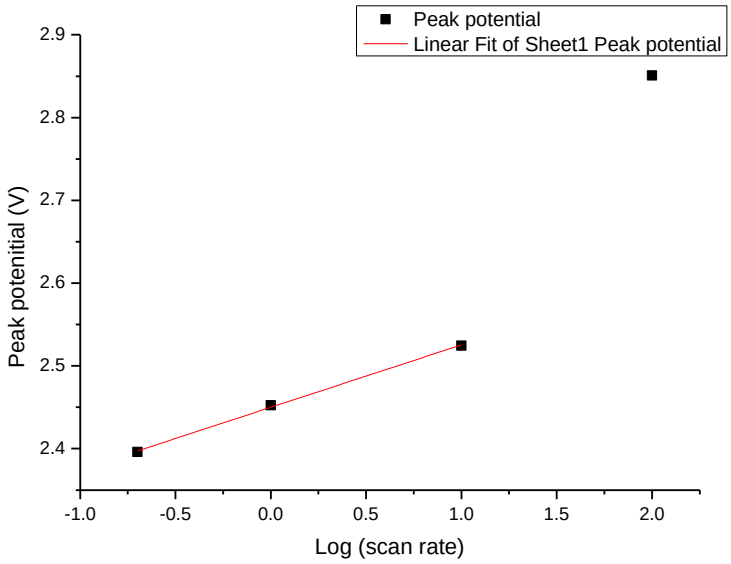

Figure 119. Peak potential vs Log scan rate for **ii/iii**-SWNT

8.25 – Elemental analysis of porphyrin-SWNT adducts

Porphyrin-SWNT adducts were dried under high vacuum for 1 week before sending to Medac Ltd for elemental analysis.

Name	% composition		Elemental ratio		Carbon atoms in SWNT per porphyrin molecule	nmoles of porphyrin per mg of carbon	
	C	N	C	N			
SWNT	79.89	0.00					
i-SWNT	78.01	1.80	202.18	4.00	158.18	527	
ii-SWNT	71.30	1.63	204.06	4.00	160.06	521	
iii-SWNT	75.23	1.87	385.23	8.00	313.23	266	
i/ii-SWNT	73.20	2.27	152.25	4.00	108.25	770	TPP and TSPP do not have differing C:N ratios therefore no need to assume 100% of either to get a porphyrin:CNT ratio
i/iii-SWNT	76.71	2.05	170.40	4.00	126.40	659	Assuming 100% TPP
			340.80	8.00	268.80	310	Assuming 100% TMPyP
ii/iii-SWNT	66.19	6.06	51.26	4.00	7.26	11478	Assuming 100% TSPP
			102.52	8.00	30.52	2730	Assuming 100% TMPyP
			76.89	6.00	18.89	4412	Assuming 1:1 salt of TSPP:TMPyP

Table 18. Elemental analysis of porphyrin-SWNT adducts

8.26 – Synthesis of 4-(3-hydroxy-3-methylbut-1-ynyl) benzaldehyde (I)[20]

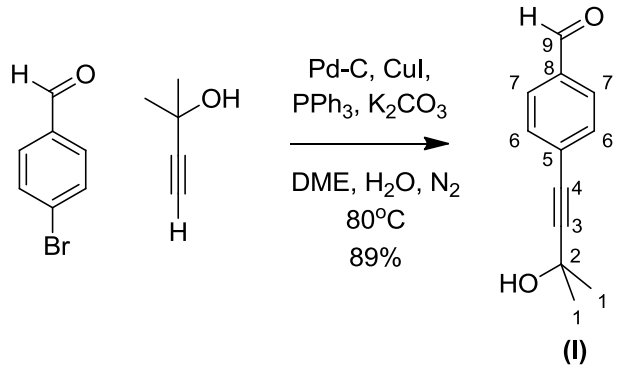

(I)

Para-bromobenzaldehyde (6.00 g. 30.0 mmol, 1.0 eq), 10 % palladium on carbon (1.26 g, 1.2 mmol, 0.04 eq), triphenylphosphine (1.28 g, 4.8 mmol, 0.16 eq), copper (I) iodide (0.46 g, 2.4 mmol, 0.08 eq) and potassium carbonate (20.58 g, 150.0 mmol, 5.0 eq) were dissolved into DME:H_2O (1:1, 120 mL) and purged with nitrogen for 30 mins. 2-methylbut-3-yne-2-ol (14.70 mL, 150.0 mmol, 5.0 eq) was added and the reaction mixture heated (90 ^oC) for 18 hours. The reaction mixture was filtered through ¾" of celite. The product was extracted into ethyl acetate (400 ml), washed with brine (2 x 100 mL), dried over Na_2SO_4 and concentrated *in vacuo*. The crude product was purified twice by column chromatography (first column; silica, eluent – 12.5 % ethyl acetate in petroleum ether → 20 % ethyl acetate in petroleum ether. Second column; silica, eluent – 100 % DCM → 100 % ethyl acetate). The product was obtained as a light yellow oil, 5.00 g (26.6 mmol, 89 %).

^{1}H NMR (400 MHz, $CDCl_3$): δ ppm 1.68 (s, 6 H, **1**), 7.52 (dd, J_{HH} = 8.19, 1.70 Hz, 2 H, **6**), 7.79 (dd, J_{HH} = 8.15, 1.55 Hz, 2 H, **7**), 9.98 (s, 1 H, **9**)

^{13}C{^{1}H} NMR (100 MHz, $CDCl_3$): δ ppm 31.3 (CH_3, **1**), 65.4 (C, **2**), 81.1 (C, **4**), 98.4 (C, **3**), 129.3 (C, **5**), 129.5 (CH, **7**), 132.1 (CH, **6**), 135.2 (C, **8**), 191.7 (CH, **9**)

GC-EI MS ($C_{12}H_{12}O_2$): Monoisotopic mass 188.22, observed *m/z* 188.2 $[M]^{+\cdot}$, 173.2 $[M–CH_3]^+$, 159.2 $[M–CHO]^+$

UV-Vis (MeCN, 16.0 µM): λ_{max} (log ε) 216 (4.17), 277 (4.46)

Emission (MeCN, 1.60 µM): No fluorescence observed

R_f (silica, 20 % EA in pet ether): 0.26

Melting Point: 55.3 – 56.2 °C (no lit. value)

8.27 – Synthesis of 5,10,15-triphenyl-20-(*p*-(3-methyl-3-hydroxyl-1-butynyl) phenyl-21*H*, 23*H*-porphyrin (II)[20]

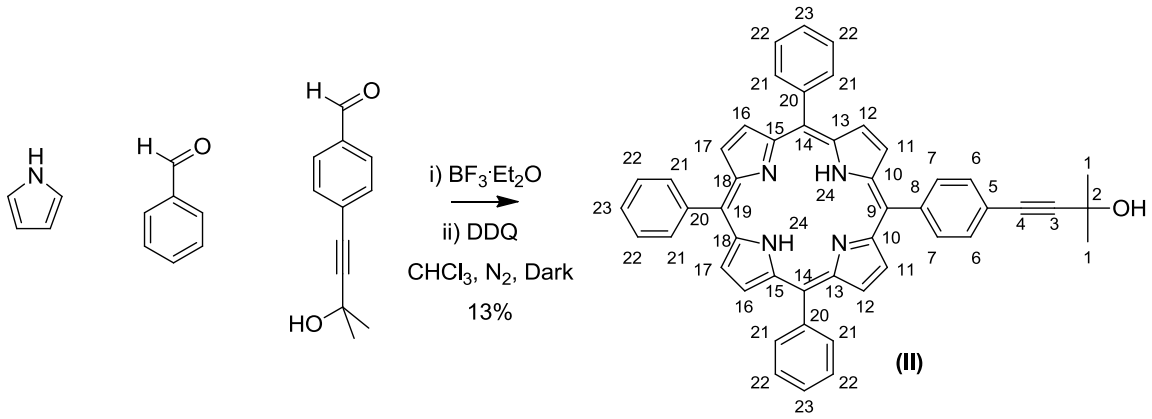

Pyrrole (2.10 mL, 30.0 mmol, 6.00 eq), benzaldehyde (3.18 g, 30.0 mmol, 6.00 eq) and 4-(3-hydroxy-3-methylbut-1-ynyl) benzaldehyde (0.94 g, 5.0 mmol, 1.00 eq) were dissolved in chloroform (500 mL) and purged with N_2 for 30 minutes in the dark. Boron trifluoride etherate (0.57 mL, 4.5 mmol, 0.90 eq) was added and the reaction stirred at room temperature. After one hour DDQ (6.81 g, 30.0 mmol, 6.00 eq) was added and left to stir overnight. The reaction mixture was concentrated *in vacuo*, DCM (200 ml) was added and the insoluble polypyrroles filtered out while loading the solution onto a column (silica/alumina, eluent – DCM → 5 % methanol in DCM). The crude product was further purified column chromatography (silica/alumina, eluent – 0.5 % methanol in DCM) to give 463.7 mg (666 µmol, 13 %) of dark purple crystals.

^{1}H NMR (400 MHz, $CDCl_3$): δ ppm -2.76 (br. s., 1 H, **24**), 1.78 (s, 6 H, **21**), 7.71-7.80 (m, 9 H, **22** & **23**), 7.83 (d, J_{HH} = 8.03 Hz, 2 H, **6**), 8.18 (d, J_{HH} = 8.16 Hz, 2 H, **7**), 8.22 (d, J_{HH} = 7.03 Hz, 6 H, **21**), 8.83 (d, J_{HH} = 4.77 Hz, 2 H, **11**), 8.86 (s, 4 H, **16** & **17**), 8.87 (d, J_{HH} = 4.77 Hz, 2 H, **12**)

^{13}C{^{1}H} NMR (100 MHz, $CDCl_3$): δ ppm 31.6 (CH_3, **1**), 65.8 (C, **2**), 82.2 (C, **4**), 95.0 (C, **3**), 119.1 (C, **10**), 120.3 (C, **13** or **15**), 120.4 (C, **13** or **15**), 122.2 (C, **18**), 126.7 (CH, **22**), 127.7 (CH, **23**), 130.0 (CH, **6**) 130.3 - 132.0 (m, CH, **11, 12, 16** & **17**), 134.5 (CH, **7**), 134.5 (CH, **21**), 142.1 (C, **20**), 142.3 (C, **8**)

MALDI-TOF ($C_{49}H_{36}N_4O$): Monoisotopic mass 696.84, Observed mass 697.97 $[M+H]^+$

UV-Vis (MeOH, 2.21 µM): λ_{max} (log ε) 400 nm (4.73), 414 nm (5.35), 512 nm (4.07), 547 nm (3.83), 589 nm (3.73), 644 nm (3.61)

Emission (MeOH, 2.21 µM): λ_{ex} 414 nm, λ_{em} (rel int) 648 nm (1), 714 nm (0.34)

***R*$_f$** (silica, DCM): 0.28

Melting Point: 195.2 – 197.5 °C (no lit. value)

8.28 – Synthesis of zinc (II) 5,10,15-triphenyl-20-(*p*-(3-methyl-3-hydroxyl-1-butynyl)-phenyl porphyrin (III)[20]

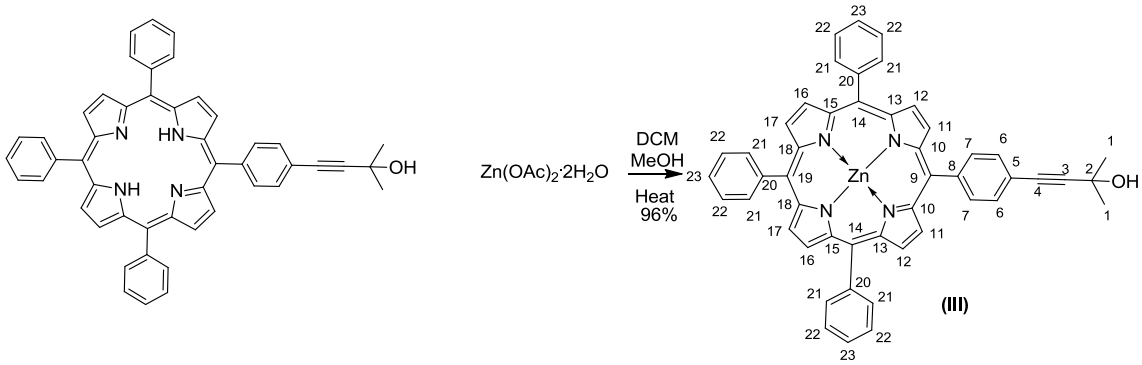

5,10,15-triphenyl-20-(*para*-(3-methyl-3-hydroxyl-1-butynyl)-phenyl-21*H*,23*H*-porphyrin (339 mg, 0.49 mmol, 1.00 eq) and zinc acetate dihydrate (5.37 g, 24.5 mmol, 50.00 eq) were dissolved in DCM (80 mL) and methanol (10 mL) before heating gently (35 °C) for 10 minutes. The reaction mixture was concentrated *in vacuo*, redissolved in DCM (200 mL), the excess zinc acetate dihydrate filtered out and the filtrate again concentrated *in vacuo*. 356.8 mg of purple powder was obtained (471 µmol, 96 %).

^{1}H NMR (400 MHz, $CHCl_3$): δ ppm 1.64 (s, 6 H, **1**), 7.73 - 7.81 (m, 9 H, **22** & **23**), 7.82 (d, J_{HH} = 8.03 Hz, 2 H, **6**), 8.20 (d, J_{HH} = 8.03 Hz, 2 H, **7**), 8.22 - 8.28 (m, 6 H, **21**), 8.95 (d, J_{HH} = 4.64 Hz, 2 H, **11**), 8.98 (s, 4 H, **16** & **17**), 8.99 (d, J_{HH} = 4.64 Hz, 2 H, **12**)

^{13}C{^{1}H} NMR (100 MHz, $CDCl_3$): δ ppm 31.4 (CH_3, **1**), 65.7 (C, **2**), 82.2 (C, **4**), 94.6 (C, **3**), 120.0 (C, **10**), 121.2 (C, **13** or **15**), 121.3 (C, **13** or **15**), 121.9 (C, **18**), 126.5 (CH, **22**), 127.5 (CH, **23**), 129.8 (CH, **6**), 131.6 (CH, **11** or **12**), 132.0 (CH, **16** or **17**), 132.0 (CH, **16** or **17**), 132.1 (CH, **11** or **12**), 134.3 (CH, **7**), 134.4 (CH, **21**), 142.8 (C, **20**), 143.0 (C, **8**), 149.8 (C, **9**), 150.2 (C, **19**), 150.2 (C, **14**), 150.23 (C, **14**)

MALDI-TOF ($C_{49}H_{34}N_4OZn$): Monoisotopic mass 758.20, observed mass 759.54 $[M+H]^+$

UV-Vis (MeOH, 2.50 µM): λ_{max} (log ε) 401 nm (4.08), 421 nm (5.06), 555 nm (3.81), 594 nm (3.60)

Emission (MeOH, 2.50 µM): λ_{ex} 421 nm, λ_{em} (rel int) 604 nm (1), 655 nm (0.64), 842 nm (0.03)

R_f (silica, DCM): 0.14

Melting Point: 217.2 – 220.1 °C (no lit. value)

8.29 – Synthesis of 5'-DMT-5-iodo-dU (IV)[20]

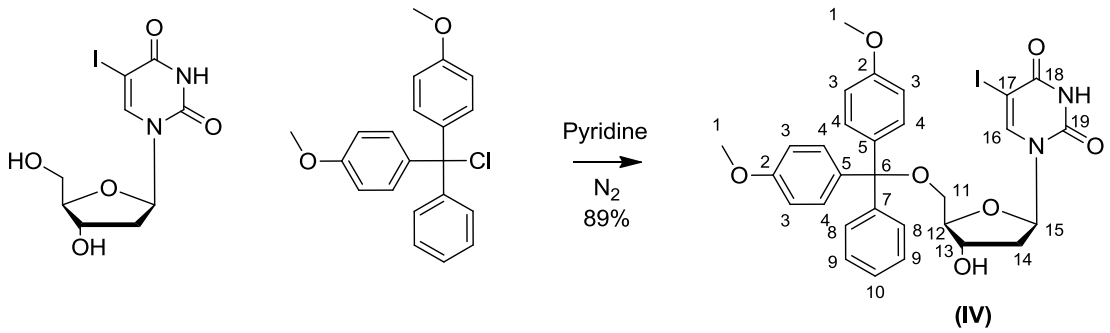

(IV)

5-iodo-2'-deoxyuridine (5-iodo-dU, 5.00 g, 14.3 mmol, 1.00 eq) was co-evaporated with pyridine (10 ml) prior to flushing with N_2 (5 mins) and dissolving in anhydrous pyridine (40 ml). 4,4'-dimethoxytrityl chloride (5.02 g, 14.8 mmol, 1.03 eq) was added in 4 portions over 4 hours and the reaction stirred for 24 hours in total. Reaction mixture was poured in brine (100 mL), extracted into DCM (200 mL) and further washed with brine (2 x 100 mL). The organic phase was dried over $MgSO_4$, filtered, concentrated *in vacuo* and co-evaporated with toluene (2 X 50 mL) and chloroform (2 x 50 mL) to produce viscous orange oil. The product was purified by column chromatography (silica neutralised with 1 mL TEA, eluent – 4:6 EA:hexane → 6:4 EA:hexane), the product was concentrated *in vacuo* to give 8.27 g of white foam (12.6 mmol, 89 %).

^{1}H NMR (400 MHz, $CDCl_3$) δ ppm 2.34 (ddd, J_{HH} = 13.6, 7.5, 6.5 Hz, 1 H, **14**), 2.54 (ddd, J_{HH} = 13.4, 5.6, 2.0 Hz, 1 H, **14**), 3.42 (dd, J_{HH} = 10.5, 3.0 Hz, 1 H, **11**), 3.47 (dd, J_{HH} = 10.5, 3.0 Hz, 1 H, **11**), 3.84 (s, 6 H, **1**), 4.14 (m, 1 H, **12**), 4.60 (ddd, J_{HH} = 5.5, 3.0 Hz, 1 H, **13**), 6.36 (dd, J_{HH} = 7.5, 6.0 Hz, 1 H, **15**), 6.90 (d, J_{HH} = 8.5 Hz, 4 H, **3**), 7.28 (t, J_{HH} = 7.0 Hz, 1 H, **10**), 7.35 (dd, J_{HH} = 14.1, 6.0 Hz, 5 H, **9**), 7.38 (dd, J_{HH} = 8.8, 2.3 Hz, 4 H, **4**), 7.46 (d, J_{HH} = 7.5 Hz, 2 H, **8**), 8.18 (s, 1 H, **16**)

^{13}C{^{1}H} NMR (100 MHz, $CDCl_3$): δ ppm 41.4 (CH_2, **14**), 55.2 (CH_3, **1**), 63.6 (CH_2, **11**), 69.7 (C, **17**), 72.2 (CH, **13**), 85.5 (CH, **15**), 86.4 (CH, **12**), 86.9 (C, **6**), 113.3 (CH, **3**), 126.9 (CH, **9**), 128.0 (CH, **10**), 128.0 (CH, **8**), 130.0 (CH, **4**), 130.0 (CH, **4**), 135.4 (C, **5**), 135.5 (C, **5**), 143.9 (CH, **16**), 144.3 (C, **7**), 151.6 (C, **19**), 158.5 (C, **2**), 162.2 (C, **18**)

GC-ESI (neg) ($C_{30}H_{29}IN_2O_7$): Monoisotopic mass 656.46, observed *m/z* 655.5 $[M-H]^-$

UV-Vis (MeCN, 14.5 µM): λ_{max} (log ε) 231 shoulder (4.32), 279 (3.94)

Emission (MeCN, 14.5 µM): No fluorescence observed

R_f (silica, 5 % MeOH in DCM): 0.13

Melting Point: 126.7 °C (dec.) (no lit. value)

8.30 – Synthesis of zinc (II) 5,10,15-triphenyl-20-*p*-ethynylphenyl porphyrin (V)[20]

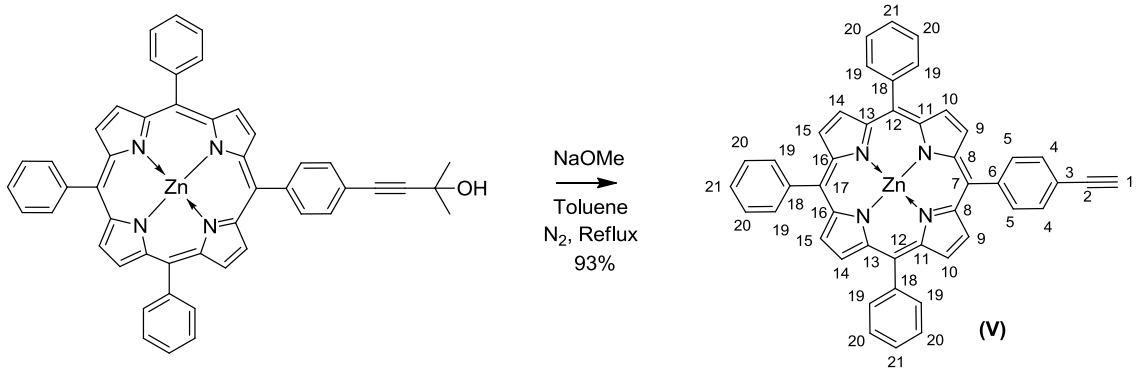

Zinc (II) 5,10,15-triphenyl-20-(*para*-(3-methyl-3-hydroxybutynyl) phenyl porphyrin (752 mg, 990 µmol, 1.00 eq) and sodium methoxide (1.60 g, 29.7 mmol, 30.00 eq) were dissolved into toluene (200 mL) and purged with N_2 (10 mins) before heating to reflux (125 °C) for 14 hours. Reaction mixture was concentrated *in vacuo*, extracted into DCM (50 mL) and washed with brine (3 x 100 mL). The reaction mixture was then dried over Na_2SO_4, filtered and concentrated *in vacuo*. No further purification was required. 647.6 mg of a purple/red powder was obtained (925 µmol, 93 %).

^{1}H NMR (400 MHz, $CDCl_3$): δ ppm 3.31 (s, 1 H, **1**), 7.75 - 7.86 (m, 9 H, **20** & **21**), 7.93 (d, J_{HH} = 8.03 Hz, 2 H, **4**), 8.22 - 8.34 (m, 6 H, **19**), 8.26 (d, J_{HH} = 7.91 Hz, 2 H, **5**), 9.01 (d, J_{HH} = 4.64 Hz, 2 H, **9**), 9.05 (s, 4 H, **14** & **15**), 9.04 (d, J_{HH} = 4.02 Hz, 2 H, **10**)

^{13}C{^{1}H} NMR (100 MHz, $CDCl_3$): δ ppm 77.9 (CH, **2**), 83.5 (C, **1**), 119.8 (C, **8**), 121.1 (CH, **11** & **13**), 121.2 (CH, **16**), 124.9 (CH, **20**), 127.3 (CH, **21**), 130.1 (CH, **4**), 131.5 (CH, **9** or **10**), 131.9 (CH, **14** or **15**), 131.9 (CH, **14** or **15**), 132.0 (CH, **9** or **10**), 134.1 (CH, **5**), 134.2 (CH, **19**), 142.5 (C, **18**), 143.3 (C, **6**), 149.6 (C, **7**), 150.0 (C, **17**), 150.1 (C, **12**), 150.1 (C, **12**)

MALDI-TOF ($C_{46}H_{28}N_4Zn$): Monoisotopic mass 700.16, observed mass 700.86 $[M+H]^+$

UV-Vis (MeOH, 1.99 µM): λ_{max} (log ε) 401 nm (4.40), 421 nm (5.44), 556 nm (4.06), 595 nm (3.78)

Emission (MeOH, 1.99 µM): λ_{ex} 421 nm, λ_{em} (rel int) 602 nm (1), 654 nm (0.65)

R_f (silica, DCM): 0.68

Melting Point: 121.5 °C (dec.) (no lit. value)

8.31 – Synthesis of 5'-DMT-5-(5''*p*-ethynylphenyl-10'',15'',20''-triphenyl-21'',23''-zinc (II) porphyrin)-dU (VI)[20]

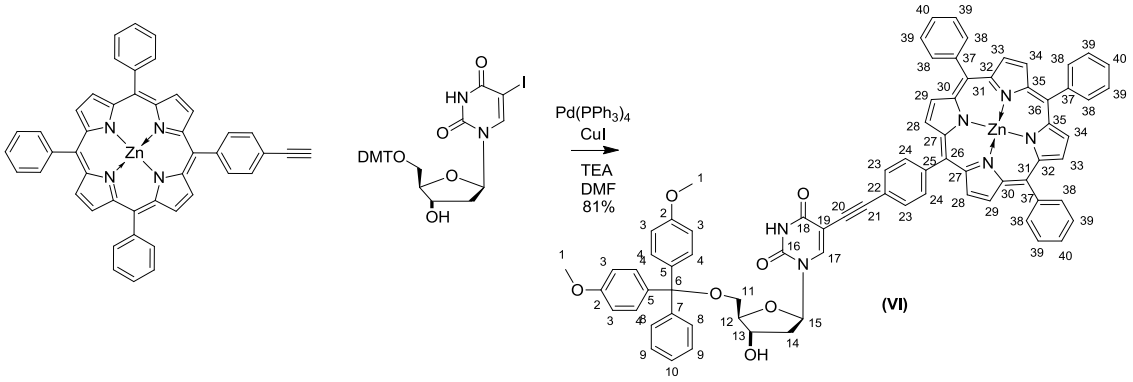

Zinc (II) 5,10,15-triphenyl-20-*para*-ethynyl phenyl porphyrin (42.2 mgs, 60.0 μmol, 1.00 eq), 5'-DMT-5-iodo-dU (106.0 mg, 160.0 μmol, 2.70 eq), copper (I) iodide (3.70 mg, 19.8 μmol, 0.33 eq) and triethylamine (16 μL) were dissolved in DMF (3 mL) in N_2 purged, flame dried glassware containing molecular sieves. The reaction vessel was shielded from light and the mixture further purged with N_2 for 20 minutes prior to the addition of palladium tetrakis(triphenylphosphine) (11.7 mg, 12.0 μmol, 0.17 eq). The reaction was stirred for 36 hours, poured into ethyl acetate (200 mL), washed with brine (3 x 100 mL), the organic phase dried over $MgSO_4$, filtered and concentrated *in vacuo*. Column chromatography was performed twice on silica neutralised with 1 mL TEA containing 20 % silica H (first column eluent – 40:1:1 DCM:MeOH:EA. Second column eluent – 50:1:1 DCM:MeOH:EA. The product was collected as a purple solid, 59.6 mg (48.4 μmol, 81 %).

^{1}H NMR (400 MHz, $CDCl_3$): δ ppm 1.49 (br. s., 1 H, **14**), 1.92 - 2.04 (m, 1 H, **14**), 2.90 (br. s., 1 H, **11**), 3.26 (br. s., 1 H, **12**), 3.48 (s, 6 H, **1**), 4.00 (br. s., 1 H, **13**), 5.48 - 5.58 (m, 1 H, **15**), 6.61 (d, J_{HH} = 7.28 Hz, 4 H, **3**), 7.02 (t, J_{HH} = 7.22 Hz, 1H, **10**), 7.07 - 7.12 (m, 4H, **9** & **23**), 7.14 (d, J_{HH} = 8.66 Hz, 4H, **4**), 7.24 (d, J_{HH} = 7.65 Hz, 2H, **8**), 7.48 - 7.63 (m, 9 H, **39** & **40**), 7.75 (s, 1 H, **17**), 7.82 (d, J_{HH} = 7.91 Hz, 2 H, **24**), 7.99 - 8.08 (m, 6 H, **36**), 8.68 (d, J_{HH} = 4.64 Hz, 2 H, **28**), 8.73 (s, 4 H, **33** & **34**), 8.75 (d, J_{HH} = 4.64 Hz, 1 H, **29**)

^{13}C{^{1}H} NMR (100 MHz, $CDCl_3$): δ ppm 41.18 (CH_2, **14**), 55.2 (CH_3, **1**), 63.1 (CH_2, **11**), 71.7 (C, **13**), 80.9 (C, **19**), 85.2 (CH, **15**), 86.2 (CH_2, **12**), 87.1 (C, **6**), 93.9 (C, **20**), 100.3 (C, **21**), 113.4 (CH, **3**), 120.0 (C, **27**), 121.0 (C, **35**), 121.1 (C, **32**), 121.5 (C, **30**), 126.5 (CH, **39**), 127.0 (CH, **10**), 127.4 (CH, **8**), 127.9 (CH, **40**), 128.1 (CH, **3**), 129.7 (CH, **4**), 129.8 (CH, **4**), 129.9 (CH, **9**), 131.6 (CH, **28**), 131.9 (CH, **33** & **34**), 132.0 (CH, **29**), 134.2 (CH, **24**), 134.5 (CH, **38**), 135.4 (C, **5**), 135.5 (C, **25**), 141.6 (C, **17**), 142.9 (C, **37**), 143.0 (C, **7**), 144.3 (C, **22**), 148.7 (C, **16**), 149.8 (C, **26**), 150.1 (C, **31**), 150.2 (C, **36**), 158.5 (C, **2**), 161.2 (C, **18**)

MALDI-TOF ($C_{76}H_{56}N_6O_7Zn$): Monoisotopic mass 1228.35, observed mass 1233.9 $[M+H]^+$

HR-ESI (pos) ($C_{76}H_{56}N_6O_7Zn$): Monoisotopic mass 1228.3496, observed *m/z* 1228.3484 $[M]^+$

UV-Vis (MeOH, 2.03 µM): λ_{max} (log ε) 402 nm (4.55), 422 nm (5.65), 557 nm (4.19), 595 nm (3.82)

Emission (MeOH, 2.03 µM): λ_{ex} 422 nm, λ_{em} (rel int) 604 nm (1), 656 (0.55)

$\boldsymbol{R_f}$ (silica, 10 % MeOH in DCM): 0.48

Melting Point: 195.1 – 196.2 °C (no lit. value)

8.32 – Synthesis of 5'-DMT-5-(5''*p*-ethynylphenyl-10'',15'',20''-triphenyl-21'',23''-zinc (II) porphyrin)-dU-3'-amidite (VII)[20]

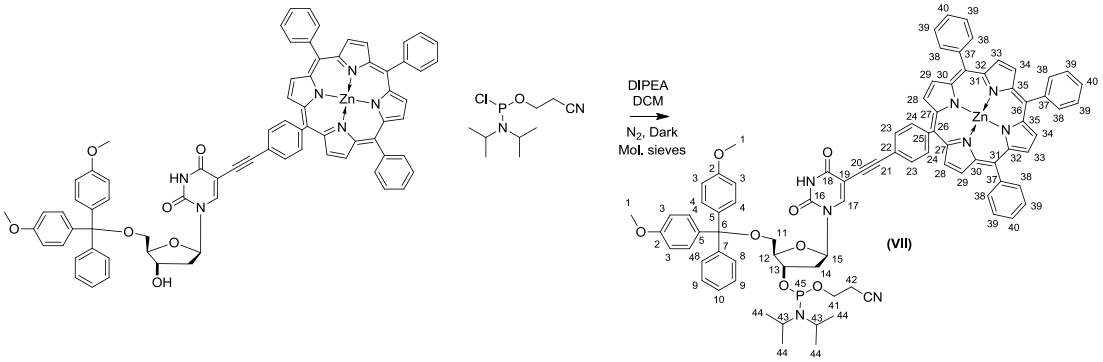

5'-DMT-5-(5''*p*-ethynylphenyl-10'',15'',20''-triphenyl-21'',23''-zinc (II)-21''-*H*-23''-*H*-porphyrin) -dU (120 mg, 97.5 µmol, 1.00 eq) and molecular sieves were added to N_2 purged, flame dried glassware. The reaction vessel was shielded from light, evacuated and purged with N_2 thrice prior to the addition of anhydrous DCM (2 mL) and DIPEA (63.8 µL, 367 µmol, 4.00 eq). The reaction mixture was purged with N_2 for a further 10 mins before the addition of CEP-Cl (66.1 µL, 282 µmol, 3.00 eq). TLC showed the reaction to have reached completion after 5 hours, the reaction mixture was filtered into another flame dried, nitrogen purged vessel, the solvent volume reduced to 1 mL. Degassed hexane (10 mL) was added and the vessel cooled (-18 °C) for 20 minutes, the product precipitated as a purple solid. The solvent was filtered off and the product washed with degassed hexane (10 mL), filtered and concentrated *in vacuo*. The partially purified product was obtained as a purple solid (199.1 mg, > 100 %).

Full characterisation of the product was not achieved due to its instability. The product was used immediately for DNA synthesis.

^{1}H NMR (400 MHz, $CDCl_3$) δ ppm 1.01 (d, J_{HH} = 6.5 Hz, 2 H, **43**), 1.12 (d, J_{HH} = 6.5 Hz, 12 H, **44**), 2.26 - 2.38 (m, 2 H, **14**), 3.23 (d, J_{HH} = 6.5 Hz, 2 H, **42**), 3.46 - 3.55 (m, 2 H, **11**), 3.66 (br. s., 6 H, **1**), 3.87 - 4.04 (m, 2 H, **41**), 4.12 - 4.19 (m, 1 H, **12**), 4.53 - 4.63 (m, 1 H, **13**), 6.23 (t, J_{HH} = 5.8 Hz, 1 H, **15**), 6.70 - 6.84 (m, 4 H, **3**), 7.17 (br. s., 1 H, **10**), 7.24 (s, 2 H, **9**), 7.34 (dd, J_{HH} = 8.8, 4.3 Hz, 4 H, **4**), 7.43 (d, J_{HH} = 3.5 Hz, 1 H, **8**), 7.60 - 7.73 (m, 9 H, **39** & **40**), 7.88 (dd, J_{HH} = 9.5, 5.5 Hz, 2 H, **23**), 8.11 (d, J_{HH} = 6.5 Hz, 8 H, **24** & **38**), 8.28 - 8.35 (m, 1 H, **17**), 8.74 (d, J_{HH} = 4.5 Hz, 2 H, **28**), 8.78 - 8.85 (m, 6 H, **29**, **33** & **34**)

MALDI-TOF ($C_{85}H_{73}N_8O_8PZn$): Monoisotopic mass 1428.46, observed mass 1446.7 $[M+O+H]^+$ (Oxidised P(V) species).

***R*$_f$** (silica, 10 % MeOH in DCM): 0.50

8.33 – Synthesis of 5-(*p*-methyl benzoate)-10,15,20-triphenyl porphyrin (VIII)

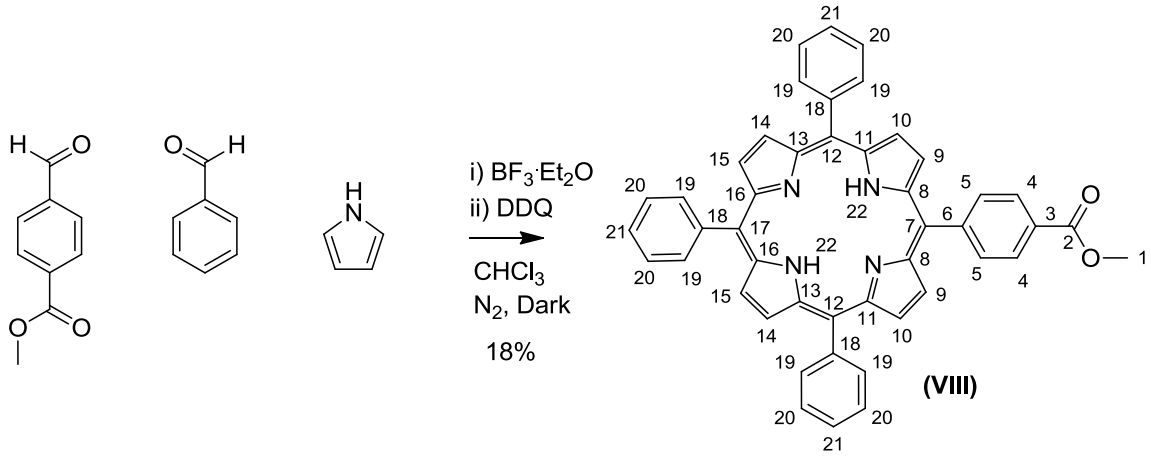

Pyrrole (2.52 mL, 36.0 mmol, 6.00 eq), benzaldehyde (3.64 mL, 36.0 mmol, 6.00 eq) and methyl-*p*-formylbenzoate (0.985 g, 6.0 mmol, 1.0 eq) were dissolved in chloroform (500 mL) and purged with N_2 for 1 hour in the dark before boron trifluoride etherate (0.69 mL, 5.4 mmol, 0.90 eq) was added and the reaction allowed to stir at room temperature. After one hour DDQ (8.14 g, 36.0 mmol, 6.00 eq) was added and left to stir overnight. The reaction mixture was concentrated *in vacuo* before purification thrice by column chromatography (first column; silica/alumina, eluent – DCM. Second and third columns; silica, eluent – toluene) to give 729.3 mg (1.08 mmol, 18 %) of dark purple crystals.

^{1}H NMR (400 MHz, $CDCl_3$): δ ppm -2.57 (s, 2 H, **22**), 4.19 (s, 3 H, **1**), 7.78 - 7.88 (m, 9 H, **20** & **21**), 8.30 - 8.37 (m, 6 H, **19**), 8.43 (d, J_{HH} = 8.16 Hz, 2 H, **4**), 8.55 (d, J_{HH} = 8.16 Hz, 2 H, **5**), 8.94 (d, J_{HH} = 4.77 Hz, 2 H, **9**), 9.00 (s, 4 H, **14** & **15**), 9.00 (d, J_{HH} = 4.77 Hz, 2 H, **10**)

^{13}C{^{1}H} NMR (100 MHz, $CDCl_3$): δ ppm 52.4 (CH_3, **1**), 118.5 (C, **8**), 120.4 (C, **13** & **16**), 120.6 (C, **11**), 126.7 (CH, **20**), 127.8 (CH, **21**), 127.9 (CH, **21**), 129.6 (C, **4**), 130.2 - 132.5 (m, C, **9, 10, 14** & **15**), 134.5 (CH, **19**), 134.6 (CH, **5**), 142.0 (C, **18**), 142.1 (C, **6**), 147.1 (C, **7, 12,** & **17**), 167.3 (C, **3**)

MALDI-TOF ($C_{46}H_{32}N_4O_2$): Monoisotopic mass 672.77, observed mass 673.76 $[M+H]^+$

UV-Vis (MeOH, 12.5 µM): λ_{max} (log ε) 399 nm (3.58), 413 nm (4.23), 512 nm (2.82), 547 nm (2.51), 589 nm (2.32), 643 nm (2.13)

Emission (MeOH, 12.5 µM): λ_{ex} 413 nm, λ_{em} (rel int) 603 nm (0.05), 648 nm (1), 712 nm (0.38). 823 nm (0.06)

R_f (silica, DCM): 0.46

Melting Point: >250 °C (lit. >300 °C[214])

8.34 – Synthesis of 5-(*p*-benzoic acid)-10,15,20-triphenyl porphyrin (IX)

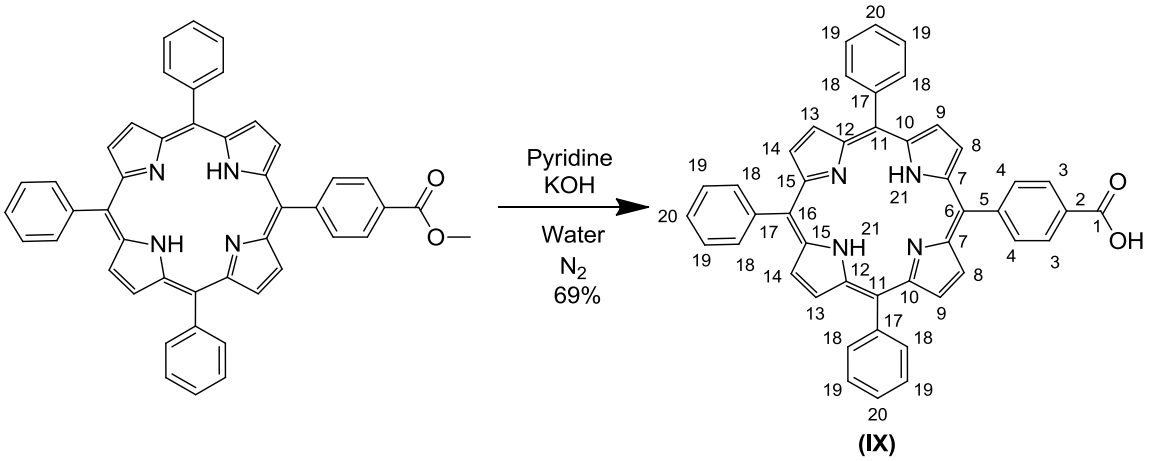

5-(*p*-methyl benzoate)-10,15,20-triphenyl porphyrin (729.3 mg, 1.1 mmol, 1.00 eq) and potassium hydroxide (2.96 g, 52.7 mmol, 50.00 eq) were dissolved in pyridine (15 mL) and water (2 mL) under a nitrogen atmosphere and the reaction mixture heated to 40 °C. After 20 hours TLC (eluent – DCM) showed the reaction to be complete so the crude mixture was poured into brine (150 mL) and DCM (300 mL), 2 M hydrochloric acid (6 mL) was added. The organic phase was washed twice with brine (2 x 100 mL) before drying over $MgSO_4$, filtering and concentrating *in vacuo*. Co-evaporation with toluene and finally chloroform was required to remove all traces of pyridine. The crude mixture was filtered twice through a 1" pad of celite 545 and eluted with chloroform (1.5 litres each), the product was concentrated *in vacuo* before recrystallisation from toluene to give 489.9 mg (744 µmol, 69 %) of a purple solid.

^{1}H NMR (400 MHz, $CDCl_3$): δ ppm -2.84 (br. s., 2 H, **21**), 7.62 - 7.81 (m, 9 H, **19** & **20**), 8.17 (dd, J_{HH} = 7.28, 1.25 Hz, 6 H, **18**), 8.27 (d, J_{HH} = 8.03 Hz, 2 H, **4**), 8.41 (d, J_{HH} = 8.03 Hz, 2 H, **3**), 8.65 - 8.94 (m, 8 H, **8, 9, 13** & **14**)

^{13}C{^{1}H} NMR (100 MHz, $CDCl_3$): δ ppm 118.5 (C, **6**), 120.2 (C, **11**), 120.3 (C, **16**), 126.6 (C, **19**), 127.7 (C, **20**), 128.0 (C, **3**), 134.4 (C, **4** & **18**), 141.9 (C, **5** & **17**), 147.0 (C, **2**), 168.7 (C, **1**)

MALDI-TOF ($C_{45}H_{30}N_4O$): Monoisotopic mass 658.75, observed mass 659.7 $[M+H]^+$

UV-Vis (MeOH, 2.98 µM): λ_{max} (log ε) 413 nm (5.40), 511 nm (4.00), 546 nm (3.65), 589 nm (3.48), 643 nm (3.32)

Emission (MeOH, 2.98 µM): λ_{ex} 413 nm, λ_{em} (rel int) 650 nm (1), 714 nm (0.36)

R_f (silica, 10 % MeOH in DCM): 0.28

Melting Point: >250 °C (lit. >300 °C[214])

8.35 – Synthesis of 5'-DMT-5-propargylamine-dU (X)

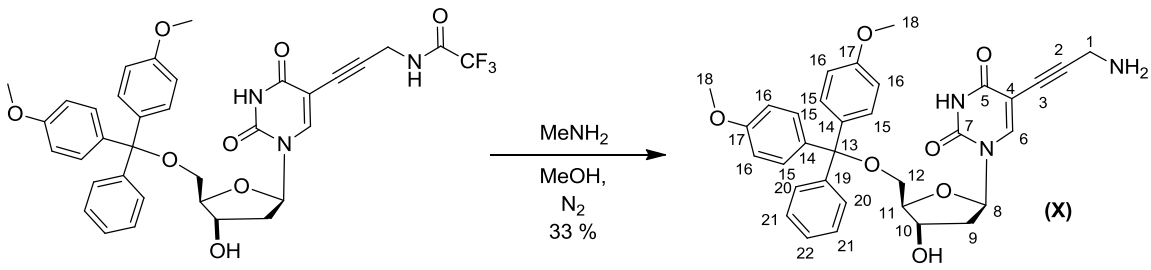

5'-DMT-5-propargyltrifluoroacetamide-dU (312.2 mg, 460 µmol, 1.00 eq) was dissolved in methanol (50 mL) and purged with N_2 for 15 minutes prior to the addition of methylamine (3.90 mL, 46.0 mmol, 100.00 eq) and the reaction heated to 40 °C for 24 hours. TLC (eluent – 30 % acetone in DCM) showed the reaction had reached completion. The reaction mixture was concentrated *in vacuo* and purified twice by column chromatography (first column; silica pretreated with 1 mL TEA, eluent – 2 % → 5 % methanol in DCM. Second column; silica pretreated with 1 mL TEA, eluent – 5 % methanol in DCM). The product was obtained as a golden foam, 90.5 mgs (155 µmol, 33 %).

^{1}H NMR (400 MHz, $CDCl_3$): δ ppm 2.33 (d, J_{HH} = 6.78 Hz, 1 H, **9**), 2.54 (d, J_{HH} = 6.65 Hz, 1 H, **9**), 3.22 (br. s., 1 H, **1**), 3.31 (d, J_{HH} = 7.91 Hz, 1 H, **12**), 3.44 (d, J_{HH} = 9.29 Hz, 1 H, **12**), 3.78 (s, 6 H, **18**), 4.13 (br. s., 1 H, **11**), 4.55 (br. s., 1 H, **10**), 6.35 (dd, J_{HH} = 6.27, 5.90 Hz, 1 H, **8**), 6.87 (d, J_{HH} = 8.53 Hz, 4 H, **16**), 7.22 (t, J_{HH} = 7.22 Hz, 1 H, **22**), 7.31 (dd, J_{HH} = 7.78, 7.53 Hz, 2 H, **21**), 7.37 (d, J_{HH} = 7.28 Hz, 4 H, **15**), 7.47 (d, J_{HH} = 7.65 Hz, 2 H, **20**), 8.19 (s, 1 H, **6**)

^{13}C{^{1}H} NMR (100 MHz, $CDCl_3$): δ ppm 31.5 (CH_2, **1**), 41.5 (CH_2, **9**), 55.2 (CH_3, **18**), 63.5 (CH_2, **12**), 71.6 (CH, **10**), 73.4 (C, **4**), 85.7 (CH, **8**), 86.6 (CH, **11**), 86.8 (C, **13**), 94.1 (C, **3**), 99.9 (C, **2**), 113.2 (CH, **16**), 126.8 (CH, **22**), 127.8 (CH, **20**), 127.9 (CH, **21**), 129.9 (CH, **15**), 130.0 (CH, **15**), 135.4 (C, **14**), 135.6 (C, **14**), 142.6 (CH, **6**), 144.6 (C, **19**), 149.5 (C, **7**), 158.5 (C, **17**), 162.3 (C, **5**)

GC-ESI (pos) ($C_{33}H_{33}N_3O_7$): Monoisotopic mass 583.63, observed *m/z* 584.30 $[M+H]^+$

UV-Vis (MeCN, 14.5 µM): λ_{max} (log ε) 233 (4.38), 285 (3.97)

Emission (MeCN, 14.5 µM): No fluorescence observed

R_f (silica, 10 % MeOH in DCM): 0.21

Melting Point: 134.2 °C (dec.) (no lit. value)

8.36 – Synthesis of 5'-DMT-5-propargylamino-dU (X)

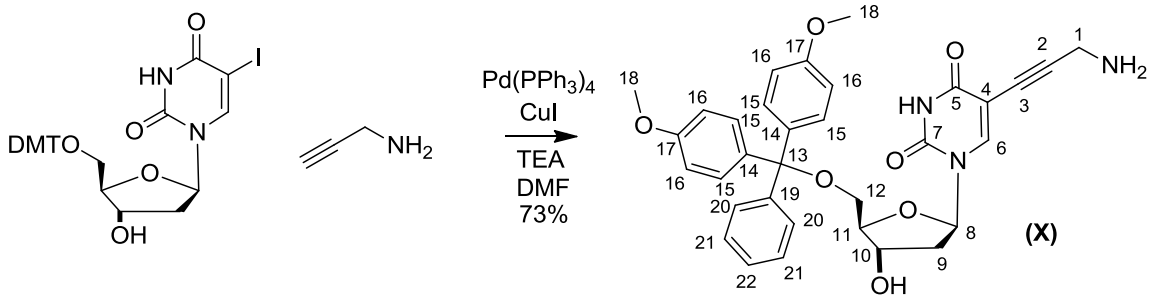

5'-DMT-5-iodo-dU (492 mg, 750.0 µmol, 1.00 eq) and triethylamine (0.73 mL, 5.3 mmol, 7.00 eq) were dissolved in anhydrous DMF (5 mL), shielded from light and purged with N_2 for 30 mins. Propargylamine (103 µL, 1.5 mmol, 2.00 eq) and copper (I) iodide (35.7 mg, 188.0 µmol, 0.25 eq) were added to the reaction mixture and further purged for 20 minutes prior to the addition of palladium tetrakis(triphenyl phosphine) (86.5 mg, 75.0 µmol, 0.10 eq). The reaction was allowed to stir at room temperature for 2.5 hours. The reaction mixture was poured into EDTA (aq, 5 % w/v, pH 9, 25 mL), partitioned with chloroform (25 mL), washed with further EDTA solution (50 mL) and brine (sat. 50 mL). The organic phase was dried over Na_2SO_4, filtered and concentrated *in vacuo*. Coevaporation with toluene and then $CHCl_3$ was needed to remove all traces of TEA and DMF. Column chromatrography (silica pretreated with 1 mL TEA, eluent – 5 % methanol in DCM) gave the product as a golden foam, 346.7 mg (594 µmol, 79 %).

^{1}H NMR (400 MHz, $CDCl_3$): δ ppm 2.33 (d, J_{HH} = 6.78 Hz, 1 H, **9**), 2.54 (d, J_{HH} = 6.65 Hz, 1 H, **9**), 3.22 (br. s., 1 H, **1**), 3.31 (d, J_{HH} = 7.91 Hz, 1 H, **12**), 3.44 (d, J_{HH} = 9.29 Hz, 1 H, **12**), 3.78 (s, 6 H, **18**), 4.13 (br. s., 1 H, **11**), 4.55 (br. s., 1 H, **10**), 6.35 (dd, J_{HH} = 6.27, 5.90 Hz, 1 H, **8**), 6.87 (d, J_{HH} = 8.53 Hz, 4 H, **16**), 7.22 (t, J_{HH} = 7.22 Hz, 1 H, **22**), 7.31 (dd, J_{HH} = 7.78, 7.53 Hz, 2 H, **21**), 7.37 (d, J_{HH} = 7.28 Hz, 4 H, **15**), 7.47 (d, J_{HH} = 7.65 Hz, 2 H, **20**), 8.19 (s, 1 H, **6**)

^{13}C{^{1}H} NMR (100 MHz, $CDCl_3$): δ ppm 31.5 (CH_2, **1**), 41.5 (CH_2, **9**), 55.2 (CH_3, **18**), 63.5 (CH_2, **12**), 71.6 (CH, **10**), 73.4 (C, **4**), 85.7 (CH, **8**), 86.6 (CH, **11**), 86.8 (C, **13**), 94.1 (C, **3**), 99.9 (C, **2**), 113.2 (CH, **16**), 126.8 (CH, **22**), 127.8 (CH, **20**), 127.9 (CH, **21**), 129.9 (CH, **15**), 130.0 (CH, **15**), 135.4 (C, **14**), 135.6 (C, **14**), 142.6 (CH, **6**), 144.6 (C, **19**), 149.5 (C, **7**), 158.5 (C, **17**), 162.3 (C, **5**)

GC ESI (pos) ($C_{33}H_{33}N_3O_7$): Monoisotopic mass 583.63, observed *m/z* 584.30 $[M+H]^+$

UV-Vis (MeCN, 14.5 µM): λ_{max} (log ε) 233 (4.38), 285 (3.97)

Emission (MeCN, 14.5 µM): No fluorescence observed

R_f (silica, 10 % MeOH in DCM): 0.21

Melting Point: 134.2 °C (dec.) (no lit. value)

8.37 – Synthesis of 2,2,2-trifluoro-*N*-(prop-2-ynyl)acetamide (XI)

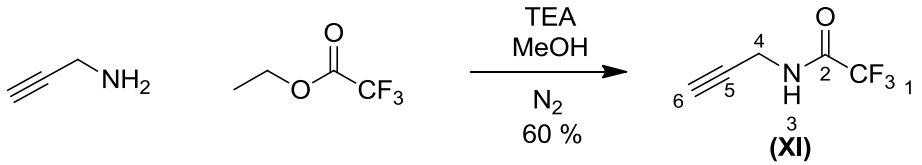

(XI)

Propargylamine (0.34 mL, 5.0 mmol, 1.00 eq) and triethylamine (0.91 mL, 6.5 mmol, 1.30 eq) were dissolved in anhydrous methanol (5 mL) and degassed with N_2 for 25 mins. The reaction mixture was cooled (0 °C), ethyl trifluoroacetate (0.77 mL, 6.5 mmol, 1.30 eq) was added dropwise and the reaction mixture allowed to warm (RT) and stir overnight. TLC showed the reaction to have reached completion. The reaction mixture was concentrated *in vacuo* before redissolving in DCM (40 mL), washing with brine (3 x 100 mL), drying over Na_2SO_4, filtering and concentrating *in vacuo*. Column chromatography (silica, eluent – 100:5 DCM:MeOH) gave the product as a pale orange oil (454 mg, 60 %).

^{1}H NMR (400 MHz, $CDCl_3$): δ ppm 2.25 (t, J_{HH} = 2.57 Hz, 1 H, **6**), 4.05 (d, J_{HH} = 2.64 Hz, 2 H, **4**), 7.89 (br. s., 1 H, **3**)

^{13}C{^{1}H} NMR (100 MHz, $CDCl_3$): δ ppm 29.3 (CH_2, **4**), 72.2 (CH, **6**), 77.2 (C, **5**), 115.6 (q, J_{CF} = 286.95 Hz, C, **1**), 157.3 (q, J_{CF} = 37.82 Hz, C, **2**)

^{19}F NMR (282 MHz, $CDCl_3$): δ ppm -76.60 (s, **1**)

GC-ESI (neg) ($C_5H_4F_3NO$): Monoisotopic mass 151.02, observed *m/z* 150.10 $[M-H]^-$

UV-Vis (MeCN, 13.2 µM): λ_{max} (log ε) 274 (1.40), 412 (0.82)

Emission (MeCN, 13.2 µM): λ_{ex} 274 nm, λ_{em} (rel int) 308 (1), 609 (0.29)

R_f (silica, 10% DCM in MeOH): 0.46

Melting Point: Oil at RT

8.38 – Synthesis of 5'-DMT-5-propargyltrifluoroacetamide-dU (XII)

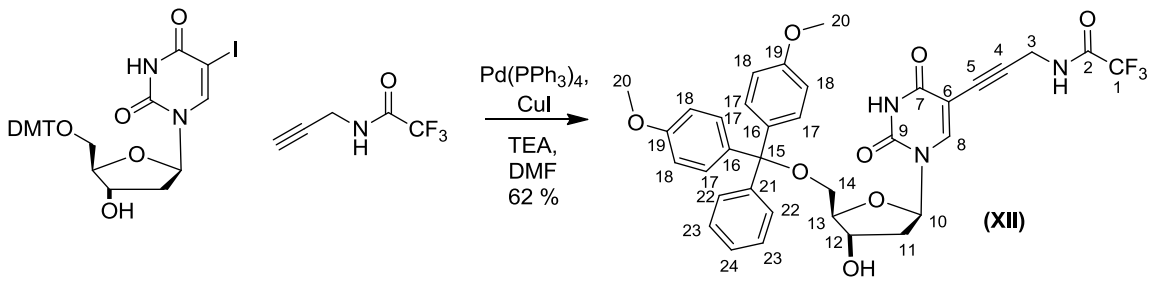

5'-DMT-5-iodo-dU (656 mg, 1.0 mmol, 1.00 eq), propargyl(trifluoroacetamide) (206 mg, 1.4 mmol, 1.40 eq), copper iodide (38.1 mg, 0.2 mmol, 0.20 eq) and triethylamine (0.97 mL, 7.0 mmol, 7.00 eq) were dissolved in anhydrous DMF (6 mL) in flame dried glassware under N_2. The reaction mixture was purged with N_2 in the dark for 1 hour prior to the addition of palladium tetrakis(triphenylphosphine) (115 mg, 0.1 mmol, 0.10 eq). The reaction reached completion after 2 hours and was poured into ethyl acetate (100 mL), washed with brine (3 x 100 mL), dried over Na_2SO_4, filtered and concentrated *in vacuo*. Column chromatography was performed (silica pretreated with 1 mL pyridine, eluent 10 → 30 % acetone in DCM) to give 443.0 mg (652 µmol, 62 %) of a golden foam.

^{1}H NMR (400 MHz, $CDCl_3$): δ ppm 2.31 - 2.49 (m, 1 H, **10**), 2.60 - 2.77 (m, 1 H, **10**), 3.43 (br. s., 2 H, **13**), 3.82 (s, 6 H, **19**), 4.00 (br. s., 2 H, **3**), 4.24 (br. s., 1 H, **12**), 4.62 - 4.77 (m, 1 H, **11**), 6.36 - 6.49 (m, 1 H, **9**), 6.91 (d, J_{HH} = 8.78 Hz, 4 H, **17**), 7.26 (t, J_{HH} = 7.22 Hz, 1 H, **23**), 7.35 (t, J_{HH} = 7.53 Hz, 2 H, **22**), 7.41 (d, J_{HH} = 8.66 Hz, 4 H, **16**), 7.51 (d, J_{HH} = 7.65 Hz, 2 H, **21**), 8.29 (s, 1 H, **8**)

^{13}C{^{1}H} NMR (100 MHz, $CDCl_3$): δ ppm 30.8 (CH_2, **3**), 42.0 (CH_2, **11**), 55.7 (CH_3, **20**), 64.0 (CH_2, **14**), 72.5 (CH, **12**), 75.8 (C, **6**), 86.6 (CH, **10**), 87.3 (C, **5**), 87.5 (CH, **13**), 88.0 (C, **15**), 99.3 (C, **4**), 113.8 (CH, **18**), 116.2 (q, *J*=287.76 Hz, C, **1**), 127.4 (CH, **24**), 128.4 (CH, **22**), 128.5 (CH, **22**), 129.0 (CH, **23**), 129.2 (CH, **23**), 130.4 (CH, **17**), 132.8 (C, **21**), 135.9 (C, **16**), 136.0 (C, **16**), 144.1 (C, **8**), 149.9 (C, **9**), 157.2 (q, *J*=37.50 Hz, C, **2**), 159.1 (C, **19**), 163.4 (C, **7**)

^{19}F NMR (282 MHz, $CDCl_3$): δ ppm –75.78

MALDI-TOF ($C_{35}H_{32}F_3N_3O_8$): Monoisotopic mass 679.64; observed mass 701.8 $[M+Na]^+$, 717.9 $[M+K]^+$

UV-Vis (MeCN, 13.2 µM): λ_{max} (log ε) 229 (4.46), 283 (3.92)

Emission (MeCN, 13.2 µM): No fluorescence observed

***R*$_f$** (silica, 30 % acetone in DCM): 0.40

8.39 – Synthesis of *N*-(5'-DMT-5-propargyl-dU)-5,10,15-triphenyl-20-(*p*-benzamide)-porphyrin (XIII)

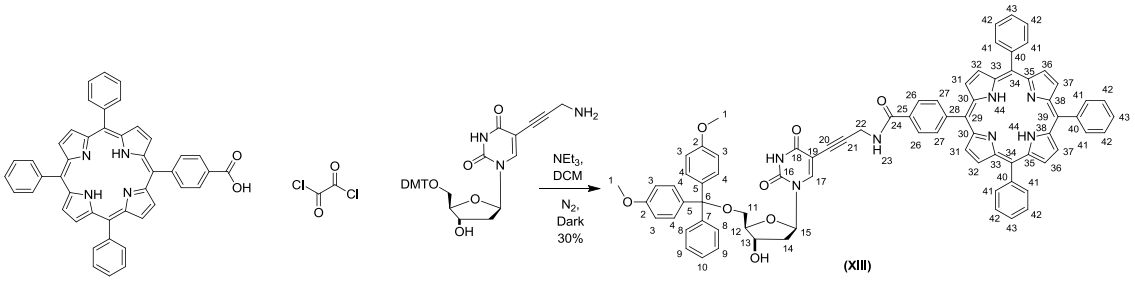

5,10,15-triphenyl-20-*para*-benzoic acid porphyrin (49.4 mg, 0.075 mmol, 1.00 eq) was dissolved in anhydrous DCM (2 mL) in oven dried glassware and purged with N_2 for 30 mins. To this oxalyl chloride (6.4 µL, 0.075 mmol, 1.00 eq) was added in one portion and the reaction shielded from light, the reaction mixture turned green. After 90 minutes the reaction had not reached completion so further oxalyl chloride (1.2 µL, 0.015 mmol, 0.20 eq) was added. TLC (10 % methanol in DCM) showed no further reaction after 30 minutes. In a separate oven dried flask the 5'-DMT-5-propargylamino-dU (44.6 mg, 0.075 mmol, 1.00 eq) and triethylamine (52 µL, 0.38 mmol, 5.0 eq) were dissolved in anhydrous DCM (5 mL) and purged with N_2 for 30 minutes. The acid chloride was added to the 5'DMT-5-propargylamino-dU *via* a cannula. The reaction mixture was then shielded from light and allowed to stir at room temperature for 18 hours, at which point TLC (10 % methanol in DCM) showed the consumption of the 5'-DMT-5-propargylamino-dU. The reaction mixture was washed with brine (50 mL), the aqueous phase re-extracted with $CHCl_3$ (50 mL) and the combined organics further washed with brine (50 mL). The organic phase was dried over Na_2SO_4, filtered and concentrated *in vacuo*. Column chromatography was carried out (silica pretreated with triethylamine, eluent – 2 % methanol in DCM), to give the product as a purple solid, 27.9 mg (22.8 µmol, 30 %).

^{1}H NMR (400 MHz, $CDCl_3$): δ ppm -2.75 (s, 2 H, **44**), 2.27 - 2.39 (m, 1 H, **14**), 2.47 - 2.59 (m, 1 H, **14**), 3.35 (dd, J_{HH} = 10.42, 2.76 Hz, 1 H, **11**), 3.41 (dd, J_{HH} = 10.67, 2.13 Hz, 1 H, **11**), 3.68 (s, 6 H, **1**), 4.09 (d, J_{HH} = 2.26 Hz, 1 H, **12**), 4.30 (dd, J_{HH} = 17.82, 4.52 Hz, 1 H, **22**), 4.37 (dd, J_{HH} = 17.94, 4.89 Hz, 1 H, **22**), 4.51 - 4.59 (m, 1 H, **13**), 6.34 (t, J_{HH} = 6.53 Hz, 1 H, **15**), 6.70 (t, J_{HH} = 4.52 Hz, 1 H, **23**), 6.82 (dd, J_{HH} = 8.78, 2.01 Hz, 4 H, **3**), 7.18 (t, J_{HH} = 7.28 Hz, 1 H, **10**), 7.28 (t, J_{HH} = 7.65 Hz, 2 H, **9**), 7.36 (d, J_{HH} = 8.16 Hz, 4 H, **4**), 7.45 (d, J_{HH} = 7.65 Hz, 2 H, **8**), 7.67 - 7.85 (m, 9 H, **42** & **43**), 7.96 (d, J_{HH} = 7.91 Hz, 2 H, **27**) 8.20 (d, J_{HH} = 7.40 Hz, 6 H, **41**), 8.22 (d, J_{HH} = 7.91 Hz, 2 H, **26**), 8.27 (s, 1 H, **17**), 8.77 (d, J_{HH} = 4.77 Hz, 2 H, **31**), 8.85 (d, J_{HH} = 4.77 Hz, 2 H, **32**), 8.86 (s, 4 H, **36** & **37**)

$^{13}C\{^{1}H\}$ NMR (100 MHz, $CDCl_3$): δ ppm 30.9 (CH_2, **22**), 41.7 (CH_2, **14**), 55.2 (CH_3, **1**), 63.5 (CH_2, **11**), 72.2 (CH, **13**), 74.6 (C, **19**), 85.9 (CH, **15**), 86.7 (CH, **12**), 87.1 (C, **6**), 89.5 (C, 20), 99.5 (C, **21**), 113.4 (CH, **3**), 118.7 (C, **30**), 120.3 (C, **35** & **38**), 120.5 (C, **33**), 125.5 (CH, **27**), 126.7 (CH, **42**), 127.0 (CH, **10**), 127.7 (CH, **8**), 127.9 (CH, **43**), 128.1 (CH, **9**), 130.0 (CH, **4**), 130.5 - 132.4 (m, CH, **31**, **32**, **36** & **37**), 133.0 (C, **40**), 134.5 (CH, **41**), 134.5 (C, **26**), 135.5 (C, **5**), 142.2 (C, **40**), 143.4 (CH, **17**), 144.5 (C, **7**), 145.6 (C, **25**), 149.2 (C, **16**), 158.6 (C, **2**), 162.1 (C, **18**), 166.9 (C, **24**)

MALDI-TOF ($C_{78}H_{61}N_7O_8$): Monoisotopic mass 1224.36, observed mass 1229.2 $[M+H]^+$

UV-Vis (MeOH, 2.45 µM): λ_{max} (log ε) 413 nm (5.49), 512 nm (4.09), 545 nm (3.74), 587 nm (3.58), 644 nm (3.42)

Emission (MeOH, 2.45 µM): λ_{ex} 413 nm, λ_{em} (rel int) 648 nm (1), 715 (0.34)

R_f (silica, 10 % MeOH in DCM) 0.26

Melting Point: 208.3 – 210.5 °C (no lit. value)

8.40 – Synthesis of *N*-(5'-DMT-5-propargyl-dU)-5,10,15-triphenyl-20-(*p*-benzamide)-porphyrin (XIII)

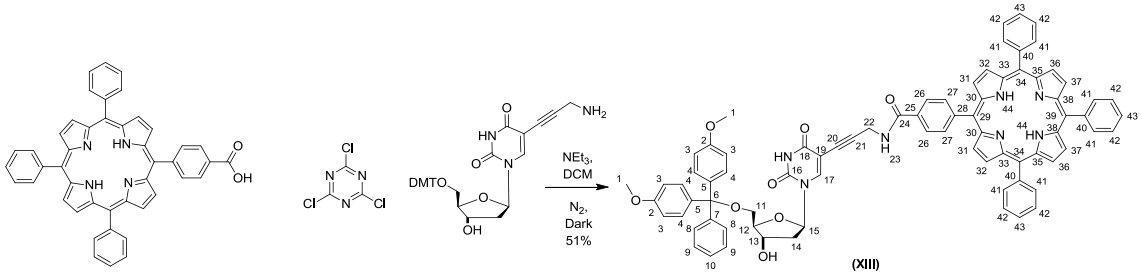

5,10,15-triphenyl-20-*para*-benzoic acid porphyrin (155.3 mg, 0.236 mmol, 1.00 eq) was dissolved in anhydrous DCM (8 mL) in oven dried glassware and purged with N_2 for 20 mins. To this triethylamine (39 µL, 0.283 mmol, 1.20 eq) and cyanuric chloride (21.7 mg, 0.120 mmol, 0.50 eq) were added in one portion and the reaction shielded from light. In a separate oven dried flask the 5'-DMT-5-propargylamino-dU (137.5 mg, 0.236 mmol, 1.00 eq) was dissolved in anhydrous DCM (8 mL) and purged with N_2 for 10 minutes. After reacting for 30 minutes TLC (10% methanol in DCM) showed complete formation of the acid chloride so the reaction mixture was added *via* a cannula in 5 portions over 5 minutes to the solution containing the 5'-DMT-5-propargylamino-dU. The reaction mixture was then shielded from light and allowed to stir at room temperature for 14 hours, at which point TLC (10 % methanol in DCM) showed the consumption of the 5'-DMT-5-propargylamino-dU. The reaction mixture was washed with brine (50 mL), the aqueous phase re-extracted with DCM (50 mL) and the combined organics further washed with brine (100 mL). The organic phase was dried over $MgSO_4$, filtered and concentrated *in vacuo*. Column chromatography was carried out (silica pretreated with triethylamine, eluent – 2 % methanol in DCM), a second column was conducted (silica pretreated with triethylamine, eluent – 1 → 3 % methanol in DCM) to give the product as a purple solid, 146.1 mg (119.3 µmol, 51 %).

^{1}H NMR (400 MHz, $CDCl_3$): δ ppm -2.75 (s, 2 H, **44**), 2.27 - 2.39 (m, 1 H, **14**), 2.47 - 2.59 (m, 1 H, **14**), 3.35 (dd, J_{HH} = 10.42, 2.76 Hz, 1 H, **11**), 3.41 (dd, J_{HH} = 10.67, 2.13 Hz, 1 H, **11**), 3.68 (s, 6 H, **1**), 4.09 (d, J_{HH} = 2.26 Hz, 1 H, **12**), 4.30 (dd, J_{HH} = 17.82, 4.52 Hz, 1 H, **22**), 4.37 (dd, J_{HH} = 17.94, 4.89 Hz, 1 H, **22**), 4.51 - 4.59 (m, 1 H, **13**), 6.34 (t, J_{HH} = 6.53 Hz, 1 H, **15**), 6.70 (t, J_{HH} = 4.52 Hz, 1 H, **23**), 6.82 (dd, J_{HH} = 8.78, 2.01 Hz, 4 H, **3**), 7.18 (t, J_{HH} = 7.28 Hz, 1 H, **10**), 7.28 (t, J_{HH} = 7.65 Hz, 2 H, **9**), 7.36 (d, J_{HH} = 8.16 Hz, 4 H, **4**), 7.45 (d, J_{HH} = 7.65 Hz, 2 H, **8**), 7.67 - 7.85 (m, 9 H, **42** & **43**), 7.96 (d, J_{HH} = 7.91 Hz, 2 H, **27**) 8.20 (d, J_{HH} = 7.40 Hz, 6 H, **41**), 8.22 (d, J_{HH} = 7.91 Hz, 2 H, **26**), 8.27 (s, 1 H, **17**), 8.77 (d, J_{HH} = 4.77 Hz, 2 H, **31**), 8.85 (d, J_{HH} = 4.77 Hz, 2 H, **32**), 8.86 (s, 4 H, **36** & **37**)

$^{13}C\{^{1}H\}$ NMR (100 MHz, $CDCl_3$): δ ppm 30.9 (CH_2, **22**), 41.7 (CH_2, **14**), 55.2 (CH_3, **1**), 63.5 (CH_2, **11**), 72.2 (CH, **13**), 74.6 (C, **19**), 85.9 (CH, **15**), 86.7 (CH, **12**), 87.1 (C, **6**), 89.5 (C, **20**), 99.5 (C, **21**), 113.4 (CH, **3**), 118.7 (C, **30**), 120.3 (C, **35** & **38**), 120.5 (C, **33**), 125.5 (CH, **27**), 126.7 (CH, **42**), 127.0 (CH, **10**), 127.7 (CH, **8**), 127.9 (CH, **43**), 128.1 (CH, **9**), 130.0 (CH, **4**), 130.5 - 132.4 (m, CH, **31**, **32**, **36** & **37**), 133.0 (C, **40**), 134.5 (CH, **41**), 134.5 (C, **26**), 135.5 (C, **5**), 142.2 (C, **40**), 143.4 (CH, **17**), 144.5 (C, **7**), 145.6 (C, **25**), 149.2 (C, **16**), 158.6 (C, **2**), 162.1 (C, **18**), 166.9 (C, **24**)

MALDI-TOF ($C_{78}H_{61}N_7O_8$): Monoisotopic mass 1224.36, observed mass 1229.2 $[M+H]^+$

UV-Vis (MeOH, 2.45 µM): λ_{max} (log ε) 413 nm (5.49), 512 nm (4.09), 545 nm (3.74), 587 nm (3.58), 644 nm (3.42)

Emission (MeOH, 2.45 µM): λ_{ex} 413 nm, λ_{em} (rel int) 648 nm (1), 715 (0.34)

$\boldsymbol{R_f}$ (silica, 10 % MeOH in DCM) 0.26

Melting Point: 208.3 – 210.5 °C (no lit. value)

8.41 – Synthesis of *N*-(5'DMT-5-propargyl-dU)-5'',10'',15''-triphenyl-20''-(*p*-benzamide)-21''-*H*-23''-*H*-porphyrin (XIII)

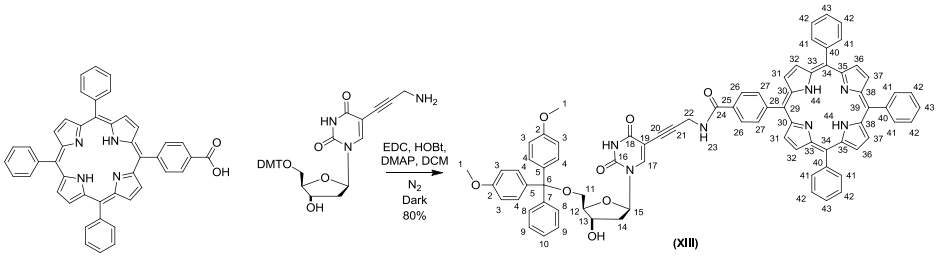

5,10,15-triphenyl-20-*para*-benzoic acid porphyrin (105 mg, 160.0 µmol, 1.00 eq), 5'DMT-5-propargylamino-dU (121 mg, 210.0 µmol, 1.30 eq), EDC (56 µL, 320.0 µmol, 2.00 eq), HOBt (24.4 mg, 0.16 mmol, 1.00 eq) and DMAP (38.9 mg, 0.32 mmol, 2.00 eq) were stirred in anhydrous DCM (5 mL) in oven dried glassware under N_2 for 5 ½ hours. The reaction mixture was washed with brine (25 mL), the aqueous phase re-extracted with DCM (50 mL). The organic phase was dried over Na_2SO_4, filtered and concentrated *in vacuo*. The product was purified by column chromatography (silica pretreated with 1 mL TEA, eluent – 0.5 % methanol in DCM → 2.5 % methanol in DCM) to give the product as a purple solid, 156.7 mg (128 µmol, 80 %).

^{1}H NMR (400 MHz, $CDCl_3$): δ ppm -2.75 (s, 2 H, **44**), 2.27 - 2.39 (m, 1 H, **14**), 2.47 - 2.59 (m, 1 H, **14**), 3.35 (dd, J_{HH} = 10.42, 2.76 Hz, 1 H, **11**), 3.41 (dd, J_{HH} = 10.67, 2.13 Hz, 1 H, **11**), 3.68 (s, 6 H, **1**), 4.09 (d, J_{HH} = 2.26 Hz, 1 H, **12**), 4.30 (dd, J_{HH} = 17.82, 4.52 Hz, 1 H, **22**), 4.37 (dd, J_{HH} = 17.94, 4.89 Hz, 1 H, **22**), 4.51 - 4.59 (m, 1 H, **13**), 6.34 (t, J_{HH} = 6.53 Hz, 1 H, **15**), 6.70 (t, J_{HH} = 4.52 Hz, 1 H, **23**), 6.82 (dd, J_{HH} = 8.78, 2.01 Hz, 4 H, **3**), 7.18 (t, J_{HH} = 7.28 Hz, 1 H, **10**), 7.28 (t, J_{HH} = 7.65 Hz, 2 H, **9**), 7.36 (d, J_{HH} = 8.16 Hz, 4 H, **4**), 7.45 (d, J_{HH} = 7.65 Hz, 2 H, **8**), 7.67 - 7.85 (m, 9 H, **42** & **43**), 7.96 (d, J_{HH} = 7.91 Hz, 2 H, **27**) 8.20 (d, J_{HH} = 7.40 Hz, 6 H, **41**), 8.22 (d, J_{HH} = 7.91 Hz, 2 H, **26**), 8.27 (s, 1 H, **17**), 8.77 (d, J_{HH} = 4.77 Hz, 2 H, **31**), 8.85 (d, J_{HH} = 4.77 Hz, 2 H, **32**), 8.86 (s, 4 H, **36** & **37**)

^{13}C{^{1}H} NMR (100 MHz, $CDCl_3$): δ ppm 30.9 (CH_2, **22**), 41.7 (CH_2, **14**), 55.2 (CH_3, **1**), 63.5 (CH_2, **11**), 72.2 (CH, **13**), 74.6 (C, **19**), 85.9 (CH, **15**), 86.7 (CH, **12**), 87.1 (C, **6**), 89.5 (C, 20), 99.5 (C, **21**), 113.4 (CH, **3**), 118.7 (C, **30**), 120.3 (C, **35** & **38**), 120.5 (C, **33**), 125.5 (CH, **27**), 126.7 (CH, **42**), 127.0 (CH, **10**), 127.7 (CH, **8**), 127.9 (CH, **43**), 128.1 (CH, **9**), 130.0 (CH, **4**), 130.5 - 132.4 (m, CH, **31**, **32**, **36** & **37**), 133.0 (C, **40**), 133.4 (C, **28**), 134.5 (CH, **41**), 134.5 (C, **26**), 135.5 (C, **5**), 142.2 (C, **40**), 143.4 (C|H, **17**), 144.5 (C, **7**), 145.6 (C, **25**), 149.2 (C, **16**), 158.6 (C, **2**), 162.1 (C, **18**), 166.9 (C, **24**)

MALDI-TOF ($C_{78}H_{61}N_7O_8$): Monoisotopic mass 1224.36, observed mass 1229.2 $[M+H]^+$

HR-ESI(pos) ($C_{78}H_{61}N_7O_8$): Monoisotopic mass 1224.3610, observed *m/z* 1224.4663 $[M]^+$

UV-Vis (MeOH, 2.45 μM) λ_{max} (log ε): 413 nm (5.49), 512 nm (4.09), 545 nm (3.74), 587 nm (3.58), 644 nm (3.42)

Emission (MeOH, 2.45 μM) λ_{ex} 413 nm, λ_{em} (rel int): 648 nm (1), 715 (0.34)

R_f (silica, 10 % methanol in DCM) 0.26

Melting Point: 208.3 – 210.5 °C (no lit. value)

8.42 – Synthesis of *N*-(5'DMT-5-propargyl-dU)-5'',10'',15''-triphenyl-20''-(*p*-benzamide)-21''-*H*-23''-*H*-porphyrin-3'-amidite (XIV)

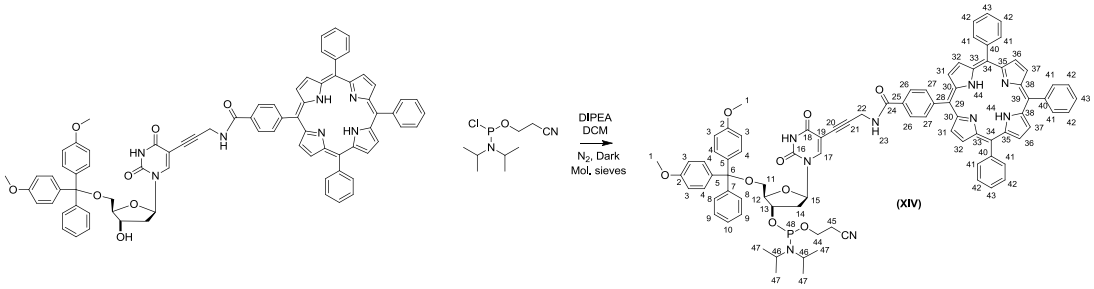

N-(5'DMT-5-propargyl-dU)-5'',10'',15''-triphenyl-20''-(*p*-benzamide)-21''-*H*-23''-*H*-porphyrin (120 mg, 98.0 µmol, 1.00 eq) and molecular sieves were added to N_2 purged, flame dried glassware. The reaction vessel was shielded from light, evacuated and purged with N_2 thrice prior to the addition of anhydrous DCM (2 mL) and DIPEA (68.3 µL, 392 µmol, 4.00 eq). The reaction mixture was purged with N_2 for a further 10 mins before the addition of CEP-Cl (69.9 µL, 294 µmol, 3.00 eq). TLC showed the reaction to have reached completion after 2.5 hours, the reaction mixture was filtered into another flame dried, nitrogen purged vessel, the solvent volume reduced to 1 mL. Degassed hexane (10 mL) was added and the vessel cooled (-18 °C) for 20 minutes, the product precipitated as a purple solid. The solvent was filtered off and the product washed with degassed hexane (10 mL), filtered and concentrated *in vacuo*. The partially purified product was obtained as a purple solid (120.5 mg, 86 %).

Full characterisation of the product was not achieved due to its instability. The product was used immediately for DNA synthesis.

$\boldsymbol{R_f}$ (10 % MeOH in DCM): 0.46

8.43 – Synthesis of *N*-(5'DMT-5-propargyl-dU)-ferrocenamide (XV)

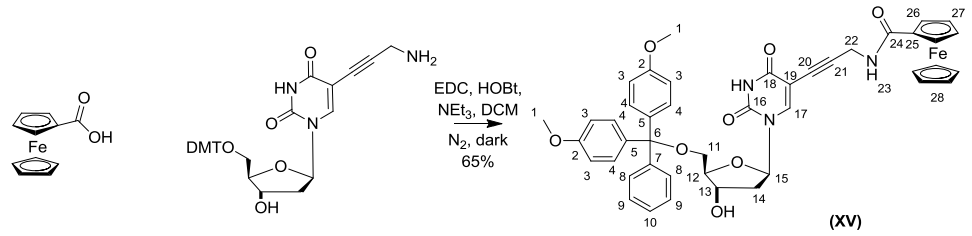

Ferrocene carboxylic acid (80.5 mg, 350.0 µmol, 1.00 eq), 5'DMT-5-propargylamino-dU (204 mg, 350.0 µmol, 1.00 eq), EDC (124 µL, 700.0 µmol, 2.00 eq), HOBt (53.6 mg, 350.0 µmol, 1.00 eq) and DMAP (85.6 mg, 700.0 µmol, 2.00 eq) were stirred in anhydrous DCM (5 mL) in oven dried glassware under N_2 for 3 hours. The reaction mixture was washed with brine (2 x 50 mL), the aqueous phase re-extracted with DCM (50 mL). The organic phase was dried over Na_2SO_4, filtered and concentrated *in vacuo*. Column chromatography was carried out (silica pretreated with 1mL TEA, eluent – 2 % methanol in DCM → 3 % methanol in DCM) to give the product as a yellow foam, 180.0 mg (226 µmol, 65 %).

^{1}H NMR (400 MHz, $CDCl_3$) δ ppm 2.30 (ddd, J_{HH} = 13.6, 6.8 Hz, 1 H, **14**), 2.55 (ddd, J_{HH} = 13.6, 5.5, 2.5 Hz, 1 H, **14**), 3.38 (d, J_{HH} = 2.5 Hz, 2 H, **11**), 3.79 (s, 6 H, **1**), 4.05 (dd, J_{HH} = 17.6, 4.5 Hz, 2 H, **22**), 4.14 (dd, J_{HH} = 17.3, 5.8 Hz, 2 H, **22**), 4.10 - 4.16 (m, 1 H, **12**), 4.18 (s, 5 H, **28**), 4.28 - 4.33 (m, 2 H, **27**), 4.55 (ddd, J_{HH} = 5.4, 2.6 Hz, 2 H, **13**), 4.63 (d, J_{HH} = 13.6 Hz, 2 H, **26**), 6.26 (t, J_{HH} = 4.8 Hz, 1 H, **23**), 6.33 (dd, J_{HH} = 6.5 Hz, 1 H, **15**), 6.87 (d, J_{HH} = 9.0 Hz, 4 H, **3**), 7.23 (t, J_{HH} = 7.5 Hz, 1 H, **10**), 7.31 (dd, J_{HH} = 8.3, 7.3 Hz, 2 H, **9**), 7.35 (d, J_{HH} = 8.5 Hz, 4 H, **4**), 7.45 (d, J_{HH} = 7.5 Hz, 2 H, **8**), 8.10 (s, 1 H, **17**)

^{13}C{^{1}H} NMR (100 MHz, $CDCl_3$) δ ppm 30.4 (CH_2, **22**), 41.7 (CH_2, **14**), 55.5 (CH_3, **1**), 63.9 (CH_2, **11**), 68.5 (CH, **26**), 70.0 (CH, **28**), 70.8 (CH, **27**), 72.4 (CH, **13**), 74.3 (C, **19**), 75.4 (C, **25**), 86.1 (CH, **15**), 86.8 (CH, **12**), 87.2 (C, **6**), 90.4 (C, **21**), 99.8 (C, **20**), 113.6 (CH, **3**), 127.3 (CH, **10**), 128.2 (CH, **9**), 128.3 (CH, **8**), 130.2 (C, **4**), 135.8 (C, **5**), 143.2 (CH, **17**), 144.8 (C, **7**), 149.6 (C, **16**), 158.9 (C, **2**), 162.6 (C, **24**), 170.5 (C, **18**)

GC-ESI(pos) ($C_{44}H_{41}FeN_3O_8$) Monoisotopic mass 795.2243, observed *m/z* 818.1 $[M+Na]^+$

HR-ESI(pos) ($C_{44}H_{41}FeN_3O_8$) Monoisotopic mass 795.2243, observed *m/z* 813.2568 $[M+NH_4]^+$

UV-Vis (MeOH, 32.6 µM): λ_{max} (log ε) 228 nm (4.35), 275 nm (3.90), 282 nm (3.90), 292 nm (3.85), 441 nm (2.04)

Emission (MeOH, 32.6 µM): No fluorescence observed

R_f (silica, 10 % MeOH in DCM): 0.33

Melting Point: 143.2 °C (dec.) (no lit. value)

8.44 – Synthesis of *N*-(5'DMT-5-propargyl-dU)-ferrocenamide-3'-amidite (XVI)

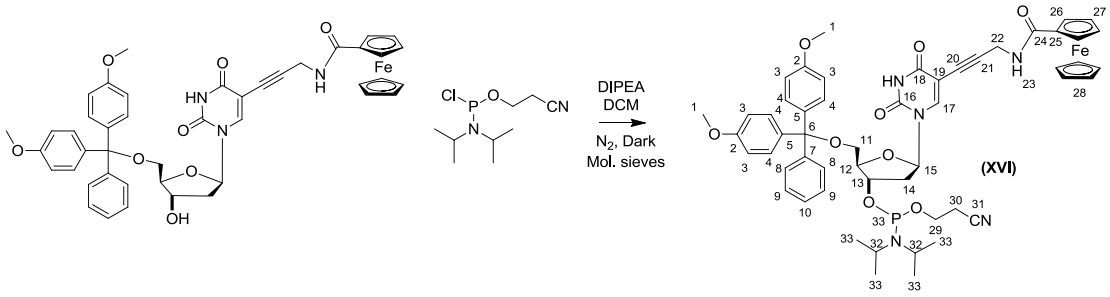

N-(5'DMT-5-propargyl-dU)-ferrocenamide (90 mg, 113.2 µmol, 1.00 eq) and molecular sieves were added to N_2 purged, flame dried glassware. The reaction vessel was shielded from light, evacuated and purged with N_2 thrice prior to the addition of anhydrous DCM (2 mL) and DIPEA (78.8 µL, 452.8 µmol, 4.00 eq). The reaction mixture was purged with N_2 for a further 10 mins before the addition of CEP-Cl (80.1 µL, 340.0 µmol, 3.00 eq). TLC showed the reaction to have reached completion after 3.5 hours, the solvent volume reduced to 1 mL. Product was purified by column chromatography under N_2 (silica neutralised with 1mL TEA, eluent – 10% MeOH in DCM), product concentrated *in vacuo* before coevaporation with toluene (2 x 5 mL) and chloroform (2 x 5 mL). The product was obtained as a golden foam (170 mgs, > 100 %).

^{1}H NMR (400 MHz, $CDCl_3$): δ ppm 0.99 (s, 2 H, **32**), 1.04 - 1.14 (m, 12 H, **33**), 2.17 - 2.31 (m, 2 H, **14**), 2.49 - 2.58 (m, 2 H, **14**), 3.28 (dd, J_{HH} = 6.8, 2.8 Hz, 2 H, **30**), 3.46 - 3.52 (m, 2 H, **11**), 3.72 (s, 6 H, **1**), 3.96 (s, 2 H, **22**), 4.03 - 4.10 (m, 6 H, **28**), 4.13 (br. s., 1 H, **12**), 4.18 - 4.26 (m, 2 H, **27**), 4.21 - 4.22 (m, 2 H, **29**), 4.40 - 4.56 (m, 3 H, **26** & **14**), 6.21 (dd, J_{HH} = 13.1, 7.0 Hz, 1 H, **15**), 6.78 (dd, J_{HH} = 8.8, 3.8 Hz, 4 H, **3**), 7.01 - 7.32 (m, 10 H, **9**, **10** & **3**), 7.37 (dd, J_{HH} = 7.5, 2.0 Hz, 2 H, **8**), 8.05 (d, J_{HH} = 17.1 Hz, 1 H, **17**)

^{13}C{^{1}H} NMR (100 MHz, $CDCl_3$): δ ppm 23.5 (CH_3, **33**), 29.0 (CH_2, **22**), 39.5 (CH_2, **14**), 39.7 (CH_2, **30**), 44.3 (CH, **32**), 54.2 (CH_3, **1**), 59.0 (CH_2, **11**), 62.2 (CH, **29**), 67.1 (CH, **13**), 67.1 (CH, **26**), 68.7 (CH, **28**), 69.4 (CH, **27**), 73.1 (C, **19**), 74.2 (C, **25**), 84.6 (CH, **15**), 84.7 (C, **31**), 85.0 (CH, **12**), 85.9 (C, **6**), 88.8 (C, **21**), 98.6 (C, **20**), 112.3 (CH, **3**), 125.9 (CH, **10**), 126.9 (CH, **9**), 127.0 (CH, **8**), 129.0 (CH, **4**), 134.7 (C, **5**), 141.8 (C, **7**), 143.4 (CH, **17**), 148.1 (C, **16**), 157.6 (C, **2**), 160.7 (C, **24**), 168.7 (C, **18**)

^{35}P{^{1}H} NMR (121 MHz, $CDCl_3$): δ ppm 149.63

GC-ESI (pos) ($C_{53}H_{58}FeN_5O_9P$): Monoisotopic mass 995.33, observed *m/z* 1018.4 $[M+Na]^+$

UV-Vis (DCM, conc. unknown due to >100% yield): λ_{max} (Relative intensity) 227 nm (0.97), 281 nm (1.00), 356 nm (0.07), 380 nm (0.09), 440 nm (0.01)

Emission (DCM, conc. unknown due to >100% yield): No fluorescence observed

$\boldsymbol{R_f}$ (silica, 10 % MeOH in DCM): 0.21

8.45 – Synthesis of 4-methyl-2-2'-bipyridyl-4' carboxaldehyde (XVII)[176]

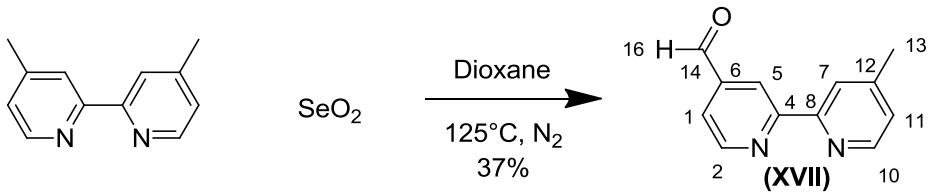

4,4'dimethyl-2-2'-bipyridine (1.105 g, 6.0 mmol, 1.00 eq) was dissolved in dioxane (15 mL) under N_2, selenium (IV) oxide (672.4 mg, 6.6 mmol, 1.10 eq) was added and the reaction mixture heated to reflux (125 °C) for 18 hours. The reaction mixture was hot filtered and the solvent removed *in vacuo*. The resulting solid was redissolved in ethyl acetate (100 mL) and the insoluble material filtered off. Sodium carbonate washes (1 M, 3 x 50 mL) removed any carboxylic acid side product, the organic phase was then extracted with sodium metabisulphite (0.3 M, 4 x 50 mL) to form the aldehyde bisulphite. The sodium metabisulphite extractions were combined and the pH adjusted to pH 10 with sodium carbonate before extracting with DCM (2 X 100 mL), the combined DCM extractions were washed with brine (50 mL), dried over Na_2SO_4 and dried *in vacuo* to give a white solid, 436.3 mg (2.20 mmol, 37 %).

^{1}H NMR (400 MHz, $CDCl_3$): δ ppm 2.43 (s, 3 H, **13**), 7.16 (d, J_{HH} = 5.0 Hz, 1 H, **11**), 7.68 (dd, J_{HH} = 5.0, 1.5 Hz, 1 H, **1**), 8.24 (s, 1 H, **7**), 8.54 (d, J_{HH} = 5.0 Hz, 1 H, **10**), 8.79 (s, 1 H, **5**), 8.85 (d, J_{HH} = 4.5 Hz, 1 H, **2**), 10.14 (s, 1 H, **16**)

^{13}C{^{1}H} NMR (100 MHz, $CDCl_3$): δ ppm 21.6 (CH_3, **13**), 121.0 (CH, **1**), 121.7 (CH, **5**), 122.5 (CH, **7**), 125.8 (CH, **11**), 143.0 (C, **6**), 148.8 (C, **12**), 149.6 (CH, **10**), 150.7 (CH, **2**), 155.1 (C, **8**), 158.7 (C, **4**), 192.1 (CH, **14**)

GC-ESI (pos) ($C_{12}H_{10}N_2O$): Monoisotopic mass 198.1, observed *m/z* 199.2 $[M+H]^+$, 231.2 $[M+H+MeOH]^+$

UV-Vis (MeOH, 44.0 µM): λ_{max} (log ε) 279 nm (4.37), 314 nm (4.19), 357 nm (2.84), 379 nm (2.81)

Emission (MeOH, 5.5 mM): λ_{ex} 279 nm, λ_{em} (rel int): 373 nm (0.17), 403 nm (0.42), 437 nm (0.81), 489 nm (0.46), 529 nm (1)

R_f (silica, 20% MeOH, 80% DCM): 0.59

Melting Point: 129.8 – 131.2 °C (lit. 131.9 – 132.9 °C[215])

8.46 – Synthesis of 4-methyl-2-2'-bipyridyl-4' carboxylic acid (XVIII)[176]

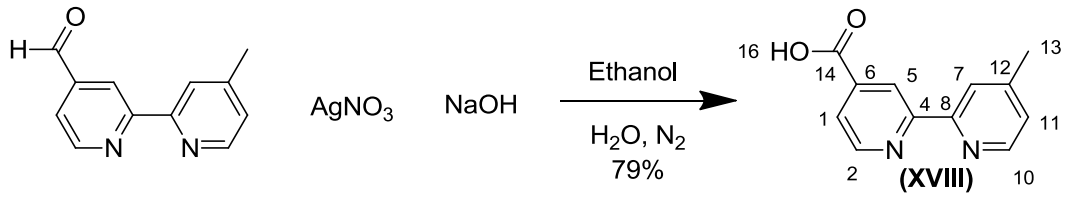

To a suspension of 4-methyl-2-2'-bipyridyl-4' carboxaldehyde (436 mg, 2.20 mmol, 1.00 eq) in ethanol (25 mL) a solution of $AgNO_3$ (448 mg, 4.6 mL, 0.58M, 2.64 mmol, 1.20 eq) was added, following this a sodium hydroxide solution (1.0M, 8.8 mL, 8.80 mmol, 4.00 eq) was added dropwise over 20 minutes. The reaction was stirred at room temperature for 24 hours. Ethanol was removed *in vacuo* to leave the crude reaction mixture in water, the insoluble silver (I) oxide was filtered off and the solid was washed with sodium hydroxide (1.3 M, 2 x 5 mL) and water (2 x 5 mL). The aqueous fraction was extracted with DCM to remove any unreacted starting material. The aqueous phase was concentrated *in vacuo* to ~7 mL and acidified (pH 4) with HCl:AcOH (1:1, ~4 M, ~5 mL), the product precipitated as a white solid, 372.4 mg (1.74 mmol, 79 %).

^{1}H NMR (400 MHz, DMSO-d_6) δ ppm 2.43 (s, 3 H, **13**), 7.34 (d, J_{HH} = 3.5 Hz, 1 H, **11**), 7.86 (d, J_{HH} = 4.0 Hz, 1 H, **1**), 8.28 (br. s., 1 H, **7**), 8.58 (d, J_{HH} = 4.0 Hz, 1 H, **10**), 8.81 (s, 1 H, **5**), 8.86 (d, J_{HH} = 4.0 Hz, 1 H, **2**), 13.04 - 14.38 (m, 1 H, **16**)

^{13}C{^{1}H} NMR (100 MHz, DMSO-d_6) δ ppm 21.3 (CH_3, **13**), 120.2 (CH, **1**), 121.8 (CH, **5**), 123.2 (CH, **7**), 125.7 (CH, **11**), 139.7 (C, **6**), 149.2 (C, **12**), 149.5 (CH, **10**), 150.7 (CH, **2**), 154.3 (C, **8**), 156.6 (C, **4**), 166.7 (C, **14**)

GC-ESI (neg) ($C_{12}H_{10}N_2O_2$): Monoisotopic mass 214.1, observed *m/z* 213.1 $[M-H]^-$

UV-Vis (MeOH, 46.7 µM): λ_{max} (log ε) 285 (4.23), 238 (4.27)

Emission (MeOH, 46.7 µM): No fluorescence observed

R_f (silica, MeOH) 0.62

Melting Point: >250 °C (lit. 280 °C[216])

8.47 – Synthesis of *N*-(prop-2-ynyl)-4-methyl-2-2'-bipyridyl-4'-carboxamide (XIX)

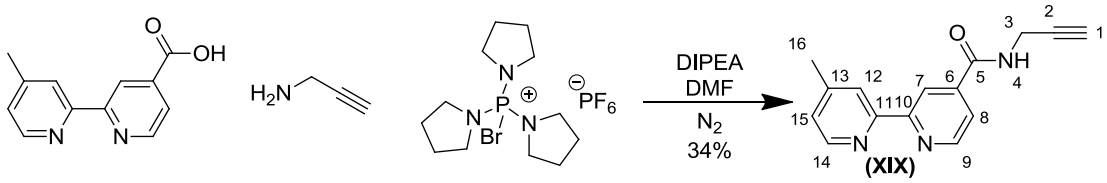

4-methyl-2-2'-bipyridyl-4'-carboxylic acid (107 mg, 0.5 mmol, 1.00 eq), PyBroP (233 mg, 0.5 mmol, 1.00 eq) and propargylamine (37.7 µL, 0.55 mmol, 1.10 eq) were dissolved in DMF (2 mL) under N_2, to this DIPEA (248 µL, 1.5 mmol, 3.00 eq) was added and the reaction stirred at RT for 2.5 hours. The reaction mixture was poured into EA (50 mL) and brine (sat. 20 mL), a white solid precipitated, this was filtered off and discarded. The organic phase was separated, dried over Na_2SO_4, filtered and concentrated *in vacuo*. The crude product was columned (silica, eluent – 1 % MeOH in $CHCl_3$) and recolumned (silica, eluent – EA). The product was obtained as an off white solid, 42.3 mg (168 µmol, 34 %).

^{1}H NMR (400 MHz, DMSO-d_6) δ ppm 2.54 (s, 3 H, **16**), 3.26 (t, J_{HH} = 5.0 Hz, 1 H, **1**), 4.23 (dd, J_{HH} = 2.8, 2.8 Hz, 2 H, **3**), 7.43 (dd, J_{HH} = 5.0, 1.0 Hz, 1 H, **15**), 7.92 (dd, J_{HH} = 5.0, 1.5 Hz, 1 H, **8**), 8.37 (s, 1 H, **12**), 8.69 (d, J_{HH} = 5.0 Hz, 1 H, **14**), 8.88 (d, J_{HH} = 1.0 Hz, 1 H, **7**), 8.93 (d, J_{HH} = 5.0 Hz, 1 H, **9**), 9.51 (t, J_{HH} = 5.5 Hz, 1 H, **4**)

^{13}C{^{1}H} NMR (100 MHz, DMSO-d_6) δ ppm 21.9 (CH_3, **16**), 29.9 (CH_2, **3**), 74.3 (CH, **1**), 82.0 (C, **2**), 119.3 (CH, **7**), 122.6 (CH, **8**), 122.7 (CH, **12**), 126.5 (CH, **15**), 143.3 (C, **6**), 149.4 (C, **13**), 150.3 (CH, **14**), 151.1 (CH, **9**), 155.7 (C, **11**), 157.4 (C, **10**), 165.8 (C, **5**)

GC-ESI (pos) ($C_{152}H_{13}N_3O$): Monoisotopic mass 251.11, observed *m/z* 252.2 $[M+H]^+$

UV-Vis (MeOH, 39.8 µM): λ_{max} (log ε) 281 (4.08), 239 (4.19)

Emission (MeOH, 39.8 µM): No fluorescence observed

R_f (silica, 10% MeOH in DCM): 0.35

Melting Point: 95.6 °C (dec.) Lit. 146 °C[176]

8.48 – Synthesis of *N*-(prop-2-ynyl)-4-methyl-2-2'-bipyridyl-4'-carboxamide (XIX)

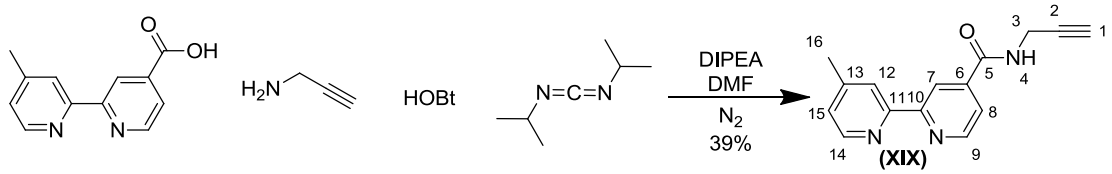

4-methyl-2-2'-bipyridyl-4'-carboxylic acid (107 mg, 0.5 mmol, 1.00 eq), HOBt (76.5 mg, 0.5 mmol, 1.00 eq), DIPEA (107 µL, 0.65 mmol, 1.30 eq) and propargylamine (34.3 µL, 0.50 mmol, 1.00 eq) were dissolved in DMF (2 mL) under N_2. DIC (85.2 µL, 0.55 mmol, 1.10 eq) was added dropwise over 45 minutes and the reaction stirred at RT for 18 hours. The reaction mixture was poured into EA (50 mL) and brine (sat. 50 mL), a white solid precipitated (urea byproduct), this was filtered off and discarded. The organic phase was separated, dried over Na_2SO_4, filtered and concentrated *in vacuo*. The crude product was columned (silica, eluent – 1 % MeOH in $CHCl_3$), the resulting solid also contained the urea byproduct, this was recrystallised and the product obtained from the supernatant as an off white solid, 49.3 mg (196 µmol, 39 %).

^{1}H NMR (400 MHz, DMSO-d_6) δ ppm 2.54 (s, 3 H, **16**), 3.26 (t, J_{HH} = 5.0 Hz, 1 H, **1**), 4.23 (dd, J_{HH} = 2.8, 2.8 Hz, 2 H, **3**), 7.43 (dd, J_{HH} = 5.0, 1.0 Hz, 1 H, **15**), 7.92 (dd, J_{HH} = 5.0, 1.5 Hz, 1 H, **8**), 8.37 (s, 1 H, **12**), 8.69 (d, J_{HH} = 5.0 Hz, 1 H, **14**), 8.88 (d, J_{HH} = 1.0 Hz, 1 H, **7**), 8.93 (d, J_{HH} = 5.0 Hz, 1 H, **9**), 9.51 (t, J_{HH} = 5.5 Hz, 1 H, **4**)

^{13}C{^{1}H} NMR (100 MHz, DMSO-d_6) δ ppm 21.9 (CH_3, **16**), 29.9 (CH_2, **3**), 74.3 (CH, **1**), 82.0 (C, **2**), 119.3 (CH, **7**), 122.6 (CH, **8**), 122.7 (CH, **12**), 126.5 (CH, **15**), 143.3 (C, **6**), 149.4 (C, **13**), 150.3 (CH, **14**), 151.1 (CH, **9**), 155.7 (C, **11**), 157.4 (C, **10**), 165.8 (C, **5**)

GC-ESI (pos) ($C_{152}H_{13}N_3O$): Monoisotopic mass 251.11, observed *m/z* 252.2 $[M+H]^+$

UV-Vis (MeOH, 39.8 µM): λ_{max} (log ε) 281 (4.08), 239 (4.19)

Emission (MeOH, 39.8 µM): λ_{ex} 281 nm, λ_{em} (rel int): No fluorescence observed

R_f (silica, 10% MeOH in DCM): 0.35

Melting Point: 95.6 °C (dec.) Lit. 146 °C[176]

8.49 – Synthesis of *N*-(prop-2-ynyl)-4-methyl-2-2'-bipyridyl-4'-carboxamide (XIX)[176]

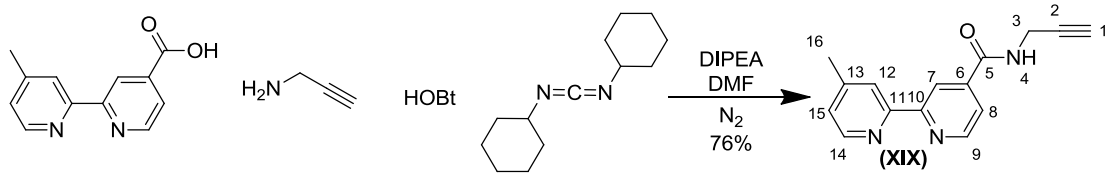

4-methyl-2-2'-bipyridyl-4'-carboxylic acid (107 mg, 0.5 mmol, 1.00 eq), HOBt (76.5 mg, 0.5 mmol, 1.00 eq), DIPEA (107 µL, 0.65 mmol, 1.30 eq) and propargylamine (34.3 µL, 0.50 mmol, 1.00 eq) were dissolved in DMF (3 mL) under N_2. DCC (113.5 mg, 0.55 mmol, 1.10 eq) was dissolved in DMF (3 mL) and added dropwise to the reaction over 30 minutes and the reaction stirred at RT for 18 hours. The resulting precipitate (urea byproduct) was filtered off and the DMF was removed by vacuum distillation. The crude product was dissolved in EA (10 mL) and washed with $NaHCO_3$ (sat. 30 mL), HCl (0.5 M, 30 mL) and brine (sat. 30 mL). The organic phase was separated, dried over Na_2SO_4, filtered and concentrated *in vacuo*. The crude product was columned (dry loaded onto silica, eluent – 1.5 % MeOH in $CHCl_3$) and the product obtained as an off white solid, 95.3 mg (379 µmol, 76 %).

^{1}H NMR (400 MHz, DMSO-d_6) δ ppm 2.54 (s, 3 H, **16**), 3.26 (t, J_{HH} = 5.0 Hz, 1 H, **1**), 4.23 (dd, J_{HH} = 2.8, 2.8 Hz, 2 H, **3**), 7.43 (dd, J_{HH} = 5.0, 1.0 Hz, 1 H, **15**), 7.92 (dd, J_{HH} = 5.0, 1.5 Hz, 1 H, **8**), 8.37 (s, 1 H, **12**), 8.69 (d, J_{HH} = 5.0 Hz, 1 H, **14**), 8.88 (d, J_{HH} = 1.0 Hz, 1 H, **7**), 8.93 (d, J_{HH} = 5.0 Hz, 1 H, **9**), 9.51 (t, J_{HH} = 5.5 Hz, 1 H, **4**)

^{13}C{^{1}H} NMR (100 MHz, DMSO-d_6) δ ppm 21.9 (CH_3, **16**), 29.9 (CH_2, **3**), 74.3 (CH, **1**), 82.0 (C, **2**), 119.3 (CH, **7**), 122.6 (CH, **8**), 122.7 (CH, **12**), 126.5 (CH, **15**), 143.3 (C, **6**), 149.4 (C, **13**), 150.3 (CH, **14**), 151.1 (CH, **9**), 155.7 (C, **11**), 157.4 (C, **10**), 165.8 (C, **5**)

GC-ESI (pos) ($C_{152}H_{13}N_3O$): Monoisotopic mass 251.11, observed *m/z* 252.2 $[M+H]^+$

UV-Vis (MeOH, 39.8 µM): λ_{max} (log ε) 281 (4.08), 239 (4.19)

Emission (MeOH, 39.8 µM): λ_{ex} 281 nm, λ_{em} (rel int): No fluorescence observed

R_f (silica, 10% MeOH in DCM): 0.35

Melting Point: 95.6 °C (dec.) Lit. 146 °C[176]

8.50 – Synthesis of Ruthenium (IV) (*N*-(prop-2-ynyl)-4-methyl-2-2'-bipyridyl-4'-carboxamide) $(bipy)_2$ *bis*-hexafluorophosphate salt (XX)[176]

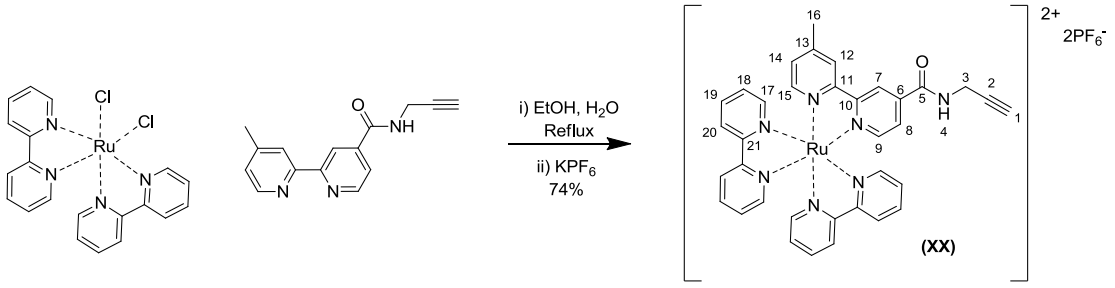

$Ru(bipy)_2(Cl)_2$ (150 mg, 0.3 mmol, 1.00 eq) and *N*-(prop-2-ynyl)-4-methyl-2-2'-bipyridyl-4'-carboxamide (80 mg, 0.3 mmol, 1.00 eq) were dissolved in EtOH:H_2O (1:1, 25 mL) and heated to reflux for 14 hours, the red solution turned lighter over the course of the reaction. The reaction mixture was cooled (RT) and the ethanol removed, a precipitate formed on standing (3 hrs), this was filtered off and discarded. KPF_6 (sat.aq. ~50 mL) was added until no further precipitation occurred. The orange solid product was filtered off, washed with water and ether and dried *in vacuo*, 211.2 mg (221 µmol, 74 %).

^{1}H NMR (400 MHz, CD_3CN): δ ppm 2.53 (t, J_{HH} = 2.5 Hz, 1 H, **1**), 2.56 (s, 3 H, **16**), 4.18 (dd, J_{HH} = 5.5, 2.5 Hz, 2 H, **3**), 7.29 (d, J_{HH} = 5.0 Hz, 1 H, **14**), 7.41 (dd, J_{HH} = 6.5, 6.0 Hz, 4 H, **18**), 7.58 (d, J_{HH} = 5.5 Hz, 1 H, **15**), 7.64 (dd, J_{HH} = 5.8, 1.3 Hz, 1 H, **8**), 7.70 - 7.78 (m, 4 H, **17**), 7.88 (d, J_{HH} = 6.0 Hz, 1 H, **9**), 8.07 (dd, J_{HH} = 7.8 Hz, 4 H, **19**), 8.51 (d, J_{HH} = 7.5 Hz, 4 H, **20**), 8.50 (s, 1 H, **12**), 8.77 (s, 1 H, **7**)

^{13}C{^{1}H} NMR (100 MHz, CD_3CN): δ ppm 19.9 (CH_3, **16**), 28.8 (CH_2, **3**), 71.2 (CH, **1**), 79.2 (C, **2**), 121.2 (CH, **7**), 124.0 (CH, **20**), 124.1 (CH, **8**), 125.2 (CH, **12**), 127.3 (CH, **16**), 128.5 (CH, **14**), 137.6 (CH, **19**), 141.4 (C, **6**), 150.4 (C, **13**), 150.5 (CH, **15**), 151.3 (CH, **17**), 151.3 (CH, **17**), 151.4 (CH, **17**), 151.4 (CH, **17**), 152.2 (CH, **9**), 155.6 (C, **11**), 156.4 (C, **21**), 156.6 (C, **21**), 156.6 (C, **21**), 156.7 (C, **21**), 157.7 (C, **10**), 162.7 (C, **5**)

GC ESI (pos) ($C_{35}H_{29}F_{12}N_7OP_2Ru$): Monoisotopic mass 955.08, observed *m/z* 810.2 $[M\text{-}PF_6^-]^+$

UV-Vis (MeCN, 10.5 µM): λ_{max} (log ε) 247 (4.48), 285 (4.87), 454 (4.17)

Emission (MeCN, 10.5 µM): λ_{ex} 285 nm, λ_{em} (rel int): 567 (0.74), 636 (1.00)

R_f (silica, 20:1:3 MeCN:$KNO_{3\,(sat.aq.)}$:H_2O): 0.40

CV (1 mM in 10 mM Tris buffer (pH 7.2) containing 1M NaCl and 50% DMSO, sweep rate 100 mV s^{-1}, potentials *vs* SCE, 5 mm Ø glassy carbon electrode, Pt counter electrode): 1.146 V / 1.013 V (ox. / red.)

Melting Point: 229.3 – 230.6 °C (no lit. value)

8.51 – Synthesis of Ruthenium (IV) (*N*-(prop-2-ynyl)-4-methyl-2-2'-bipyridyl-4'-carboxamide) $(bipy)_2$ *bis*-nitrate (XXI)

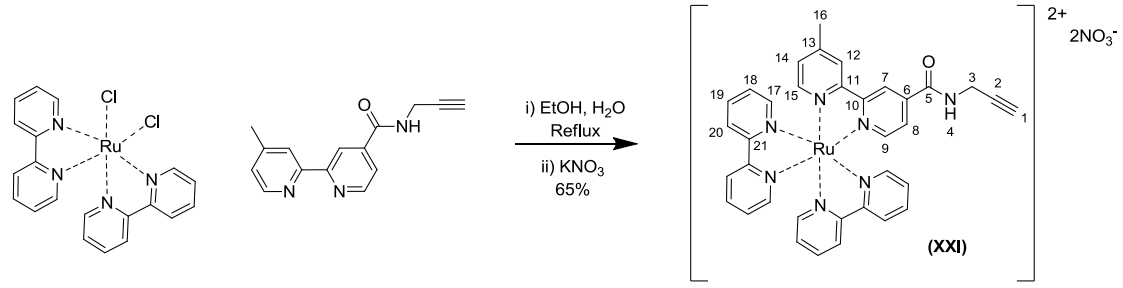

$Ru(bipy)_2(Cl)_2$ (150 mg, 0.3 mmol, 1.00 eq) and *N*-(prop-2-ynyl)-4-methyl-2-2'-bipyridyl-4'-carboxamide (80 mg, 0.3 mmol, 1.00 eq) were dissolved in EtOH:H_2O (70:30, 25 mL) and heated to reflux for 16 hours. KNO_3 (4.00 g) was added and the reaction mixture agitated at room temperature for 5 minutes before drying *in vacuo*. Crude product was redissolved in DCM:MeOH (20:1, 10 mL), filtered and the solvent removed *in vacuo*. The product was purified by column chromatography (silica, eluent - MeCN:$KNO_{3\ (sat.\ aq.)}$:H_2O 20:1:3), product dried, redissolved in DCM:MeOH (20:1, 10 mL), filtered, the solvent removed and the red solid product dried *in vacuo*, 151.1 mg (192 µmol, 65 %).

^{1}H NMR (400 MHz, CD_3CN): δ ppm 2.46 (t, J_{HH} = 2.5 Hz, 1 H, **1**), 2.53 (s, 3 H, **16**), 4.16 (dd, J_{HH} = 5.5, 2.5 Hz, 2 H, **3**), 7.28 (d, J_{HH} = 5.0 Hz, 1 H, **14**), 7.42 (dd, J_{HH} = 6.5, 6.0 Hz, 4 H, **18**), 7.59 (d, J_{HH} = 5.5 Hz, 1 H, **15**), 7.76 (dd, J_{HH} = 5.8, 1.3 Hz, 1 H, **8**), 7.84 (dd, J_{HH} = 6.0, 1.5 Hz, 4 H, **17**), 7.86 - 7.91 (m, 1 H, **9**), 8.06 (br. s., 4 H, **19**), 8.60 (d, J_{HH} = 8.0 Hz, 4 H, **20**), 8.61 - 8.65 (m, 1 H, **12**), 8.77 - 8.83 (m, 1 H, **7**), 9.61 (t, J_{HH} = 5.5 Hz, 1 H, **4**)

^{13}C{^{1}H} NMR (100 MHz, CD_3CN): δ ppm 19.9 (CH_3, **16**), 28.7 (CH_2, **3**), 70.5 (CH, **1**), 79.5 (C, **2**), 121.4 (CH, **7**), 124.1 (CH, **20**), 124.8 (CH, **8**), 125.6 (CH, **12**), 127.3 (CH, **16**), 128.3 (CH, **14**), 137.5 (CH, **19**), 141.4 (C, **6**), 150.3 (C, **13**), 151.2 (CH, **15**), 151.4 (CH, **17**), 152.0 (CH, **9**), 155.9 (C, **11**), 156.5 (C, **21**), 156.6 (C, **21**), 156.7 (C, **21**), 156.7 (C, **21**), 157.7 (C, **10**), 162.9 (C, **5**)

GC ESI (pos) ($C_{35}H_{29}N_9O_7Ru$): Monoisotopic mass 789.12, observed *m/z* 727.5 $[M\text{-}NO_3^-]^+$

UV-Vis (MeCN, 15.5 µM): λ_{max} (log ε) 245 (4.38), 288 (4.79), 455 (4.12)

Emission (MeCN, 15.5 µM): λ_{ex} 455 nm, λ_{em} (rel int): 634 (1.00)

λ_{ex} 288 nm, λ_{em} (rel int): 635 (1.00)

R_f (silica, 20:1:3 MeCN:$KNO_{3\ (sat.aq.)}$:H_2O): 0.44

Melting Point: >250 °C (no lit. value)

8.52 – Synthesis of 5'-hydroxyl ruthenium *tris*-bipyridyl monomer *bis*-nitrate (XXII)

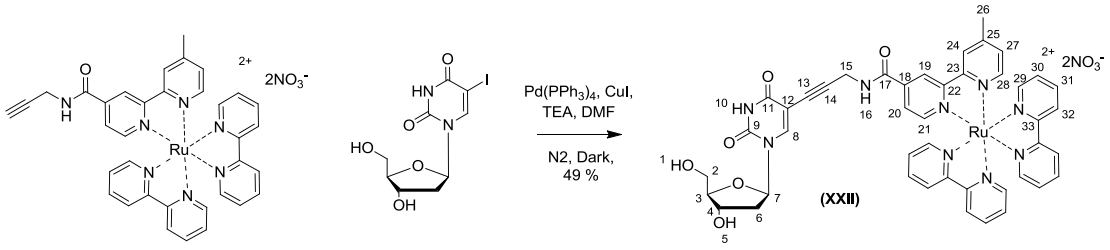

Ruthenium (IV) (*N*-(prop-2-ynyl)-4-methyl-2-2'-bipyridyl-4'-carboxamide) $(bipy)_2$ *bis*-nitrate (38.6 mg, 48.9 µmol, 1.00 eq), 5-iodo-dU (17.3 mg, 48.9 µmol, 1.00 eq) and copper (I) iodide (1.9 mg, 9.79 µmol, 0.20 eq) were dissolved in DMF (1.5 mL) and purged with N_2 for 10 minutes. Palladium tetrakis triphenyl phosphine (5.7 mg, 4.89 µmol, 0.10 eq) and TEA (13.6 µL, 97.9 µmol, 2.00 eq) were added and the reaction stirred in the dark for 18 hours. The product was isolated by column chromatography (silica, eluent – 50:1:3 $MeCN:KNO_{3\ (sat.\ aq.)}:H_2O$. The isolated product was dried, redissolved in DCM, filtered and concentrated *in vacuo* to remove KNO_3 to give 24.5 mg (24.1 µmol, 49 %) of an orange solid.

^{1}H NMR (400 MHz, DMSO-d_6): δ ppm 2.09 - 2.15 (m, 2 H, **6**), 2.55 (s, 3 H, **26**), 3.52 - 3.65 (m, 2 H, **2**), 3.81 (q, J_{HH} = 3.4 Hz, 1 H, **3**), 4.20 - 4.27 (m, 1 H, **4**), 4.38 (d, J_{HH} = 6.1 Hz, 2 H, **15**), 5.14 (t, J_{HH} = 5.1 Hz, 1 H, **1**), 5.28 (d, J_{HH} = 4.0 Hz, 1 H, **5**), 6.11 (t, J_{HH} = 6.6 Hz, 1 H, **7**), 7.42 (d, J_{HH} = 6.1 Hz, 1 H, **27**), 7.54 (dd, J_{HH} = 7.1, 6.1 Hz, 4 H, **30**), 7.59 (d, J_{HH} = 6.1 Hz, 1 H, **28**), 7.73 (d, J_{HH} = 5.6 Hz, 4 H, **29**), 7.84 (dd, J_{HH} = 5.8, 1.8 Hz, 1 H, **20**), 7.90 - 7.93 (m, 1 H, **21**), 8.17 (t, J_{HH} = 7.8 Hz, 4 H, **31**), 8.20 - 8.22 (m, 1 H, **8**), 8.82 - 8.83 (m, 1 H, **24**), 8.85 (d, J_{HH} = 8.1 Hz, 4 H, **32**), 9.18 - 9.24 (m, 1 H, **19**), 9.66 (t, J_{HH} = 5.3 Hz, 1 H, **16**)

^{13}C{^{1}H} NMR (100 MHz, DMSO-d_6): δ ppm 20.6 (CH_3, **26**), 29.5 (CH_2, **15**), 40.3 (CH_2, **6**), 63.0 (CH_2, **2**), 70.1 (CH, **4**), 74.8 (C, **12**), 84.7 (CH, **7**), 87.6 (CH_2, **3**), 88.7 (C, **14**), 97.8 (C, **13**), 121.4 (CH, **19**), 124.3 (CH, **32**), 125.1 (CH, **20**), 125.5 (CH, **24**), 127.7 (CH, **30**), 128.8 (CH, **27**), 137.9 (CH, **31**), 141.0 (C, **18**), 143.8 (C, **9**), 149.3 (C, **25**), 149.8 (CH, **28**), 150.2 (CH, **8**), 151.0 (CH, **29**), 151.1 (CH, **29**), 151.3 (CH, **29**), 152.0 (CH, **21**), 155.5 (C, **23**), 156.3 (C, **33**), 156.4 (C, **33**), 156.5 (C, **33**), 156.5 (C, **33**), 157.3 (C, **22**), 161.6 (C, **17**), 162.6 (C, **11**)

GC ESI (pos) ($C_{44}H_{39}N_{11}O_{12}Ru$): Monoisotopic mass 1015.18, observed *m/z* 976.2 $[M\text{-}NO_3^- + Na^+ - e^-]^+$, 891.2 $[M\text{-}2NO_3^- + e^-]^+$

HR-ESI(pos) ($C_{44}H_{39}N_{11}O_{12}Ru$) Monoisotopic mass 1015.1834, observed *m/z* 445.6030 $[M\text{-}2NO_3]^{2+}$

UV-Vis (MeCN, 12.3 µM): λ_{max} (log ε) 287 (4.53), 455 broad. (3.80)

Emission (MeCN, 12.3 μM): λ_{ex} 287 nm, λ_{em} (rel int): 634 (1.0)

λ_{ex} 455 nm, λ_{em} (rel int): 634 (1.0)

$\boldsymbol{R_f}$ (silica, 20:1:3 MeCN:$KNO_{3\,(sat.aq.)}$:H_2O): 0.08

Melting Point: 191.3 – 193.2 °C (dec.) (no lit. value)

8.53 – Synthesis of Ruthenium (IV) (4-methyl-2-2'-bipyridyl-4'-carboxylic acid) $(bipy)_2$ *bis*-nitrate (XXIII)

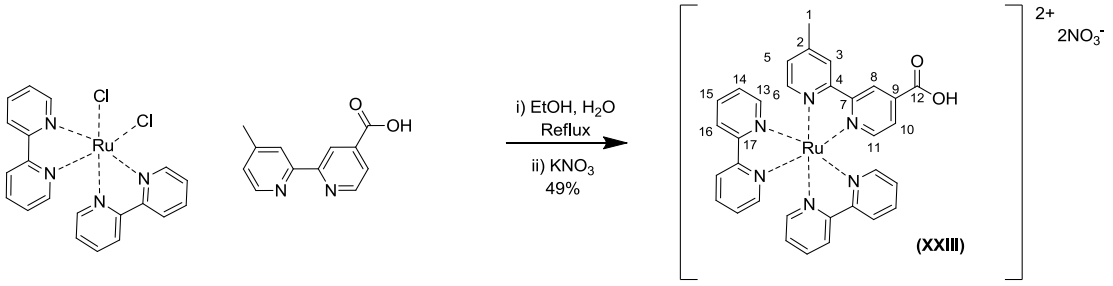

Ruthenium $(bpy)_2Cl_2$ (150 mg, 0.3 mmol, 1.00 eq) and 4-methyl-2-2'-bipyridyl-4'-carboxylic acid (64.2 mg, 0.3 mmol, 1.00 eq) were heated to 110 °C in ethanol:water (70:30, 25 mL) for 16 hours, the ethanol was removed *in vacuo*, KNO_3 (4.0 g) was added and the reaction mixture agitated at room temperature for 5 minutes. The crude product was dried, redissolved in DCM:MeOH (1:1 25 mL), filtered and concentrated *in vacuo*. Purified by column chromatography (silica, eluent – MeCN:$KNO_{3\ sat\ aq}$:H_2O 50:1:3). The product was obtained as a red solid, 110.4 mg (147 µmol, 49 %).

^{1}H NMR (400 MHz, CD_3CN): δ ppm 3.09 (br. s., 3 H, **1**), 7.82 (d, J_{HH} = 5.6 Hz, 1 H, **5**), 7.96 (d, J_{HH} = 7.1 Hz, 4 H, **14**), 8.12 (d, J_{HH} = 5.6 Hz, 1 H, **6**), 8.28 (d, J_{HH} = 4.0 Hz, 4 H, **13**), 8.36 (d, J_{HH} = 6.1 Hz, 1 H, **10**), 8.40 (d, J_{HH} = 5.6 Hz, 1 H, **11**), 8.62 (dd, J_{HH} = 8.1, 6.6 Hz, 4 H, **15**), 9.12 (d, J_{HH} = 7.6 Hz, 4 H, **16**), 9.15 (br. s., 1 H, **3**), 9.55 (br. s., 1 H, **8**)

^{13}C{^{1}H} NMR (100 MHz, CD_3CN): δ ppm 59.4 (CH_3, **1**), 162.5 (CH, **8**), 163.6 (CH, **16**), 164.9 (CH, **10**), 165.7 (CH, **3**), 166.8 (CH, **14**), 167.8 (CH, **5**), 177.1 (CH, **15**), 190.0 (C, **2**), 190.8 (CH, **6**), 190.9 (CH, **13**), 191.5 (CH, **11**), 195.4 (C, **4**), 196.2 (C, **17**), 196.3 (C, **7**), 197.1 (C, **12**)

MALDI ToF (pos) ($C_{32}H_{26}N_8O_8Ru$): Monoisotopic mass 752.09, observed *m/z* 627.9 $[M\text{-}2NO_3^-]^{2+}$

UV-Vis (MeCN, 16.0 µM): λ_{max} (log ε) 243 (3.91), 287 (4.39), 453 (3.65)

Emission (MeCN, 16.0 µM): No fluorescence observed

R_f (silica, 3:1:1 MeCN:KNO_3 sat.aq.:H_2O): 0.25

Melting Point: 190.2 °C (dec.) (no lit. value)

8.54 – Synthesis of *N*-(prop-2-yne)-*N'*-(ethylbenzene)-napthalene diimide (XXIV)

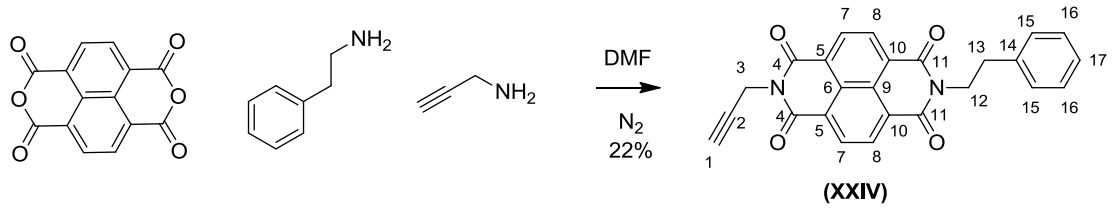

(XXIV)

Phenylethylamine (252 µL, 2.0 mmol, 1.00 eq) and propargylamine (137 µL, 2.0 mmol, 1.00 eq) were dissolved in DMF (10 mL) and purged with N_2 for 10 minutes prior to the addition of naphthalene-1,4,5,8-tetracarboxylate dianhydride (536 mg, 2.0 mmol, 1.00 eq) and heating to 120 °C. The reaction mixture was cooled (RT) after 16 hours and concentrated *in vacuo*. The product was isolated through repeated column chromatography on silica, column 1 eluent; 5% MeOH in DCM, column 2 eluent; 0.5% MeOH in DCM → 1% MeOH in DCM, column 3 eluent; 0.2% MeOH in DCM, column 4 eluent; 0.2% MeOH in DCM, column 5 eluent; 0.05% MeOH in DCM → 0.1% MeOH in DCM, column 6 eluent; DCM (dry loaded onto column). 177.7 mgs (435 µmol, 22 %) of an off white solid was isolated.

^{1}H NMR (400 MHz, $CDCl_3$); δ ppm 2.16 (t, J_{HH} = 2.5 Hz, 1 H, **1**), 2.97 (t, J_{HH} = 8.3 Hz, 2 H, **13**), 4.36 (t, J_{HH} = 8.3 Hz, 2 H, **12**), 4.91 (d, J_{HH} = 2.5 Hz, 2 H, **3**), 7.15 (t, J_{HH} = 7.0 Hz, 1 H, **17**), 7.20 - 7.31 (m, 2 H, **16**), 7.24 (d, J_{HH} = 11.5 Hz, 2 H, **15**), 8.70 (d, J_{HH} = 7.5 Hz, 2 H, **7**), 8.74 (d, J_{HH} = 7.5 Hz, 2 H, **8**)

^{13}C{^{1}H} NMR (100 MHz, $CDCl_3$); δ ppm 35.0 (CH_2, **13**), 43.1 (CH_2, **12**), 72.1 (CH, **1**), 78.7 (C, **2**), 127.2 (CH, **17**), 127.5 (C, **10**), 127.6 (C, **6** & **9**), 127.8 (C, **5**), 129.4 (CH, **15**), 129.8 (CH, **16**), 131.9 (CH, **8**), 132.2 (CH, **7**), 139.1 (C, **14**), 162.9 (C, **11**), 163.4 (C, **4**)

GC-ESI (pos) ($C_{25}H_{16}N_2O_4$): Monoisotopic mass 408.4, observed *m/z* 431.4 $[M+Na]^+$

UV-Vis (DCM, 16.5 µM): λ_{max} (log ε) 341 nm (4.30), 358 nm (4.53), 379nm (4.63)

Emission (DCM, 12.5 mM): λ_{ex} 379 nm, λ_{em} (rel int): 408 nm (1), 433 (0.57)

R_f (silica, 5% MeOH in DCM); 0.60

Melting Point: >250 °C (no lit. value)

8.55 – Synthesis of 5'-DMT-5-(*N*-(ethylbenzene)-*N'*-(prop-2-ynyl)-napthalene diimide) dU (XXV)

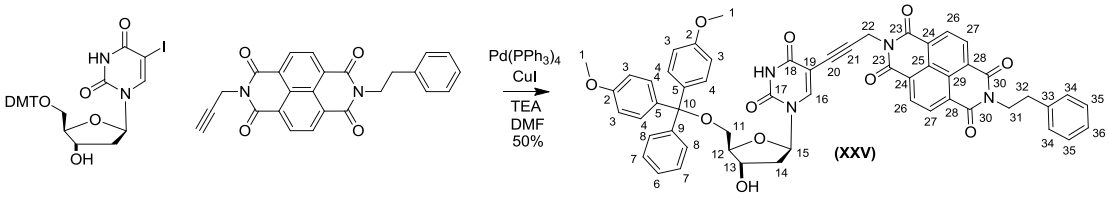

N-prop-2-yne-*N'*-ethylbenzene naphthalene diimide (51.1 mg, 125 µmol, 1.00 eq), 5'-DMT-5-iodo-dU (86.16 mg, 131 µmol, 1.05 eq), copper (I) iodide (7.86 mg, 41.3 µmol, 0.33 eq) and TEA (435 µL, 3.13 mmol, 25.00 eq) were dissolved in DMF (5 mL) in flame dried glassware, shielded from light and purged with N_2 for 10 minutes prior to the addition of $Pd(PPh_3)_4$ (24.5 mg, 21.2 µmol, 0.17 eq). After 5.5 hours additional CuI (3.9 mg, 20.65 µmol, 0.17 eq) and $Pd(PPh_3)_4$ (12.2 mg, 10.6 µmol, 0.09 eq) was added and the reaction allowed to stir at RT for 24 hours in total. Reaction mixture poured into EDTA solution (5% w/v, pH 9, 20 mL), extracted into DCM (50 mL), washed with additional EDTA solution (5% w/v, pH 9, 2 x 20 mL), dried over Na_2SO_4, filtered and concentrated *in vacuo*. Column chromatography was carried out twice (First column; silica pretreated with TEA, eluent – DCM → 2% MeOH in DCM. Second column; silica pretreated with TEA, sample dry loaded, eluent – 60% EA 40% pet. ether) to give the product as a yellow solid, 58.2 mg (62.1 µmol, 50 %).

^{1}H NMR (400 MHz, $CDCl_3$); δ ppm 2.01 - 2.14 (m, 1 H, **14**), 2.34 (dd, J_{HH} = 7.8, 2.8 Hz, 1 H, **14**), 2.94 (t, J_{HH} = 7.5 Hz, 2 H, **32**), 3.27 (dd, J_{HH} = 21.6, 10.5 Hz, 2 H, **11**), 3.58 - 3.71 (m, 6 H, **1**), 3.91 (s, 1 H, **12**), 4.25 (br. s., 1 H, **13**), 4.31 (t, J_{HH} = 7.5 Hz, 2 H, **31**), 4.81 (br. s., 2 H, **22**), 6.06 (t, J_{HH} = 5.0 Hz, 1 H, **15**), 6.65 - 6.74 (m, 4 H, **3**), 6.98 - 7.07 (m, 1 H, **6**), 7.08 - 7.26 (m, 11 H, **4**, **7**, **34**, **35** & **36**), 7.31 (d, J_{HH} = 7.5 Hz, 2 H, **6**), 7.93 (s, 1 H, **16**), 8.42 (d, J_{HH} = 7.5 Hz, 2 H, **26**), 8.53 (d, J_{HH} = 7.5 Hz, 2 H, **27**)

^{13}C{^{1}H} NMR (100 MHz, $CDCl_3$); δ ppm 31.4 (CH_2, **22**), 35.0 (CH_2, **32**), 42.2 (CH_2, **14**), 43.0 (CH_2, **31**), 56.1 (CH_3, **1**), 64.3 (CH_2, **11**), 73.0 (CH, **13**), 74.5 (C, **19**), 86.8 (CH, **15**), 87.4 (CH, **12**), 87.9 (C, **10**), 88.9 (C, **21**), 100.3 (C, **20**), 114.1 (CH, **3**), 127.2 (CH, **27**), 127.4 (CH, **24**), 127.4 (CH, **36**), 127.5 (CH, **6**), 127.8 (C, **25** & **29**), 128.8 (CH, **8**), 129.5 (CH, **7**), 129.8 (CH, **34**), 130.8 (CH, **35**), 130.9 (CH, **4**), 131.8 (CH, **27**), 132.0 (CH, **26**), 136.5 (C, **6**), 139.1 (CH, **39**), 143.9 (CH, 16), 145.4 (C, **9**), 150.1 (C, **17**), 159.4 (C, **2**), 162.2 (C, **18**), 162.5 (C, **30**), 163.5 (C, **23**)

GC-ESI (pos) ($C_{55}H_{44}N_4O_{11}$): Monoisotopic mass 936.3, observed *m/z* 959.4 $[M+Na]^+$

HR-ESI(pos) ($C_{55}H_{44}N_4O_{11}$) Monoisotopic mass 936.3007, observed *m/z* 954.3347 $[M+NH_4]^+$

UV-Vis (DCM, 0.11 mM): λ_{max} (log ε) 233 nm (3.96), 284 nm (3.37), 342 nm (3.30), 356 nm (3.51), 377 nm (3.57)

Emission (DCM, 12.7 mM): λ_{ex} 377 nm, λ_{em} (rel int): 447 nm (0.56), 488 nm (0.41), 535 nm (0.47), 652 (1), 716 nm (0.38)

$\boldsymbol{R_f}$ (silica, 90% EA, 10% pet. ether); 0.35

CV (1 mM in MeCN containing 1M TBAP, sweep rate 100 mV s^{-1}, potentials *vs* Ag/AgCl, 5 mm Ø glassy carbon electrode, Pt counter electrode): -0.332 V / -0.434 V (ox. / red.)

Melting Point: 99.8 °C (dec.) (no lit. value)

8.56 – Synthesis of naphthalene diimide dU phosphoramidite (XXVI)

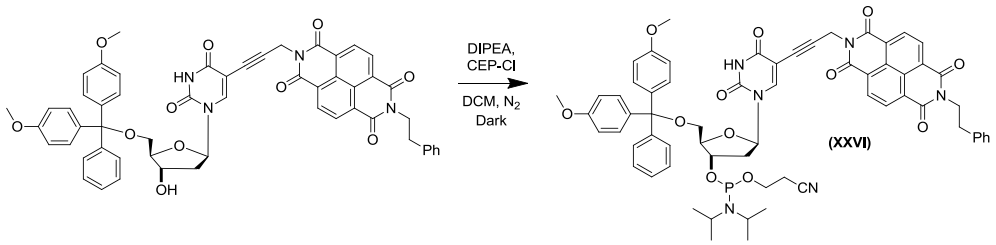

5'-DMT-5-(*N*-(ethylbenzene)-*N'*-(prop-2-ynyl)-napthalene diimide) dU (28.0 mg, 30.0 µmole, 1.00 eq) was dissolved in DCM (2 mL) under an N_2 atmosphere. DIPEA (20.1 µL, 90.0 µmoles, 3.00 eq) and CEP-Cl (20.1 µL, 60.0 µmoles, 2.00 eq) were added and the reaction stirred in the dark. The reaction had not reached completion after 3 hours so an additional portion of CEP-Cl (14.3 µL, 60.0 µmoles, 2.00 eq) was added. After 5 hours the reaction volume was reduced to 1 mL, hexanes added (10 mL) and the reaction chilled (-18 °C) for 90 minutes. The hexanes were removed and the solid product was washed with additional hexanes (5 mL). The crude product was dissolved in 600 µL DCM for immediate use in DNA synthesis.

Full characterisation of the product was not achieved due to its instability. The product was used immediately for DNA synthesis.

$\boldsymbol{R_f}$ (10% MeOH in DCM): 0.48

8.57 – Synthesis of 5'-DMT-5-propargyl-(anthraquinone-2''-carboxamidyl)-dU (XXVII)

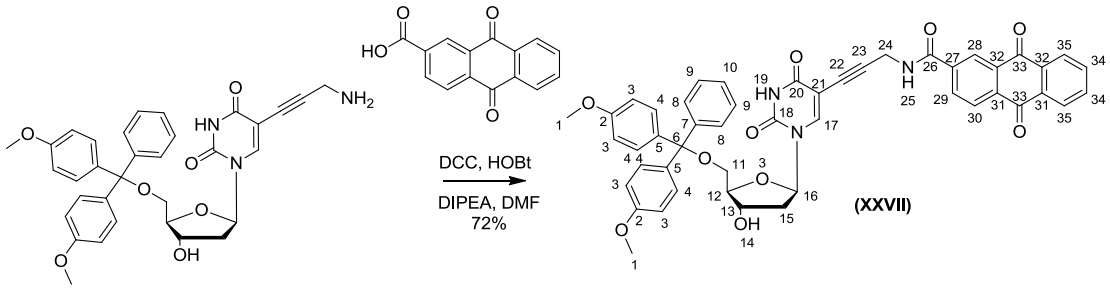

5'-DMT-5-propargylamino-dU (58.3 mg, 0.1 mmol, 1.00 eq), anthraquinone-2-carboxylic acid (25.2 mg, 0.1 mmol, 1.00 eq), HOBt (15.3 mg, 0.1 mmol, 1.00 eq) and DIPEA (21.4 µL, 0.13 mmol, 1.30 eq) were dissolved in DMF (3 mL) and purged with nitrogen. DCC (22.7 mg, 0.11 mmol, 1.10 eq) was dissolved in DMF (1 mL), this was added to the reaction mixture portion-wise over 20 minutes and the reaction stirred for 16 hours. The solvent was removed *in vacuo*, the resulting solid redissolved in DCM (10 mL), washed with brine (2 x 20 mL), dried over Na_2SO_4, filtered and concentrated *in vacuo*. The crude product was purified by column chromatography (silica, eluent 5 % MeOH in DCM), the product was obtained as a yellow foam, 59.9 mg (73.2 µmol, 72 %).

^{1}H NMR (400 MHz, CD_3CN): δ ppm 2.20 - 2.30 (m, 1 H, **15**), 2.44 - 2.53 (m, 1 H, **15**), 3.23 (br. s., 2 H, **11**), 3.61 (s, 6 H, **1**), 4.02 (d, J_{HH} = 3.0 Hz, 1 H, **12**), 4.08 (br. s., 2 H, **24**), 4.46 - 4.52 (m, 1 H, **13**), 6.22 (t, J_{HH} = 6.6 Hz, 1 H, **16**), 6.68 (dd, J_{HH} = 9.1, 1.5 Hz, 4 H, **4**), 7.06 (s, 1 H, **10**), 7.16 (t, J_{HH} = 7.8 Hz, 2 H, **9**), 7.20 (dd, J_{HH} = 8.8, 1.8 Hz, 4 H, **3**), 7.27 - 7.30 (m, 2 H, **7**), 7.32 (d, J_{HH} = 7.6 Hz, 1 H, **29**), 7.62 - 7.72 (m, 2 H, **34**), 8.02 (dd, J_{HH} = 8.1, 1.5 Hz, 1 H, **33**), 8.06 (s, 1 H, **17**), 8.12 (dd, J_{HH} = 6.6, 2.0 Hz, 1 H, **35**), 8.16 (d, J_{HH} = 8.1 Hz, 1 H, **30**), 8.50 (d, J_{HH} = 1.5 Hz, 1 H, **26**)

^{13}C{1H} NMR (100 MHz, CD_3CN): δ ppm 30.8 (CH_2, **24**), 41.6 (CH_2, **15**), 55.2 (CH_3, **1**), 63.6 (CH_2, **11**), 72.2 (CH, **13**), 74.8 (C, **21**), 86.0 (CH, **16**), 86.7 (CH, **12**), 87.0 (C, **6**), 89.1 (C, **23**), 99.3 (C, **22**), 113.3 (CH, **4**), 125.7 (CH, **26**), 126.9 (CH, **10**), 127.3 (CH, **35**), 127.3 (CH, **30**), 127.6 (CH, **33**), 127.9 (CH, **8**), 128.0 (CH, **9**), 130.0 (CH, **3**), 133.1 (C, **27**), 133.3 (CH, **33**), 134.4 (CH, **34**), 135.0 (C, **32**), 135.5 (C, **5**), 138.7 (C, **31**), 143.3 (CH, **17**), 149.7 (C, **18**), 158.5 (C, **2**), 163.0 (C, **20**), 165.1 (C, **26**), 182.4 (C, **33**)

GC ESI (pos) ($C_{48}H_{39}N_3O_{10}$): Monoisotopic mass 817.26, observed *m/z* 840.5 $[M+Na]^+$, 499.3 $[M-(DMTO^-)]^+$

HR-ESI(pos) ($C_{48}H_{39}N_3O_{10}$) Monoisotopic mass 817.2635, observed *m/z* 840.2521 $[M+Na]^+$

UV-Vis (MeCN, 6.10 μM): λ_{max} (log ε) 237 (4.89), 256 (4.99), 273 shoulder (4.66), 298 shoulder (4.40), 333 shoulder (3.99)

Emission (MeCN, 6.10 μM): No fluorescence observed

$\boldsymbol{R_f}$ (silica, 10% MeOH in DCM): 0.37

CV (0.5 mM in 50 % DMSO/50 % 1.0 M NaCl 10 mM Tris pH 7.2, sweep rate 100 mVs^{-1}, potentials *vs* SCE, 1 mm Ø glassy carbon working electrode, Pt counter electrode): -0.479 / -0.524 V

Melting Point: 141.7 °C (dec.) (no lit. value)

8.58 – Synthesis of 5'-DMT-5-propargyl-(anthraquinone-2''-carboxamidyl)-dU-3'-amidite (XXVIII)

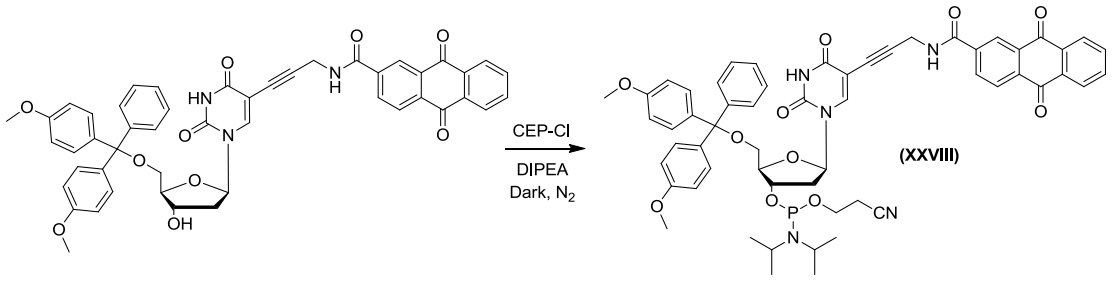

5'-DMT-5-propargyl-(anthraquinone-2''-carboxamidyl)-dU (22.5 mg, 27.5 mmol, 1.00 eq) was dissolved in DCM (1.5 mL) with molecular sieves and purged with nitrogen while shielded from light for 5 minutes. DIPEA (19 µL, 110.0 mmol, 4.00 eq) and CEP-Cl (20 µL, 82.5 mmol, 3.00 eq) were added and the reaction stirred at RT for 2 hours. The crude product was precipitated with hexanes (5 mL) and cooled (-18 °C) for 10 minutes, the hexanes were decanted off and the crude product washed with further hexanes (5 mL). The crude product was used immediately for DNA synthesis.

Full characterisation of the product was not achieved due to its instability. The product was used immediately for DNA synthesis.

$\boldsymbol{R_f}$ (silica, 10 % MeOH in DCM): 0.56

GC ESI (pos) ($C_{57}H_{56}N_5O_{11}P$): Monoisotopic mass 1017.37, observed *m/z* 1040.8 $[M+Na]^+$

8.59 – Synthesis of 5'-hydroxyl amide linked porphyrin monomer (XXIX)

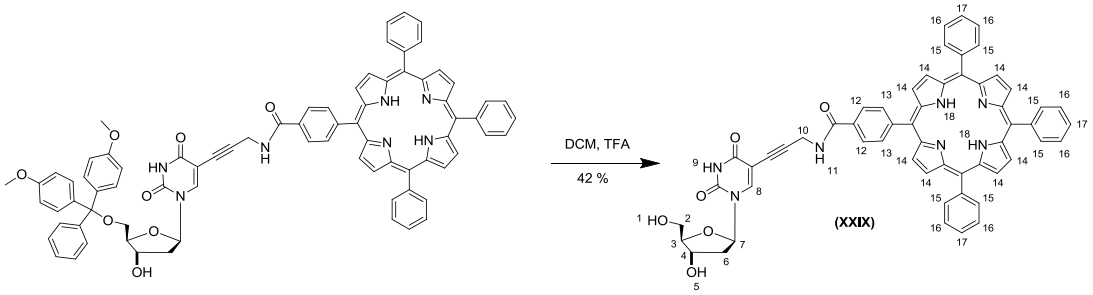

Amide linked porphyrin monomer (20 mg, 16.3 µmol, 1.00 eq) was dissolved in DCM (2 mL) and TFA (6.1 µL, 81.7 mmol, 5.00 eq) was added, the reaction mixture was agitated for 5 minutes before loading onto a column (silica neutralised with TEA, eluent – 5 % MeOH in DCM). The product was concentrated *in vacuo* before redissolving in DCM (10 mL), and washing with 1M HCl (15 mL), sat. Na_2CO_3 solution (15 mL) and brine (15 mL). The organic phase was dried over Na_2SO_4, filtered and concentrated *in vacuo*. The product was recolumned (silica, eluent – 5 % MeOH in DCM) and obtained as a purple solid 6.3 g (6.8 µmol, 42 %).

^{1}H NMR (400 MHz, CD_3CN): δ ppm -2.93 (br. s, 2 H, **18**), 2.09 - 2.23 (m, 2 H, **6**), 3.56 - 3.70 (m, 2 H, **2**), 3.83 (q, J_{HH} = 3.0 Hz, 1 H, **3**), 4.23 - 4.30 (m, 1 H, **4**), 4.47 (d, J_{HH} = 5.5 Hz, 2 H, **10**), 5.14 (t, J_{HH} = 5.0 Hz, 1 H, **1**), 5.25 (d, J_{HH} = 4.5 Hz, 1 H, **5**), 6.15 (t, J_{HH} = 6.5 Hz, 1 H, **7**), 7.79 - 7.87 (m, 9 H, **16** & **17**), 8.22 (d, J_{HH} = 7.5 Hz, 6 H, **15**), 8.25 (s, 1 H, **8**), 8.34 (s, 4 H, **12** & **13**), 8.84 (s, 8 H, **14**), 9.39 (t, J_{HH} = 5.5 Hz, 1 H, **11**), 11.61 - 11.74 (m, 1 H, **9**)

^{13}C{^{1}H} NMR (100 MHz, CD_3CN): δ ppm Insufficient material for conclusive ^{13}C{^{1}H} NMR analysis

GC ESI (pos) ($C_{57}H_{43}N_7O_6$): Monoisotopic mass 921.32, observed *m/z* 922.6 $[M+H]^+$, 944.8 $[M+Na]^+$

HR-ESI (pos) ($C_{57}H_{43}N_7O_6$) Monoisotopic mass 921.3271, observed *m/z* 922.3343 $[M+H]^+$

UV-Vis (2.67 % EtOH in DCM, 3.51 µM): λ_{max} (log ε) 290 (4.28), 414 (5.45), 511 (4.07), 546 (3.72), 589 (3.55), 644 (3.37)

Emission (2.67 % EtOH in DCM, 3.51 µM): λ_{ex} 414 nm, λ_{em} (rel int) 649 (1), 716 (0.36)

R_f (silica, 10 % MeOH in DCM): 0.22

CD (2.67 % EtOH in DCM, 3.51 µM): (–) 414 nm

8.60 – Synthesis of 5'-hydroxyl acetylene linked porphyrin monomer (XXX)

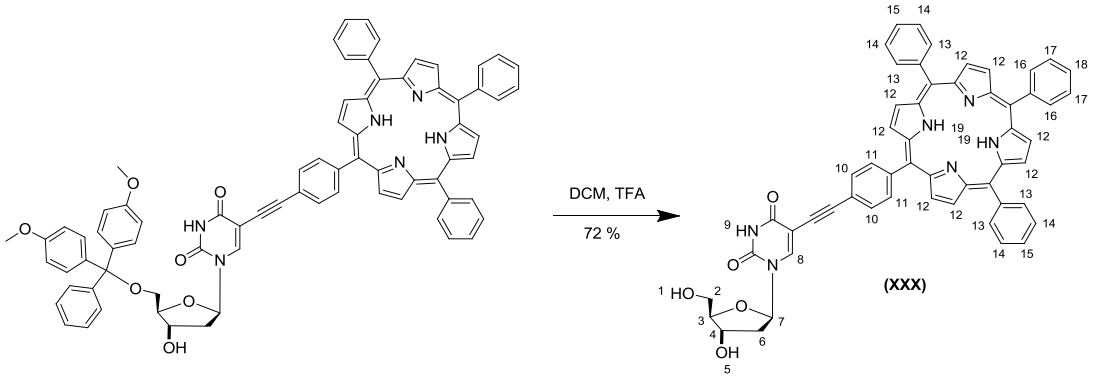

Acetylene linked porphyrin monomer (20 mg, 16.3 µmol, 1.00 eq) was dissolved in DCM (2 mL) and TFA (12.2 µL, 163 mmol, 10.00 eq) was added, the reaction mixture was agitated for 5 minutes before loading onto a column (silica neutralised with TEA, eluent – 5 % MeOH in DCM). The product was concentrated *in vacuo* before redissolving in DCM (10 mL), and washing with 1M HCl (15 mL), sat. Na_2CO_3 solution (15 mL) and brine (15 mL). The organic phase was dried over Na_2SO_4, filtered and concentrated *in vacuo*. The product was recolumned (silica, eluent – 5 % MeOH in DCM) and obtained as a purple solid 10.1 g (11.7 µmol, 72 %).

^{1}H NMR (400 MHz, CD_3CN): δ ppm -2.89 (s, 2 H, **5**), 2.14 - 2.35 (m, 3 H, **6**), 3.66 (ddd, J_{HH} = 11.5, 4.3, 3.8 Hz, 1 H, **2**), 3.74 (ddd, J_{HH} = 11.5, 4.5, 3.5 Hz, 1 H, **2**), 3.88 (q, J_{HH} = 3.3 Hz, 1 H, **3**), 4.34 (ddd, J_{HH} = 9.5, 8.0, 4.0 Hz, 2 H, **4**), 5.27 (t, J_{HH} = 5.0 Hz, 1 H, **1**), 5.31 (d, J_{HH} = 4.5 Hz, 1 H, **5**), 6.21 (t, J_{HH} = 6.3 Hz, 1 H, **7**), 7.74 - 7.89 (m, 9 H, **14**, **15**, **17** & **18**), 7.91 (d, J_{HH} = 8.5 Hz, 2 H, **11**), 8.15 - 8.23 (m, 4 H, **10** & **16**), 8.25 (d, J_{HH} = 8.5 Hz, 2 H, **13**), 8.56 (s, 1 H, **8**), 8.73 - 8.93 (m, 8 H, **12**), 11.70 - 11.85 (m, 1 H, **9**)

^{13}C{1H} NMR (100 MHz, CD_3CN): δ ppm Insufficient material for conclusive ^{13}C{1H} NMR analysis

GC ESI (pos) ($C_{55}H_{40}N_6O_5$): Monoisotopic mass 864.31, observed *m/z* 865.6 $[M+H]^+$

HR-ESI(pos) ($C_{55}H_{40}N_6O_5$) Monoisotopic mass 864.3060, observed *m/z* 865.3128 $[M+H]^+$

UV-Vis (2.67 % EtOH in DCM, 3.01 µM): λ_{max} (log ε) 308 (4.35), 416 (5.44), 513 (4.03), 551 (3.91), 593 (3.64), 645 (3.34)

Emission (2.67 % EtOH in DCM, 3.01 µM): λ_{ex} 416 nm, λ_{em} (rel int): 650 (1), 716 (0.31)

R_f (silica, 10 % MeOH in DCM): 0.28

CD (2.67 % EtOH in DCM, 3.51 µM): (–) 416 nm

8.61 – Testing the stability of *N*-propynyl-*N'*-phenethyl-napthalene diimide to DNA deprotection conditions

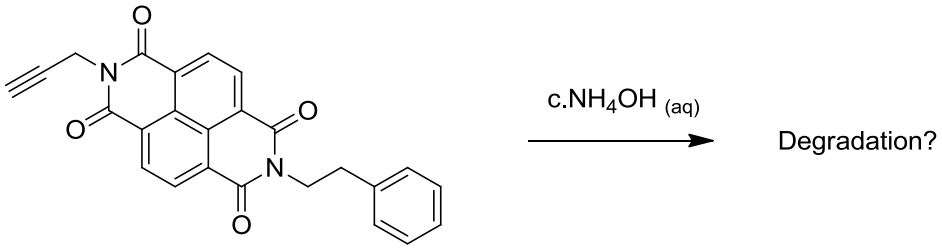

N-propynyl-*N'*-phenethyl-napthalene diimide (4.7 mg, 11.5 µmole, 1.00 eq) was suspended in concentrated aqueous ammonia (35%, SG = 0.88, 2.5 mL) and shaken at RT for 18 hours. The sample was partioned with $CHCl_3$ (5 mL), separated and concentrated *in vacuo*. The starting material, 4.5 mg (96%), was recovered unchanged.

^{1}H NMR (400 MHz, $CDCl_3$); δ ppm 2.16 (t, J_{HH} = 2.5 Hz, 1 H, **1**), 2.97 (t, J_{HH} = 8.3 Hz, 2 H, **13**), 4.36 (t, J_{HH} = 8.3 Hz, 2 H, **12**), 4.91 (d, J_{HH} = 2.5 Hz, 2 H, **3**), 7.15 (t, J_{HH} = 7.0 Hz, 1 H, **17**), 7.20 - 7.31 (m, 2 H, **16**), 7.24 (d, J_{HH} = 11.5 Hz, 2 H, **15**), 8.70 (d, J_{HH} = 7.5 Hz, 2 H, **7**), 8.74 (d, J_{HH} = 7.5 Hz, 2 H, **8**)
^{13}C{^{1}H} NMR (100 MHz, $CDCl_3$); δ ppm 35.0 (CH_2, **13**), 43.1 (CH_2, **12**), 72.1 (CH, **1**), 78.7 (C, **2**), 127.2 (CH, **17**), 127.5 (C, **10**), 127.6 (C, **6** & **9**), 127.8 (C, **5**), 129.4 (CH, **15**), 129.8 (CH, **16**), 131.9 (CH, **8**), 132.2 (CH, **7**), 139.1 (C, **14**), 162.9 (C, **11**), 163.4 (C, **4**)
GC-ESI (pos) ($C_{25}H_{16}N_2O_4$): Monoisotopic mass 408.4, observed *m/z* 426.3 $[M+NH_4]^+$
R_f (silica, 5 % MeOH in DCM); 0.60
Melting Point: >250 °C (no lit. value)

8.62 – Synthesis of acetylene linked porphyrin DNA strands (3) and (4)

Strand Name	Sequence	Scale (µmoles)
3	3' TAT TA**P**^{1} A**P**^{1}A **P**^{1}A**P**^{1} A**P**^{1}A **P**^{1}CG CTG CTA CCG **G*** 5'	1
4	3' AGC GA**P**^{1} A**P**^{1}A **P**^{1}A**P**^{1} A**P**^{1}A **P**^{1}AA TAC CGT ATG **G*** 5'	1

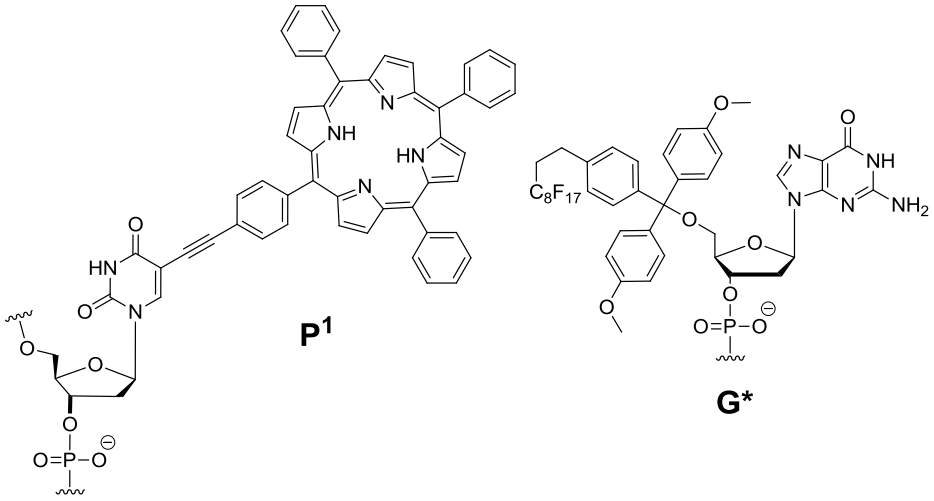

Crude acetylene linked porphyrin phosphoramidite (**VII**) (199.1 mg, ~ 98 µmoles) was dissolved in DCM:MeCN (1:1, 3.90 mL, 25.0 mM), porphyrin monomer couplings were achieved by passing the amidite solution (192 µL, 4.8 eq.) through the CGP support over a period of 5 minutes. DNA strands were cleaved from the resin and deprotected with ammonia solution (35 % in H_2O, S.G. = 0.88, 1 mL) in the presence of a nitromethane scavenger (12 µL, 8.0 eq per phosphate) at 30 °C for 18 hours. Strands were purified by FluoroPak II columns before concentrating *in vacuo*, desalting with NAP-5 columns and concentrated *in vacuo*.

3

Yield (nmoles): 69

HPLC conditions: 0.0 min 100 % buffer, 3.0 min 100 % buffer, 25.0 min 100 % THF, 35.0 min 100 % buffer. Buffer – 100 mM TEAA, 1 % MeCN in H_2O. Column – Merck 250 X 4 mm C18 LiChroCART at 55 °C.

HPLC retention time (mins): 16.52

Calculated ε_{260} (mol^{-1} dm^3 cm^{-1}): 277,500

UV-Vis (100 mM sodium phosphate, 100 NaCl, 1 mM Na_2EDTA, pH 7.0, 1.00 µM): λ_{max} (log ε) 261 (5.44), 418 (5.83), 520 (4.74), 557 (4.52), 594 (4.35), 651 (4.41)

Emission (100 mM sodium phosphate, 100 NaCl, 1 mM Na_2EDTA, pH 7.0, 1.00 µM): λ_{ex} 420 nm, λ_{em} (rel int) 656 (1.0), 720 (0.32)

CD (100 mM sodium phosphate, 100 NaCl, 1 mM Na_2EDTA, pH 7.0, 3.97 µM): λ_{abs} (Molar $\Delta\varepsilon$) (-)250 (34.1), (+)276 (36.4)

CD (100 mM sodium phosphate, 100 NaCl, 1 mM Na_2EDTA, pH 7.0, 1.61 µM): λ_{abs} (Molar $\Delta\varepsilon$) (+)407 (5.6), (-)425 (17.0), (+)440 (18.5)

GC ESI (neg): Unobservable by mass spectrometry

4

Yield (nmoles): 81

HPLC conditions: 0.0 min 100 % buffer, 3.0 min 100 % buffer, 25.0 min 100 % THF, 35.0 min 100 % buffer. Buffer – 100 mM TEAA, 1 % MeCN in H_2O. Column – Merck 250 X 4 mm C18 LiChroCART at 55 °C.

HPLC retention time (mins): 16.35

Calculated ε_{260} (mol^{-1} dm^3 cm^{-1}): 296,300

UV-Vis (100 mM sodium phosphate, 100 NaCl, 1 mM Na_2EDTA, pH 7.0, 1.48 µM): λ_{max} (log ε) 258 (5.47), 418 (5.78), 520 (4.68), 556 (4.45), 594 (4.29), 651 (4.43)

Emission (100 mM sodium phosphate, 100 NaCl, 1 mM Na_2EDTA, pH 7.0, 1.48 µM): λ_{ex} 420 nm, λ_{em} (rel int): 656 (1.0), 720 (0.32)

CD (100 mM sodium phosphate, 100 NaCl, 1 mM Na_2EDTA, pH 7.0, 3.94 µM): λ_{abs} (Molar $\Delta\varepsilon$) (-)251 (45.4), (+)278 (33.9)

CD (100 mM sodium phosphate, 100 NaCl, 1 mM Na_2EDTA, pH 7.0, 1.82 µM): λ_{abs} (Molar $\Delta\varepsilon$) (+)406 (5.8), (-)425 (17.6), (+)439 (5.5)

GC ESI (neg): Unobservable by mass spectrometry

8.63 – Synthesis of amide linked porphyrin DNA strands (5) and (6)

Strand Name	Sequence	Scale (μmoles)
5	3' TAT TA**P²** A**P²**A **P²**A**P²** A**P²**A **P²**CG CTG CTA CCG **G*** 5'	1
6	3' AGC GA**P²** A**P²**A **P²**A**P²** A**P²**A **P²**AA TAC CGT ATG **G*** 5'	1

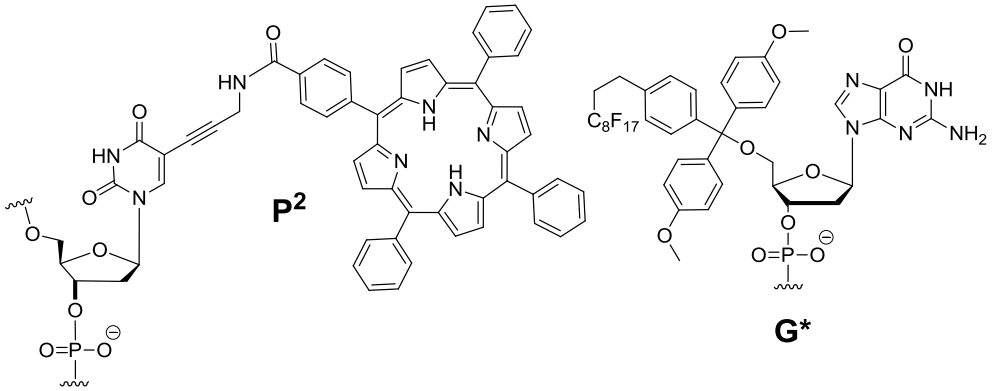

Crude amide linked porphyrin phosphoramidite **(XIV)** (120.5 mg, ~ 85 μmoles) was dissolved in DCM:MeCN (1:1, 3.90 mL, 21.2 mM), porphyrin monomer couplings were achieved by passing the amidite solution (192 μL, 4.17 eq.) through the CGP support over a period of 5 minutes. DNA strands were cleaved from the resin and deprotected with ammonia solution (35 % in H_2O, S.G. = 0.88, 1 mL) in the presence of a nitromethane scavenger (12 μL, 8.0 eq per phosphate) at 30 °C for 18 hours. Strands were purified by FluoroPak II columns before concentrating *in vacuo*, desalting with NAP-5 columns and concentrated *in vacuo*.

5

Yield (nmoles): 218

HPLC conditions: 0.0 min 100 % buffer, 3.0 min 100 % buffer, 25.0 min 100 % THF, 35.0 min 100 % buffer. Buffer – 100 mM TEAA, 1 % MeCN in H_2O. Column – Merck 250 X 4 mm C18 LiChroCART at 55 °C.

HPLC retention time (mins): 15.47

Calculated ε_{260} (mol^{-1} dm^3 cm^{-1}): 277,500

UV-Vis (100 mM sodium phosphate, 100 NaCl, 1 mM Na_2EDTA, pH 7.0, 1.05 μM): λ_{max} (log ε) 260 (5.44), 419 (5.80), 520 (4.77), 555 (4.49), 593 (4.35), 649 (4.27)

Emission (100 mM sodium phosphate, 100 NaCl, 1 mM Na_2EDTA, pH 7.0, 1.05 μM): λ_{ex} 419 nm, λ_{em} (rel int) 654 (1.0), 720 (0.34)

CD (100 mM sodium phosphate, 100 NaCl, 1 mM Na_2EDTA, pH 7.0, 5.20 μM): λ_{abs} (Molar $\Delta\varepsilon$) (-)253 (43.7), (+)274 (36.9)

CD (100 mM sodium phosphate, 100 NaCl, 1 mM Na_2EDTA, pH 7.0, 1.83 µM): λ_{abs} (Molar $\Delta\varepsilon$) (+)423 (12.9), (-)438 (19.7)

GC ESI (neg): Unobservable by mass spectrometry

6

Yield (nmoles): 138

HPLC conditions: 0.0 min 100 % buffer, 3.0 min 100 % buffer, 25.0 min 100 % THF, 35.0 min 100 % buffer. Buffer – 100 mM TEAA, 1 % MeCN in H_2O. Column – Merck 250 X 4 mm C18 LiChroCART at 55 °C.

HPLC retention time (mins): 16.52

Calculated ε_{260} (mol^{-1} dm^3 cm^{-1}): 296,300

UV-Vis (100 mM sodium phosphate, 100 NaCl, 1 mM Na_2EDTA, pH 7.0, 1.32 µM): λ_{max} (log ε) 258 (5.47), 418 (5.85), 520 (4.80), 555 (4.52), 593 (4.38), 649 (4.36)

Emission (100 mM sodium phosphate, 100 NaCl, 1 mM Na_2EDTA, pH 7.0, 1.32 µM): λ_{ex} 420 nm, λ_{em} (rel int): 654 (1.0), 720 (0.34)

CD (100 mM sodium phosphate, 100 NaCl, 1 mM Na_2EDTA, pH 7.0, 4.50 µM): λ_{abs} (Molar $\Delta\varepsilon$) (-)253 (49.3), (+)276 (37.6)

CD (100 mM sodium phosphate, 100 NaCl, 1 mM Na_2EDTA, pH 7.0, 1.31 µM): λ_{abs} (Molar $\Delta\varepsilon$) (+)415 (24.3), (-)439 (14.7)

GC ESI (neg): Unobservable by mass spectrometry

8.64 – Synthesis of unmodified DNA strands (7) and (8)

Strand Name	Sequence	Scale (μmoles)
7	3' TAT TAT ATA TAT ATA TCG CTG CTA CCG G 5'	1
8	3' AGC GAT ATA TAT ATA TAA TAC CGT ATG G 5'	1

DNA strands were cleaved from the resin and deprotected with ammonia solution (35% in H_2O, S.G. = 0.88, 1 mL) in the presence of a nitromethane scavenger (12 μL, 8.0 eq per phosphate) at 30 °C for 18 hours. Strands were purified by FluoroPak II columns before concentrating *in vacuo*, desalting with NAP-5 columns and concentrated *in vacuo*.

7

Yield (nmoles): 591

HPLC conditions: 0.0 min 100% buffer, 3.0 min 100% buffer, 25.0 min 100% MeOH, 30.0 min 100% MeOH, 37.0 min 100% buffer, 40 min 100% buffer. Buffer – 100 mM TEAA, 1% MeCN in H_2O. Column – Merck 250 X 4 mm C18 LiChroCART at 55 °C.

HPLC retention time (mins): 12.09

Calculated ε_{260} (mol^{-1} dm^3 cm^{-1}): 277,500

UV-Vis (100 mM sodium phosphate, 100 NaCl, 1 mM Na_2EDTA, pH 7.0, 1.02 μM): λ_{max} (log ε) 260 (5.44)

Emission (100 mM sodium phosphate, 100 NaCl, 1 mM Na_2EDTA, pH 7.0, 1.02 μM): λ_{ex} 260 nm, No fluorescence observed

CD (100 mM sodium phosphate, 100 NaCl, 1 mM Na_2EDTA, pH 7.0, 4.50 μM): λ_{abs} (Molar $\Delta\varepsilon$) (-)247 (61.3), (+)274 (69.0)

GC ESI (neg): Calculated mass: 8552, observed *m/z*: 8555 $[M\text{-}H^+]^-$, 8577 $[M\text{-}2H^+\text{+}Na^+]^-$, 8600 $[M\text{-}3H^+\text{+}2Na^+]^-$, 8623 $[M\text{-}4H^+\text{+}3Na^+]^-$

8

Yield (nmoles): 486

HPLC conditions: 0.0 min 100% buffer, 3.0 min 100% buffer, 25.0 min 100% MeOH, 30.0 min 100% MeOH, 37.0 min 100% buffer, 40 min 100% buffer. Buffer – 100 mM TEAA, 1% MeCN in H_2O. Column – Merck 250 X 4 mm C18 LiChroCART at 55 °C.

HPLC retention time (mins): 11.97

Calculated ε_{260} (mol^{-1} dm^3 cm^{-1}): 296,300

UV-Vis (100 mM sodium phosphate, 100 NaCl, 1 mM Na_2EDTA, pH 7.0, 1.21 μM): λ_{max} (log ε) 258 (5.47)

Emission (100 mM sodium phosphate, 100 NaCl, 1 mM Na_2EDTA, pH 7.0, 1.21 µM): λ_{ex} 258 nm, λ_{em} (rel int): No fluorescence observed

CD (100 mM sodium phosphate, 100 NaCl, 1 mM Na_2EDTA, pH 7.0, 3.80 µM): λ_{abs} (Molar $\Delta\varepsilon$) (-)249 (31.1), (+)272 (33.4)

GC ESI (neg): Calculated mass: 8634, observed *m/z*: 8637 $[M\text{-}H^+]^-$, 8659 $[M\text{-}2H^+\text{+}Na^+]^-$, 8681 $[M\text{-}3H^+\text{+}2Na^+]^-$

8.65 – General synthetic procedure for metallation of porphyrin DNA

Single stranded porphyrin DNA (1.0 eq), was heated with a $Co(OAc)_2{\cdot}4H_2O$, $Cu(OAc)_2{\cdot}H_2O$ or $Zn(OAc)_2{\cdot}2H_2O$ (100 mM, 200 eq. per porphyrin) to 85 °C for 5 minutes, the DNA precipitated. EDTA solution (0.5 M, pH 8.1, 100 eq. per Co ion) was added to redissolve the DNA and sequester excess metal ions. An equal volume of NaCl solution (100 mg mL^{-1} NaCl in H_2O) was added to the metallated porphyrin DNA sample prior to loading onto a conditioned GlenPak column, excess EDTA and cobalt salts were eluted with 'salt wash' (2 mL, 5 % MeCN, 100 mg mL^{-1} NaCl in H_2O), metallated DNA was eluted with MeCN:H_2O (1:1, 4 mL), concentrated *in vacuo* and desalted with a NAP-5 column.

8.66 – Cobalt metallated porphyrin DNA (3Co)

Single stranded porphyrin DNA (**3**, 5.0 nmoles) was cobalt metallated as per the general method, the product was obtained as a purple solid, 5.0 nmoles (100 %).

UV-Vis (H_2O, 5.27 µM): λ_{max} (log ε) 259 (5.22), 422 (5.44), 519 (4.59), 554 (4.41), 593 (4.21), 649 (4.05)
Emission (H_2O, 5.27 µM): No fluorescence observed
CD (100 mM sodium phosphate, 100 mM NaCl, 1 mM Na_2EDTA pH 7.0, 3.62 µM): λ_{abs} (Molar $\Delta\varepsilon$) (-)249 (16.2), (+)275 (31.4)
CD (100 mM sodium phosphate, 100 mM NaCl, 1 mM Na_2EDTA pH 7.0, 2.77 µM): λ_{abs} (Molar $\Delta\varepsilon$) (+)398 (12.0), (-)423 (0.83), (+)436 (9.7)

8.67 – Cobalt metallated porphyrin DNA (5Co)

Single stranded porphyrin DNA (**5**, 5.0 nmoles) was cobalt metallated as per the general method, the product was obtained as a purple solid, 4.5 nmoles (90 %).

UV-Vis (H_2O, 4.53 µM): λ_{max} (log ε) 259 (5.17), 422 (5.44), 519 (4.58), 554 (4.39), 593 (4.21), 649 (4.02)
Emission (H_2O, 4.53 µM): No fluorescence observed
CD (100 mM sodium phosphate, 100 mM NaCl, 1 mM Na_2EDTA pH 7.0, 3.24 µM): λ_{abs} (Molar $\Delta\varepsilon$) (-)250 (20.0), (+)272 (39.8)
CD (100 mM sodium phosphate, 100 mM NaCl, 1 mM Na_2EDTA pH 7.0, 2.19 µM): λ_{abs} (Molar $\Delta\varepsilon$) (+)398 (1.87), (-)420 (12.5), (+)434 (0.4)

8.68 – Copper metallated porphyrin DNA (3Cu)

Single stranded porphyrin DNA (**3**, 5.0 nmoles) was copper metallated as per the general method, the product was obtained as a purple solid, 3.6 nmoles (72 %).

UV-Vis (H_2O, 3.64 µM): λ_{max} (log ε) 260 (4.92), 414 (5.34), 525 (4.44), 544 (4.17), 590 (3.63), 648 (3.48)
Emission (H_2O, 1.34 µM): λ_{ex} 415 nm, λ_{em} (rel int) 652 (1.00), 719 (0.30)
CD (100 mM sodium phosphate, 100 mM NaCl, 1 mM Na_2EDTA pH 7.0, 3.22 µM): λ_{abs} (Molar $\Delta\varepsilon$) (-)249 (10.7), (+)276 (21.3)
CD (100 mM sodium phosphate, 100 mM NaCl, 1 mM Na_2EDTA pH 7.0, 1.92 µM): λ_{abs} (Molar $\Delta\varepsilon$) (+)404 (16.8), (-)430 (0.5)

8.69 – Copper metallated porphyrin DNA (5Cu)

Single stranded porphyrin DNA (**5**, 5.0 nmoles) was copper metallated as per the general method, the product was obtained as a purple solid, 2.5 nmoles (50 %).

UV-Vis (H_2O, 2.48 µM): λ_{max} (log ε) 260 (5.06), 414 (5.58), 525 (4.27), 544 (4.42), 590 (3.87), 648 (3.64)
Emission (H_2O, 0.832 µM): λ_{ex} 413 nm, λ_{em} (rel int) 649 (1.00), 717 (0.31)
CD (100 mM sodium phosphate, 100 mM NaCl, 1 mM Na_2EDTA pH 7.0, 3.48 µM): λ_{abs} (Molar $\Delta\varepsilon$) (-)251 (8.5), (+)271 (36.4)
CD (100 mM sodium phosphate, 100 mM NaCl, 1 mM Na_2EDTA pH 7.0, 2.31 µM): λ_{abs} (Molar $\Delta\varepsilon$) (+)398 (12.3), (-)418 (4.5)

8.70 – Zinc metallated porphyrin DNA (3Zn)

Single stranded porphyrin DNA (**3**, 5.0 nmoles) was zinc metallated as per the general method, the product was obtained as a purple solid, 2.1 nmoles (42 %).

UV-Vis (H_2O, 2.09 µM): λ_{max} (log ε) 257 (5.29), 427 (5.31), 520 (4.66), 558 (4.59), 597 (4.44), 649 (4.25)
Emission (H_2O, 2.09 µM): λ_{ex} 427 nm, λ_{em} (rel int) 653 (1.00), 718 (0.31)
CD (100 mM sodium phosphate, 100 mM NaCl, 1 mM Na_2EDTA pH 7.0, 4.52 µM): λ_{abs} (Molar $\Delta\varepsilon$) (-)249 (19.1), (+)276 (30.5)

CD (100 mM sodium phosphate, 100 mM NaCl, 1 mM Na_2EDTA pH 7.0, 1.87 µM): λ_{abs} (Molar $\Delta\varepsilon$) (-)402 (1.2), (+)430 (54.1), (-)444 (25.5)

8.71 – Zinc metallated porphyrin DNA (5Zn)

Single stranded porphyrin DNA (**5**, 5.0 nmoles) was zinc metallated as per the general method, the product was obtained as a purple solid, 2.3 nmoles (46 %).

UV-Vis (H_2O, 2.32 µM): λ_{max} (log ε) 258 (5.27), 427 (5.49), 519 (4.67), 557 (4.59), 596 (4.41), 647 (4.19)
Emission (H_2O, 2.32 µM): λ_{ex} 427 nm, λ_{em} (rel int) 653 (1.00), 718 (0.33)
CD (100 mM sodium phosphate, 100 mM NaCl, 1 mM Na_2EDTA pH 7.0, 4.15 µM): λ_{abs} (Molar $\Delta\varepsilon$) (-)254 (9.8), (+)275 (36.8)
CD (100 mM sodium phosphate, 100 mM NaCl, 1 mM Na_2EDTA pH 7.0, 1.13 µM): λ_{abs} (Molar $\Delta\varepsilon$) (+)419 (16.6), (-)441 (12.9)

8.72 – Analysis of duplex DNA systems

Duplex	Absorbance (log *A*)[a]	Fluorescence (Rel. Em.)[a]	T_m (°C)	CD (nm)[a]
3•4	259 (5.65), 418 (6.05), 519 (4.97), 555 (4.70), 592 (4.45), 648 (4.36)	655 (1.00), 720 (0.30)	50.8[a,d]	-251, +277, +406, -425, +442
5•6	259 (5.65), 416 (6.12), 519 (5.06), 555 (4.75), 592 (4.57), 648 (4.44)	655 (1.00), 720 (0.31)	45.9[b,c]	-254, +275, +420, -438
3•6	259 (5.65), 418 (6.03), 519 (4.96), 555 (4.68), 592 (4.46), 648 (4.33)	655 (1.00), 720 (0.32)	51.3[a,d]	-253, +277, +411, -436
7•8	259 (5.65)	N/A	47.2[a,c], 41.2[b,c]	-250, +274
3•8	259 (5.65), 418 (5.76), 519 (4.66), 555 (4.38), 592 (4.18), 648 (4.11)	655 (1.00), 720 (0.29)	53.3[a,d]	-249, +273, +406, -424, +439
4•7	259 (5.65), 418 (5.73), 519 (4.67), 555 (4.41), 592 (4.18), 648 (4.09)	655 (1.00), 720 (0.30)	51.4[a,d]	-250, +274, +405, -425, +440
5•8	259 (5.65), 417 (5.90), 519 (4.87), 555 (4.57), 592 (4.38), 648 (4.38)	655 (1.00), 720 (0.32)	51.8[a,d], 48.8[b,d], 46.2[b,c]	-251, +273, +422, -437
6•7	259 (5.65), 416 (5.89), 519 (4.84), 555 (4.54), 592 (4.36), 648 (4.21)	655 (1.00), 720 (0.32)	52.1[a,d], 50.1[b,d], 47.3[b,c]	-250, +275, +420, -437
3Zn•4	259 (5.65), 420 (6.00), 521 (4.97), 558 (4.98)	N/A	N/A	-249, +275, +411, -425, +433, -444
3Cu•4	259 (5.65), 419 (5.94), 520 (4.97), 554 (4.93)	N/A	N/A	-249, +275, +410, -422, +433
3Co•4	259 (5.65), 420 (6.89), 521 (4.99), 556 (4.94)	N/A	N/A	-249, +274, +405, -423, +436
5Zn•6	259 (5.65), 417 (6.04), 520 (5.12), 557 (5.04)	N/A	N/A	-253, +274, +421, -438
5Cu•6	259 (5.65), 417 (6.00), 520 (5.05), 554 (4.95)	N/A	N/A	-252, +272, +406, -437
5Co•6	259 (5.65), 419 (6.05), 520 (5.24), 556 (5.20)	N/A	N/A	-252, +275, +421, -437
3Zn•6	259 (5.65), 418 (6.02), 522 (5.00), 558 (4.94)	N/A	N/A	-252, +275, +424, -441
3Cu•6	259 (5.65), 418 (6.05), 520 (5.03), 554 (4.92)	N/A	N/A	-253, +275, +409, -436
3Co•6	259 (5.65), 418 (5.97), 520 (5.00), 556 (4.87)	N/A	N/A	-252, +275, +420, -437

Table 19. Photospectrometric data of synthesised duplexes

[a] = 100 mM sodium phosphate, 100 mM NaCl, 1 mM Na_2EDTA, pH 7.0 [b] = 9:1 100 mM sodium phosphate, 100 mM NaCl, 1 mM Na_2EDTA, pH 7.0:DMF [c] = Fluorescence melt [d] = UV melt

8.73 – Variable temperature UV-vis of 3•4, 5•6 and 3•6

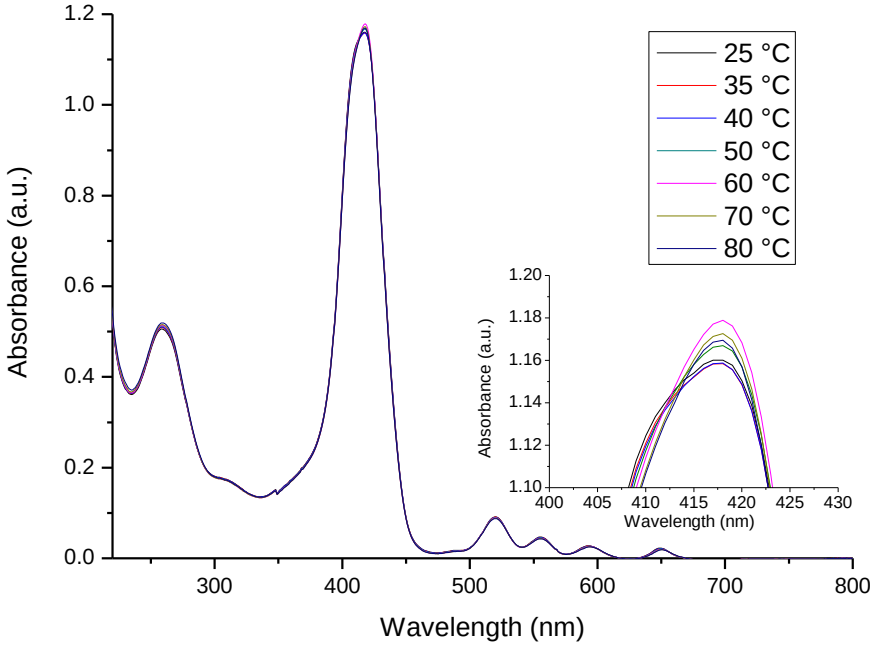

Figure 120. Variable temperature UV-vis of **3•4**

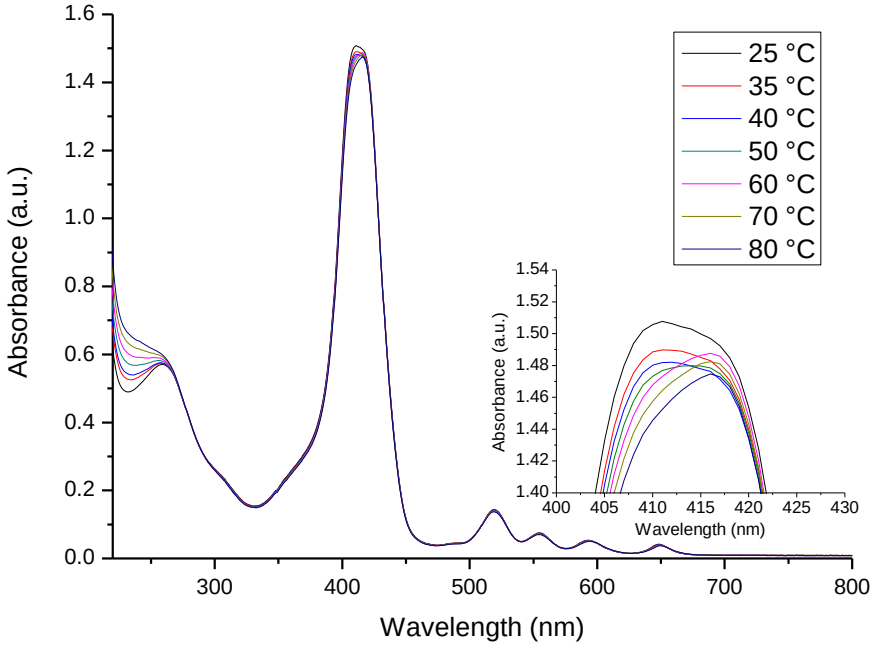

Figure 121. Variable temperature UV-vis of **5•6**

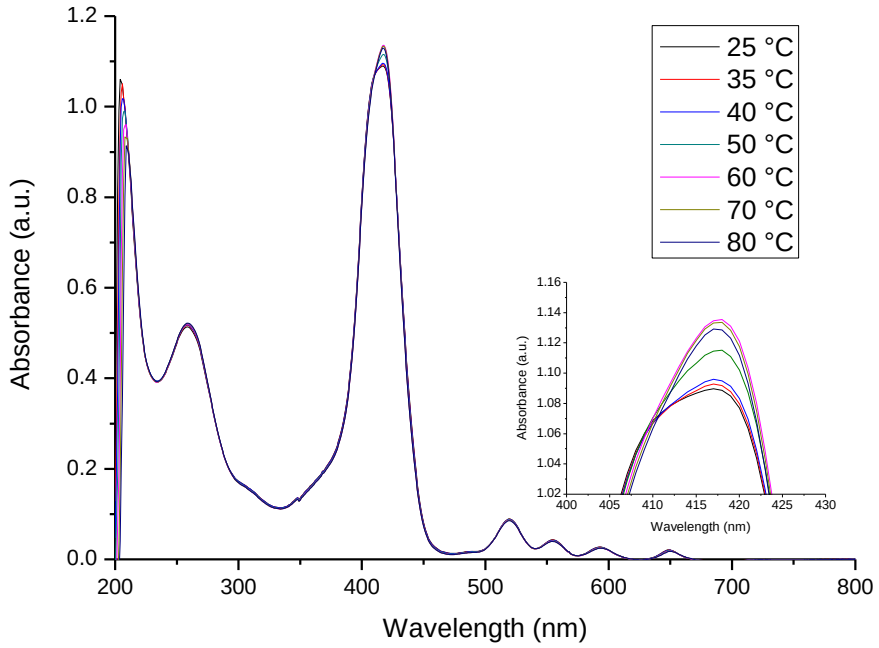

Figure 122. Variable temperature UV-vis of **5•6**

8.74 – Variable temperature fluorescence of 3•4, 5•6 and 3•6

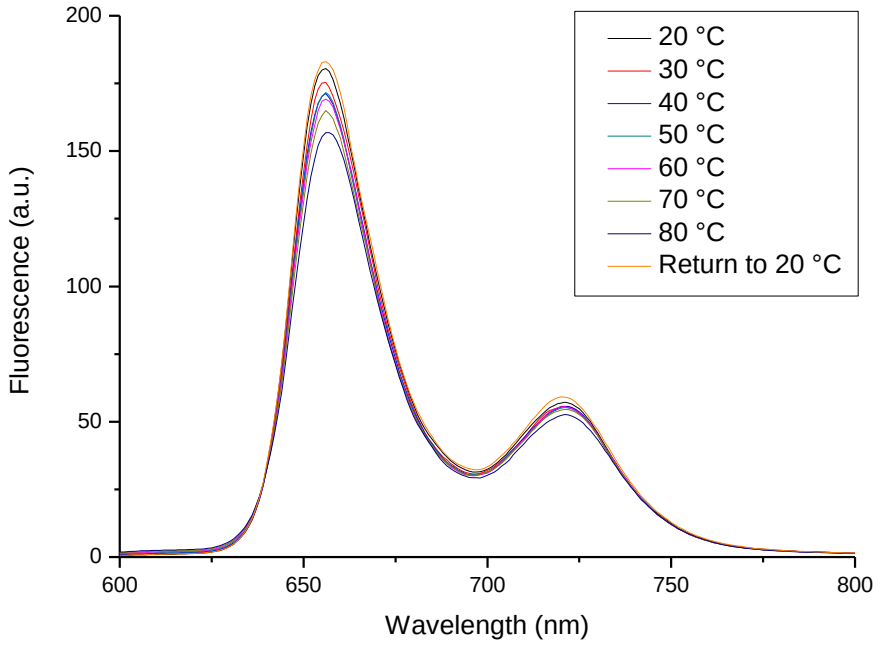

Figure 123. Variable temperature fluorescence of **3•4**

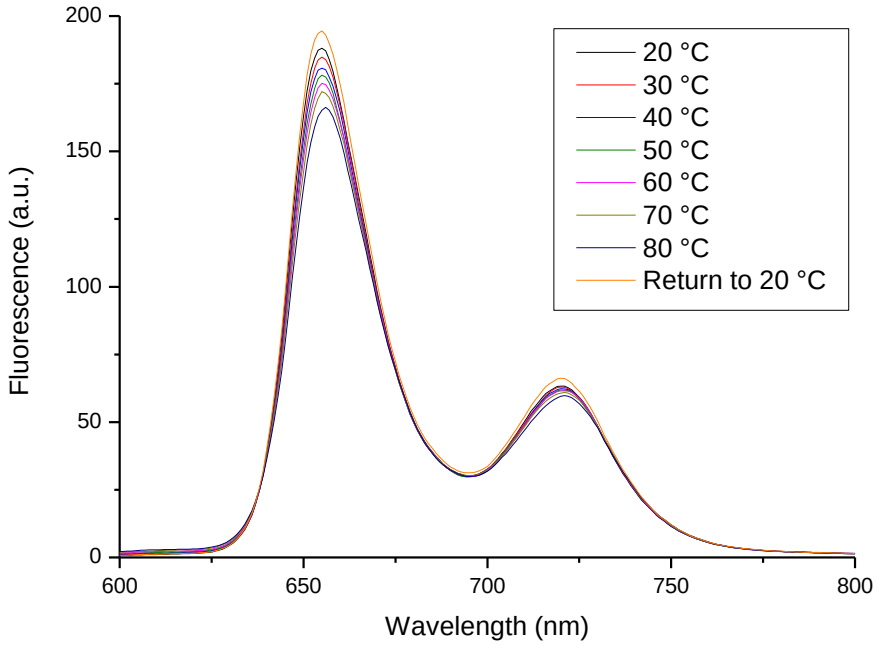

Figure 124. Variable temperature fluorescence of **5•6**

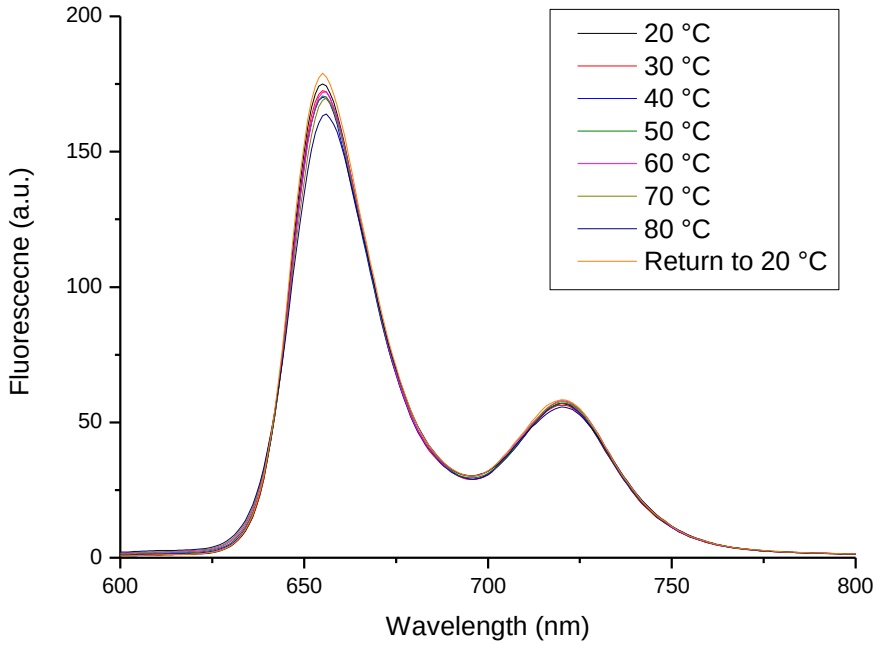

Figure 125. Variable temperature fluorescence of **3•6**

8.75 – Serial Dilution of 5•6

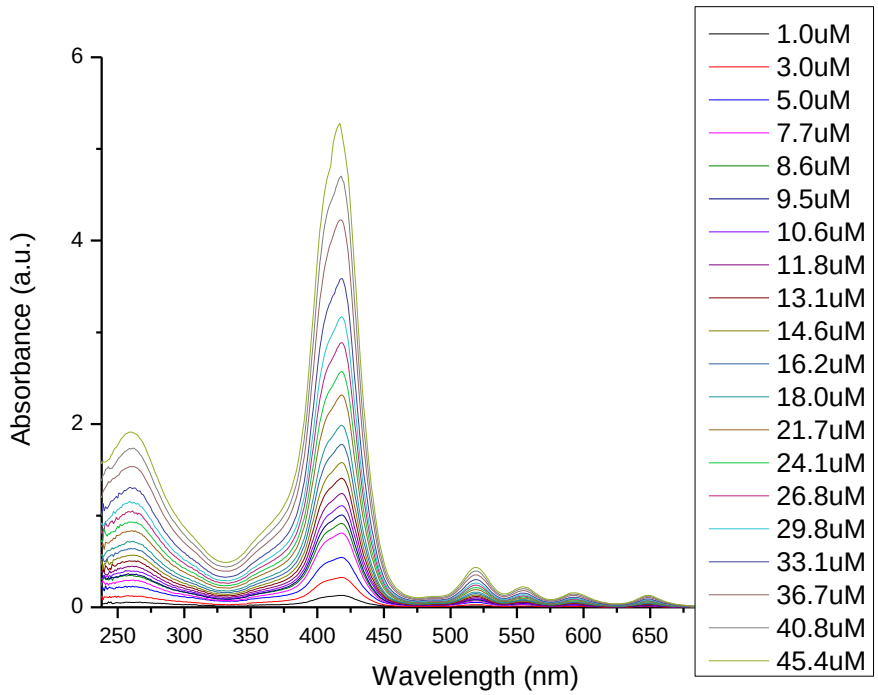

Figure 126. UV-vis of a serial dilution of **5•6**

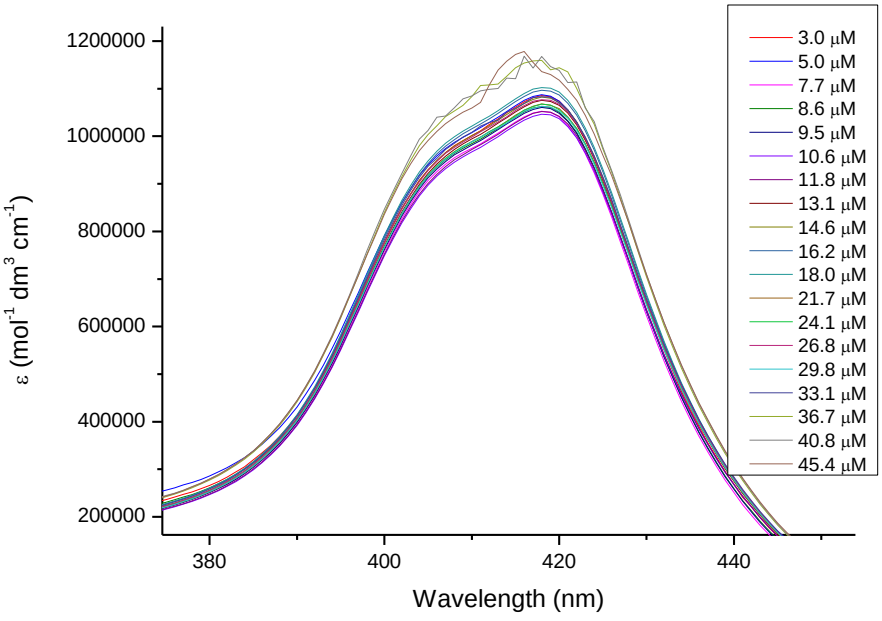

Figure 127. UV-vis of a serial dilution of **5•6**

8.76 – Testing coupling times of ferrocene monomer (XVI)

Strand Name	Sequence	Coupling time (min)	Scale (µmoles)
10a	3' ACT TAG **F**GA ACC GAT 5'	5	1
10b	3' ACT TAG **F**GA ACC GAT 5'	10	1

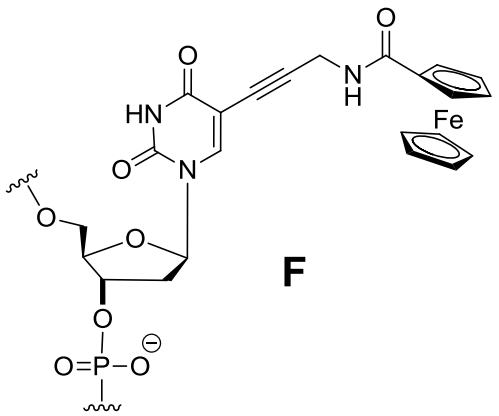

Crude ferrocene phosphoramidite **(XVI)** (190.5 mg, ~ 120 µmoles) was dissolved in DCM:MeCN (1:1, 1.20 mL, 100 mM), the ferrocene monomer was coupled using two different methods, for **10a**; amidite coupling (116 µL, 11.20 eq.) over 5 minutes, for **10b**; amidite coupling (116 µL, 11.20 eq.) over 5 minutes, an acetonitrile wash (800 µL) and a further amidite coupling (116 µL, 11.20 eq.) over 5 minutes. Protecting groups were cleaved using a diethylamine wash (20 % in MeCN, 640 µL) over 20 minutes, DNA strands were cleaved from the resin with ammonia solution (35 % in H_2O, S.G. = 0.88, 1 mL) at RT for 16 hours. Strands were purified by GlenPak columns before concentrating *in vacuo*.

10a

Yield (nmoles): 347

Calculated ε_{260} (mol^{-1} dm^3 cm^{-1}): 151,000

UV-Vis (100 mM sodium phosphate, 100 NaCl, 1 mM Na_2EDTA, pH 7.0, 0.65 µM): λ_{max} (log ε) 260 (5.18)

Emission (100 mM sodium phosphate, 100 NaCl, 1 mM Na_2EDTA, pH 7.0, 0.65 µM): No fluorescence observed

GC ESI (neg): Calculated mass: 4807, observed *m/z*: 4828.5 $[M-2H+Na]^-$, 4850.0 $[M-3H+2Na]^-$

10b

Yield (nmoles): 446

Calculated ε_{260} (mol^{-1} dm^3 cm^{-1}): 151,000

UV-Vis (100 mM sodium phosphate, 100 NaCl, 1 mM Na_2EDTA, pH 7.0, 0.68 µM): λ_{max} (log ε) 260 (5.18)

Emission (100 mM sodium phosphate, 100 NaCl, 1 mM Na_2EDTA, pH 7.0, 0.68 µM): No fluorescence observed

GC ESI (neg): Calculated mass: 4807, observed *m/z*: 4828.0 $[M-2H+Na]^-$, 4850.0 $[M-3H+2Na]^-$

.

8.77 – Synthesis of thiol/porphyrin/ferrocene modified DNA (11) and (12)

Strand Name	Sequence	Scale (μmoles)
11	3' (**Thiol Heg**)$_3$ **P^1**A**P^1** A**P^1**A **P^1**A**P^1** A**F**C GCT AC**A*** 5'	1
12	3' TGT AGC GA**P^2** A**P^2**A **P^2**A**P^2** A**P^{2}A*** 5'	1
11a	3' (**Thiol Heg**)$_2$ TAT ATA TAT A**F**C GCT ACA 5'	1
12a	3' TGT AGC GAT ATA TAT ATA 5'	1

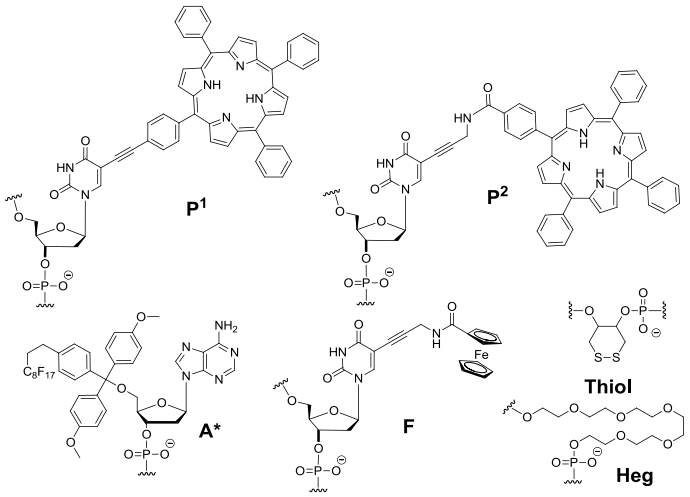

Crude acetylene linked porphyrin phosphoramidite (**VII**, 70 mg, 32.6 μmoles) was dissolved in DCM:MeCN (1:1, 1.20 mL, 100 mM), crude amide linked porphyrin (**XIV**, 60 mg, 32.7 μmoles) was dissolved in DCM:MeCN (1:1, 1.3 mL, 25 mM), crude ferrocene phosphoramidite (**XVI**, 190.5 mg, ~ 120 μmoles) was dissolved in DCM:MeCN (1:1, 560 μL, 100 mM). Porphyrin monomers were coupled over 5 minutes (112 μM, 2.4 eq), ferrocene monomer was coupled over 10 minutes (224 μL, 22.5 eq). Commercially available heg and thiol linkers were coupled as per the manufacturer's recommendation. Synthesis was conducted on a universal support. Deprotection of the protecting groups and cleavage of the strands was achieved by shaking in ammonia solution (35 % in H_2O, S.G. = 0.88, 1 mL) for 18 hours at RT. Purification was achieved by FluoroPak II columns and samples desalted with NAP-5 columns before concentrating *in vacuo*.

11

Yield (nmoles): 8

Calculated ε_{260} (mol^{-1} dm^3 cm^{-1}): 184,900

UV-Vis (100 mM sodium phosphate, 100 NaCl, 1 mM Na_2EDTA, pH 7.0, 1.50 μM): λ_{max} (log ε) 260 (5.27), 420 (5.58), 519 (4.43), 554 (4.18), 594 (4.09), 649 (4.26)

Emission (100 mM sodium phosphate, 100 NaCl, 1 mM Na_2EDTA, pH 7.0, 1.50 μM): λ_{ex} 420 nm, λ_{em} (rel int) 651 (1.00), 716 (0.29)

12

Yield (nmoles): 12

Calculated ε_{260} (mol^{-1} dm^3 cm^{-1}): 192,100

UV-Vis (100 mM sodium phosphate, 100 NaCl, 1 mM Na_2EDTA, pH 7.0, 0.723 μM): λ_{max} (log ε) 255 (5.28), 420 (5.16), 517 (3.83), 554 (3.62), 594 (3.33), 650 (3.86)

Emission (100 mM sodium phosphate, 100 NaCl, 1 mM Na_2EDTA, pH 7.0, 0.723 μM): λ_{ex} 420 nm, λ_{em} (rel int) 652 (1.00), 714 (0.31)

11•12

Calculated ε_{260} (mol^{-1} dm^3 cm^{-1}): 288819

UV-Vis (100 mM sodium phosphate, 100 NaCl, 1 mM Na_2EDTA, pH 7.0, 0.919 μM): λ_{max} (log ε) 259 (5.46)

T_m (100 mM sodium phosphate, 100 NaCl, 1 mM Na_2EDTA, pH 7.0): 51.0 °C

11a

Yield (nmoles): 37

Calculated ε_{260} (mol^{-1} dm^3 cm^{-1}): 184,900

UV-Vis (100 mM sodium phosphate, 100 NaCl, 1 mM Na_2EDTA, pH 7.0, 0.65 μM): λ_{max} (log ε) 260 (5.27)

Emission (100 mM sodium phosphate, 100 NaCl, 1 mM Na_2EDTA, pH 7.0, 0.65 μM): No fluorescence observed

MALDI ToF (pos): Calculated mass: 6900, unobservable by mass spectrometry

12a

Yield (nmoles): 555

Calculated ε_{260} (mol^{-1} dm^3 cm^{-1}): 192,100

UV-Vis (100 mM sodium phosphate, 100 NaCl, 1 mM Na_2EDTA, pH 7.0, 0.64 μM): λ_{max} (log ε) 255 (5.28)

Emission: No fluorescence spectrum collected

GC ESI (neg): Calculated mass: 5537, observed *m/z*: 5537.0 $[M-H]^-$, 5559.0 $[M-2H+Na]^-$, 5583.0 $[M-3H+2Na]^-$

8.78 – Synthesis of naphthalene diimide modified DNA (13) and (14)

Strand Name	Sequence	Scale (µmoles)
13	3' ACT TAG TGA **N**CC GAG CAG TC 5'	1
14	3' ACT TAG TGA **N**C**N** GAG CAG TC 5'	1
13a	3' ACT TAG TGA TCC GAG CAG TC 5'	1
14a	3' ACT TAG TGA TCT GAG CAG TC 5'	1
13b	3' GAC TGC TCG GAT CAC TAA GT 5'	1
14b	3' GAC TGC TCA GAT CAC TAA GT 5'	1

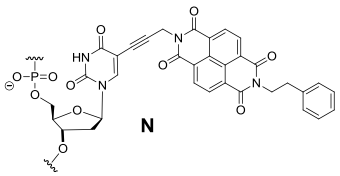

Crude naphthalene diimide phosphoramidite (**XXVI**, ~ 30 µmoles) was dissolved in DCM:MeCN (1:1, 600 µL, 50 mM), monomer was coupled over 5 minutes (112 µL, 5.6 eq). Deprotection of the protecting groups and cleavage of the strands was achieved by shaking in ammonia solution (35 % in H_2O, S.G. = 0.88, 1 mL) for 18 hours at RT. Purification was achieved by GlenPak columns, modified samples were eluted using MeCN:H_2O (1:1, 1 mL), MeCN (1 mL) and MeOH (1 mL). Samples desalted with NAP-5 columns before concentrating *in vacuo*.

13

Yield (nmoles): 69

Calculated ε_{260} (mol^{-1} dm^3 cm^{-1}): 193,600

UV-Vis (100 mM sodium phosphate, 100 NaCl, 1 mM Na_2EDTA, pH 7.0, 0.99 µM): λ_{max} (log ε) 260 (5.29)

Emission (100 mM sodium phosphate, 100 NaCl, 1 mM Na_2EDTA, pH 7.0, 0.99 µM): No fluorescence observed

GC ESI (neg): Calculated mass: 6508, unobservable by mass spectrometry

14

Yield (nmoles): 23

Calculated ε_{260} (mol^{-1} dm^3 cm^{-1}): 196,300

UV-Vis (100 mM sodium phosphate, 100 NaCl, 1 mM Na_2EDTA, pH 7.0, 1.14 µM): λ_{max} (log ε) 260 (5.29)

Emission (100 mM sodium phosphate, 100 NaCl, 1 mM Na_2EDTA, pH 7.0, 1.14 μM): No fluorescence observed

GC ESI (neg): Calculated mass: 6915, unobservable by mass spectrometry

13a

Yield (nmoles): 264

Calculated ε_{260} (mol^{-1} dm^3 cm^{-1}): 193,600

UV-Vis (100 mM sodium phosphate, 100 NaCl, 1 mM Na_2EDTA, pH 7.0, 1.07 μM): λ_{max} (log ε) 260 (5.29)

Emission: No fluorescence spectrum collected

GC ESI (neg): Calculated mass: 6117, observed *m/z*: 6116.03 $[M-H]^-$

14a

Yield (nmoles): 232

Calculated ε_{260} (mol^{-1} dm^3 cm^{-1}): 196,300

UV-Vis (100 mM sodium phosphate, 100 NaCl, 1 mM Na_2EDTA, pH 7.0, 0.95 μM): λ_{max} (log ε) 260 (5.29)

Emission: No fluorescence spectrum collected

GC ESI (neg): Calculated mass: 6132, observed *m/z*: 6131.08 $[M-H]^-$

13b

Yield (nmoles): 234

Calculated ε_{260} (mol^{-1} dm^3 cm^{-1}): 192,800

UV-Vis (100 mM sodium phosphate, 100 NaCl, 1 mM Na_2EDTA, pH 7.0, 1.02 μM): λ_{max} (log ε) 260 (5.29)

Emission: No fluorescence spectrum collected

GC ESI (neg): Calculated mass: 6117, observed *m/z*: 6116.03 $[M-H]^-$

14b

Yield (nmoles): 342

Calculated ε_{260} (mol^{-1} dm^3 cm^{-1}): 196,100

UV-Vis (100 mM sodium phosphate, 100 NaCl, 1 mM Na_2EDTA, pH 7.0, 1.12 μM): λ_{max} (log ε) 260 (5.29)

Emission: No fluorescence spectrum collected

GC ESI (neg): Calculated mass: 6101, observed *m/z*: 6100.08 $[M-H]^-$

8.79 – Synthesis of thiol/porphyrin/anthraquinone modified DNA for CV (15 - 20)

Strand Name	Sequence	Scale (µmoles)
15	3' **Thiol PAP** A**P**A **PAP** A**Q**C GCT AC**A*** 5'	1
16	3' TGT AGC GA**P** A**P**A **PAP** A**PA*** 5'	1
17	3' **Thiol** TAT ATA TAT A**Q**C GCT AC**A*** 5'	0.2
18	3' TGT AGC GAT ATA TAT ATA 5'	1
19	3' **Thiol** TAT A**P**A **P**AT A**Q**C GCT AC**A*** 5'	0.2
20	3' TGT AGC GAT ATA **P**AT AT**A*** 5'	1

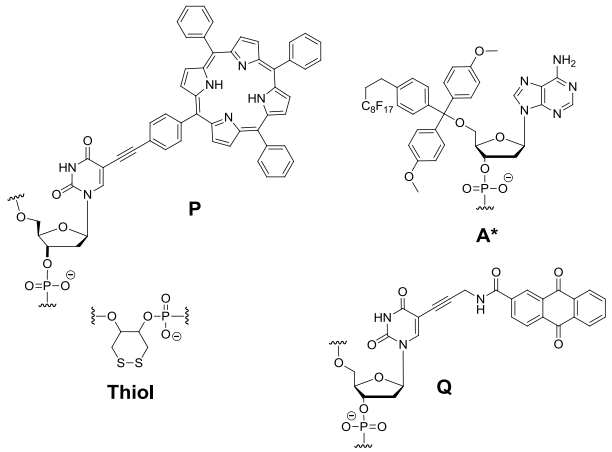

Crude acetylene porphyrin monomer phosphoramidite (**VII**, ~ 64 µmoles) was dissolved in DCM:MeCN (1:1, 1.8 mL, 35.5 mM), crude anthroquinone monomer phosphoramidite (**XXVIII**, ~ 27.5 µmoles) was dissolved in DCM:MeCN (1:1, 900 µL, 30.5 mM). Porphyrin monomer was coupled over 5 minutes (112 µM, 4.0 eq), anthraquinone monomer was coupled over 5 minutes (112 µL, 3.4 eq). Commercially available thiol linker was coupled as per the manufacturer's recommendation. Synthesis of thiol modified strands was conducted on universal supports, other strands were synthesised on standard nucleoside modified CPG supports. Strands were cleaved from the supports with; methanolic ammonia (2M, 1 mL) at RT for 16 hours, methanolic ammonia (2M, 1 mL) at 60°C for 4 hours and MeOH:aqueous ammonia (70:30, 1 mL) at 60 °C for 1 hour. Protecting groups were cleaved with aqueous ammonia (35 %, S.G. = 0.88, 1 mL) at RT for 16 hours, samples were dried before purification with FluoroPak II or GlenPak columns. Samples were desalted with NAP-5 columns.

15

Yield (nmoles): 37

HPLC conditions: 0.0 min 100 % buffer, 40.0 min 60 % buffer 40 % MeOH, 55.0 min 60 % MeOH 40 % buffer, 70.0 min 100 % MeOH, 85.0 min 100 % MeOH, 100 min 100 % buffer.

Buffer – 100 mM HFIPA, 8.4 mM TEA in H_2O. Column – Waters 50 X 4.6 mm C18 XBridge at 50 °C.

HPLC retention time (mins): 71.17

Calculated ε_{260} (mol^{-1} dm^3 cm^{-1}): 184,900

UV-Vis (100 mM sodium phosphate, 100 NaCl, 1 mM Na_2EDTA, pH 7.0, 0.70 µM): λ_{max} (log ε) 262 (5.27), 422 (5.49), 521 (4.53), 557 (4.38), 597 (4.21), 651 (4.12)

Emission (100 mM sodium phosphate, 100 NaCl, 1 mM Na_2EDTA, pH 7.0, 0.70 µM): λ_{ex} 421 nm, λ_{em} (rel int) 654 (1.00), 721 (0.33)

16

Yield (nmoles): 29

HPLC conditions: 0.0 min 100 % buffer, 40.0 min 60 % buffer 40 % MeOH, 55.0 min 60 % MeOH 40 % buffer, 70.0 min 100 % MeOH, 85.0 min 100 % MeOH, 100 min 100 % buffer. Buffer – 100 mM HFIPA, 8.4 mM TEA in H_2O. Column – Waters 50 X 4.6 mm C18 XBridge at 50 °C.

HPLC retention time (mins): 71.04

Calculated ε_{260} (mol^{-1} dm^3 cm^{-1}): 192,100

UV-Vis (100 mM sodium phosphate, 100 NaCl, 1 mM Na_2EDTA, pH 7.0, 1.23 µM): λ_{max} (log ε) 260 (5.27), 420 (5.54), 520 (4.51), 557 (4.28), 594 (4.09), 650 (4.04)

Emission (100 mM sodium phosphate, 100 NaCl, 1 mM Na_2EDTA, pH 7.0, 1.23 µM): λ_{ex} 419 nm, λ_{em} (rel int) 655 (1.00), 719 (0.32)

17

Yield (nmoles): 11

HPLC conditions: 0.0 min 100 % buffer, 40.0 min 60 % buffer 40 % MeOH, 55.0 min 60 % MeOH 40 % buffer, 70.0 min 100 % MeOH, 85.0 min 100 % MeOH, 100 min 100 % buffer. Buffer – 100 mM HFIPA, 8.4 mM TEA in H_2O. Column – Waters 50 X 4.6 mm C18 XBridge at 50 °C.

HPLC retention time (mins): 9.80

Calculated ε_{260} (mol^{-1} dm^3 cm^{-1}): 184,900

UV-Vis (100 mM sodium phosphate, 100 NaCl, 1 mM Na_2EDTA, pH 7.0, 3.27 µM): λ_{max} (log ε) 260 (5.27), 335 (3.92)

Emission (100 mM sodium phosphate, 100 NaCl, 1 mM Na_2EDTA, pH 7.0, 3.27 µM): No fluorescence observed

18

Yield (nmoles): 75

HPLC conditions: 0.0 min 100 % buffer, 40.0 min 60 % buffer 40 % MeOH, 55.0 min 60 % MeOH 40 % buffer, 70.0 min 100 % MeOH, 85.0 min 100 % MeOH, 100 min 100 % buffer. Buffer – 100 mM HFIPA, 8.4 mM TEA in H_2O. Column – Waters 50 X 4.6 mm C18 XBridge at 50 °C.

HPLC retention time (mins): 5.75

Calculated ε_{260} (mol^{-1} dm^3 cm^{-1}): 192,100

UV-Vis (100 mM sodium phosphate, 100 NaCl, 1 mM Na_2EDTA, pH 7.0, 0.83 µM): λ_{max} (log ε) 260 (5.28)

Emission: No fluoresence spectrum collected

19

Yield (nmoles): 17

HPLC conditions: 0.0 min 100 % buffer, 40.0 min 60 % buffer 40 % MeOH, 55.0 min 60 % MeOH 40 % buffer, 70.0 min 100 % MeOH, 85.0 min 100 % MeOH, 100 min 100 % buffer. Buffer – 100 mM HFIPA, 8.4 mM TEA in H_2O. Column – Waters 50 X 4.6 mm C18 XBridge at 50 °C.

HPLC retention time (mins): 69.16

Calculated ε_{260} (mol^{-1} dm^3 cm^{-1}): 184,900

UV-Vis (100 mM sodium phosphate, 100 NaCl, 1 mM Na_2EDTA, pH 7.0, 1.29 µM): λ_{max} (log ε) 260 (5.27), 423 (5.25), 521 (4.21), 558 (4.03), 595 (3.86), 651 (3.86)

Emission (100 mM sodium phosphate, 100 NaCl, 1 mM Na_2EDTA, pH 7.0, 1.29 µM): λ_{ex} 421 nm, λ_{em} (rel int) 652 (1.00), 715 (0.30)

20

Yield (nmoles): 115

HPLC conditions: 0.0 min 100 % buffer, 40.0 min 60 % buffer 40 % MeOH, 55.0 min 60 % MeOH 40 % buffer, 70.0 min 100 % MeOH, 85.0 min 100 % MeOH, 100 min 100 % buffer. Buffer – 100 mM HFIPA, 8.4 mM TEA in H_2O. Column – Waters 50 X 4.6 mm C18 XBridge at 50 °C.

HPLC retention time (mins): 71.10

Calculated ε_{260} (mol^{-1} dm^3 cm^{-1}): 192,100

UV-Vis (100 mM sodium phosphate, 100 NaCl, 1 mM Na_2EDTA, pH 7.0, 1.17 µM): λ_{max} (log ε) 260 (5.28), 423 (5.44), 520 (4.25), 558 (4.18), 595 (4.06), 654 (4.20)

Emission (100 mM sodium phosphate, 100 NaCl, 1 mM Na_2EDTA, pH 7.0, 1.17 μM): λ_{ex} 422 nm, λ_{em} (rel int) 653 (1.00), 717 (0.28)

8.80 – Synthesis of thiol/porphyrin modified DNA for CV (21) and (21a)

Strand Name	Sequence	Scale (µmoles)
21	3' **Thiol PAP APA*** 5'	1
21a	3' **Thiol** TAT AT**A*** 5'	1

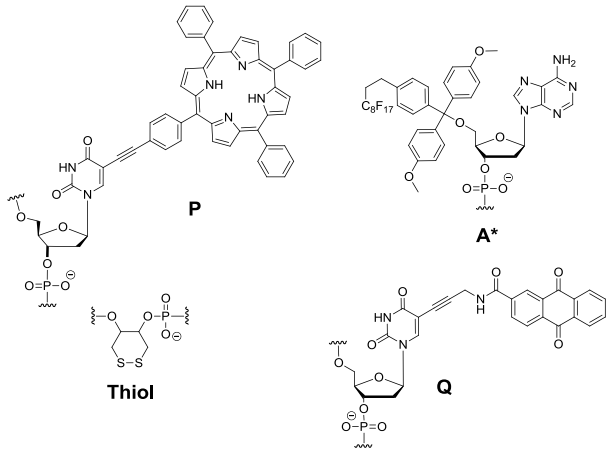

Crude acetylene porphyrin monomer phosphoramidite (**VII**, ~ 64 µmoles) was dissolved in DCM:MeCN (1:1, 1.8 mL, 35.5 mM) and coupled over 5 minutes (112 µM, 4.0 eq). Commercially available thiol linker was coupled as per the manufacturer's recommendation. Synthesis was conducted on universal supports. Strands were cleaved from the supports with; methanolic ammonia (2M, 1 mL) at RT for 16 hours, methanolic ammonia (2M, 1 mL) at 60°C for 4 hours and MeOH:aqueous ammonia (70:30, 1 mL) at 60 °C for 1 hour. Protecting groups were cleaved with aqueous ammonia (35%, S.G. = 0.88, 1 mL) at RT for 16 hours, samples were dried before purification with FluoroPak II or GlenPak columns. Samples were desalted with NAP-5 columns.

21

Yield (nmoles): 22

HPLC conditions: 0.0 min 100 % buffer, 40.0 min 60 % buffer 40 % MeOH, 55.0 min 60 % MeOH 40 % buffer, 70.0 min 100 % MeOH, 85.0 min 100 % MeOH, 100 min 100 % buffer. Buffer – 100 mM HFIPA, 8.4 mM TEA in H_2O. Column – Waters 50 X 4.6 mm C18 XBridge at 50 °C.

HPLC retention time (mins): 64.89

Calculated ε_{260} (mol^{-1} dm^3 cm^{-1}): 67,000

UV-Vis (100 mM sodium phosphate, 100 NaCl, 1 mM Na_2EDTA, pH 7.0, 0.96 µM): λ_{max} (log ε) 259 (4.83), 421 (5.12), 520 (4.15), 555 (3.94), 594 (3.65), 648 (3.51)

Emission (100 mM sodium phosphate, 100 NaCl, 1 mM Na_2EDTA, pH 7.0, 0.96 µM): λ_{ex} 420 nm, λ_{em} (rel int) 653 (1.0), 717 (0.26)

21a

Yield (nmoles): 46

HPLC conditions: 0.0 min 100 % buffer, 40.0 min 60 % buffer 40 % MeOH, 55.0 min 60 % MeOH 40 % buffer, 70.0 min 100 % MeOH, 85.0 min 100 % MeOH, 100 min 100 % buffer. Buffer – 100 mM HFIPA, 8.4 mM TEA in H_2O. Column – Waters 50 X 4.6 mm C18 XBridge at 50 °C.

HPLC retention time (mins): 5.15

Calculated ε_{260} (mol^{-1} dm^3 cm^{-1}): 67,000

UV-Vis (100 mM sodium phosphate, 100 NaCl, 1 mM Na_2EDTA, pH 7.0, 1.93 µM): λ_{max} (log ε) 260 (4.83)

Emission:No fluorescence spectrum collected

8.81 – Preparation of DNA modified electrodes for cyclic voltammetry

Sample preparation and acquisition of cyclic voltammograms was performed by Robert Johnson of Dr. Phil Bartlett's research group (University of Southampton) in the following manner.

A 0.5 mm Ø gold wire was mounted in epoxy resin and polished sequentially with 1200 grit sand paper, 1 µm micropolish and 0.3 µm micropolish. The electrode surfaces were cleaned by cycling in H_2SO_4 (1M) between 0.3 V and 1.8 V (vs. SCE) twenty times. The electrode was then held at 1.8 V (vs. SCE) for 60 seconds to oxidise the gold surface before returning to 0.3 V (vs.SCE) and the absolute surface area of the gold electrode calculated from the resulting reduction peak. The electrode was washed with deionised water before use.

A solution of 1 µM DNA (single stranded or duplex) was prepared in 100 mM NaCl, 10 mM Tris buffer (pH 7.2). The electrode was functionalised with the DNA solution for 24-48 hours before washing excess unbound solution with 100 mM NaCl, 10 mM Tris buffer (pH 7.2). The functionalised electrode was then capped with 6-mercaptohexan-1-ol solution (0.5 mM) for 20 minutes before washing with 100 mM NaCl, 10 mM Tris buffer (pH 7.2).

Cyclic voltammograms were acquired using a degassed 100 mM NaCl, 10 mM Tris buffer solution (pH 7.2) with a saturated calomel (SCE) reference electrode and a platinum gauze counter electrode. All measurements were made inside a Faraday cage.

8.82 – Cyclic voltammetry of strand 15

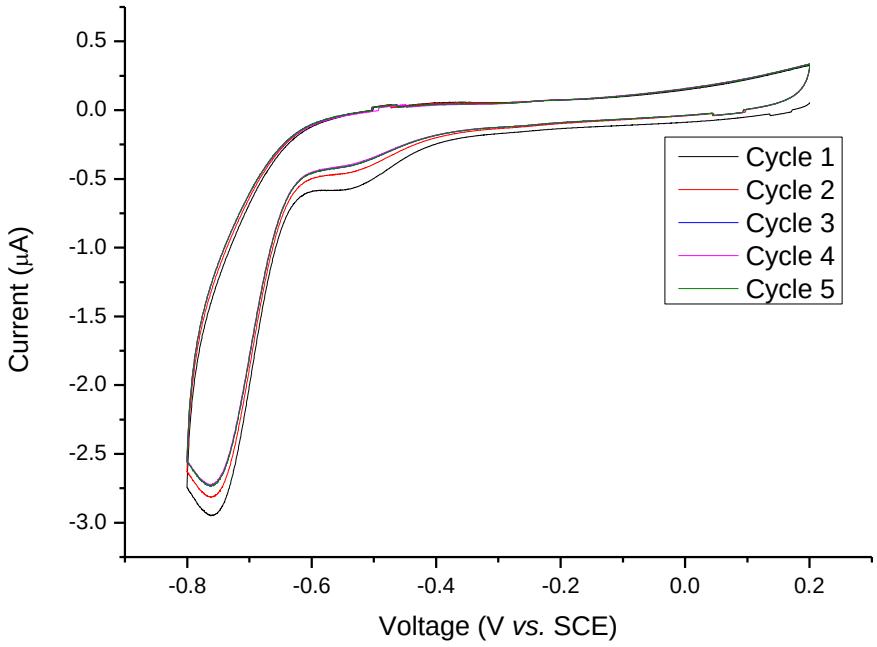

Figure 128. CV of **15** in 100 mM NaCl, 10 mM Tris buffer, pH 7.2

8.83 – Cyclic voltammetry of strand 17

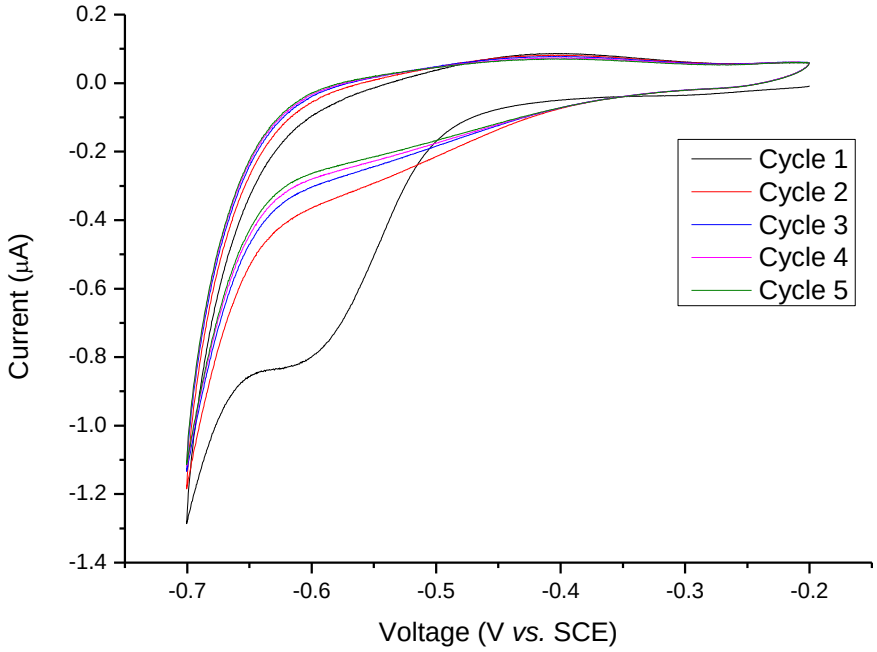

Figure 129. CV of **17** in 100 mM NaCl, 10 mM Tris buffer, pH 7.2

8.84 – Cyclic voltammetry of 15•16

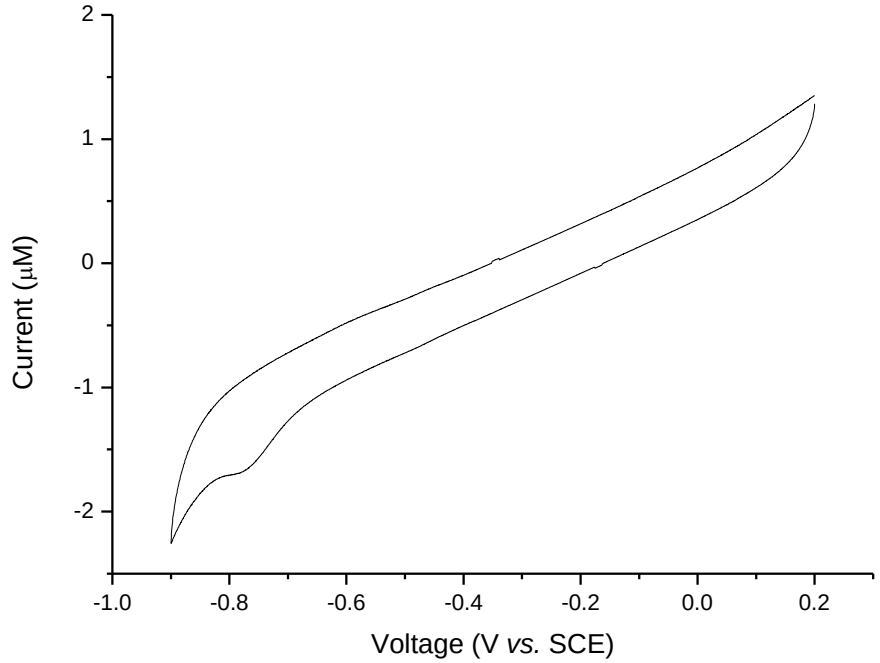

Figure 130. CV of **15•16** in 100 mM NaCl, 10 mM Tris buffer, pH 7.2

8.85 – Cyclic voltammetry of 17•18

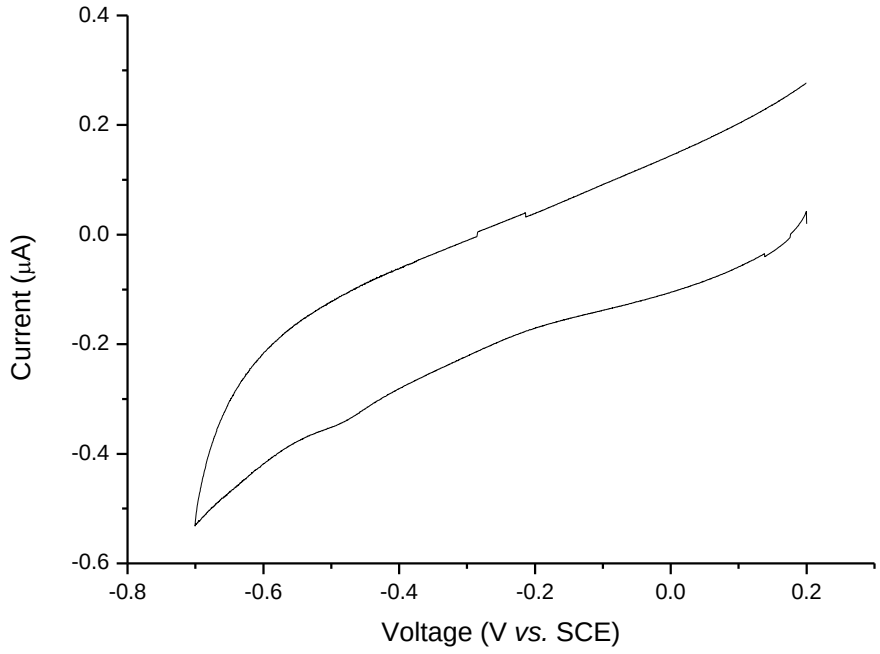

Figure 131. CV of **17•18** in 100 mM NaCl, 10 mM Tris buffer, pH 7.2

8.86 – Differential Pulse Voltammetry of 15•16

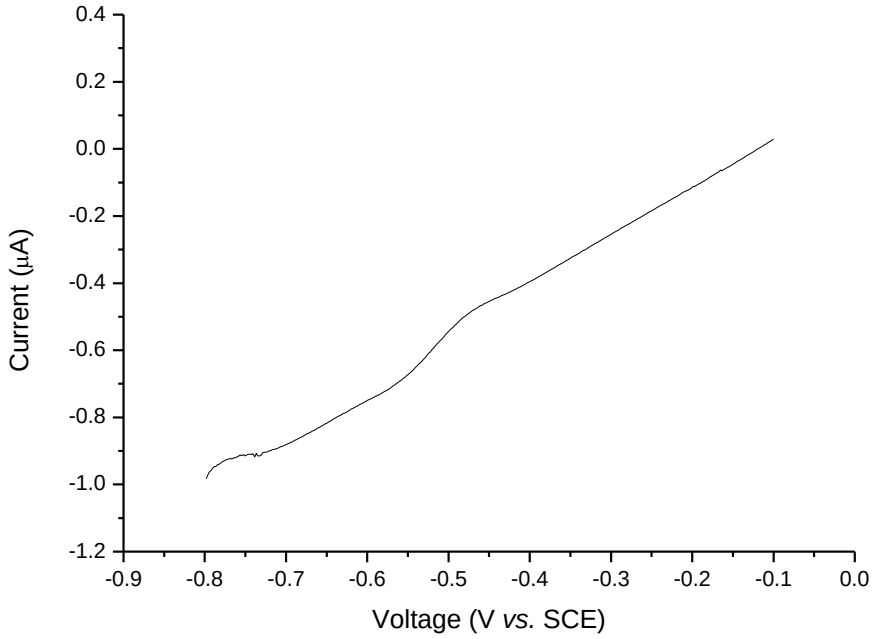

Figure 132. DPV of **15•16** in 100 mM NaCl, 10 mM Tris buffer, pH 7.2

8.87 – Differential Pulse Voltammetry of 17•18

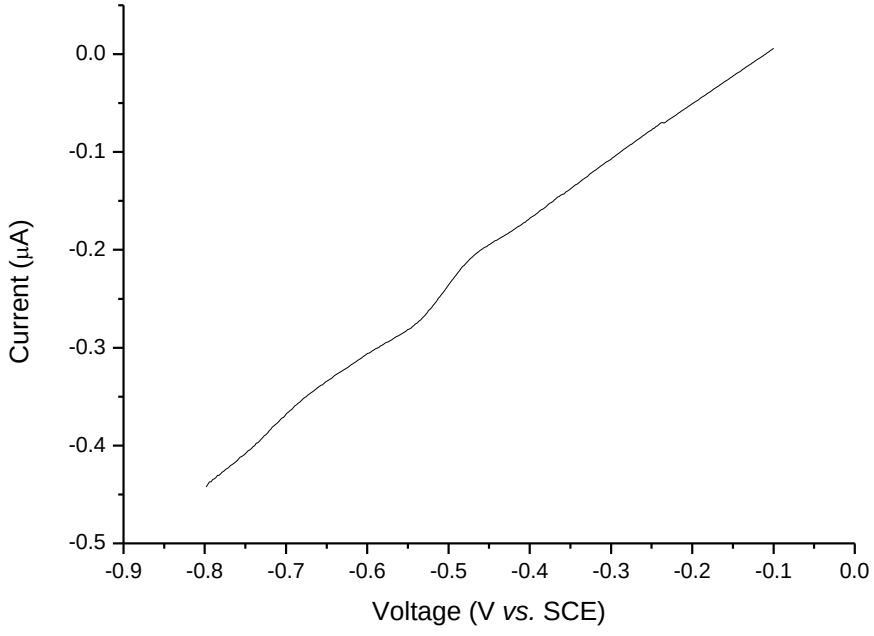

Figure 133. DPV of **17•18** in 100 mM NaCl, 10 mM Tris buffer, pH 7.2

8.88 – Synthesis of *N,N'*-di(prop-2-ynyl) napthalene diimide (XXXI)

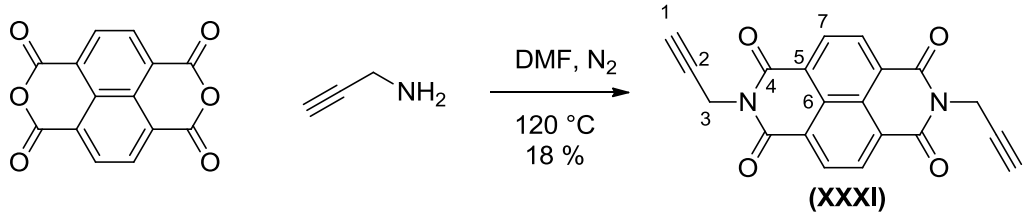

(XXXI)

Napthalene-1,4,5,8-tetracarboxylic acid di-anhydride (536 mg, 2.0 mmol, 1.00 eq) and propargylamine (274 µL, 4.0 mmol, 2.00 eq) were dissolved in DMF (10 mL) under N_2 and heated to 120 °C for 28 hours. The reaction mixture was concentrated *in vacuo* and purified by column chromatography (silica, eluent – DCM). The product was obtained as an off white solid, 121 mg (353 µmol, 18 %).

^{1}H NMR (400 MHz, $CDCl_3$): δ ppm 2.17 (t, J_{HH} = 2.5 Hz, 2 H, **1**), 4.92 (d, J_{HH} = 2.5 Hz, 4 H, **3**), 8.76 (s, 4 H, **7**)

^{13}C{^{1}H} NMR (100 MHz, $CDCl_3$) δ ppm 32.09 (CH_2, **3**), 73.42 (CH, **1**), 79.90 (C, **2**), 128.11 (CH, **7**), 128.85 (C, **5**), 133.63 (C, **6**), 163.27 (C, **4**)

GC ESI (pos) ($C_{20}H_{10}N_2O_4$): Monoisotopic mass 342.06, observed *m/z* 365.1 $[M+ Na]^+$

UV-Vis (MeCN, 13.0 µM): λ_{max} (log ε) 235 (4.21), 356 (4.02), 376 (4.10)

Emission (MeCN, 0.78 mM): λ_{ex} 376 nm, λ_{em} (rel int): 431 nm (1.0)

R_f (silica, 5 % MeOH in DCM): 0.75

Melting Point: 244.5 – 246.7 °C (no lit. value)

8.89 – Synthesis of $Os(bipy)_2Cl_2$ (XXXII)

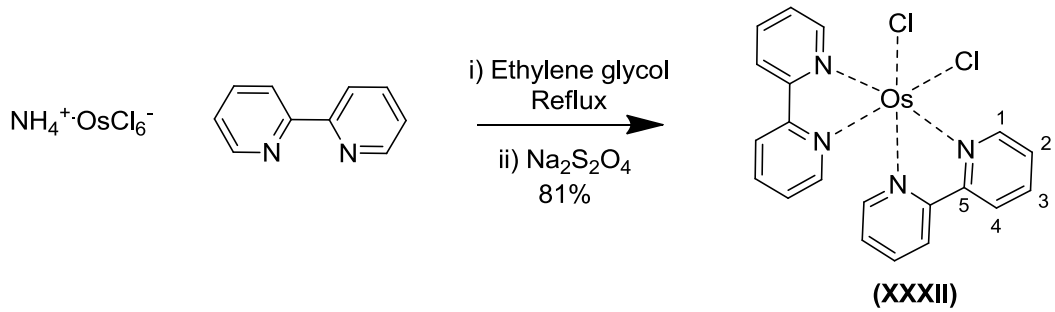

(XXXII)

Ammonium hexafluoro-osmate (421 mg, 1.0 mmol, 1.00 eq) and 2,2'-bipyridyl (312 mg, 2.0 mmol, 2.00 eq) were dissolved in ethylene glycol (15 mL) and heated to reflux (150 °C) for 1 hr. The reaction mixture was cooled and a solution of sodium dithionite (0.5 M, 1.74 g, 10.0 mmol, 10.00 eq) was added and stirred over ice for 30 minutes. The precipitate that formed was filtered off, washed with water (20 mL) and ether (100 mL) and dried *in vacuo*, 467.3 mg (815 µmol, 81 %).

^{1}H NMR (400 MHz, DMSO-d_6): δ ppm 6.55 - 6.64 (m, 4 H, **2**), 7.17 - 7.25 (m, 4 H, **3**), 8.57 (d, J_{HH} =6.0 Hz, 4 H, **4**), 8.85 - 8.92 (m, 4 H, **1**)

^{13}C{^{1}H} NMR (100 MHz, DMSO-d_6) δ ppm 122.85 (CH, **4**), 125.28 (CH, **2**), 135.22 (CH, **3**), 151.28 (CH, **1**), 162.67 (C, **5**)

GC ESI (pos) ($C_{20}H_{16}Cl_2N_4Os$): Monoisotopic mass 574.04, observed *m/z* 574.2 $[M]^+$

CV (1mM in 10 mM Tris buffer (pH 7.2) containing 1M NaCl and 50% DMSO, sweep rate 100 mV s^{-1}, potentials *vs* SCE, 5 mm Ø glassy carbon working electrode, Pt counter electrode): -0.015 V / -0.067 V (ox. / red.)

UV-Vis (MeCN, 17.4 µM): λ_{max} (log ε) 296 (4.65), 380 (3.87), 461 (3.81), 553 (3.90)

Emission (MeCN 17.4 µM): No fluorescence observed

R_f (silica, 20:1:3 MeCN:$KNO_{3\ sat.\ aq.}$:H_2O): 0.43

IR (solid): cm^{-1} 3040 (C-H aromatic), 2335 (C=C aromatic), 2365 (C=N aromatic), 1012 (Os-N)

Melting Point: >250 °C (no lit. value)

8.90 – Synthesis of Osmium (IV) (*N*-(prop-2-ynyl)-4-methyl-2-2'-bipyridyl-4'-carboxamide) $(bipy)_2$ *bis*-nitrate (XXXIII)

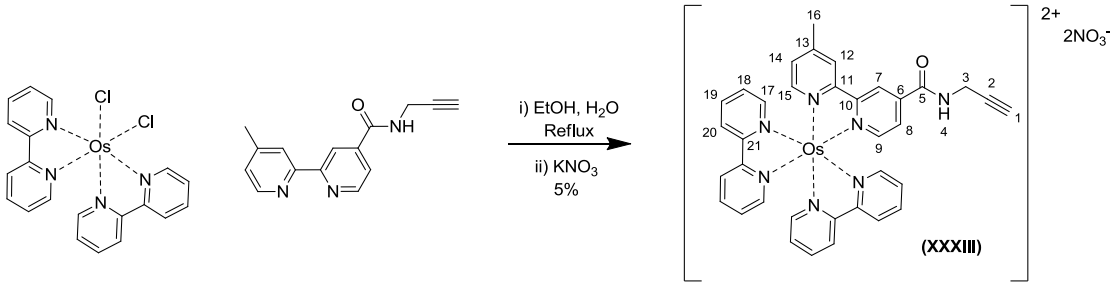

$Os(bipy)_2(Cl)_2$ (172.1 mg, 0.3 mmol, 1.00 eq) and *N*-(prop-2-ynyl)-4-methyl-2-2'-bipyridyl-4'-carboxamide (80 mg, 0.3 mmol, 1.00 eq) were dissolved in EtOH:H_2O (70:30, 25 mL) and heated to reflux for 16 hours. KNO_3 (4.00 g) was added and the reaction mixture agitated at room temperature for 5 minutes before drying *in vacuo*. Crude product was redissolved in DCM:MeOH (1:1, 50 mL), filtered and the solvent removed *in vacuo*. The product was purified by column chromatography (silica, eluent - MeCN:$KNO_{3\ sat.\ aq.}$:H_2O 50:1:3), product dried, redissolved in DCM:MeOH (1:1, 20 mL), filtered, the solvent removed and the dark green solid product dried *in vacuo*, 14 mg (15.9 µmol, 5 %).

^{1}H NMR (400 MHz, DMSO-d_6): δ ppm 2.66 (s, 3 H, **16**), 3.22 (t, J_{HH} = 2.5 Hz, 1 H, **1**), 4.16 (dd, J_{HH} = 5.3, 2.3 Hz, 2 H, **3**), 7.34 (d, J_{HH} = 5.1 Hz, 1 H, **14**), 7.42 - 7.48 (m, 4 H, **18**), 7.50 (d, J_{HH} = 6.1 Hz, 1 H, **15**), 7.63 (dd, J_{HH} = 5.6, 4.5 Hz, 4 H, **17**), 7.66 - 7.70 (m, 1 H, **8**), 7.83 (d, J_{HH} = 5.6 Hz, 1 H, **9**), 7.94 - 8.03 (m, 4 H, **19**), 8.79 (s, 1 H, **12**), 8.84 (d, J_{HH} = 8.1 Hz, 4 H, **20**), 9.12 (d, J_{HH} = 1.5 Hz, 1 H, **7**), 9.47 (t, J_{HH} = 5.3 Hz, 1 H, **4**)

^{13}C{^{1}H} NMR (100 MHz, DMSO-d_6): δ ppm 20.57 (CH_3, **16**), 28.82 (CH_2, **3**), 73.60 (CH, **1**), 80.51 (C, **2**), 121.76 (CH, **7**), 124.76 (CH, **20**), 125.67 (CH, **8**), 126.14 (CH, **12**), 128.41 (CH, **18**), 129.27 (CH, **14**), 137.44 (CH, **19**), 139.97 (C, **6**), 149.55 (C, **13**), 150.17 (CH, **15**), 150.57 (CH, **17**), 151.01 (CH, **9**), 157.68 (C, **11**), 158.54 (C, **21**), 159.45 (C, **10**), 162.72 (C, **5**)

MALDI ToF (pos) ($C_{35}H_{29}N_9O_7Os$): Monoisotopic mass 879.18, observed mass 755.6 [M-$2NO_3$]$^{2+}$

UV-Vis (MeCN, 15.9 µM) λ_{max} (log ε): 245 (4.29), 291 (4.71), 375 (3.85), 446 (3.95), 486 (3.97)

Emission (MeCN, 15.9 µM): No fluorescence observed

R_f (silica, 20:1:3 MeCN:$KNO_{3\ sat.\ aq.}$:H_2O): 0.41

Melting Point: >250 °C (no lit. value)

9 – Bibliography

(1) Ryter, S. W.; Tyrrell, R. M. *Free Radic. Biol. Med.* **2000**, *28*, 289-309.
(2) Rabinowitch, E. *Rev. Mod. Phys.* **1944**, *16*, 226-235.
(3) Fromme, P.; Mathis, P. *Photosynth. Res.* **2004**, *80*, 109-124.
(4) Rhee, K.-H. *Annu. Rev. Biophys. Biomol. Struct.* **2001**, *30*, 307-328.
(5) Buchanan, B. B. *Ann. Rev. Plant Physiol.* **1980**, *31*, 341-374.
(6) Pilgrim, J. L.; Gerostamoulos, D.; Drummer, O. H. *Forensic Sci Med. Pathol.* **2011**, *7*, 162-184.
(7) Ganapathy, S.; Oostergetel, G. T.; Wawrzyniak, P. K.; Reus, M.; Gomez Maqueo Chew, A.; Buda, F.; Boekema, E. J.; Bryant, D. A.; Holzwarth, A. R.; de Groot, H. J. M. *Proc. Natl. Acad. Sci. USA* **2009**, *106*, 8525-8530.
(8) Fleischer, E. B. *Acc. Chem. Res.* **1970**, *3*, 105-112.
(9) Adler, A. D.; Longo, F. R.; Finarelli, J. D.; Goldmacher, J.; Assour, J.; Korsakoff, L. *J. Org. Chem.* **1967**, *32*, 476-476.
(10) Twyman, L. J.; Sanders, J. K. M. *Tet. Lett.* **1999**, *40*, 6681-6684.
(11) Richeter, S.; Hadj-Aissa, A.; Taffin, C.; van der Lee, A.; Leclercq, D. *ChemComm.* **2007**, 2148-2150.
(12) Silvers, S. J.; Tulinsky, A. *J. Am. Chem. Soc.* **1967**, *89*, 3331-3337.
(13) Lavallee, D. K.; Anderson, O. P. *J. Am. Chem. Soc.* **1982**, *104*, 4707-4708.
(14) Ostfeld, D.; Tsutsui, M. *Acc. Chem. Res.* **1974**, *7*, 52-58.
(15) Prodi, A.; Indelli, M. T.; Kleverlaan, C. J.; Scandola, F.; Alessio, E.; Gianferrara, T.; Marzilli, L. G. *Chem. Eur. J.* **1999**, *5*, 2668-2679.
(16) Mansuy, D.; Battioni, J. P.; Dupre, D.; Sartori, E.; Chottard, G. *J. Am. Chem. Soc.* **1982**, *104*, 6159-6161.
(17) Ryu, S.; Kim, J.; Yeo, H.; Kim, K. *Inorg. Chim. Acta* **1995**, *228*, 233-236.
(18) Ricciardi, G.; Rosa, A.; Baerends, E. J.; van Gisbergen, S. A. J. *J. Am. Chem. Soc.* **2002**, *124*, 12319-12334.
(19) Huang, X. F.; Nakanishi, K.; Berova, N. *Chirality* **2000**, *12*, 237-255.
(20) Fendt, L. A.; Bouamaied, I.; Thoni, S.; Amiot, N.; Stulz, E. *J. Am. Chem. Soc.* **2007**, *129*, 15319-15329.
(21) Nguyen, T.; Brewer, A.; Stulz, E. *Angew. Chem. Int. Ed.* **2009**, *48*, 1974-1977.
(22) Gouterman, M. *J. Chem. Phys.* **1959**, *30*, 1139-1161.
(23) Spellane, P. J.; Gouterman, M.; Antipas, A.; Kim, S.; Liu, Y. C. *Inorg. Chem.* **1980**, *19*, 386-391.
(24) Watson, J. D.; Crick, F. H. C. *Nature* **1953**, *171*, 737-738.
(25) Wilkins, M. H. F.; Seeds, W. E.; Stokes, A. R.; Wilson, H. R. *Nature* **1953**, *172*, 759-762.
(26) Franklin, R. E.; Gosling, R. G. *Nature* **1953**, *171*, 740-741.
(27) Wing, R.; Drew, H.; Takano, T.; Broka, C.; Tanaka, S.; Itakura, K.; Dickerson, R. E. *Nature* **1980**, *287*, 755-758.
(28) Potaman, V. N.; Bannikov, Y. A.; Shlyachtenko, L. S. *Nucleic Acids Res.* **1980**, *8*, 635-642.
(29) Gould, I. R.; Kollman, P. A. *J. Am. Chem. Soc.* **1994**, *116*, 2493-2499.
(30) Jurecka, P.; Hobza, P. *J. Am. Chem. Soc.* **2003**, *125*, 15608-15613.
(31) Yakovchuk, P.; Protozanova, E.; Frank-Kamenetskii, M. D. *Nucleic Acids Res., 34*, 564-574.
(32) Wang, A. H. J.; Quigley, G. J.; Kolpak, F. J.; Crawford, J. L.; van Boom, J. H.; van der Marel, G.; Rich, A. *Nature* **1979**, *282*, 680-686.
(33) Arnott, S. *Trends Biochem. Sci.* **2006**, *31*, 349-354.
(34) Somoza, A. *Angew. Chem. Int. Ed.* **2009**, *48*, 9406-9408.
(35) Rothemund, P. W. K. *Nature* **2006**, *440*, 297-302.
(36) Jager, S.; Rasched, G.; Kornreich-Leshem, H.; Engeser, M.; Thum, O.; Famulok, M. *J. Am. Chem. Soc.* **2005**, *127*, 15071-15082.

(37) Hobbs, F. W. *J. Org. Chem.* **2002**, *54*, 3420-3422.
(38) Mokhir, A. A.; Tetzlaff, C. N.; Herzberger, S.; Mosbacher, A.; Richert, C. *J. Comb. Chem.* **2001**, *3*, 374-386.
(39) Nakamura, M.; Shimomura, Y.; Ohtoshi, Y.; Sasa, K.; Hayashi, H.; Nakano, H.; Yamana, K. *Org. Biomol. Chem.* **2007**, *5*, 1945-1951.
(40) Zhu, L.; Lukeman, P. S.; Canary, J. W.; Seeman, N. C. *J. Am. Chem. Soc.* **2003**, *125*, 10178-10179.
(41) Krider, E. S.; Rack, J. J.; Frank, N. L.; Meade, T. J. *Inorg. Chem.* **2001**, *40*, 4002-4009.
(42) Sorensen, M. D.; Petersen, M.; Wengel, J. *ChemComm.* **2003**, 2130-2131.
(43) Koshkin, A. A.; Singh, S. K.; Nielsen, P.; Rajwanshi, V. K.; Kumar, R.; Meldgaard, M.; Olsen, C. E.; Wengel, J. *Tetrahedron* **1998**, *54*, 3607-3630.
(44) Fukuda, M.; Nakamura, M.; Takada, T.; Yamana, K. *Tetrahedron Lett.* **2010**, *51*, 1732-1735.
(45) Morales-Rojas, H.; Kool, E. T. *Org. Lett.* **2002**, *4*, 4377-4380.
(46) Brotschi, C.; Mathis, G.; Leumann, C. J. *Chem. Euro. J.* **2005**, *11*, 1911-1923.
(47) Zimmermann, N.; Meggers, E.; Schultz, P. G. *Bioorg. Chem.* **2004**, *32*, 13-25.
(48) Tanaka, K.; Clever, G. H.; Takezawa, Y.; Yamada, Y.; Kaul, C.; Shionoya, M.; Carell, T. *Nat. Nanotech.* **2006**, *1*, 190-U5.
(49) Yang, H.; Rys, A. Z.; McLaughlin, C. K.; Sleiman, H. F. *Angew. Chem. Int. Ed.* **2009**, *48*, 9919-9923.
(50) Malinovskii, V. L.; Samain, F.; Haner, R. *Angew. Chem. Int. Ed.* **2007**, *46*, 4464-4467.
(51) Czlapinski, J. L.; Sheppard, T. L. *J. Am. Chem. Soc.* **2001**, *123*, 8618-8619.
(52) Bouamaied, I.; Nguyen, T.; Ruhl, T.; Stulz, E. *Org. Biomol. Chem.* **2008**, *6*, 3888-3891.
(53) Iijima, S. *Nature* **1991**, *354*, 56-58.
(54) Iijima, S. *Physica B.* **2002**, *323*, 1-5.
(55) Wang, X.; Li, Q.; Xie, J.; Jin, Z.; Wang, J.; Li, Y.; Jiang, K.; Fan, S. *Nano Lett.* **2009**, *9*, 3137-3141.
(56) Thess, A.; Lee, R.; Nikolaev, P.; Dai, H.; Petit, P.; Robert, J.; Xu, C.; Lee, Y. H.; Kim, S. G.; Rinzler, A. G.; Colbert, D. T.; Scuseria, G. E.; Tomanek, D.; Fischer, J. E.; Smalley, R. E. *Science* **1996**, *273*, 483-487.
(57) Hafner, J. H.; Bronikowski, M. J.; Azamian, B. R.; Nikolaev, P.; Rinzler, A. G.; Colbert, D. T.; Smith, K. A.; Smalley, R. E. *Chem. Phys. Lett.* **1998**, *296*, 195-202.
(58) Nikolaev, P.; Bronikowski, M. J.; Bradley, R. K.; Rohmund, F.; Colbert, D. T.; Smith, K. A.; Smalley, R. E. *Chem. Phys. Lett.* **1999**, *313*, 91-97.
(59) Dai, H.; Rinzler, A. G.; Nikolaev, P.; Thess, A.; Colbert, D. T.; Smalley, R. E. *Chem. Phys. Lett.* **1996**, *260*, 471-475.
(60) Katz, E.; Willner, I. *ChemPhysChem* **2004**, *5*, 1084-1104.
(61) Chen, Z.; Du, X.; Du, M.-H.; Rancken, C. D.; Cheng, H.-P.; Rinzler, A. G. *Nano Lett.* **2003**, *3*, 1245-1249.
(62) Chattopadhyay, D.; Galeska, I.; Papadimitrakopoulos, F. *J. Am. Chem. Soc.* **2003**, *125*, 3370-3375.
(63) Li, H.; Zhou, B.; Lin, Y.; Gu, L.; Wang, W.; Fernando, K. A. S.; Kumar, S.; Allard, L. F.; Sun, Y. P. *J. Am. Chem. Soc.* **2004**, *126*, 1014-1015.
(64) Ho, K. H. L.; Rivier, L.; Jousselme, B.; Jegou, P.; Filoramo, A.; Campidelli, S. *Chem. Comm.* **2010**, *46*, 8731-8733.
(65) Baskaran, D.; Mays, J. W.; Zhang, X. P.; Bratcher, M. S. *J. Am. Chem. Soc.* **2005**, *127*, 6916-6917.
(66) Ehli, C.; Rahman, G. M. A.; Jux, N.; Balbinot, D.; Guldi, D. M.; Paolucci, F.; Marcaccio, M.; Paolucci, D.; Melle-Franco, M.; Zerbetto, F.; Campidelli, S.; Prato, M. *J. Am. Chem. Soc.* **2006**, *128*, 11222-11231.
(67) Chitta, R.; Sandanayaka, A. S. D.; Schumacher, A. L.; D'Souza, L.; Araki, Y.; Ito, O.; D'Souza, F. *J. Phys. Chem. C.* **2007**, *111*, 6947-6955.
(68) Nakashima, N.; Tomonari, Y.; Murakamiy, H. *Chem. Lett.* **2002**, *31*, 2.
(69) Guldi, D. M.; Rahman, G. M. A.; Jux, N.; Tagmatarchis, N.; Prato, M. *Angew. Chem. Int. Ed* **2004**, *43*, 5526-5530.

(70) Li, C.; Chen, Y.; Wang, Y.; Iqbal, Z.; Chhowalla, M.; Mitra, S. *J. Mater. Chem.* **2007**, *17*, 2406-2411.
(71) Martin, N.; Sanchez, L.; Herranz, M. Ã.; Illescas, B.; Guldi, D. M. *Acc. Chem. Res.* **2007**, *40*, 1015-1024.
(72) D'Souza, F.; Chitta, R.; Sandanayaka, A. S. D.; Subbaiyan, N. K.; D'Souza, L.; Araki, Y.; Ito, O. *J. Am. Chem. Soc.* **2007**, *129*, 15865-15871.
(73) Yang, Q.-H.; Gale, N.; Oton, C. J.; Li, F.; Vaughan, A.; Saito, R.; Nandhakumar, I. S.; Tang, Z.-Y.; Cheng, H.-M.; Brown, T.; Loh, W. H. *Nanotechnology* **2007**, *18*, 405706.
(74) Dillon, A. C.; Jones, K. M.; Bekkedahl, T. A.; Kiang, C. H.; Bethune, D. S.; Heben, M. J. *Nature* **1997**, *386*, 377-379.
(75) Khlobystov, A. N.; Porfyrakis, K.; Kanai, M.; Britz, D. A.; Ardavan, A.; Shinohara, H.; Dennis, T. J. S.; Briggs, G. A. D. *Angew. Chem. Int. Ed.* **2004**, *43*, 1386-1389.
(76) Agnihotri, S.; Rostam-Abadi, M.; Rood, M. J. *Carbon* **2004**, *42*, 2699-2710.
(77) Jang, S.-R.; Vittal, R.; Kim, K.-J. *Langmuir* **2004**, *20*, 9807-9810.
(78) Campidelli, S.; Ballesteros, B.; Filoramo, A.; Diaz, D. D.; de la Torre, G.; Torres, T.; Rahman, G. M. A.; Ehli, C.; Kiessling, D.; Werner, F.; Sgobba, V.; Guldi, D. M.; Cioffi, C.; Prato, M.; Bourgoin, J.-P. *J. Am. Chem. Soc.* **2008**, *130*, 11503-11509.
(79) Bahr, J. L.; Tour, J. M. *Chem. Mater.* **2001**, *13*, 3823-3824.
(80) Georgakilas, V.; Kordatos, K.; Prato, M.; Guldi, D. M.; Holzinger, M.; Hirsch, A. *J. Am. Chem. Soc.* **2002**, *124*, 760-761.
(81) Alvaro, M.; Atienzar, P.; de la Cruz, P.; Delgado, J. L.; Troiani, V.; Garcia, H.; Langa, F.; Palkar, A.; Echegoyen, L. *J. Am. Chem. Soc.* **2006**, *128*, 6626-6635.
(82) Guldi, D. M.; Marcaccio, M.; Paolucci, D.; Paolucci, F.; Tagmatarchis, N.; Tasis, D.; Vazquez, E.; Prato, M. *Angew. Chem. Int. Ed.* **2003**, *42*, 4206-4209.
(83) Guo, Z.; Du, F.; Ren, D.; Chen, Y.; Zheng, J.; Liu, Z.; Tian, J. *J. Mater. Chem.* **2006**, *16*, 3021-3030.
(84) Shi Kam, N. W.; Jessop, T. C.; Wender, P. A.; Dai, H. *J. Am. Chem. Soc.* **2004**, *126*, 6850-6851.
(85) Zhao, Q.; Gu, Z. N.; Zhuang, Q. K. *Electrochem. Commun.* **2004**, *6*, 83-86.
(86) Hasobe, T.; Fukuzumi, S.; Kamat, P. V. *J. Phys. Chem. B* **2006**, *110*, 25477-25484.
(87) Hasobe, T.; Fukuzumi, S.; Kamat, P. V. *J. Am. Chem. Soc.* **2005**, *127*, 11884-11885.
(88) Murakami, H.; Nomura, T.; Nakashima, N. *Chem. Phys. Lett.* **2003**, *378*, 481-485.
(89) Rahman, G. M. A.; Guldi, D. M.; Campidelli, S.; Prato, M. *J. Mater. Chem* **2006**, *16*, 62-65.
(90) Boul, P. J.; Cho, D.-G.; Rahman, G. M. A.; Marquez, M.; Ou, Z.; Kadish, K. M.; Guldi, D. M.; Sessler, J. L. *J. Am. Chem. Soc.* **2007**, *129*, 5683-5687.
(91) Gigliotti, B.; Sakizzie, B.; Bethune, D. S.; Shelby, R. M.; Cha, J. N. *Nano Lett.* **2006**, *6*, 159-164.
(92) Zheng, M.; Jagota, A.; Strano, M. S.; Santos, A. P.; Barone, P.; Chou, S. G.; Diner, B. A.; Dresselhaus, M. S.; Mclean, R. S.; Onoa, G. B.; Samsonidze, G. G.; Semke, E. D.; Usrey, M.; Walls, D. J. *Science* **2003**, *302*, 1545-1548.
(93) Yang, Q.-H.; Gale, N.; Oton, C. J.; Li, H.; Nandhakumar, I. S.; Tang, Z.-Y.; Brown, T.; Loh, W. H. *Carbon* **2007**, *45*, 2701-2703.
(94) Fujitsuka, M.; Okada, A.; Tojo, S.; Takei, F.; Onitsuka, K.; Takahashi, S.; Majima, T. *J. Phys. Chem. B.* **2004**, *108*, 11935-11941.
(95) Shimidzu, T.; Segawa, H. *Thin Solid Films* **1996**, *273*, 14-19.
(96) Anderson, H. L. *Inorg. Chem.* **1994**, *33*, 972-981.
(97) Dunetz, J. R.; Sandstrom, C.; Young, E. R.; Baker, P.; Van Name, S. A.; Cathopolous, T.; Fairman, R.; de Paula, J. C.; Akerfeldt, K. S. *Org. Lett.* **2005**, *7*, 2559-2561.
(98) Hasobe, T.; Kamat, P. V.; Troiani, V.; Solladie, N.; Ahn, T. K.; Kim, S. K.; Kim, D.; Kongkanand, A.; Kuwabata, S.; Fukuzumi, S. *J. Phys. Chem. B.* **2005**, *109*, 19-23.
(99) Hasobe, T.; Kashiwagi, Y.; Absalom, M. A.; Sly, J.; Hosomizu, K.; Crossley, M. J.; Imahori, H.; Kamat, P. V.; Fukuzumi, S. *Adv. Mater.* **2004**, *16*, 975-979.
(100) D'Souza, F.; Rogers, L. M.; Islam, D. M. S.; Araki, Y.; Ito, O.; Wada, T. *Chem. Lett.* **2008**, *37*, 460-461.

(101) Drain, C. M. *P. Natl. Acad. Sci. USA* **2002**, *99*, 5178-5182.
(102) Sun, K.; Mauzerall, D. *Biophys. J.* **1996**, *71*, 295-308.
(103) Nam, Y. S.; Shin, T.; Park, H.; Magyar, A. P.; Choi, K.; Fantner, G.; Nelson, K. A.; Belcher, A. M. *J. Am. Chem. Soc.*, *132*, 1462-+.
(104) Martin, K. E.; Wang, Z. C.; Busani, T.; Garcia, R. M.; Chen, Z.; Jiang, Y. B.; Song, Y. J.; Jacobsen, J. L.; Vu, T. T.; Schore, N. E.; Swartzentruber, B. S.; Medforth, C. J.; Shelnutt, J. A. *J. Am. Chem. Soc.* **2010**, *132*, 8194-8201.
(105) Wang, Z. C.; Medforth, C. J.; Shelnutt, J. A. *J. Am. Chem. Soc.* **2004**, *126*, 15954-15955.
(106) Osuka, A.; Zhang, R. P.; Maruyama, K.; Ohno, T.; Nozaki, K. *B. Chem. Soc. Jpn.* **1993**, *66*, 3773-3782.
(107) Borjesson, K.; Tumpane, J.; Ljungdahl, T.; Wilhelmsson, L. M.; Norden, B.; Brown, T.; Martensson, J.; Albinsson, B. *J. Am. Chem. Soc.* **2009**, *131*, 2831-2839.
(108) Asano-Someda, M.; Kaizu, Y. *Inorg. Chem.* **1999**, *38*, 2303-2311.
(109) Guldi, D. M.; Imahori, H.; Tamaki, K.; Kashiwagi, Y.; Yamada, H.; Sakata, Y.; Fukuzumi, S. *J. Phys. Chem. A.* **2004**, *108*, 541-548.
(110) Ambroise, A.; Wagner, R. W.; Rao, P. D.; Riggs, J. A.; Hascoat, P.; Diers, J. R.; Seth, J.; Lammi, R. K.; Bocian, D. F.; Holten, D.; Lindsey, J. S. *Chem. Mater.* **2001**, *13*, 1023-1034.
(111) Jolliffe, K. A.; Langford, S. J.; Ranasinghe, M. G.; Shephard, M. J.; Paddon-Row, M. N. *J. Org. Chem.* **1999**, *64*, 1238-1246.
(112) Bennett, N.; Xu, G. Z.; Esdaile, L. J.; Anderson, H. L.; Macdonald, J. E.; Elliott, M. *Small*, *6*, 2604-2611.
(113) Sedghi, G.; Sawada, K.; Esdaile, L. J.; Hoffmann, M.; Anderson, H. L.; Bethell, D.; Haiss, W.; Higgins, S. J.; Nichols, R. J. *J. Am. Chem. Soc.* **2008**, *130*, 8582-+.
(114) Chang, M.-H.; Hoffmann, M.; Anderson, H. L.; Herz, L. M. *J. Am. Chem. Soc.* **2008**, *130*, 10171-10178.
(115) Susumu, K.; Frail, P. R.; Angiolillo, P. J.; Therien, M. J. *J. Am. Chem. Soc.* **2006**, *128*, 8380-8381.
(116) Berman, A.; Izraeli, E. S.; Levanon, H.; Wang, B.; Sessler, J. L. *J. Am. Chem. Soc.* **1995**, *117*, 8252-8257.
(117) Stulz, E.; Bouamaied, I. *Synlett* **2004**, *9*, 1579-1583.
(118) Brewer, A.; Siligardi, G.; Neylon, C.; Stulz, E. *Org. Biomol. Chem.* **2011**, *9*, 777-782.
(119) Bouamaied, I.; Fendt, L.-A.; Wiesner, M.; Haussinger, D.; Amiot, N.; Thoni, S.; Stulz, E. *Pure.Appl.Chem.* **2006**, *78*, 2003-2014.
(120) Stulz, E.; Bouamaied, I. *Chimia* **2005**, 101-104.
(121) Bouamaied, I.; Fendt, L.-A.; Haussinger, D.; Wiesner, M.; Thoni, S.; Amiot, N.; Stulz, E. *Nucleos. Nucleot. Nucl.* **2007**, *26*, 1533-1538.
(122) Solladie, N.; Gross, M.; Gisselbrecht, J.-P.; Sooambar, C. *ChemComm.* **2001**, 2.
(123) Ruhl, T.; Stulz, E. *Supramol. Chem.*, *22*, 103-108.
(124) Solladie, N.; Gross, M. *Tet. Lett.* **1999**, *40*, 3359-3362.
(125) Boutorine, A. S.; Le Doan, T.; Battioni, J. P.; Mansuy, D.; Dupre, D.; Helene, C. *Bioconj. Chem.* **1990**, *1*, 350-356.
(126) Mammana, A.; Asakawa, T.; Bitsch-Jensen, K.; Wolfe, A.; Chaturantabut, S.; Otani, Y.; Li, X. X.; Li, Z. M.; Nakanishi, K.; Balaz, M.; Ellestad, G. A.; Berova, N. *Bioorgan. Med. Chem.* **2008**, *16*, 6544-6551.
(127) Ohya, Y.; Hashimoto, N.; Jo, S.; Nohori, T.; Yoshikuni, T.; Ouchi, T.; Tamiaki, H. *Supramol. Chem.* **2009**, *21*, 301-309.
(128) Fischer, H.; Zeile, K. *Liebigs Ann. Chem.* **1929**, *468*, 98-116.
(129) Rothemund, P. *J. Am. Chem. Soc.* **1935**, *57*, 2010-2011.
(130) Rothemund, P. *J. Am. Chem. Soc.* **1936**, *58*, 625-627.
(131) Lindsey, J. S.; Schreiman, I. C.; Hsu, H. C.; Kearney, P. C.; Marguerettaz, A. M. *J. Org. Chem.* **1987**, *52*, 827-836.
(132) Zaidi, S. H. H.; Muthukumaran, K.; Tamaru, S.-i.; Lindsey, J. S. *J. Org. Chem.* **2004**, *69*, 8356-8365.

(133) Dogutan, D. K.; Zaidi, S. H. H.; Thamyongkit, P.; Lindsey, J. S. *J. Org. Chem.* **2007**, *72*, 7701-7714.
(134) Karotki, A.; Kruk, M.; Drobizhev, M.; Rebane, A.; Nickel, E.; Spangler, C. W. *IEEE J. Sel. Top. Quant. Electron.* **2001**, *7*, 971-975.
(135) Venkataraman, K.; Wagle, D. R. *Tetrahedron Lett.* **1979**, 3037-3040.
(136) J. Nurminen, E.; K. Mattinen, J.; Lonnberg, H. *J. Chem. Soc., Perkin Trans. 2* **1998**, 1621-1628.
(137) Connors, K. A.; Pandit, N. K. *Anal. Chem.* **1978**, *50*, 1542-1545.
(138) Borjesson, K.; Wiberg, J.; El-Sagheer, A. H.; Ljungdahl, T.; Martensson, J.; Brown, T.; Norden, B.; Albinsson, B. *ACS Nano*, *4*, 5037-5046.
(139) Malinovskii, V. L.; Wenger, D.; Haner, R. *Chem. Soc. Rev.*, *39*, 410-422.
(140) Shkirman, S.; Solov'ev, K.; Kachura, T.; Arabei, S.; Skakovskii, E. *J. Appl. Spec.* **1999**, *66*, 68-75.
(141) Kottysch, T.; Ahlborn, C.; Brotzel, F.; Richert, C. *Chem. Euro. J.* **2004**, *10*, 4017-4028.
(142) Bucholz, T. L.; Loo, Y.-L. *Macromol.* **2008**, *41*, 4069-4070.
(143) Davis, T. M.; McFail-Isom, L.; Keane, E.; Williams, L. D. *Biochemistry* **1998**, *37*, 6975-6978.
(144) Berova, N.; Bari, L. D.; Pescitelli, G. *Chem. Soc. Rev.* **2007**, *36*, 914-931.
(145) Pescitelli, G.; Sreerama, N.; Salvadori, P.; Nakanishi, K.; Berova, N.; Woody, R. W. *J. Am. Chem. Soc.* **2008**, *130*, 6170-6181.
(146) Georgakopoulou, S.; van Grondelle, R.; van der Zwan, G. *J. Phys. Chem. B* **2006**, *110*, 3344-3353.
(147) Nakano, S.-I.; Uotani, Y.; Uenishi, K.; Fujii, M.; Sugimoto, N. *Nucleic Acids Res.*, *33*, 7111-7119.
(148) Harada, N.; Chen, S. L.; Nakanishi, K. *J. Am. Chem. Soc.* **1975**, *97*, 5345-5352.
(149) Nehira, T.; Parish, C. A.; Jockusch, S.; Turro, N. J.; Nakanishi, K.; Berova, N. *J. Am. Chem. Soc.* **1999**, *121*, 8681-8691.
(150) Pescitelli, G.; Gabriel, S.; Wang, Y.; Fleischhauer, J.; Woody, R. W.; Berova, N. *J. Am. Chem. Soc.* **2003**, *125*, 7613-7628.
(151) Hsu, M. C.; Woody, R. W. *J. Am. Chem. Soc.* **1971**, *93*, 3515-+.
(152) Riazance, J. H.; Baase, W. A.; Johnson, W. C.; Hall, K.; Cruz, P.; Tinoco, I. *Nucleic Acids Res.* **1985**, *13*, 4983-4989.
(153) Xueguang, S.; Enhua, C.; Chunli, B.; Yujian, H.; Jingfen, Q. *Chinese Sci. Bull.* **1998**, *43*, 1456-1460.
(154) Snatzke, G. *Angew. Chem. Int. Ed* **1979**, *18*, 363-377.
(155) Mammana, A.; Pescitelli, G.; Asakawa, T.; Jockusch, S.; Petrovic, A. G.; Monaco, R. R.; Purrello, R.; Turro, N. J.; Nakanishi, K.; Ellestad, G. A.; Balaz, M.; Berova, N. *Chem. Euro. J.* **2009**, *15*, 11853-11866.
(156) Aghdaei, S.; Morgan, H.; De Planque, M. *54th Annual Meeting of the Biophysical Society.* **2010**, *20th - 24th February 2010*, 401a-402a.
(157) Morgan, H.; De Planque, M. *NanoBioTech.* **2010**, *15th - 17th November*.
(158) Ricci, F.; Zari, N.; Caprio, F.; Recine, S.; Amine, A.; Moscone, D.; Palleschi, G.; Plaxco, K. W. *Bioelectrochemistry* **2009**, *76*, 208-213.
(159) Hartwich, G.; Caruana, D. J.; de Lumley-Woodyear, T.; Wu, Y. B.; Campbell, C. N.; Heller, A. *J. Am. Chem. Soc.* **1999**, *121*, 10803-10812.
(160) Anne, A.; Demaille, C. *J. Am. Chem. Soc.* **2008**, *130*, 9812-9823.
(161) Jacobsen, M. F.; Ferapontova, E. E.; Gothelf, K. V. *Org. Biomol. Chem.* **2009**, *7*, 905-908.
(162) Beilstein, A. E.; Grinstaff, M. W. *J. Organomet. Chem.* **2001**, *637*, 398-406.
(163) Brazdilova, P.; Vrabel, M.; Pohl, R.; Pivonkova, H.; Havran, L.; Hocek, M.; Fojta, M. *Chem. Euro. J.* **2007**, *13*, 9527-9533.
(164) Pike, A. R.; Ryder, L. C.; Horrocks, B. R.; Clegg, W.; Connolly, B. A.; Houlton, A. *Chem. Euro. J.* **2005**, *11*, 344-353.
(165) Pike, A. R.; Ryder, L. C.; Horrocks, B. R.; Clegg, W.; Elsegood, M. R. J.; Connolly, B. A.; Houlton, A. *Chem. Euro. J.* **2002**, *8*, 2891-2899.

(166) Mucic, R. C.; Herrlein, M. K.; Mirkin, C. A.; Letsinger, R. L. *ChemComm.* **1996**, 555-557.
(167) Navarro, A. E.; Spinelli, N.; Chaix, C.; Moustrou, C.; Mandrand, B.; Brisset, H. *Bioorg. Med. Chem. Lett.* **2004**, *14*, 2439-2441.
(168) Prins, R.; Korswage.Ar; Kortbeek, A. G. *J. Organomet. Chem.* **1972**, *39*, 335-&.
(169) Kang, D.; Zuo, X. L.; Yang, R. Q.; Xia, F.; Plaxco, K. W.; White, R. J. *Anal. Chem.* **2009**, *81*, 9109-9113.
(170) Wang, J.; Rivas, G.; Jiang, M. A.; Zhang, X. J. *Langmuir* **1999**, *15*, 6541-6545.
(171) Steel, A. B.; Herne, T. M.; Tarlov, M. J. *Anal. Chem.* **1998**, *70*, 4670-4677.
(172) Ho, P. S.; Frederick, C. A.; Saal, D.; Wang, A. H. J.; Rich, A. *J. Biomol. Struct. Dyn.* **1987**, *4*, 521-534.
(173) Khan, S. I.; Beilstein, A. E.; Sykora, M.; Smith, G. D.; Hu, X.; Grinstaff, M. W. *Inorg. Chem.* **1999**, *38*, 3922-3925.
(174) Hu, X.; Smith, G. D.; Sykora, M.; Lee, S. J.; Grinstaff, M. W. *Inorg. Chem.* **2000**, *39*, 2500-2504.
(175) Vrabel, M.; Horakova, P.; Pivonkova, H.; Kalachova, L.; Cernocka, H.; Cahova, H.; Pohl, R.; Sebest, P.; Havran, L.; Hocek, M.; Fojta, M. *Chem. Euro. J.* **2009**, *15*, 1144-1154.
(176) Khan, S. I.; Beilstein, A. E.; Smith, G. D.; Sykora, M.; Grinstaff, M. W. *Inorg. Chem.* **1999**, *38*, 2411-2415.
(177) Balzani, V.; Juris, A.; Venturi, M.; Campagna, S.; Serroni, S. *Chem. Rev.* **1996**, *96*, 759-833.
(178) Kanvah, S.; Joseph, J.; Schuster, G. B.; Barnett, R. N.; Cleveland, C. L.; Landman, U. *Acc. Chem. Res.*, *43*, 280-287.
(179) Arinaga, K.; Rant, U.; Knezevic, J.; Pringsheim, E.; Tornow, M.; Fujita, S.; Abstreiter, G.; Yokoyama, N. *Biosens. Bioelectron.* **2007**, *23*, 326-331.
(180) Gorodetsky, A. A.; Buzzeo, M. C.; Barton, J. K. *Bioconj. Chem.* **2008**, *19*, 2285-2296.
(181) Shiratori, H.; Ohno, T.; Nozaki, K.; Yamazaki, I.; Nishimura, Y.; Osuka, A. *J. Org. Chem.* **2000**, *65*, 8747-8757.
(182) Staab, H. A.; Nikolic, S.; Krieger, C. *Eur. J. Org. Chem.* **1999**, 1459-1470.
(183) Langford, S. J.; Latter, M. J.; Woodward, C. P. *Photochem. Photobiol.* **2006**, *82*, 1530-1540.
(184) Katz, H. E.; Johnson, J.; Lovinger, A. J.; Li, W. J. *J. Am. Chem. Soc.* **2000**, *122*, 7787-7792.
(185) Barros, T. C.; Brochsztain, S.; Toscano, V. G.; Berci, P.; Politi, M. J. *J. Photoch. Photobio. A.* **1997**, *111*, 97-104.
(186) Tierney, M. T.; Grinstaff, M. W. *Org. Lett.* **2000**, *2*, 3413-3416.
(187) Gorodetsky, A. A.; Green, O.; Yavin, E.; Barton, J. K. *Bioconjugate Chem.* **2007**, *18*, 1434-1441.
(188) Whittemore, N. A.; Mullenix, A. N.; Inamati, G. B.; Manoharan, M.; Cook, P. D.; Tuinman, A. A.; Baker, D. C.; Chambers, J. Q. *Bioconjugate Chem.* **1999**, *10*, 261-270.
(189) Yamana, K.; Kumamoto, S.; Nakano, H.; Sugie, Y. *Nucleic Acids Res. Suppl.* **2001**, 35-6.
(190) Yamana, K.; Nishijima, Y.; Ikeda, T.; Gokota, T.; Ozaki, H.; Nakano, H.; Sangen, O.; Shimidzu, T. *Bioconjugate Chemistry* **1990**, *1*, 319-324.
(191) Mahajan, S.; Richardson, J.; Ben Gaied, N.; Zhao, Z. Y.; Brown, T.; Bartlett, P. N. *Electroanalysis* **2009**, *21*, 2190-2197.
(192) Ben Gaied, N.; Zhao, Z. Y.; Gerrard, S. R.; Fox, K. R.; Brown, T. *ChemBioChem* **2009**, *10*, 1839-1851.
(193) Mori, K.; Subasinghe, C.; Cohen, J. S. *Febs Lett.* **1989**, *249*, 213-218.
(194) Wang, G.; Fu, X.; Huang, J.; Wu, L.; Du, Q. *Electrochim. Acta*, *55*, 6933-6940.
(195) Laviron, E. *J. Electroanal. Chem.* **1979**, *101*, 19-28.
(196) Yu, J. X.; Mathew, S.; Flavel, B. S.; Johnston, M. R.; Shapter, J. G. *J. Am. Chem. Soc.* **2008**, *130*, 8788-8796.
(197) Guldi, D. M.; Rahman, G. M. A.; Prato, M.; Jux, N.; Qin, S.; Ford, W. *Angew. Chem. Int. Ed.* **2005**, *44*, 2015-2018.

(198) Hecht, D. S.; Ramirez, R. J. A.; Briman, M.; Artukovic, E.; Chichak, K. S.; Stoddart, J. F.; Gruner, G. *Nano. Lett.* **2006**, *6*, 2031-2036.
(199) Casey, J. P.; Bachilo, S. M.; Weisman, R. B. *J. Mater. Chem.* **2008**, *18*, 1510-1516.
(200) Chichak, K. S.; Star, A.; Altoé, M. V. P.; Stoddart, J. F. *Small* **2005**, *1*, 10.
(201) Chen, J.; Collier, C. P. *J. Phys. Chem. B.* **2005**, *109*, 7605-7609.
(202) Nakashima, N.; Tomonari, Y.; Murakami, H. *Chem. Lett.* **2002**, *31*, 638-639.
(203) Genady, A. R.; El-Zaria, M. E.; Gabel, D. *J. Organomet. Chem.* **2004**, *689*, 3242-3250.
(204) Franco, R.; Jacobsen, J. L.; Wang, H.; Wang, Z.; Istvan, K.; Schore, N. E.; Song, Y.; Medforth, C. J.; Shelnutt, J. A. *Phys. Chem. Chem. Phys.*, *12*, 4072-7.
(205) George, R. C.; Egharevba, G. O.; Nyokong, T. *Polyhedron*, *29*, 1469-1474.
(206) Brown, S. D. M.; Corio, P.; Marucci, A.; Dresselhaus, M. S.; Pimenta, M. A.; Kneipp, K. *Phys. Rev. B.* **2000**, *61*, R5137.
(207) Azoulay, J.; Debarre, A.; Richard, A.; Tchenio, P.; Bandow, S.; Iijima, S. *Europhys. Lett.* **2001**, *53*, 7.
(208) Dresselhaus, M. S.; Dresselhaus, G.; Jorio, A.; Souza Filho, A. G.; Pimenta, M. A.; Saito, R. *Acc. Chem. Res.* **2002**, *35*, 1070-1078.
(209) Guldi, D. M.; Rahman, G. M. A.; Jux, N.; Tagmatarchis, N.; Prato, M. *Angew. Chem. Int. Ed.* **2004**, *43*, 5526-5530.
(210) Ojadi, E.; Selzer, R.; Linschitz, H. *J. Am. Chem. Soc.* **1985**, *107*, 7783-7784.
(211) Vanwilligen, H.; Das, U.; Ojadi, E.; Linschitz, H. *J. Am. Chem. Soc.* **1985**, *107*, 7784-7785.
(212) Kelley, S. O.; Barton, J. K.; Jackson, N. M.; Hill, M. G. *Bioconj. Chem.* **1997**, *8*, 31-37.
(213) Fisher, A. C. *Oxford University Press.* **1996**, *3rd Edition*.
(214) Matile, S.; Berova, N.; Nakanishi, K.; Novkova, S.; Philipova, I.; Blagoev, B. *J. Am. Chem. Soc.* **1995**, *117*, 7021-7022.
(215) Dellaciana, L.; Hamachi, I.; Meyer, T. J. *J. Org. Chem.* **1989**, *54*, 1731-1735.
(216) Khairoutdinov, R. F.; Doubova, L. V.; Haddon, R. C.; Saraf, L. *J. Phys. Chem. B.* **2004**, *108*, 19976-19981.